UNIVERSITY OF SOUTHAMPTON

FACULTY OF NATURAL AND ENVIRONMENTAL SCIENCES

School of Chemistry

TRANSIENT STUDIES OF OXYGEN REDUCTION AT MICROELECTRODES

By

Laila AL-Shandoudi

Thesis submitted for the degree of Doctor of Philosophy

May 2015

UNIVERSITY OF SOUTHAMPTON

ABSTRACT

FACULTY OF ENGINERING, SCIENCE AND MATHEMATICS
SCHOOL OF CHEMISTRY

Doctor of Philosophy

TRANSIENT STUDIES OF OXYGEN REDUCTION AT MICROELECTRODES

By Laila AL-Shandoudi

Our group has previously reported the successful development of a steady state microelectrode sensor for the determination of dissolved oxygen concentrations in sea water. The work presented here underpins the development of a fast oxygen sensor for oceanographic applications; the overall aim is to determine the best conditions to measure dissolved oxygen concentrations with microdiscs on a time scale ranging from sub-milliseconds to seconds. Previous studies with rotating disc and microelectrodes have shown how the apparent number of electrons, n_{app}, varies between 4 and 2 as the steady mass transfer coefficient increases. The present study also aims to provide insight into the oxygen reduction reaction (ORR) and in particular to probe whether and how n_{app}, depends on the time scale of the reaction.

This thesis will describe the results of transient amperometric experiments recorded with microdisc electrodes. The experiments were carried out with different size Pt microdisc electrodes, using fast scan cyclic voltammetry, chronoamperometry and sampled current voltammetry. Model experiments were first conducted with ferrocene, $FeCp_2$, in acetonitrile to validate the experimental approach. Subsequent model experiments were conducted with hexaammineruthenium (III) chloride, $Ru(NH_3)_6Cl_3$, in aqueous chloride solutions. The ORR was also probed in aqueous chloride solutions. Experiments were also systematically conducted in absence of redox couple to investigate the role of background processes in determining the overall amperometric response over the different time scales considered. Where possible, fast scan voltammograms, chronoamperograms and sampled current voltammograms were compared to theoretical expressions or simulations. The work will also describe attempts to develop a potentiostatic conditioning waveform capable of pre-treating the microdisc electrode in order to produce reliable oxygen reduction chronoamperograms.

Various coatings were used for simultaneous determination of dopamine and oxygen species for biological application. The conditioning waveform at bare electrode was found to give more reproducible ORR amperometric response than the coatings alone.

Contents

هذا من فضل ربي

DECLARATION OF AUTHORSHIP

I, Laila Mohammed AL-shandoudi

declare that the thesis entitled

TRANSIENT STUDIES OF OXYGEN REDUCTION AT MICROELECTRODES

and the work presented in the thesis are both my own, and have been generated by me as the result of my own original research. I confirm that:

- this work was done wholly or mainly while in candidature for a research degree at this University;
- where any part of this thesis has previously been submitted for a degree or any other qualification at this University or any other institution, this has been clearly stated;
- where I have consulted the published work of others, this is always clearly attributed;
- where I have quoted from the work of others, the source is always given. With the exception of such quotations, this thesis is entirely my own work;
- I have acknowledged all main sources of help;
- where the thesis is based on work done by myself jointly with others, I have made clear exactly what was done by others and what I have contributed myself;
- none of this work has been published before submission.

Signed: …………………………………………………………………..

Date:…………………………………………………………………….

Acknowledgements

Firstly, thank God for giving me patience and initiation to achieve my wish to continue my study in the field I like very much.

My utmost gratitude to Dr. Guy Denuault who was a source of inspiration and encouragement for his advice.

I would like to express my sincere gratitude to Dr. Peter Birkin for allowing me to undertake this work. They are highly acknowledged.

I am grateful to my supervisors Associate for Dr. Maciej Sosna for his continuous guidance, advice, effort and suggestion throughout the research.

I would also like to thank, my sponsor, Ministry of Higher Education (Oman) for providing me the financial support and special thanks for them for valuable opportunity to carry out my research successfully in Britain.

I would also like to thank members of Electrochemistry and Surface Science department, especially Guy and Phil groups for helping and encouraging me to carry out my research.

Lastly I would like to express my sincere appreciation to my parents for encouraging and supporting me throughout the study.

Definitions and abbreviations

Meaning	Abbreviation
boron-doped diamond	BDD
conductivity, temperature, depth probe	CTD
dissolved oxygen	DO
electrochemical quartz crystal microbalance	EQCM
electrochemical quartz crystal nanobalance	EQCN
environmental scanning electron microscope	ESEM
normal hydrogen electrode	NHE
oxygen reduction reaction	ORR
polypyrrole	PPy
diaminobenzene	DAB
dopamine	DA
rotating disc electrode	RDE
reference electrode	RE
roughness factor	RF
rotating ring-disc electrode	RRDE
saturated calomel electrode	SCE
standard deviation	SD
scanning electron microscopy	SEM
saturated mercurous sulphate electrode	SMSE
working electrode	WE

List of Symbols

Symbol	Description	usual unit
A	(a) area	cm^2
a	microdisc electrode radius	μm
a_j	activity of species j	-
C	conductivity	S
C_{dl}	double layer capacitance	F
c_j	molar concentration of species j	$mol\ dm^{-3}$
c_{mj}	molal concentration (molality) of species j	$mol\ kg^{-1}$
c_{sat}	oxygen concentration in oxygen saturated solution	$mol\ dm^{-3}$
c_∞	molar concentration in the bulk solution	$mol\ dm^{-3}$
D_j	diffusion coefficient of species j	$cm^2\ s^{-1}$
D_w	oxygen diffusion coefficient in water	$cm^2\ s^{-1}$
$E_{1/2}$	half-wave potential	V
$E_{1/4}, E_{3/4}$	quartile potentials	V
E_{cl}	cleaning potential	V
E_{ref}	reference electrode potential	V
F	the Faraday constant, 96485	$C\ mol^{-1}$
f	resonant frequency of a piezoelectric	Hz

Chapter 1

Introduction

1 Overview

The present work gives an overview of the study of Oxygen Reduction Reaction (ORR) under non-steady state conditions with microelectrodes.

Oxygen electrochemistry, particularly the reaction mechanism of oxygen reduction and the role of electrocatalyst in this reaction is one of the attractive research areas among electrochemists. In many fields, e.g. fuel cells, metal-air batteries, hydrogen–oxygen fuel cells, corrosion, electro-organic reactions, industrial electrolytic processes and sensor development, the O_2 reduction reaction is a key reaction. Although a large part of the investigations in the literature relates to ORR in acidic and alkaline solutions, there is a lack of studies in neutral unbuffered medium. However, there are many difficulties faced with the complexity of this reaction (e.g. intermediates and number of electron involved). Therefore, it is of great importance to study the fundamental issues related to its time dependence in order to develop a microelectrode DO sensor. We also report attempts to investigate the same issue for model systems such as ferrocene oxidation and ruthenium complex ion reduction.

The O_2 sensor previously developed for oceanography is based on steady state measurement. Since it could be affected by convection and the measurement takes long times, there is an urgent need to shorten the response time. Therefore there is an interest to reconstruct a DO sensor that works under transient conditions enabling to overcome all previously mentioned problems. The question raised here is how the reaction occurs over the timescale of the measurement. Also, much of the work presented here has focused on the development of an applied conditioning waveform to obtain a reliable response for the electroreduction of O_2. This work tries to identify ongoing critical questions regarding the surface condition and reproducibility that will likely be

the focus of sensor development. It also tries to understand how and why electrode performance changes with time and preconditioning. Understanding the fundamental aspects of ORR will improve the speed of the design of a sensor and may help towards the development of better catalysts.

Of particular interest is the dependence of the apparent number of electron on the timescale of the measurement. This thesis explores the ORR reaction performance at short time.

1.1 The importance of Dissolved Oxygen (DO) sensing

There has been considerable interest in determining DO in various environments. Significantly, numerous works have been devoted to the development of new dissolved oxygen sensors. Monitoring of oxygen levels *in situ* is of great important in many fields including:

- environmental fields, where O_2 can serve as a tracer for water quality in terms of pollution or eutrophication in natural waters and as an indicator of biochemical breakdown of waste in sewage water treatment.
- environmental control, where there is a demand for O_2 monitoring in modified atmospheres (e.g. greenhouses, gas industries, and respiratory gases), safety in industrial environments, emissions control, engineered biofilms and combustion optimisation.
- some applications which are related to biological systems such as blood or tissues as they can give information on metabolic process or medical diagnosis as well as pharmaceutical industry, particularly biomedical preparation of drugs, using bacteria culture.
- the automotive industry and fuel cells technology, mainly batteries and related electrochemical technology depend greatly on DO measurements to investigate its role in corrosion processes.
- food storage where a certain amount of oxygen is necessary to avoid spoilage of foodstuff.
- metallurgy, where corrosion phenomenon is caused by presence of oxygen.
- power plant cooling system, where there is a demand for reduced oxygen levels to avoid corrosion.

Apart from all above mentioned areas where determination of oxygen is of great importance, it is vital to measure DO for marine applications and oceanography. Dissolved oxygen levels in deep-sea waters are of great interest as they offer a platform for oceanographic research, in

particular climate change studies that correlate positively with biological activity of photosynthesising organisms on short timescales, or negatively with the respiration processes of aquatic flora and fauna. Additionally, they provide an indicator of water masses movement and mixing.

It is believed that DO is a key parameter for prediction of global climate change. This in turn results in the necessity for long time measurement to investigate this environmental issue. The work in this thesis underpins the development of microelectrode of a faster cathode material for DO sensing. The next section provides detailed information about microelectrodes.

1.2 Use of Microelectrodes

1.2.1 Definition

During the last two decades, microelectrodes have been established as powerful tools for electrochemical studies. In particular, they are attractive as the active components of sensors; microelectrode sensors require only very simple and low power circuitry. In addition, they can offer high sensitivity, a signal less affected by flow rate, short response times and the ability to operate in media of high or variable resistivity [1]. They can be differentiated from conventional electrodes by having a characteristic dimension (radius, width or thickness depending on geometry), mostly $\leq 50\mu m$. Their size can give unique electrochemical properties. Most of them offer the combination between the ease of fabrication and robustness [2].

Generally, the materials used for fabrication of microelectrodes are Pt, Au, C, Ag, Ni, Cu, Hg on C, Pd and W and the insulating material used can be glass, epoxy resin, wax, etc while the body where the microelectrode wire can be sealed into can be Pyrex capillary, pipette tip, PTFE tubing, etc. In order to make electrical contact to a copper wire several materials were tried such as Ag epoxy resin, indium and solder.

Basically, there are different designs of microelectrodes such as disc, hemispherical, channel and band shapes. Figure 1.1 represents some of the different designs. The diffusion regime depends on the geometry of the microelectrode.
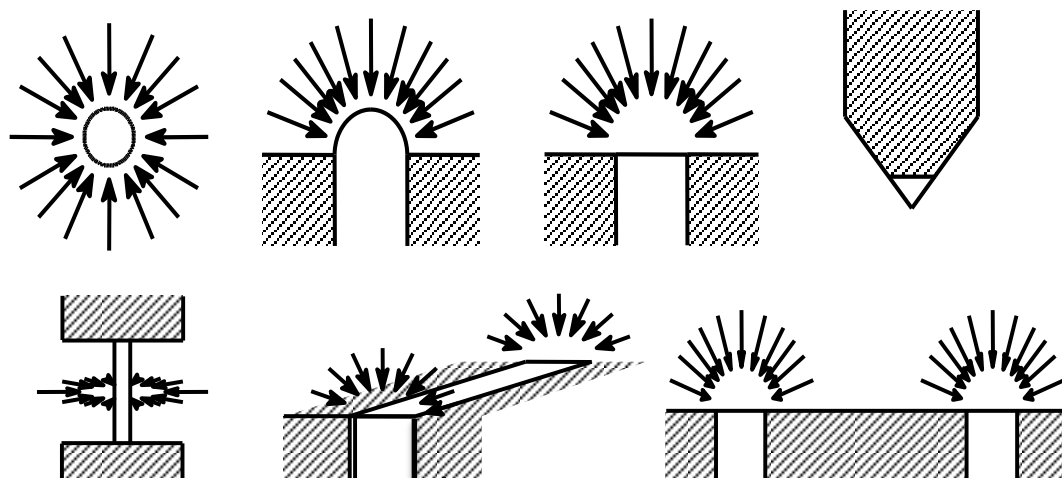
Figure 1.1 Schematic illustration of microelectrode designs. Sphere, Hemisphere, Disc, STM tips partially coated, Cylinder, Line and Rings.

1.2.2 Properties of microelectrodes

There are some attractive features related to microelectrodes that have made significant impact in electrochemistry. The decreased ohmic distortions allow electrochemical measurements to be made on new and unique chemical environments such as highly resistive solutions [3]. Additionally, the greatly reduced double-layer capacitance of microelectrodes, associated with their small area, results in electrochemical cells with small resistor–capacitor RC time constant. Moreover, enhanced rates of mass transport of electroactive species result in formation of a spherical diffusion layer at long times leading to a steady state current [4-15].

Many interested applications which require small electrodes like medicine, bioengineering and microanalysis can be investigated.

1.2.3 Chronoamperometry at microelectrodes

Assuming that the potential step is applied to a microdisc, the charging current is not negligible at the beginning, but quickly, exponentially decays with time. After a time such that the charging current can be neglected, the diffusion controlled faradaic current at the microdisc can be analysed with the Shoup and Szabo equation (1) [16]. This function was obtained by fitting both short and

long time analytical expressions derived by Aoki and Osteryoung [17] and was noted to agree with a 0.6% deviation of the theoretical current [16].

$$i = 4nFDc^{\infty}a \left\{ \begin{array}{l} 0.7854 + 0.4431\left(\dfrac{Dt}{a^2}\right)^{-1/2} \\ + 0.2146\exp\left[-0.3912\left(\dfrac{Dt}{a^2}\right)^{-1/2}\right] \end{array} \right\}$$ Equation 1.1

where n is the number of electrons involved, F is the Faraday constant, D and c^{∞} are the diffusion coefficient and the bulk concentration of the species, a is the radius of the electrode and t is the time.

Figure 1.2 shows a typical plot of i-t curve for typical conditions ($D = 1\text{x}10^{-5}$ cm^2 s^{-1}, $C = 5$ mM). It is clear the largest current is observed immediately after the potential step was applied, which is followed by a decay in current till it levels off. Basically, a log-log plot displays three diffusion regimes depending on the time scales: short, intermediate and long-time domains. Corresponding diffusion regimes for three time domains are expected to be linear, convergent and then a radial diffusion should be observed. Also, a linear relationship is obtained for the current versus $t^{-0.5}$.
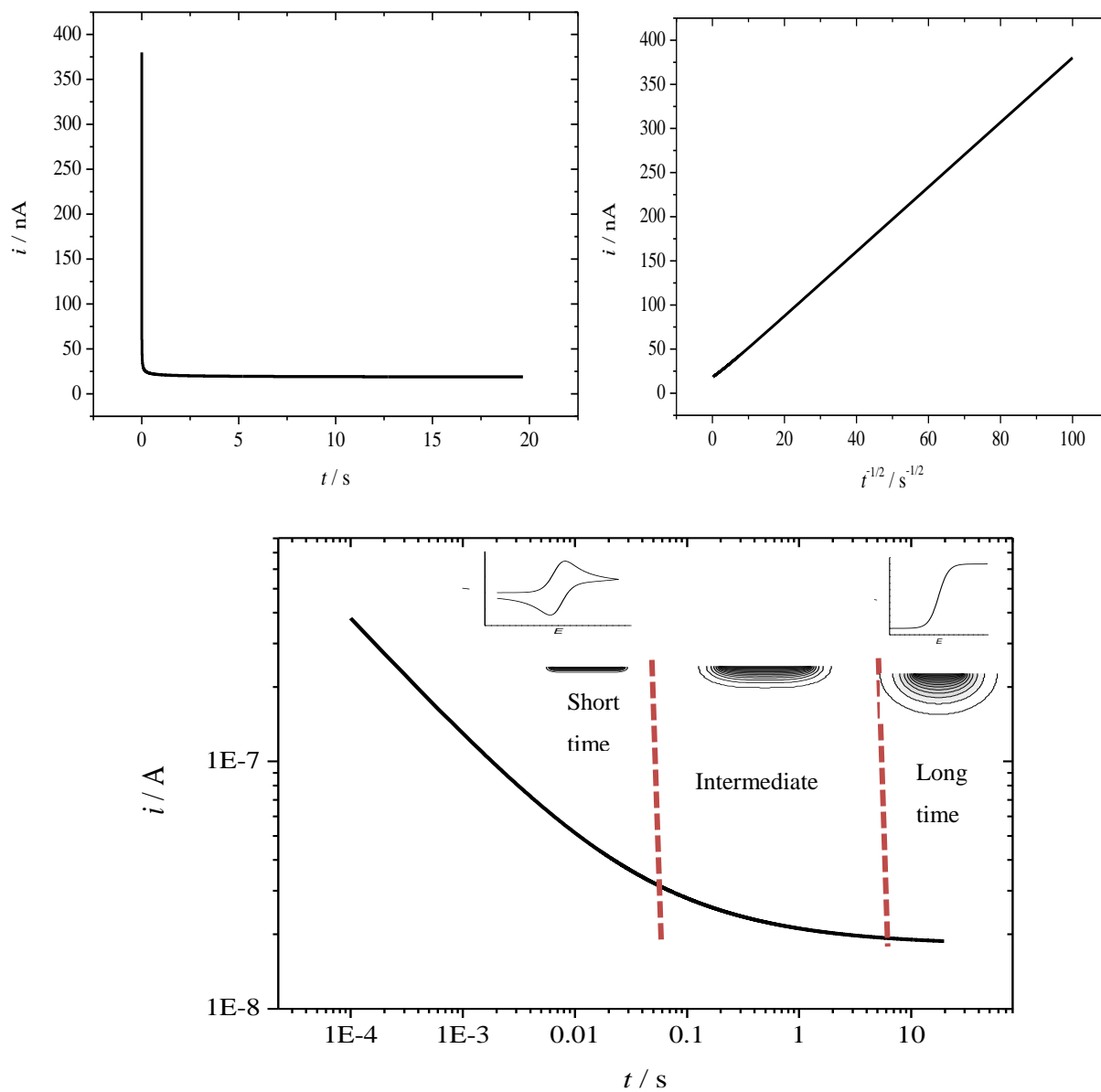
Figure 1.2 Diffusion controlled current transients at a microdisc electrode. The conditions in this case are as follows $D = 1 \times 10^{-5}$ cm^2 s^{-1}, $c^{\infty} = 5$ mM and $a = 1.25 \times 10^{-3}$ cm.

A more accurate version of the equation for the diffusion controlled current at a microdisc was derived by Mahon and Oldham [18] (Equation 2).

$$\frac{i}{nFDc^{\infty}a} = \begin{cases} \dfrac{1}{\sqrt{\pi\theta}} + \sqrt{\dfrac{\theta}{4\pi}} - \dfrac{3\theta}{25} + \dfrac{3\theta^{3/2}}{226}, \theta \leq 1.281 \\[3mm] \dfrac{4}{\pi} + \dfrac{8}{\sqrt{\pi^{5}\theta}} + \dfrac{25\theta^{-3/2}}{2792} - \dfrac{\theta^{-5/2}}{3380} - \dfrac{\theta^{-7/2}}{4500}, \theta \geq 1.281 \end{cases} \qquad \text{Equation 1.2}$$

where $$\theta = \frac{Dt}{a^{2}}$$

The difference between the Shoup and Szabo and the Mahon and Oldham equations can be clearly seen when $(i_{S\&S} - i_{M\&O})/i_{M\&O} \times 100$ versus time is plotted in Figure 1.3. The relative difference increases significantly in milliseconds domain. This is important in our study of ORR since the milliseconds to second region is the focus where the exploration and the investigation of the ORR is conducted and studied. The difference between them is nevertheless small.
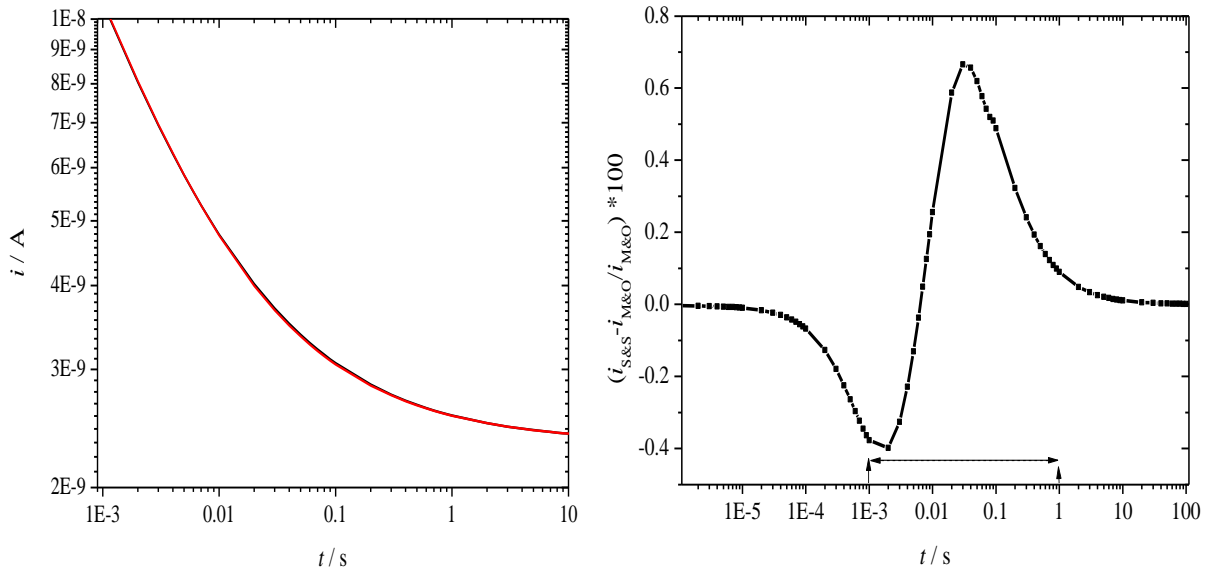
Figure 1.3 Relative differences between Shoup and Szabo (black) and Mahon and Oldham (red) equations at microdisc electrodes. The conditions in this case are as follows $D = 1 \times 10^{-5}$ cm^2 s^{-1}, $C^{\infty} = 1 \times 10^{-7}$ mol cm^{-3} and $a = 1.25 \times 10^{-3}$ cm.

There have been some applications of this theoretical treatment. Aoki and Osteryoung found a good agreement between the theoretical and experimental values of the diffusion coefficient for hexacyanoferrate (II) ion after applying the Shoup-Szabo equation for chronoamperometric curves at microdisc electrode [19]. Ikeuchi and Kanakubo proposed an easy method for determining the

diffusion coefficients of electrode reaction products by double potential step chronoamperometry at small disc electrodes using this equation [20]. The method was also verified successfully by an experiment in which the diffusion coefficients of both the elements of the $[Fe(CN)_6]^{4-}/[Fe(CN)_6]^{3-}$ redox couple were determined by the usual potential step chronoamperometry and by this method [20]. Also, direct determination of diffusion coefficients for some systems by chronoamperometry at microdisc was reported by Denuault *et al.*[21].

At short times planar diffusion dominates and the current at the microdisc electrode tends towards that given by Cottrell equation

$$i = \frac{nFAD^{1/2}c^{\infty}}{\pi^{1/2}t^{1/2}}$$ Equation 1.3

Using the Shoup and Szabo equation, it is possible to derive k_m for a microdisc, where k_m is the mass transfer coefficient.

$$i = nFAk_m c^{\infty} = nF\pi a^2 k_m c^{\infty} = 4nFDa\ c^{\infty} f(t)$$ Equation 1.4

where $f(t)$ is a term taken from the Shoup-Szabo equation.

$$f(t) = \left\{ \begin{array}{l} 0.7854 + 0.4431 \left(\dfrac{Dt}{a^2}\right)^{-1/2} \\[2em] + \ 0.2146\ \exp\left[-0.3912\left(\dfrac{Dt}{a^2}\right)^{-1/2}\right] \end{array} \right\}$$ Equation 1.5

Hence

$$k_m(t) = \frac{4D}{\pi a} f(t)$$ Equation 1.6

The same mass transport coefficient can also be obtained from the Mahon and Oldham equation. However the time term expression $f(t)$ differs and it includes two terms as follows

8

$$f(t) = \begin{cases} \dfrac{1}{\sqrt{\pi\theta}} + \sqrt{\dfrac{\theta}{4\pi}} - \dfrac{3\theta}{25} + \dfrac{3\theta^{3/2}}{226}, \theta \leq 1.281 \\ \dfrac{4}{\pi} + \dfrac{8}{\sqrt{\pi^5\theta}} + \dfrac{25\theta^{-3/2}}{2792} - \dfrac{\theta^{-5/2}}{3380} - \dfrac{\theta^{-7/2}}{4500}, \theta \geq 1.281 \end{cases}$$

Equation 1.7

Where $\qquad \theta = \dfrac{Dt}{a^2}$

In the potential step experiment the mass transfer coefficient at short time tends towards that of planar electrode and

$$k_m = \sqrt{\dfrac{D}{\pi t}}$$

Equation 1.8

While at long times, a hemispherical diffusion field occurs at the microdisc electrode surface. Here, the rate of mass transfer is still high at small microdisc electrode. The diffusion controlled current measured in the steady state condition is given by.

$$i_{ss} = 4nFDc^\infty a$$

Equation 1.9

As the $f(t)$ expressions tend to 1 when time goes to infinity. In this case, the steady state mass transfer coefficient, k_m can be calculated using the following equation

$$k_m = \dfrac{4D}{\pi a}$$

Equation 1.10

As the present work describes transient studies at different time scales at microdisc electrodes, some pulse techniques were used for this investigation which will be briefly reviewed in subsequent sections of the introduction.

1.3 Oxygen Reduction Reaction

The literature concerning ORR is very rich. This is mainly due to some basic interest in some areas such as fuel cells, energy sources and the chlor-alkali industry, where ORR can be used instead of the hydrogen evolution reaction. Extensive reviews in various fields, corrosion, fuel

cell, batteries and sensors have been published. Corrosion studies also consider ORR as a basic reaction that is coupled with the dissolution or passivation of a metal. This reaction takes place at the cathode. In this section, some fundamental issues related to O_2 sensor (measurement in unbuffered chloride containing solutions on Pt and Au microelectrodes) are discussed.

1.3.1 Mechanism of ORR and kinetics of the cathodic reduction of oxygen

The mechanism for the electrochemical reduction of oxygen has been extensively studied at various electrode materials over a wide range of solution conditions [10, 22-24]. The mechanism is complicated and has been found to be dependent on solution pH, electrode material, and mass transport rate. The oxygen reduction reaction is a multi-electron reaction that may have a number of elementary steps involving different reaction intermediates and there has been some debate over that. A modified Wroblowa *et al.* scheme has been demonstrated to be the most effective one to describe the complicated reaction pathway of O_2 reduction at metal surfaces among the different proposed schemes [25]. The mechanism suggested by Wroblowa [26] is shown below (Scheme 1.1).

This model does not allow us to predict which reaction pathway dominates at different timescales. Hence it is not possible to predict how the apparent number of electron depends on time.
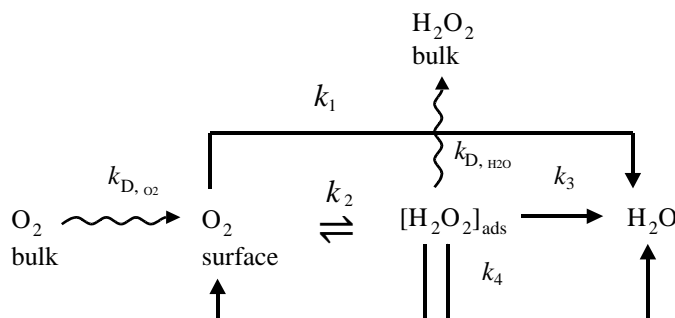
Scheme 1.1 Mechanism suggested by Wroblowa for oxygen reduction. O_2 can be electrochemically reduced either directly to water without intermediate formation of $H_2O_{2(ad)}$ (direct 4e[-] reduction) with the rate constant as depicted (k_1), or to $H_2O_{2(ad)}$ (2e[-] reduction) as represented by (k_2). The adsorbed peroxide can be electrochemically reduced to water with the rate constant (k_3) (2e[-] pathway), catalytically (chemically) decomposed on the electrode surface (k_4) or desorbed into the bulk of the solution ($k_{D,H2O}$) [25-26].

1.3.1.1 Electrode materials effect

The electrochemical reactions of oxygen are influenced by the nature of the cathode materials. On the basis of the pathways of ORR noted above, two main electrode materials categories can be recognised as indicated in Table1.1: those that promote the 2e- reduction pathway to peroxide and those that promote the 4e- reduction pathway to water.

Table 1.1 Electrode materials and reaction pathways for oxygen reduction.

Reaction Pathway	Electrode Material
Four-electron	
	Platinum group metals
	Other metals: Ag
	Oxides: Pyrochlores (e.g., lead ruthenate)
Two-electron	
	Graphite
	Metals: Au, Hg, most oxide-covered metals(e.g., Ni, Co)
	Oxides: most transition metal oxides(e.g., NiO, spinels)

On Au electrodes, two waves for ORR were recorded. The first one is a well-defined wave which corresponds to the reaction ($O_2 + 2e^- \rightarrow H_2O_2$) while the second is a poorly defined and potential independent wave, which suggests a chemical step for decomposition of H_2O_2 to take place. The mechanism proposed is as follows:

$$H_2O_2 \rightarrow 2\ OH^{\bullet} \qquad\qquad \text{Equation 1.11}$$

or

$$H_2O_2 \rightarrow H_2O + O^{\bullet} \qquad\qquad \text{Equation 1.12}$$

$$O^{\bullet} + H_2O_2 + e^- \rightarrow OH^{\bullet} + OH^- \qquad\qquad \text{Equation 1.13}$$

and it is followed by a charge transfer step

$$OH^{\bullet} + e^- \rightarrow OH^- \qquad\qquad \text{Equation 1.14}$$

Using Pt electrodes, the reaction proceeds through 4e$^-$ transfer. The exact role of the platinum electrode surface in the mechanism for oxygen reduction is uncertain [11-12, 27]. Some other

alternatives have been used. Metal alloys have shown the most promise towards ORR. Pt/Pd (111), however, shows superior and higher catalytic activity compared with bare Pt electrode. This higher activity of the alloy Pt/ Pd is associated with the reduced OH coverage, thus the binding energy of OH is weaker on Pt/Pd (111) than on Pt (111). Also this alloy exhibits the lowest current for H_2O_2 oxidation [28].

The use of different electrode designs for ORR can be exploited. Huang et *al.* developed a dual disc microelectrode which has interelectrode gap widths of 5 to 48 μm for the measurement of the electron transfer number n_{app} of dioxygen reduction. This electrode benefits from generation-collection properties. They found that the reduction of dioxygen is dominated by a four-electron reaction on bare platinum electrode [29].

The binding of molecular oxygen to the metal atoms on the electrode surface, can determine whether the overall reduction reaction will follow the four-electron or the two electron pathway. Three suggested binding modes are illustrated in Figure 1.4. From molecular orbital representations, it can be seen that with the Griffith and bridge-type interactions, the two atoms of an O$_2$ molecule form M-O bonds. Therefore, they favour the dissociation of O$_2$ resulting in the direct four electron process.
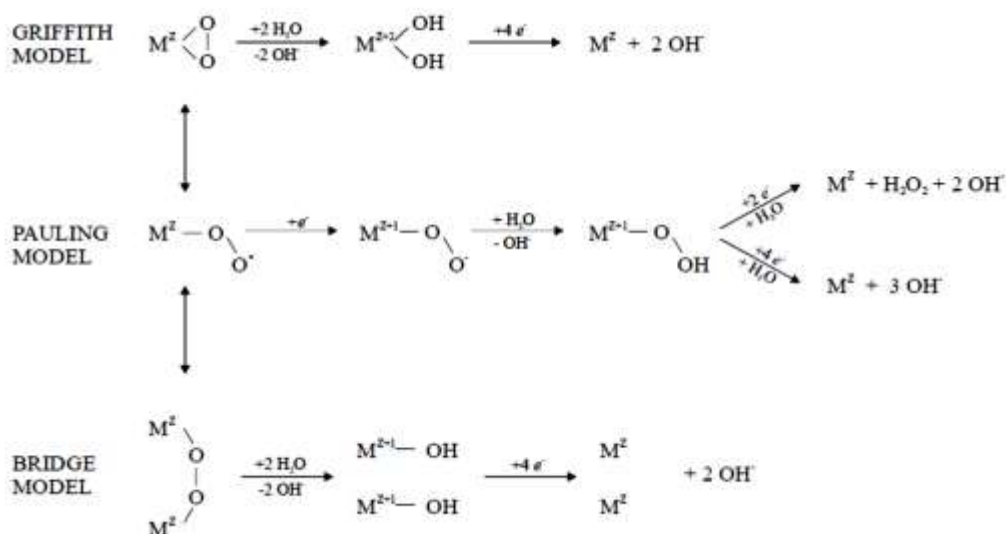

Figure 1.4 Representations of the types of interactions of molecular oxygen with metal atoms.

There are some approaches to change the kinetics of ORR. One of them is the modification of the cathode materials. There are many investigations with nanostructured Pt microelectrodes, where the increase in the active area for the reaction promotes the increase in the activity for the electrode towards ORR. It has been reported, that Pt mesoporous modified microelectrodes have significantly altered oxygen reduction kinetics when compared to polished platinum microelectrodes of the same dimensions within the same solution [30-32]. Another investigation on ORR was the comparison between Pt electrodeposited using a mixture of Brij 56 and n-heptane and Pt deposited without structure-directing additives. Oxygen reduction experiments revealed a threefold increase in catalytic activity due to templating [33].

Basically, three main issues regarding the presented work will be discussed in details; along with their consequences on ORR pathway, their influence on the position of the wave and on the recorded response.

- pH
- adsorption of chloride
- adsorption of other species
- Mass transport conditions

1.3.1.2 pH effect

Enormous and rich literature has dealt with acidic and alkaline media for fuel cell development purpose. However, ORR in neutral unbuffered solutions is seldom available. Some work was published for ORR on Ni [34], Fe [35], Cu [36], Ag [12] and Au [37] electrodes in neutral solutions. An understanding of the mechanism of different electrochemical processes is therefore possible only if account is taken of the state of the Pt electrode surface which is strongly affected by oxide formation and reduction, H adsorption and also anion adsorption [38]. Yang and Denuault were able to observe the changes in pH, using Scanning Electrochemical Microscopy (SECM) technique in acidic media. They concluded that an increase in pH accompanied the adsorption of hydrogen and oxide reduction processes while oxide formation and hydrogen desorption contributed in creating an acidic environment [38].

The chemical environment significantly influences the ORR. Pletcher and Sotiropoulos investigated *i-E* relationship for the reduction of oxygen at Pt, Ag and Au microdiscs in purified water and other media of low ionic strength and identified the effects of pH changes at the cathode

surface in unbuffered neutral solutions [37, 39]. In neutral solution, an alteration in $E_{3/4} - E_{1/4}$ was observed, and it was attributed to the local build-up of the reaction products (OH$^-$).

It was also observed by Pletcher and Sotiropoulos that there are two waves corresponding to ORR on Au microelectrode in unbuffered chloride solution. The first one is ascribed to the first 2e$^-$ reduction step and the second for 4 e$^-$ transfer. Interestingly, the separation between the two waves was much greater than reported in the literature for buffered media [40].

Since the response at the electrode can be affected by the presence of anions, previous investigations of the effect of adsorption at noble metals is reviewed in the next section.

1.3.1.3 Adsorption of anions

A large body of work has been devoted to the investigation of adsorption of ions on the electrodes. Pt and Au electrochemistry are affected significantly by the purity of the electrolyte under study, the distilled water quality for aqueous solutions preparation and the cleanliness of the glassware used. A selection of works reporting different detection methods of the adsorbed ions on Pt and Au electrodes is shown in Table 1.2.

There are numerous works directed towards addressing or assessing the influence of the surface structure on the electrocatalysis process [41-43]. Anion adsorption at electrodes has been an interesting subject for many researchers, in particular, its influence on the structure of the double-layer and electrode kinetics. The degree of anion adsorption on the electrode surface varies. Two categories of adsorption can be classified.

- Non Specific Adsorption (e.g F$^-$, ClO$_4^-$, OH$^-$)

An interesting study was conducted to assess the adsorption of various ions on Pt electrodeposited on Au quartz in EQCM experiments. It was concluded that the mass incorporations in the double layer region and H$_{UPD}$ (Under Potential Deposition) regions were associated to adsorption of the corresponding hydrated anions, i.e., ClO$_4^-$.2H$_2$O, HSO$_4^-$.2H$_2$O, HPO$_4^{2-}$ and Cl$^-$·6H$_2$O. Calculated anion coverage values varied from 7 (perchlorate) to 19% (phosphate) on the Pt surface [44].

- Specific Adsorption (e.g Cl$^-$, Br$^-$, SO$_4^{2-}$)

This phenomenon has some consequences: those associated with electrostatic interactions with charged electrode surfaces and those related to chemisorption (so-called 'specific adsorption') associated with localized charge redistribution [45-46]. Only chloride adsorption will be investigated in details. A list of detection methods for chloride adsorption on Pt and Au electrodes is presented in Table 1.3.

Table 1.2 Comparison of literature investigation methods for detection of adsorbing ions.

Adsorbing Ion	Electrode Material	Method of detection	Reference
Perchlorate adsorption			
ClO_4^-	Pt	RRDE	[44]
	Au(111)	EQCM	[47]
Chloride adsorption			
Cl^-	Au(111)	EQCM	[48]
		STM	
		SXS*	
Bisulphate adsorption			
HSO_4^-	Pt	FT-IR	[47]
	Pt	UHV (Ultrahigh vacuum)	[49]
Bromide adsorption			
Br^-	Pt	EQCM	[45, 48]
	Au(111)	EQCM	[48]
Phosphate adsorption			
PO_4^{3-}	Pt	FT-IR	
	Pt	Multipulse Potentiodynamic	[50]

*Surface X-ray Scattering

Table 1.3 Comparison of literature investigation methods for adsorption of chloride detection on Pt electrode.

Adsorbing Ion	Electrode Material	Method of detection	Reference
Chloride adsorption			
	Pt	tracer technique	[51]
		RRDE	
		nanogravimetry	[45]
		ellipsometry	[52]
		CO displacement method	[53]
		In Situ Surface scattering	[54]
		Multipulse Potentiodynamic	[50]

Since this work was carried out mostly in chloride solutions, the following sections will detail previous studies regarding the effect of chloride on the ORR and the features of Pt in different electrolytes. Hence, the adsorption of chloride on the electrode materials will be reviewed.

1.3.1.4 The effect of chloride on various electrode materials: specific adsorption

The effect of halide on Au and Pt especially has been addressed for long times. It was shown by different investigators that anions adsorption on Pt and Au is sensitive to surface structure and electrode pretreatment. This section focuses on the effect of adsorption on the response of the electrode.

1.3.1.4.1 Platinum electrode

The phenomenon of adsorption of chloride has been studied by different techniques (Table 1.3). The dependency of adsorption of chloride on potential and pH has been confirmed by several researchers. There is also a strong tendency of halide ions to be specifically adsorbed on platinum as demonstrated by several workers. It was found, using tracer method that Cl^- adsorbs on Pt in the whole potential window: from H_2 evolution till Cl_2 evolution [55]. The same observation was made, by combination of EQCM with cyclic voltammetry indicating Cl_2 evolution when the concentration of Cl^- exceeded 10^{-1} M [45].

Additionally, there were three characteristic regions of Cl coverage relative to the potential on single crystal Pt electrodes: double layer region, a region where Cl_{ads} is displaced by OH_{ads} and a region of co-adsorption of Cl and hydrogen [56]. Significantly, with help of impedance spectroscopy, an estimation of a monolayer coverage of Cl^- on Pt electrode was found when chloride bulk concentration is 0.01 M, indicating the strong effect of halide ions on the capacitance of the double layer on Pt electrode [57]. A similar observation was made, using EQCM. An extension in the double layer region towards the positive going scan in sulphuric acid was observed. It was also reported that a decrease in the oxide reduction peak was observed when the concentration of Cl^- increases (ppm levels) which also promotes a narrower H_{UPD} peaks [58]. The presence of chloride even at the nanomolar concentration, e.g., arising from electrolyte leakage from the reference electrode, makes the oxide monolayer formation ill-defined, shifts the hydrogen adsorption/desorption potentials and causes the double layer region [59] to either be

significantly diminished or totally absent. Significantly, it was reported that the addition of chloride to sulphuric acid medium results in inhibition of strongly adsorbed hydrogen [60].

Interestingly, passivation of platinum electrode in aqueous NaCl is also well studied and it is attributed to formation of the oxide film. However, the chloride ions can retard the film formation. Obrucheva observed that when HCl was added to sulphuric acid, the extent of anodization was significantly reduced at the same anodic potential. The inhibition is attributed to competition between specifically adsorbed chloride ions and oxygen [57]. In the presence of NaCl, chloride ions compete with water molecules to occupy the electrode surface. Kuhn and Wright have also shown that in the presence of NaCl, the oxide film grows in two stages with increasing potential. The first stage is the formation of PtO. This occurs at lower potentials. The second involves formation of PtO_2 at higher potential [57]. Presence of chloride also promotes the blockage of O species coverage at the Pt surface. Some investigators suggested that there is a competitive adsorption between Cl and OH, in some studies of the effect of the adsorption on Pt single crystal [56].

Using ICP-MS, AFM and EQCM, revealed that Pt dissolves in chloride solutions in ppm concentration level [58]. A complete change in recorded H_2SO_4 CV features was observed, when 100 and 1000 ppm of Cl⁻ was added. In addition, a massive mass change was observed. This behaviour is attributed to the formation of chloride complexes ($PtCl_4^{2-}$ and $PtCl_6^{2-}$) in oxide formation region, according to Equations 1.15 and 1.16. Additionally, the contribution of Cl⁻ adsorption is ascribed and accounts for the mass change in H_{UPD} (Under Potential Deposition) region [58].

$$Pt + 4Cl^- \rightarrow PtCl_4^{2-} + 2e^- \qquad\qquad\qquad \text{Equation 1.15}$$

$$Pt + 6Cl^- \rightarrow PtCl_6^{2-} + 4e^- \qquad\qquad\qquad \text{Equation 1.16}$$

There is also the probability of Pt etching but this normally requires large potential excursions [61].

More recently, it has been demonstrated that the Cl⁻ contamination, even in trace levels influences the degradation of the fuel cell performance. With help of Electrochemical Impedance Spectroscopy (EIS) technique, the findings indicated an increase in both the charge (electron)

transfer and mass transfer resistances on the cathode side as a result of chloride contamination, and the cell performance loss is attributed to an increase in charge (electron) transfer resistance [62].

1.3.1.4.1.1   Influence of chloride on ORR at Platinum electrode

The electrochemistry of oxygen in presence of chloride was explored by several investigators and some limitations of ORR have been reported. The oxygen molecule adsorption can be inhibited by the chloride ion adsorption, and the rate of ORR decreases as the concentration of chloride ions increases [63]. Electrochemical Impedance Spectroscopy (EIS) and Rotating Disc Electrode (RDE) voltammetry investigations also supported the previous observation in terms of inhibition of oxygen molecule adsorption by the chloride ion adsorption [63]. To assess the effects of Cl^- and other atmospheric trace species on ORR, Imabayashi *et al*. reported the role of Cl_{ad} as a site blocking species on the Pt surface. It leads to a decrease in the catalyst activity towards the ORR by reducing the surface sites available for breaking O–O bond, which in turn results in enhancement of H_2O_2 intermediate [64] . A similar study by Schmidt *et al*. with a rotating ring-disc electrode (RRDE), aiming to assess the effects of chloride adsorption on (ORR) arrived to the same conclusion [65] .

It was also found that the effect on the kinetic, particularly the value of k^0 decreases and the Tafel slope increases as the chloride ion concentration increases, which is consistent with the results of EIS that the R_t-O_2 (charge transfer resistance) increases as the chloride ion concentration increases. This result further proves that the ORR is inhibited by the presence of chloride ion.

Another study was conducted to observe the role of chloride on the inhibition of H_2O_2 oxidation at Pt electrode. It was found that in case of saline solutions, there is a possible inhibition of the decomposition of H_2O_2 due to chloride adsorption on Pt. The investigators pointed out that the presence of chloride can lead to a marked decrease in the rate of the oxidation due to formation of platinum chloride complex film on the surface [58].

Additionally, the ORR wave in NaCl shifted cathodically relative to $NaClO_4$ in the pH range 8-10, suggesting the adsorption of Cl^- ion on Pt electrode. The latter solution exhibits an inhibiting effect by chloride, which inhibits Pt-OH formation. Moreover, Kaska *et al*. concluded that the rate determining step for ORR is the first electron transfer in presence or absence of chloride [51].

1.3.1.4.2 Gold electrode

Gold was also used as a cathode material for ORR investigation in some studies. Sosna *et al.* observed the effect of chloride on the dissolution of gold at more positive potentials [11] . They concluded that the dissolution of gold is in agreement with the thermodynamic model of gold-chloride-water system [66]. The resulting product is $AuCl_4^-$. The dissolution of Au in Cl$^-$ containing solutions was also proved using EQCM and *in situ* STM [48].

1.3.1.4.2.1   Influence of chloride on ORR at Gold electrode

The investigation of ORR on Au suggests that it proceeds via the sequential route. It was also revealed that the position of the ORR wave is affected by presence of adsorbing ions. There is a lack of data in the literature regarding ORR in saline electrolyte although Ref [12] illustrates some work in NaCl at Au microdisc.

1.3.2   Adsorption of other species

Apart from anions adsorption, other kinds of adsorption can be detected at the solid/liquid interface. The following sections concentrate on that together with the influence of other possible adsorbents on the electrochemical response in general and ORR in particular.

1.3.2.1 Water adsorption

It was revealed using EQCM study in solutions of $HClO_4$, H_2SO_4, H_3PO_4 and HCl that the change of mass is due to the adsorption of water molecules. A full monolayer of adsorbed water replacing the H_{UPD} atoms was observed in every case [44]. A similar observation was made by Shimazu and Kita [67], in which they used EQCM technique to detect mass changes due to water adsorption. They observed an increase in mass in the double layer and hydrogen potential region. Bokris and Reddy [68] also pointed out in their double layer model that the first layer at the interface at the electrode surface is water molecules. Another similar finding was demonstrated by Cordon and Johnson, showing an increase in mass. They suggested it could be ascribed from rearrangement of water molecules. However, surprisingly, water molecule was found to be expelled from the surface by adsorption of halide in another study [48]. Hence, there are still on-going attempts to identify the contribution of water molecules adsorption on the electrode behaviour.

1.3.2.2 Hydrogen-like species

There are some general behaviours for the effect of cations (e.g. hydrogen or another Under Potential Deposition (UPD) species like Cu) on the electrode surface. A modification of the

electrode surface was observed as a consequence of pH changes induced by those cations that affect the reactions in the electrolyte [69]. The effect of adsorbed hydrogen on Pt - EQCM response was studied by Wilde *et al*. They found that as the pH of the contacting electrolyte increases, large frequency changes at the surface of the electrode were recorded especially in the region of weakly adsorbed hydrogen occurrence [70].

Moreover, some observations were made on the role of H_{UPD} in inhibition of the kinetics of the ORR on Pt single crystal surfaces. Some studies have related that to the blocking of the pairs of platinum sites which are required for the O–O bond breaking when H_{UPD} is adsorbed onto the Pt (111) surface. It was found that there was a difference in the surface catalytic activity between the H_{UPD}-free surface and the surface fully covered with the H_{UPD} resulting in 4e$^-$ reduction for the former and a 2e$^-$ reduction for the latter [71]. Some studies have also revealed that the most pronounced effect of deactivation by the adsorbed hydrogen on O_2 reduction occurs in the order Pt(111), Pt(100) and Pt(110) respectively [72].

1.3.2.3 Oxygen-like species

The coverage with oxide on the electrode and its influence on the activity of the electrode has been well studied by many investigators. According to Johnson and Bruckenstein, the reduction of oxygen follows two mechanisms depending on whether the reduction takes place either on "clean" or "oxide-covered" platinum [73] (the mechanism is provided afterwards in the next paragraph). It is worth mentioning the effect of the surface coverage of chemisorbed oxide species in suppressing the kinetics of the ORR on a polycrystalline platinum electrode reported by Markovi *et al* [25]. Adsorbed oxygen and hydroxyl are considered to be stable intermediates at potentials close to ORR equilibrium according to a study by Nørskov *et al* study [74].

To highlight the effect of surface condition (when it is clean or oxide covered) on the inhibition of the kinetics of ORR, H_2O_2 catalytic decomposition can be considered at Pt electrode. The mechanism for H_2O_2 decomposition can be an electrochemical step on an oxide free electrode, according to Gerischer [75] in the following reaction and it is favourable as the free energy = -210 kJ mol^{-1}.
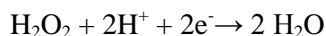
$H_2O_2 + 2H^+ + 2e^- \rightarrow 2\ H_2O$ 	Equation 1.17

or according to Bianchi *et al.* [76] it undergoes a chemical step on oxide covered electrode

$$2\ H_2O_2 \rightarrow 2\ H_2O + O_2 \hspace{4cm} \text{Equation 1.18}$$

Additionally, in another EQCM study, Jun Omura *et al* were able to detect a reversible mass change for one or more adsorbed oxygen species on Pt, within O_2 saturated and Helium-purged in two different electrolytes: HF and $HClO_4$ solutions [47]. The CV, EQCM and Auger Electron Spectroscopy) (AES) data show that the charge density, interfacial mass variation and intensity of the O-to-Pt signal ratio increase as the potential is raised towards positive potentials, indicating that the surface oxidation proceeds by a progressive coordination of O-containing species to the Pt substrate [77].

All the above investigations show that the Pt and Au surface electrochemistry is highly affected by the experimental conditions (electrolyte type, concentration and pH), in particular when employing them as ORR cathode materials. That was taken into account for the investigations in this work.

Electrode contamination also arises from adsorption of impurities from the bulk electrolyte. One can suspect that the contamination problem would be severe on a bare electrode. Due to the lack of a membrane, therefore, an electrochemical cleaning to desorb those impurities should be tried. Indeed, every electrode has a past history of use that affects its performance [73]. Therefore, every electrode needs to be first pretreated in order to make it ready for the electrochemical measurement. Studies of the best conditions for pretreatment of noble metals have constituted a major area in electrochemical surface science. It has been reported that appropriate pretreatment of the electrode is of great importance to produce a mass transfer controlled current for the reduction of oxygen at platinum electrodes. Variation in the oxygen reduction current can be attributed to one or more reasons such as some changes in the Pt surface structure, chemisorption of oxygen, an adsorption of anions and/or cations and adsorption of organic materials [78]. The loss of noble metal activity is commonly attributed to "fouling" of electrode surfaces by adsorbed organic reactants and/or reaction products, as well as the formation of surface oxides at large, positive potential values, therefore, maintaining a uniform and reproducible electrode activity is essential. Some suggestions have been to apply pulsed amperometric detection (PAD) which is based on multistep potential waveforms, which incorporate amperometric detection with alternated anodic and cathodic polarizations to clean and reactivate the electrode surface. This

method makes it possible to obtain predictable and renewable electrode surfaces without polishing [2, 5, 69, 79]. Sosna used PAD to achieve the reproducibility of the DO sensor response [11]. There are some benefits for the application of electrochemical methods to activate electrocatalysts for oxygen reduction. The removal of adsorbed impurities from the electrode surface could be achieved. Moreover these treatments can lead to the modification of electrode surface or in other words the change of the surface composition. The next subsection illustrates the rates of mass transport on ORR mechanism.

1.4 Mass transport rate effects

Mass transport conditions are also another contributing factor to the overall ORR. More details on the major effects on ORR mechanism will be presented in the following subsections.

The effect of the mass transfer coefficient of reactant and product species during the oxygen reduction reaction, ORR, on platinum in different media has been the subject of research for many years and has been experimentally examined and kinetically modeled. The enhancement of mass transport can be achieved either under steady state conditions or transient conditions. A list of works reporting the rate of mass transport on the ORR is presented in Table 1.4.

Table 1.4 Studies where the role of mass transport on ORR was investigated.

Electrode Material	Method of enhancement	Reference
Steady State conditions		
Pt	RDE	[39, 80]
Pt /C	single submicrometer-sized	[80]
Pt	various sizes of microelectrodes	[11]
(array of platinised carbon fibres)	recessed electrode	[81]
Pt & Au	recessed microelectrode	[82]
Transient Conditions		
Au	flow rates	[83]
Pt, H_1-ePt*	Vibration	[11]
Pt & Au	time dependence potential steps	This work

*Hexagonal electrodeposited platinum

1.4.1 Steady state responses

Enhanced mass transport conditions have some important consequences for the ORR pathway and final products of the reaction. The great dependence of mass transfer coefficient on electrode radius, as defined in Equation 1.10, allows examining the effect of mass transport on the ORR using different experimental techniques such as shown in the study conducted by Chen and Kucernak to investigate the dependence of n_{app} on mass transfer coefficients using submicrometer sized electrodeposited Pt single particles [80]. Those very small electrodes (down to several tens of nanometers) were advantageous in allowing the extension of the range of mass transfer studied to high values, which are inaccessible to conventional microdisc electrodes. The authors kinetically modeled the experimental data using analytically derived expressions. Hence, they demonstrated that at the smallest of these Pt particles, mass transport coefficients equivalent to a rotating disc electrode at rotation rates (ω) greater than 10^8 rpm are obtainable [80]. Similar trend of the dependence of the enhancement of k_m on the size of the electrode and rotation rates of RDE was also demonstrated by Pletcher and Sotiropoulos [39]. The n_{app} was found to decrease smoothly with increasing rotation rates when using the RDE or the microelectrodes with smaller size [39]. The two electron reduction to hydrogen peroxide becomes more important with increasing rate of mass transport (higher rotation rates for RDE and smaller microelectrodes radii) and results in the decrease of the n_{app}. This proves not only that the series pathway of the ORR takes place, but also that its contribution to the overall mechanism is increasing under high mass transport regimes.

Importantly, it was observed that when increasing the mass transfer coefficient the ORR voltammetric waves tend to shift to more negative potentials indicating the increased irreversibility of oxygen reduction. This was observed not only on Pt but also on Au and Ag microelectrodes [102]. Rapid transport of oxygen reduction products (OH$^-$) away from the electrode also minimises any localised pH changes which could influence the reaction. Sosna arrived to the same conclusion regarding the decrease in microelectrode size which promotes higher rates of steady state the mass transport [11].

Steady state measurements of ORR can be affected by convection. Convection effects can be minimised by decreasing the electrode size, thus microelectrodes are common choice when developing new DO sensors. However, even the response of micrometer size electrodes is affected

at high flow rates (e.g. a conductivity-temperature-depth probe, CTD, falls at ~ 1 ms^{-1}). Higher immunity to convection can be achieved by placing the electrode in a recess [84]. Morita and Shimizu [81] designed a sensor with an array of platinised carbon fibres as working cathode. Each carbon fibre (diameter 4 –7 μm) was at the bottom of a recess. The authors reported much lower sensitivity to flow compared to an inlaid microdisc: at a flow rate of 50 cm s^{-1}. Sensors based on the microhole cathode were later tested on a CTD profiler [54]. This sensor is moderately flow-rate-insensitive and less susceptible to poisons. Recessed electrodes were also employed by other research groups. Braun *et al*. used recessed microelectrodes to investigate tumour and normal tissue oxygenation [82]. Other investigators, Rychen *et al.* demonstrated the ability to reduce flow dependence of recessed gold microdiscs array for monitoring oxygen in sewage water environment [85]. Another deep ocean sensor with recessed electrode was implemented. Atkinson *et al.* [86] came up with a potentiostatic oxygen sensor with recessed cathodes that have different response times; 10-100 fold faster than membrane sensors. However, their relatively long turn-on transient compared to membrane sensor is one of their difficulties found. Another issue is the slow long-term downward drift of the current output.

Other applications involve the modification of a Clark-type oxygen microelectrode. Its use in the aquatic sciences was preceded by measurements with Au-plated Pt microelectrode with a recessed tip and resin coating [10]. The Needle-type DO microelectrode array sensor exhibits fast response times and high sensitivity and was successfully applied to evaluate DO microprofiles in a multi-species aerobic bacterial film [87].

In the work reported by Sosna [11], linearity between i_{lim} and DO concentration was achieved. Stability tests were also successful over a long period of time for oceanographic use. Since then, some trials on eliminating convection, caused by flow, have been carried out. A stop-flow pump system can be used but it leads to power consumption as well as increasing the size of the microelectrodes. A non-steady state sensor could achieve vast improvements in spatial resolution when profiling the water column. The next section will highlight the documented work in enhancement of mass transport under non-steady state conditions.

1.4.2 Non- Steady state responses

Early work on the velocity sensitivity or stirring effect of polarographic oxygen microelectrodes was reported by Gust *et al* [88]. Similarly Sosna *et al*. [89] observed the dependence of the limiting current on flow rate and microdisc radius. The fast measurements should produce thinner diffusion layers and thus offer significantly smaller flow sensitivity than steady state measurements but this has not been proven yet. Furthermore, some successful attempts were done by Atkinson *et al*. in designing a CTDO (Conductivity Temperature Depth Oxygen Probe) sensor, which is insensitive to flow [83]. The vibration of the electrodes in the bulk solution and in the vicinity of an insulating surface can create controlled forced convection; this approach was tried by Sosna [11].

Sosna [11] also carried out a preliminary investigation of transient determination of DO. The first results, using double potential steps, were promising. He performed transient measurements with the potential step durations down to 1 ms. The approach was shown to be capable of quantitative determination of dissolved oxygen.

The present work allows insight into the dependence of mass transport coefficient and n_{app} on the time scale of the experiment, using potential step techniques and other transient techniques. It is expected that the number of electrons involved will be 2 if the reaction ends with the formation of hydrogen peroxide or 4 if there is complete reduction to hydroxyl ions [90] and that this should depend on the time dependent mass transfer coefficient by analogy with the observed dependence of n_{app} on the steady state mass transfer coefficient.

1.5 Determination of DO

  The three main methods for determining DO concentrations in marine fields will be presented in this section: optical, chemical and electrochemical, followed by a detailed review of the sensor structure along with its advantages and drawbacks.

1.5.1   Optical methods for detection of O_2

DO can be detected optically with optodes based on luminescence quenching. The basic principle depends on the use of molecules able to absorb light and form excited states and then emit the absorbed energy in the form of luminescence. Interestingly, those molecules have specific luminescence time (excited state lifetime or the decay time of luminescence).

1.5.2   Chemical determination of O_2

The Winkler titration [91] is well known to be the most accurate method of determination of dissolved oxygen concentration. In principle, it depends on adding manganese (II) salt to the sample, followed by alkalisation of the solution. That in turn leads to precipitation of manganese (II) hydroxide and reduction of molecular oxygen. An acidified iodide solution is then added to facilitate iodide oxidation by Mn(III) species and as a consequence iodine is liberated. The iodine is then titrated with thiosulphate ion (iodometric method).

It should be mentioned that some drawbacks for this method are reported. The laboriousness and use of chemical reagents are two main issues, indicating unsuitability of this method for *in situ* analysis as well as inability to measure oxygen on a continuous basis. Hence, samples are collected on board to be sent for analysis, using automated Winkler titration. However, to minimise artefacts during sampling *in situ* measurement should be performed in marine environment.

1.5.3   Applications of electrodes to electrochemical sensing of DO
1.5.3.1   Membrane covered cathode sensor

A Clark oxygen probe involves a metallic sensing cathode covered with an oxygen permeable membrane which surrounding entraps a thin layer of internal electrolyte. A schematic representation of a Clark type sensor is shown in Figure 1.5. At present, most commercially available electrochemical oxygen sensors are based on Clark type design. Several designs of Clark type sensors have been constructed. They usually differ in reference and counter electrodes used, depending on their applications. Also, there are varieties of cathode materials with different sizes ranging from macro to micro scales and even a needle type sensor has been reported. The latter offers sub-second response times, despite employing a membrane [92-93].
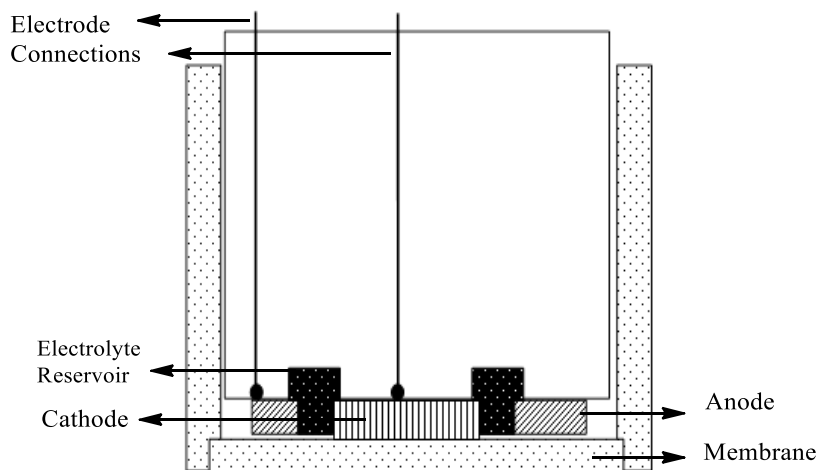
Figure 1.5 Schematic illustration of Clark sensor design.

The use of the internal electrolyte is advantageous. It provides sufficient conductivity between the electrodes but must be appropriate for the anodic reaction. For example, when using an Ag/AgCl anode, a chosen internal electrolyte is concentrated chloride salt solutions whereas alkaline electrolytes are employed for metal/metal oxide type anodes. It should be stressed that the choice of internal electrolyte can be critical in insuring no interference with the membrane and no effect on the electrode reactions. However, some problems can be encountered such as losses of internal electrolyte due to diffusion through the membrane. This can be minimised by incorporating a sufficiently large internal electrolyte reservoir in the sensor body.

There have been some developments in Clark sensor design to have 3-electrode system [94] or even 4-electrode system with two working electrodes. One working electrode functions as the sensing part for O_2 that undergoes reduction while the other consumes O_2 diffusing from the back of the electrode.

Another challenge comes from variations in the internal electrolyte pH. As a result of continuous operation the concentration of hydroxide generated on the cathode will build up and increase the pH of the internal electrolyte, thus resulting in a shift of the ORR wave and subsequently an alteration of the recorded reduction current. This in turn limits the sensor lifetime. It has to be stressed that the overall current response has a contribution from the background DO present in the internal electrolyte. However, polarising the cathode for sufficiently long times before taking

27

the measurements is efficient in reducing this effect. As an alternative, an additional electrode, called guard cathode with large surface area plays a key role in depleting DO [95].

The membrane serves as a permeable part to protect the cathode from any fouling agents, resulting in enhanced selectivity of the probe towards oxygen. Very reproducible mass transport conditions were achieved in the recorded current due to the diffusion of oxygen within the layer of internal electrolyte and the membrane thickness. This in turn resulted in a response that is less susceptible to external flow. Indeed, some criteria such as membrane thickness which determine diffusivity and solubility of O_2 should be met in constructing a sensitive and fast response sensor. Some typical membrane materials are made of hydrophobic polymers, e.g. polyethylene, Mylar, silicone rubber, halogenated hydrocarbons: polytetrafluoroethylene (PTFE), polyvinyl chloride (PVC), with thicknesses down to fractions of a micrometer [96].

On the other hand, there are some serious effects related to the permeability of the membrane which decreases with pressure and temperature, when employed in ocean or other environments; in most cases the diffusivity of oxygen within the membrane is strongly affected [94, 97]. In oceanography, the apparent hysteresis between upcast and downcast is caused by response-time mismatch of the compensation temperature sensor to the time characteristic of the DO sensor's inherent temperature dependency. All of these drawbacks lead to slow response. It was found that increased pressure causes very significant signal losses when measurements are performed at large depths (up to 50% signal loss at pressure corresponding to the depth of 5000 m). To overcome this problem, oceanographers have to take bottle samples for every cast and analyse these with standard laboratory methods such as Winkler titration on board the research vessel to obtain calibration points for the measured oxygen profiles [89, 98].

The Clark-type electrode also exhibits age effects. As a consequence, the electrode becomes blocked and its reliability is compromised. Therefore, a routine conditioning or membrane replacement is common [27]. Additionally, other errors are caused by impairment of the silver anode, plating of anode metal on the cathode, and the presence of chemical contaminants in the sensor's plastic body. It is still of great importance to design a reliable sensor that produces a stable, accurate response under extreme pressures in deep oceans.

As a result of the above mentioned problems, there is a need to replace the sensor regularly. There is a strong renewed demand for accurate, durable and low maintenance marine DO sensors. Some

key factors for a new sensor design are working longevity, physical dimensions, and energy consumption. Such constraints come from the different platforms, e.g. CTD or fixed rigs, on which the DO sensors are installed.

1.5.3.2 Bare cathode sensor

Some striking consequences were recorded when removing the membrane. There is an improvement in the response time of the sensor as oxygen does not have to diffuse through the membrane. The dependence of the sensor response on temperature and pressure originates only from the changes in the value of the oxygen diffusion coefficient. A bare cathode sensor is still sensitive to temperature variations because the diffusion coefficient of O_2 in the solution is a function of temperature but the sensor is much less sensitive to pressure variations because the diffusion coefficient has a weak dependence on pressure. However, the sensitivity of the response to external flow and convective mass transport becomes severe. Additionally, the electrode is subjected to fouling due to the absence of internal electrolyte. Hence, the introduction of surface reconditioning procedures with bare electrode is required.

There is still a great deal of scientific difficulties hindering the development of such a reliable sensor. To address this problem, some attempts to design a waveform for preconditioning the electrode have been reported. In order to achieve a reproducible response and constant activity of the electrode surface towards oxygen reduction periodic electrochemical cleaning has been implemented. In case of platinum electrodes, the cleaning procedure involved cycling the potential between oxide formation and hydrogen evolution or stepping the potential to the oxide formation region.

Long-term stability is one of the targets. Minimizing drift and the effect of bio-fouling of the sensor has been achieved by the introduction of 'cleaning pulses' that also act as preconditioning for the microelectrode. This technique was introduced to clean the electrode surface, strip any metals that could be plated during the measuring step and to recondition the electrode for the next measurement to avoid drift due to fouling. Pletcher and Sotiropoulos developed a waveform which consists of a repetitive fast potential square wave to recondition the microelectrode surface as a short sweep and a long step for measuring the reduction of dissolved oxygen current [69]. A stable response over periods of 12 h and longer was recorded by Pletcher and Sotiropoulos, using microelectrodes. More interestingly, Preidel *et al*. were able to maintain a stable response for over 60 h in saline solutions by holding glassy carbon electrodes at potentials of 0 V *vs.* Ag/AgCl

between measuring steps at -1 V *vs.* Ag/AgCl [99]. By applying conditioning potential steps, the activity of mercury coated gold microelectrodes for voltammetry in seawater remained constant, as reported by Brendel and Luther [100]. Furthermore, Rychen reported the use of a boron-doped diamond (BDD) auxiliary electrode to periodically generate oxidising hydroxyl radicals to clean a gold microdisc array cathode [85].

Previous work towards the development of electrode cleaning procedure on steady state oxygen sensor was carried out by Sosna *et al.* They applied a preconditioning waveform, which consists of cleaning steps (1 s) and measuring (12 s) [23]. This is a square-type waveform, in which the potential is stepped from a value chosen to clean the electrode (removing any adsorbed species from the microelectrode) to a value chosen to reduce oxygen (to measure i_{lim}). It is very simple to produce, with amplitudes and durations easily modified. Although this waveform performed very well for steady state measurements it is expected to produce significant transient background faradaic current. This comes from the fact that the reduction of the oxide occurs simultaneously with the reduction of the dissolved oxygen. In the present work we report the development of a more complex waveform consisting of a series of potential excursions (steps or sweeps) in the oxide formation and hydrogen adsorption regions, a rest period to allow the oxygen concentration to recover and step to oxygen reduction region to record the transient current of interest. This will be discussed in details in chapters 4 and 5. We show that by using this waveform, the residual transient current is minimised, hence providing a more accurate derivation of the DO concentration.

1.6 Fast measuring techniques for ORR investigation

To date, there has been great success in the research into DO determination, using microelectrodes under the steady state conditions which produces linear correlations between i_{lim} and oxygen concentration. Steady state stability tests for DO sensor have also proved successful, indicating good performance for long-term oceanographic as shown by the results of the RRS Discovery transatlantic cruise D279 [11, 22].

The high rates of steady state mass transport are achievable without any problem of capacitance or oxide film reduction. This is one of the key advantages of steady state operations. In this work we are keen to explore the possibility of enhancing mass transport by working at short times and more importantly the possibly of reducing the diffusion layer thickness to minimise the effects of

convection on the amperometric response of O_2 reduction. However, in this case the issues of capacitance and transient response of adsorbed species need to be considered.

Some transient techniques have been used to investigate ORR, background processes effects and the capacitance of the electrode at fast measurements[101]. In order to design a fast response sensor to enhance mass transport of oxygen towards the electrode surface, one must take into account the transient faradaic response due to the formation/removal of oxide, adsorption/desorption of hydrogen and the involvement of other adsorbing species such as anions.

The ORR at Pt exhibits slow and complicated kinetic behaviour which it is still not fully understood. It was reported that in neutral and acidic solutions under enhanced mass transport (RDE and microelectrodes), the shape of the ORR becomes distorted [39]. This study also found that the ORR is irreversible at large sweep rates.

A range of transient electrochemical techniques is available. Four have been selected and are considered in the next sections.

1.7 Electrochemical Impedance Spectroscopy (EIS) study

This technique is based on time dependency (frequency) and is used to explore any redox couples reactions as well as adsorption/desorption phenomena at different timescales. Some groups have tried to use EIS to investigate the ORR. Since they have done this over a range of frequencies, then this is like exploring the ORR mechanism at different time scales.

The ORR is a complicated process involving many elementary reactions that may generate various intermediate reactive oxygen species and the adsorption of the anions strongly influences the electrode surface state [23]. An EIS equivalent circuit for ORR was proposed [63] and is shown in Figure 1.6. This study confirmed the inhibition effect of chloride ion on ORR on carbon steel electrode.
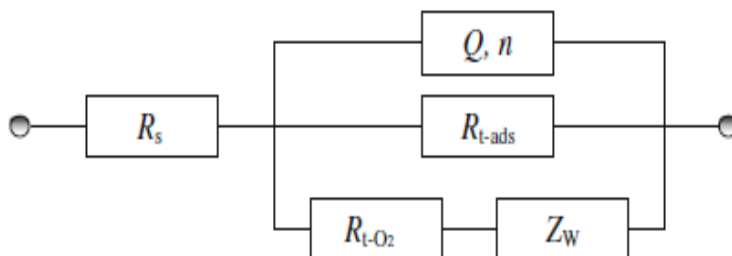
Figure 1.6 The schematic illustration of the equivalent circuit for ORR [63]. R_s is the solution resistance, R_{t-O2} is the electron transfer resistance, R_{t-ads} is the resistance for adsorption, Z_w is the Warburg impedance. Q,n is the constant phase element for the capacitive element.

To the best of our knowledge, there is no EIS study in the literature which compares the state of the polycrystalline Pt/electrolyte interface in the absence and presence of O_2. In neutral conditions indeed, there have been some studies on detecting and distinguishing different adsorbate structures, using EIS study. The first study, using potentiodynamic EIS together with numerical calculations, that compares the state of the Pt(111)/electrolyte interface in the absence and the presence of O_2 in 0.1 M $HClO_4$ was conducted by Bondarenko *et al*. [102]. Their findings rejected any co-adsorption of $ClO_4^{\cdot}$ and $Cl^{\cdot}$ with $OH^{\cdot}$.

Itagaki *et al*.[103] reported a comprehensive EIS study of ORR on Pt, Ag and GC in 0.1 M NaOH. In each case he compares experimental impedance diagrams to theoretical impedance values derived for the Wroblova ORR mechanisms. Significantly, he does not propose an equivalent circuit but uses different expressions depending on the reaction pathway considered.

Although EIS is a useful technique to explore the transient response, the interpretation of the results depends on the choice of an equivalent circuit. This is a difficult task and often the circuit has to rely on adjustable parameters such as the constant phase element. We have therefore made no attempt to use EIS for the ORR at microdisc electrodes.

1.8 Fast Scan Voltammetry (FSV) & chronoamperometry

When employing a fast (corresponding to miliseconds or microseconds range) measurement, there are three important considerations to take into account: the instrument bandwidth, ohmic drop, and charging current. All of these factors play a major role in acquiring accurate measurements.

It is of great importance for a current amplifier to offer a fast response with sufficient gain without distortion. In brief, the work presented here concentrates on fast measurements, where the condition for predominance of linear diffusion conditions is when $Dt/a^2<1$. Hence the timescales considered will range from 1 s down to sub milliseconds.

At short times we expect a significant contribution from the additional currents which originate from charging the double layer and surface-associated processes [1]. To obtain undistorted faradaic response in chronoamperometry or cyclic voltammetry, this extra current is typically subtracted after recording the data in presence and absence of the redox couple of interest.

The feasibility of cyclic voltammetry at ultramicroelectrodes in the submicrosecond domain in organic medium has also been reported by many researchers[3, 104-105] [106]. Amatore *et al.* were able to investigate the reduction of anthracene at scan rates, up to 100 kV s^{-1} [106]. Also, ferrocene oxidation on various electrode materials such as Au, Pt and Hg at scan rates 0.5, 2, 10 and 20 kV s^{-1} was elucidated by Wightman and Wipf [105, 107] and the same investigators were successful in recording the reduction of 9-fluorenone at a scan rate of 1 000 000 V s^{-1} [108]. Very fast scan rates up to several MV s^{-1} order was reported by two groups [109-110]. These investigations were done specifically to determine rate constants at different electrode materials.

There is a limited work carried out on Pt microelectrodes for transient investigations in aqueous medium presumably because oxide formation/reduction and hydrogen adsorption/desorption affect the faradaic response. Beriet *et al.* [111] investigated the ruthenium hexaammine system to determine its rate constant. The maximum scan rate used was 1000 V s^{-1}. They tried to investigate other systems such as ferrocyanide ion oxidation and the reduction of sodium hexachloroiridate (both are aqueous solutions), using Pt microelectrodes. The observation recorded was the increase of peak potential separation along with the increase of the scan rates. Similar work on ruthenium hexaammine reduction on Hg and Au was reported by Wightman [104]. The rest of the work found in the literature focuses on the use of either Hg microelectrodes or carbon fibre electrodes, in which the potential window can be widened. Most comment on the dominating effect of the surface processes at fast measurements.

Ohmic drop is another parameter which needs to be tackled in fast measurements. It can cause the potential at the working electrode, E_w, to differ from the applied potential, E_a according to the equation

$$E_w(t) = E_a(t) + i_t R_s \qquad\qquad\qquad \text{Equation 1.19}$$

where is i_t the total current. At large electrodes this is a major issue but this effect can be significantly reduced with microelectrodes. Nevertheless at very high scan rates it remains a non-negligible problem.

The following sections details other transient methods in which charging current (background current) can be reduced by applying a particular waveform.

1.9 Normal Pulse Voltammetry (NPV)

The principle of this technique consists in applying a sequence of potential steps of variable amplitude with a period at a fixed potential in between the steps (Figure 1.7). The fixed potential is called base potential E_{base} or E_{rest} (E_1) and it is chosen where there is no faradaic reaction occurring on the electrode surface. A short pulse of increasing amplitude is applied, and the current is measured at the end of each pulse. The pulse time and interval time between the pulses can be varied; typically a ratio of 1/10 is used.

This method provides insight on kinetic information by obtaining virtual steady state voltammograms at different pulse times. For experimental convenience, it is often preferred to run NPV as quickly as possible using pulses of short and equal duration to avoid contamination.
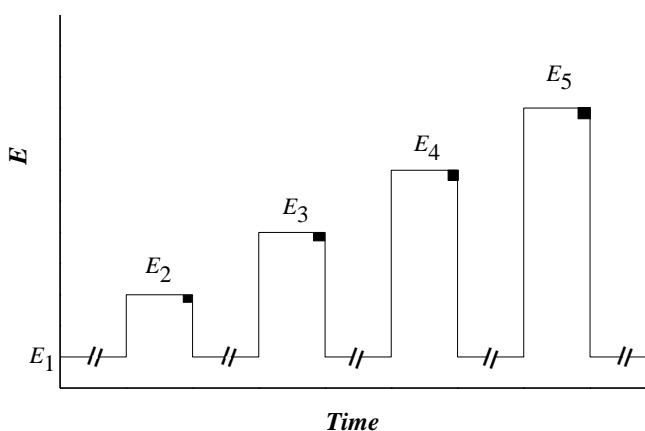
Figure 1.7 Waveform used in NPV. E_1 is the base or rest potential. Square dots show that the current is only measured at the end of the pulse time.

This technique has been used to study a range of reactions but it is not often used as differential methods, such as DPV, are better to discriminate between faradaic and background currents.

1.10 Sampled Current Voltammetry (SCV)

In this technique, series of potential step experiments are performed along the wave for reduction or oxidation of the system. The corresponding current transients are plotted and the current is sampled at fixed time (τ) to reconstruct sampled current voltammograms as shown in Figure 1.8. As in NPV, the obtained *i-E* curve has the shape of a steady-state voltammetric wave.
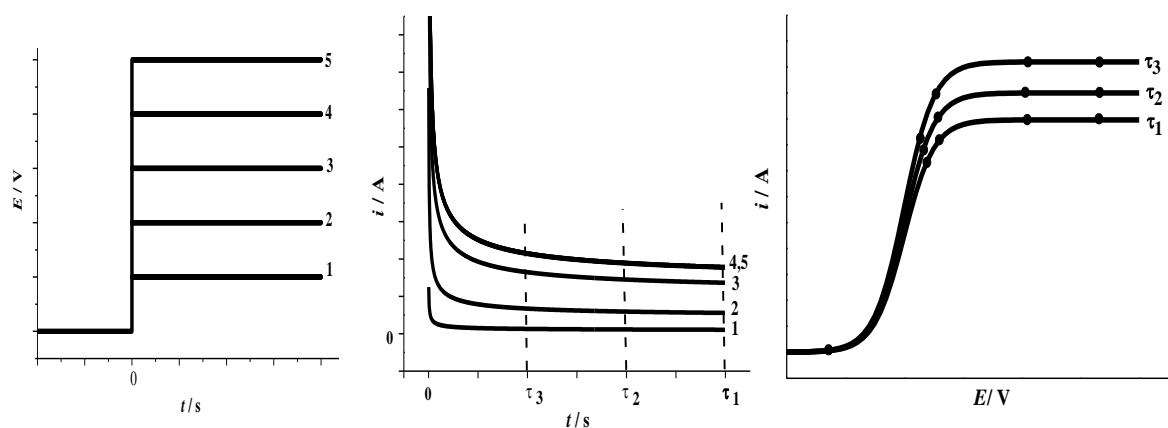
Figure 1.8 Sampled current voltammetry: a) series of potential steps experiments, b) corresponding current transients for potential step experiments, c) reconstructed sampled current voltammograms.

In the cyclic voltammetry, the staircase or linear sweep mode of increasing the potentials implies that the current response for the subsequent step depends on the previous measurement. In the NPV waveform the measurement for each step depends on the value of E_{base} (in which the current equals zero). Therefore, the source of current is the same step. The present study is therefore undertaken with the objective of studying the system with electrodes treated in such a way that every point on the current voltage curve has the same electrode history.

1.11 The need to control the history of the electrode

In voltammetry the current at a particular potential depends on the potential previously applied to the electrode. Thus every point on the voltammogram has a different history from its predecessor

along the sweep. This is particularly important when the electrode is known to undergo surface processes in parallel with the redox process of interest.

In NPV each potential step is in principle carried out with the electrode history in the same state since the return to the base potential reconditions the electrode. In reality the NPV obtained depends on the base potential chosen and on the direction of the potential increments. For example, if the base potential is not sufficiently negative to remove oxides, starting the NPV from large positive potentials leaves an oxide film for all the potential steps considered. In contrast with the same base potential, starting the NPV from negative potentials produces a clean electrode only covered with oxide when the step potentials enter the oxide region.

In this work we chose to use sampled current voltammetry so that the conditioning waveform mentioned previously could be used before each potential step. This strategy ensures that each point on the pseudo steady state voltammogram has been recorded in identical conditions.

1.12 Modification of the electrode

While a significant part of the work presented here focused on potential waveforms to recondition the electrode, an alternative approach based on surface modification was investigated. This was motivated by two questions: 1) could surface modification reliably control the surface and produce a constant amperometric response for the ORR, 2) could a surface modification be found to prevent biofouling, e.g. protein adsorption. Depending on the deposition protocol and material deposited, a monolayer to multilayers could cover the surface leading to significant changes in the sensitivity and permeability of the coated electrode. These coating were tested by means of cyclic voltammetry technique in the presence of different redox probe molecules. In order to assess the effect of the coating on the behaviour of the probe electrode, experiments were performed at the same scan rate before and after coating.

A range of coatings was considered. All had in common the possibility to initiate and control their growth electrochemically. Several polymeric films, namely polypyrrole, polyaniline, poly(phenylene oxide), poly(1,2 diaminobenzene) were chosen to allow the growth of thick (up to several micrometers thick) layers. Two other coatings, poly 4-(N-Boc-aminomethyl) benzene diazonium tetrafluoroborate and COOH-diazonium tetrafluoroborate films were chosen to provide very thin (molecular thick) films. The aim of these experiments was to investigate whether

coatings could provide a systematic way of altering the electrode surface and to compare the results obtained with the cleaning waveform with those obtained with the coatings.

1.13 Aims of the work

The long-term aim of this research is to build upon the previous research on bare microdisc electrodes for deep-sea DO concentration applications. Two strategies were followed, one investigated the possibilities of improved waveform design, the other investigated the role of surface modifications. Another aim was to gain insight into the ORR under transient conditions; in particular a key objective was to determine the dependence of n_{app} on time. A large part of the work focused on the design of potential waveforms to recondition the microelectrode and obtain reproducible O_2 reduction transients.

To achieve the abovementioned aims, significant effort was devoted to choose the best experimental conditions for miliseconds measurements, to validate experimental conditions using model redox systems, and to probe the influence of faradaic and non-faradaic processes on the transient response.

The following section briefly describes the structure and organisation of the thesis.

1.14 Structure of the thesis

Chapter 2 details the experimental work and the methodology of the work including the reagents, cells, instrumentation used on a regular basis and the preparation and characterisation of the electrodes.

Chapter 3 describes the use of ruthenium hexaammine reduction as a model system for ORR. It also presents non-steady state measurements for ruthenium hexaammine reduction. It describes transient measurements, where the performance of the applied conditioning waveform at the microelectrode is presented, and reconstructed voltammograms at different time scales are compared to theory.

Chapters 4 reports the ORR system investigated in chloride and chloride-free containing solutions, using different techniques. The effectiveness of the various applied waveforms is outlined. Also, the data on n_{app} as a function of time is presented.

Chapter 5 investigates the role of coatings on the sensor performance. The influence of various coating materials on ORR and the background is presented. The reconstructed voltammograms are compared with those on bare electrodes. Also, the dopamine oxidation was investigated with coated Pt and Carbon fibre (CF) electrodes.

Chapter 6 outlines the conclusion of this work and further work, along with Appendix and a list of references.
The appendix includes numerous experimental results of model experiments (the oxidation of ferrocene in acetonitrile) designed to probe the experimental procedure, the instrumentation, and the analysis of the data.

Chapter 2

Experimental

2 Experimental

The general experimental procedures are presented in this chapter. However, any special or particular experimental conditions are given in details in the relevant results chapters. The characterisation of the electrodes to ensure reproducible surface conditions is also described.

2.1 Solutions

Reagent solutions were prepared without any further purification in 18.2 MΩ cm resistivity water purified using a Still Plus system (Whatman). All glassware was frequently cleaned with Decon, and then rinsed thoroughly with deionised water, left to dry, rinsed once again with deionised water then with the solution for electrochemical study. The chemicals used in the present work, together with their purity and supplier, are listed in Table 2.1 below. The argon (Pureshield Argon, 99.998%) was obtained from BOC Gases in highest purity, while compressed air was taken from the compressed air laboratory supply. Solutions were kept at a desired temperature in jacketed cells using a water bath (G120, Grant).

2.2 Electrodes, Instruments, and Cells

Reference electrode

Homemade saturated calomel (SCE) and saturated mercury (I) sulphate (SMSE) electrodes were stored in saturated KCl or K_2SO_4 solutions respectively and served as the reference electrodes in most experimental work. For experiments in organic media, a Pt mesh was used as a quasi-reference electrode.

Working Electrodes

The working electrode used in all the experiments was a Pt or Au microdisc electrode (25 and 50 μm diameter); in all the cases it was initially polished (as it will be described in a separate section later) before a series of experiments was carried out. When the currents measured were very small, a counter electrode was not necessary. However, at very short times, the current was in the microampere range, therefore, the system was switched to a three electrode configuration and a counter electrode made of a Pt mesh was used.

Table 2.1 Chemicals and materials used in the experimental work.

Name	Formula	Purity	Manufacturer
Reagents			
Hexaammineruthenium (III) Chloride	$Ru(NH_3)_6Cl_3$	98%	Aldrich
Mercury (I) Chloride	Hg_2Cl_2	ACS 99.5%	Alfa Aesar
Mercury (I) Sulphate	Hg_2SO_4	>97%	Fluka
Potassium Chloride	KCl	Aristar 99.999%	BDH
Potassium Ferrocyanide	$K_4Fe(CN)_6$	Analar 99%	BDH
Ferrocene	$Fe(Cp)_2$	-	BDH
Ferricinium tertrafluoroborate	-	-	Aldrich
TBTAFB*	-	-	Aldrich
Ferrocenmethanol	-	97%	Aldrich
Phenol			
Sodium Perchlorate	$NaClO_4.XH_2O$	99%	Aldrich
Potassium Nitrate	KNO3	Analar 99%	BDH
Potassium Sulphate	K_2SO4	Analar	BDH
Sodium Chloride	NaCl	Analar Aristar	BDH
Sulphuric Acid	H_2SO_4	Aristar sp. gr. 1.84	BDH
Phospheric Acid	H_3PO_4		BDH
Wires			
Platinum (wire, Ø=25 μm)	Pt	99.9+%	Goodfellow
Gold (wire, Ø=25 μm)	Au	99.9+%	Goodfellow
Indium (wire, Ø =1 mm)	In	99.99%	Alfa Aesar

* stands for Tetrabutylammoniumtetrafluoroborate

Instrumentation

The electrochemical cell was a glass vessel that contained ports for entry of electrodes and purging of gases. In the reported experiments, the working (Pt wire, 99.997% purity, Goodfellow) and reference (either saturated calomel electrode, SCE or SMSE (saturated mercurous sulphate

electrode) electrodes were held in the same compartment. The electrochemical experiments were carried out in a two- or three-electrode system configuration at room temperature, $23 \pm 1°C$ or $25°C$. The cell was enclosed in a grounded Faraday cage in order to minimize electrical interferences. The solution was purged with argon gas for ca. 20 min or aerated with open air or compressed air, after which gas was introduced through one arm of the cell for set of experiments. All electrochemical experiments were performed using either a computer-controlled μ-Autolab or PGSTAT30 (which is coupled with ADC750 module for fast measurements) (Eco-Chemie, Utrecht, The Netherlands) connected to a PC using GPES (version 4.9). The software package Origin 8 SR4 (OriginLab Corporation.) was used to fit and plot the experimental data.

Background subtraction

The background current observed in voltammetry and chronoamperometry reflects the physical charging of the electrode double layer and some faradaic surface reactions. It was reported that both the amount of surface oxygen as well as the roughness of the electrode surface have a tendency to change during voltammetric experiments, which leads to significant changes in the background current [112], and can create a significant problem when a stable background is needed for accurate background subtraction such as in fast scan voltammetry. The strategy employed to retrieve an accurate background current was to record the response at the working electrode in the supporting electrolyte in the absence of analyte. Then, analyte solution was injected into the electrochemical cell with a pipet (to avoid removing the electrodes) and scanned in the same experimental potential window as that for background solution. This insured that data for the redox process considered were recorded without removal of the electrode from the solution. In order to allow rapid switching between the electrolyte alone and electrolyte plus redox couple, all cell ports were identified and one port was used to inject the redox couple of interest.

2.3 Pretreatment

The voltammetric responses of platinum and gold electrodes vary with the electrochemical or chemical history of the electrode. As a result, some methods of routine electrode pretreatment are usually necessary to obtain reproducible experimental results. Therefore, Pt and Au electrodes were cleaned and activated by cycling in 1 M H_2SO_4 between potentials where hydrogen evolution occurs and potentials where oxygen evolution occurs. The cycling was ended with the cathodic potential to ensure no oxide was present on the electrode. After several cycles, a reproducible voltammogram should show peaks for the formation and removal of both adsorbed hydrogen and

adsorbed oxygen (in case of Pt) and the formation and removal of adsorbed oxygen (in case of Au electrode) [5, 37]. This procedure was used throughout the work.

2.3.1   Polishing of microelectrodes

A series of polishing procedures was employed. After fabricating the electrodes, they were ground with wet SiC paper with different sizes 240, 600 and 1200 on polishing wheel. This produces deep scratches and grooves. Therefore, it was followed by polishing with finer abrasive particles of 5 and 1 μm aluminium oxide powder (Buehler Ltd). The dampened powder was placed on a clean microcloth (Buehler Ltd), which was stuck in a Petri dish. For better results, the microelectrode was held perpendicular to the surface of the cloth and polished gently. Also, the electrodes were washed with ultrapure water in between each polishing to remove any particles. In presence of any bubble by the side of the disc, further polishing would be required since the bubble would increase the electroactive area of the microelectrode. Finally, inspection under an optical microscope revealed a "mirror finish" surface.

2.4 Scanning Electron Microscopy

Scanning electron microscopy in combination with cyclic voltammetry offers a reliable platform of techniques for a reasonably complete characterization of the geometrical and electrochemical properties of the microelectrode. It was employed to assess the quality of the seal between the metal wire and the insulating material, and to gain more insight of the morphology of the electrode surface.

A Philips XL30 ESEM microscope was used to characterise the microelectrodes prepared in this work. In order to prevent charging up of the glass surrounding the electrode, the wet mode was chosen. In most cases, the gaseous secondary electron (GSE) detector was used. The recorded image was taken from two angles; 70 and 0, see figure 2.1 below, degree when the electrode is facing the electron source.

It should be stressed that, the presence of any microscopic cracks between the electrode and the glass insulation can be another source of residual current, particularly important for short time experiments.
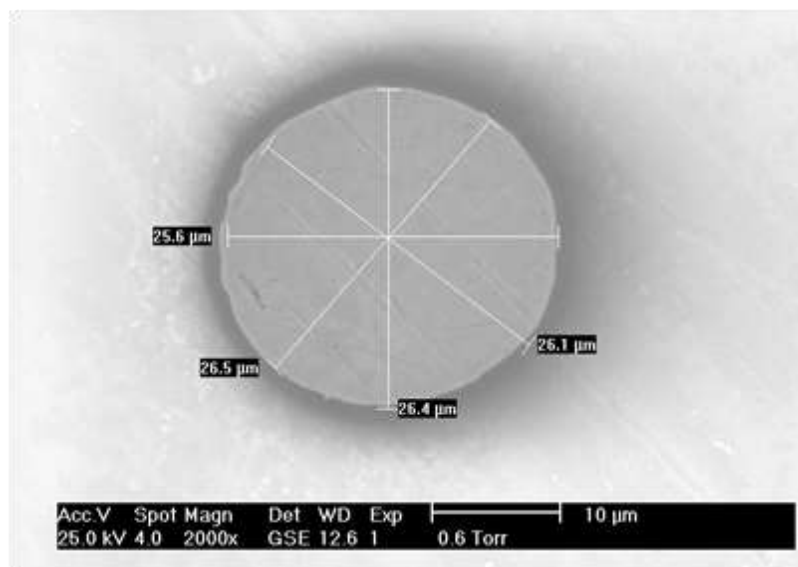
Figure 2.1 SEM image of a microdisc microelectrode Pt (a=12.5 μm) embedded in glass.

2.5 Shielding of the electrode

Since the capacitive coupling between the inner conductor and the electrolyte solution can contribute to an increase in the electrode capacitance at short time scale, construction of an electrode with a conductive shield connected to electrical ground is necessary. Figure 2.2 represents the design of shielded electrode as suggested by Wipf [113].
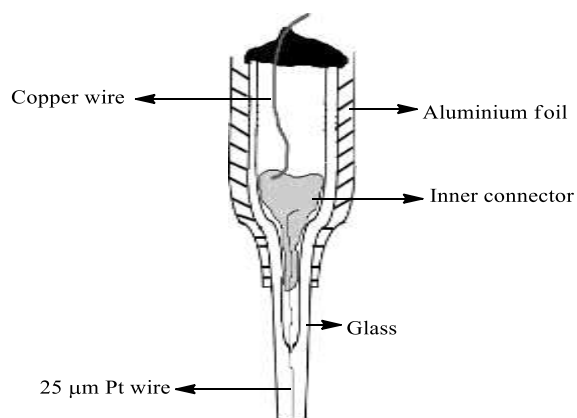
Figure 2.2 Cross sectional representation of the shielded 25 μm diameter Pt microdisc electrode.

2.6 Characterisation of microelectrodes

2.6.1 Characterisation of Pt and Au microelectrodes in acid

A cyclic voltammogram at a 25 μm diameter platinum microdisc electrode in sulphuric acid was recorded before proceeding with further measurements. The experiment was carried out in a closed cell at room temperature. The solution was degassed with argon. A stable response recorded after approximately ten cycles is shown in Figure 2.3.

The chosen scan limits are the onsets of oxygen (D) and hydrogen evolution (G) with respect to the SMSE reference electrode. Full characteristics of platinum can be observed on the cyclic voltammogram (several features, characteristic for clean platinum surface are visible) which is divided into several regions, namely, the hydrogen zone (evolution of hydrogen gas – G, hydrogen monolayer adsorption (strong – F', weak – F) and desorption (strong – A', weak – A)), the double layer region, the oxide region (Pt oxide formation –C) and reduction (stripping –E)) respectively, and the oxygen evolution –D.

This 'acid CV' can show all the features of the electrode and ensure that the electrode is clean for use before proceeding with experiments. In addition, some criteria can be used to assess the electrode roughness and detect the presence of any contaminants on the surface, such as the shape, position and magnitude of the observed peaks. The roughness factor of Pt electrode was calculated and found to be 1.8.
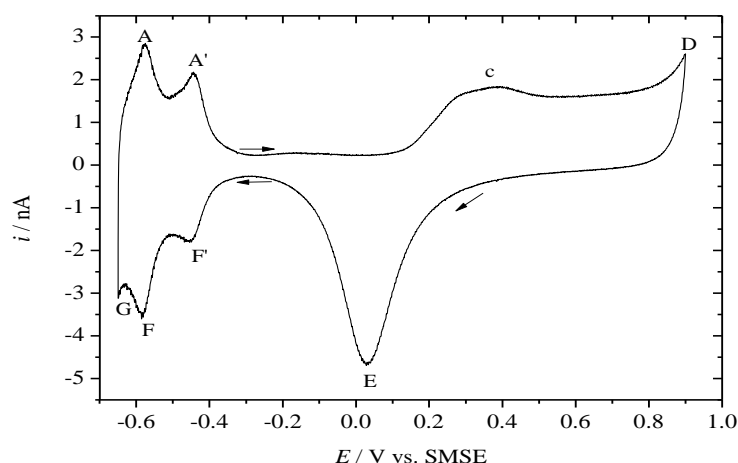
Figure 2.3 Stable cyclic voltammogram of a 25 µm diameter platinum microdisc electrode in 1 M sulphuric acid solution, deoxygenated with argon, recorded at scan rate, $v = 200$ mV s^{-1} at room temperature, using SMSE as a reference electrode. C, D, and E represent oxide formation, oxygen evolution and oxide stripping respectively while F', F are strongly and weakly bound hydrogen

adsorption followed by G hydrogen evolution and A, A' for desorption of strongly and weakly bound hydrogen.

Similarly, since gold electrodes were used in this work, characterisation was carried out in sulphuric acid to obtain information reflecting the surface state (Figure 2.4). The voltammogram shows the double layer region, gold oxide formation and its corresponding stripping peak.
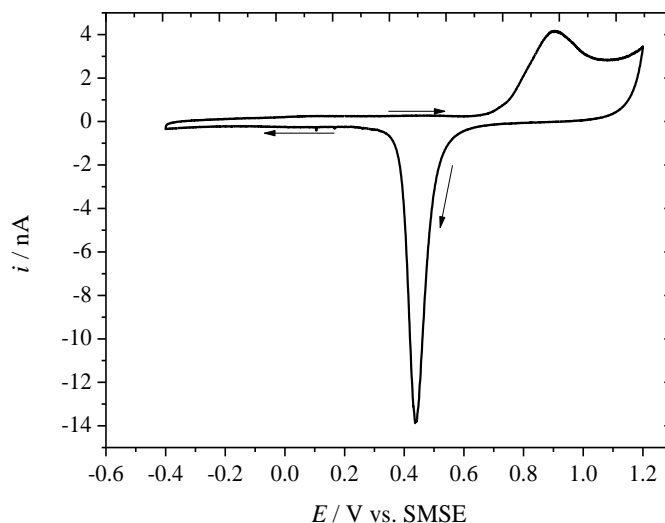
Figure 2.4 Stable cyclic voltammogram of a 25 µm diameter gold microdisc electrode in 1 M sulphuric acid solution, deoxygenated with argon, recorded at scan rate, v = 200 mV s^{-1} at room temperature, using SMSE as a reference electrode.

2.6.2 Steady state voltammetry in hexaammineruthenium (III) chloride solution

The reaction routinely used for microdisc electrode characterisation is the one-electron reduction of aqueous solution of hexaammineruthenium (III) trichloride in KCl (excess of supporting electrolyte to avoid migration current). A steady state voltammogram for this model system is shown in Figure 2.5. The experiment was carried out in a closed cell at room temperature. The voltammogram was recorded at a slow scan rate (2 mV s^{-1}) at the 25 µm Ø Pt microelectrode. Clearly, the CV has the expected sigmoidal shape with little hysteresis for steady state diffusion at a microdisc electrode.

In order to obtain the radius of the electrode, we use the equation 9 where i_{lim} is the steady state limiting current, taking c^∞= 5 mM and the diffusion coefficient of 5 mM Ru(NH$_3$)$_6$Cl$_3$ in 0.5 M KCl solution from the literature as D = 8.8×10^{-6} cm^2 s^{-1}. The calculated radius (a = 12.5×10^{-4} cm)

or 12.5 µm is in good agreement with the radius reported by the manufacturer of the wire and with the measurement from the SEM image in Figure 2.1.
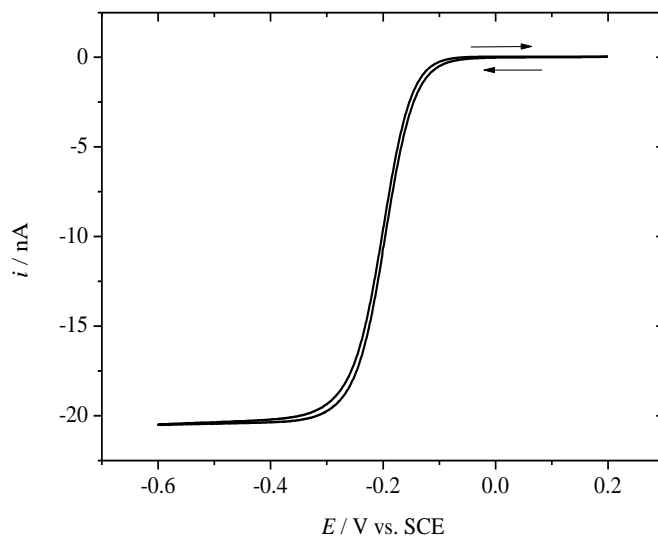
Figure 2.5 Steady state voltammetry at 5 mV s^{-1} for a 25 microns diameter Pt microdisc in 5 mM Ru(NH$_3$)$_6$Cl$_3$ / 0.5 M KCl system, SCE as reference electrode and Pt mesh as counter electrode.

2.7 Transient amperometry at microelectrodes? Is double layer a problem?

In amperometry, the measured current, i_{tot}, consists of both the faradaic current (i_F) and the capacitive current (i_C). One of the properties of the microelectrode is the improvement of the faradaic-to-charging current ratio, i_F/i_C, as the charging current decreases in proportion to decreasing area of the electrode.

After applying a potential step the capacitive current dominates the faradaic current at very short times. However, as shown in equation 18 below, it decays exponentially with a time constant (R_uC_{dl}) where R_u and C_{dl} are respectively the uncompensated resistance (in ohms) and the double layer capacitance (in farads). Assuming a diffusion controlled process the Faradaic current is given by the Mahon and Oldham expression, Equation 1.2. Figure 2.6 below shows the theoretical contribution of the charging current to the total current over a range of relevant time scales.

$$i_c = \frac{\Delta E}{R_u} \exp\left(-\frac{t}{R_u C_{dl}}\right)$$

Equation 2.1

where ΔE = magnitude of the applied potential step (V), R_u = solution resistance (Ω), t = time (s) and C_{dl}= double-layer capacitance (F).

The solution resistance is given by equation2.2 below

$$R_u \approx \frac{1}{4\kappa a}$$

Equation 2.2

where κ is the solution conductivity.

The electrode capacitance is given by

$$C_{dl} \approx \pi a^2 R_f C$$

Equation 2.3

where R_f is the roughness factor and C the capacitance of the electrode material per unit area in the given solution. For a microdisc the RC time constant is thus proportional to the radius of the electrode.

$$\tau \approx R_u C_{dl} \approx \frac{\pi R_f a C}{4\kappa}$$

Equation 2.4

Therefore at microdisc electrodes the charging time can be significantly reduced since a is small. Since the charging time limits the availability of the faradaic information (no faradaic data for $t <$ 3τ), the use of microelectrodes enables the investigation of short lived species and very fast electron transfer. The small RC constants allow high-speed voltammetric experiments to be performed at the microsecond timescale (with some experiments reported with voltammetry at the MV s^{-1} [109].

In general if $t < \tau$, then $i_C > i_F$, it is concluded that electrochemical information is lost when

$t < 3\ \tau$

$t = \tau$ $i_c = 37\%\ \Delta E\ /\ R_u$

$t = 3\ \tau$ $i_c = 5\%\ \Delta E\ /\ R_u$
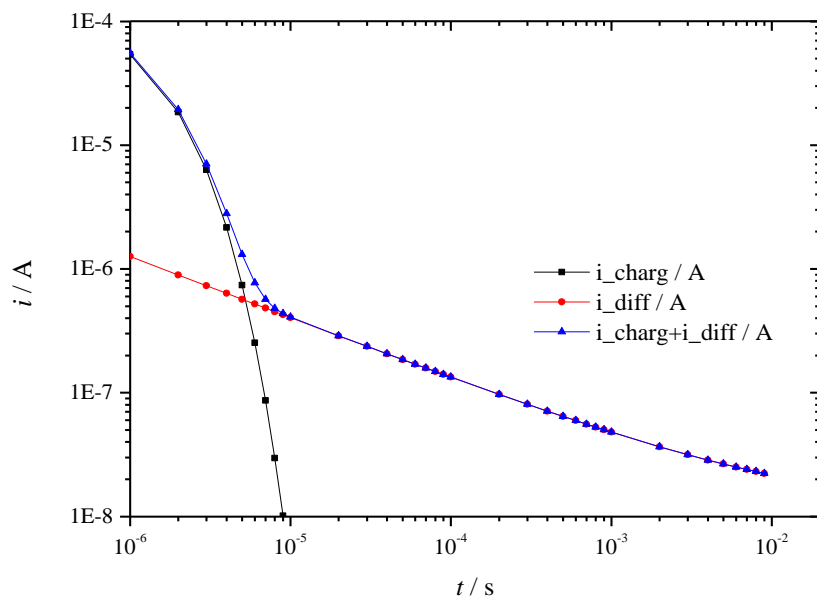
Figure 2.6 Theoretical Faradaic, double layer charging and total currents for a hypothetical 0.5 V step into the ORR plateau on a 25 μm diameter Pt disc electrode in aerated 0.5 M NaCl, taking C_{dl} ≈ 20 μF cm^{-2} for Pt in water, a conductivity κ ≈ 0.0632 Ω^{-1} cm^{-1} for 0.5 M NaCl, a roughness factor of R_f = 3, D_{O2} = 2.2×10^{-5} cm^2 s^{-1} and c^b_{O2} = 1×10^{-6} mol cm^{-3}.

Some calculations were done to determine the effect of charging current on the measurement. We took into account the following values when using microdisc electrodes: C ≈ 20 μF cm^{-2} for Pt in water , κ ≈ 0.0632 Ω^{-1} cm^{-1} for 0.5 M NaCl, R_f = 3. The previous equations were used to achieve this purpose. We found that charging current has no effect after 1 μs.

a/μm	R_u/ Ω	C_{dl} /pF	3τ / ns
12.5	1,000	300	900

Capacitive coupling to the contact inside the microelectrode (indium or silver epoxy), can, at very short times (high frequencies), accounts for an additional charging current in the transient experiments. It was reported by Wipf *et al* [113] that the magnitude of the electrode capacitance depends on its construction, as this excess capacitive current can be due to the capacitance between the inner conductor and the electrolyte solution. In order to avoid this effect, a special design for the electrode was used in which a conductive shield around the electrode was used and connected to the ground, as described in Chapter 2- Section 2.5.

Chapter 3

Transient studies with a model system: ruthenium hexaammine reduction

3 Overview

This chapter presents the results of transient chronoamperometric experiments at microdisc electrodes for a model redox reaction: the reduction of $[Ru(NH_3)_6]^{3+/2+}$ in chloride. The $[Ru(NH_3)_6]^{3+/2+}$ couple was chosen as a model for the following reasons:

-        In chloride, its reduction wave at Pt electrodes appears in the same potential range as that for oxygen reduction.

-        It is known to be a fast outer sphere electron transfer process which involves 1 electron.

Thus its reduction should be affected by the same surface processes as for the ORR. Being a fast couple (without complication from adsorption/desorption processes) its chronoamperometric response should be diffusion controlled over most of the timescale considered. Furthermore, the number of electron involved in the reduction should be equal to 1 at all timescales. Overall the reduction of $[Ru(NH_3)_6]^{3+}$ is used as a model reaction to validate the experimental approach and analytical treatment of the data.

The study presented in this chapter includes the voltammetry and amperometry of $[Ru(NH_3)_6]^{3+}$ at short times, using two different cathode materials, Au and Pt. Due to the necessity of investigating

the role of background currents (the electrolyte in absence of any redox couple), Fast Scan Voltammetry (FSV), potential step experiments, Normal Pulse Voltammetry (NPV) and conditioning waveform were used to study the reduction of the ruthenium hexaammine complex. Being a simple, fast one electron transfer process this should lead to a purely diffusion controlled response in approximately the same potential region as oxygen reduction and should allow an assessment of the effect of background processes.

3.1 FSV in Hexaammineruthenium (III) chloride solution at Pt microelectrodes

3.1.1 Pt electrode

Fast voltammetric investigations of $Ru(NH_3)_6^{3+/2+}$ experiments were carried out at both Pt and Au disc microelectrodes. A series of cyclic voltammograms were recorded at various scan rates. They were run first in the background (electrolyte alone or argon degassed KCl solution). Then the ruthenium complex was injected in the cell and the CVs were recorded again. Figure 3.1 shows the CVs before and after the subtraction of the background.
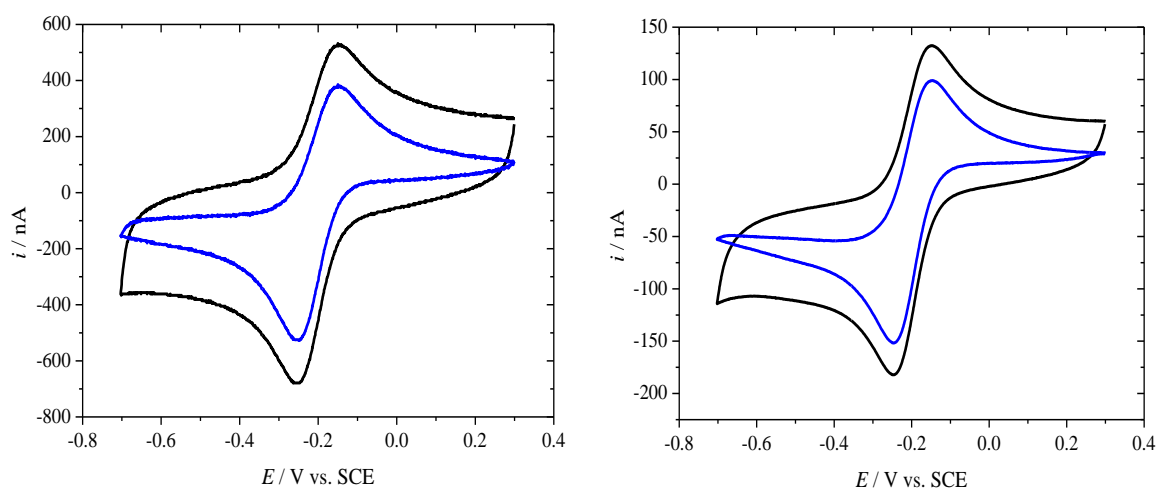
Figure 3.1 FSV in 5 mM $Ru(NH_3)_6Cl_3$ in 0.5 M KCl solution (deoxygenated with argon), using SCE as a reference electrode, Pt microdisc (25 μm Ø) as a working electrode and Pt mesh as a CE, at 50 V s^{-1} (right) and 500 V s^{-1} (left) and room temperature.

The background, Figure 3.2, originates from the double layer capacitance of the electrode which produces more current with higher scan rates, although this is negligible for the sweep rates used

here, and to some surface processes such as the reduction of Pt oxide and adsorption of hydrogen. Therefore, it was important to discriminate it from the signal for the reduction of the ruthenium complex ion.

The reduction of the ruthenium complex ion is as follows

$$Ru(NH_3)_6^{3+} \quad + \quad 1e^- \quad \rightarrow \quad Ru(NH_3)_6^{2+}$$
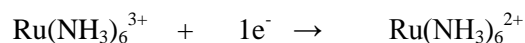
As the scan rate increases the appearance of peaks was observed together with an increase in current magnitude (data is not shown). This can be attributed to the transition from hemispherical (at low scan rate) to planar diffusion (at high scan rate).
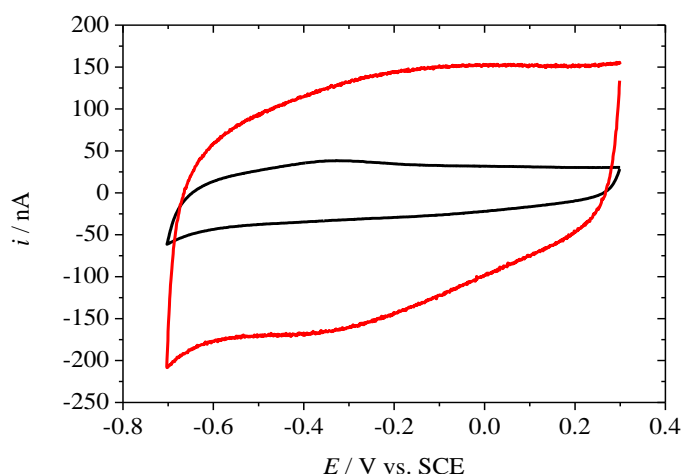
Figure 3.2 FSV in 0.5 M KCl solution (deoxygenated with argon), using SCE as a reference electrode, Pt microdisc (25 µm Ø) as a working electrode and Pt mesh as a CE at 50 V s^{-1} (black line) and 500 V s^{-1} (red line) at room temperature.

The kinetics of this system was reported to depend on the electrode materials used. It was reported previously that ruthenium complex undergoes a relatively fast reduction process with a k^0 between 0.5 and 1 cm s^{-1}. A difference in rate constant between Pt and Au electrode was reported in literature. The ideal behaviour of ruthenium metal complex cation was studied by Weaver and co-workers [114]. A high rate of electron transfer with large standard rate constant is expected for the homogeneous self-exchange of Ru(NH$_3$)$_6^{3+/2+}$ couple [115].

The cathodic peak current was measured after background subtraction and its dependence on scan rates was analysed according to the equation given by Aoki *et al.* [116]. However, excellent agreement with theory was achieved only for scan rates below 200 V s^{-1}. Then a deviation from

theory at higher scan rates was observed even after excluding the current recorded in absence of the redox species (ruthenium complex ion in this case). This enhancement could be attributed to a faradaic contribution from surface processes. This suggests that background subtraction is not working at very high scan rates. It is possible that the background current observed in presence of the redox couple is different from that in absence of the redox couple.
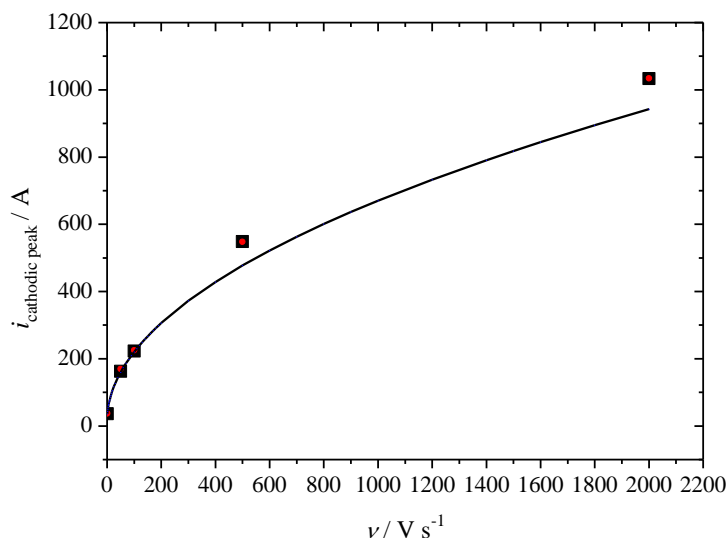
Figure 3.2 Relationship between the peak current and the scan rate for a series of cyclic voltammograms at a 25 μm diameter Pt disc in 5 mM $Ru(NH_3)_6Cl_3$ + 0.5 M KCl (argon degassed). Symbols are the experimental peak currents (red points for raw data whereas black points represent data after subtraction of the CV recorded in absence of ruthenium complex), the line is from the theory of Aoki *et al* [117], using D=8.50x10^{-6} cm^2 s^{-1} at 25°C a=12.5 x10^{-4} cm, and C^∞=5 x10^{-6} mol cm^{-3}.

Beriet and Pletcher observed a deviation from reversibility for ruthenium reduction system in 300-1000 V s^{-1} range which resulted in a large shift between the coupled oxidation and reduction peaks [111]. However, they only refer to the peak potential difference. They did not analyse the peak currents against the Aoki *et al*. [116]. The fact that results show more current than expected for diffusion control cannot be attributed to electron transfer kinetics.

3.1.2 Au electrode

FSV was also run on gold microdiscs to observe the effect of the electrode material on the reduction of the ruthenium complex. Similar experiments were conducted using Au microdisc electrodes to investigate the effect of the background and compare it with that observed on Pt

microdisc electrode. Since no hydrogen adsorption/desorption process takes place on Au the faradaic contribution for surface processes is expected to be lower than on Pt.

At Au electrodes the same behaviour was observed for the reduction of the ruthenium complex when increasing the applied scan rate. The peaks evolved indicating the transition from hemispherical diffusion at low scan rates to linear diffusion at high scan rates (data is not shown). The magnitude of the peak currents also increased with the scan rates. The background current becomes more significant at high scan rates, so it is necessary to discriminate it. Figure 3.4 presents the recorded CVs.
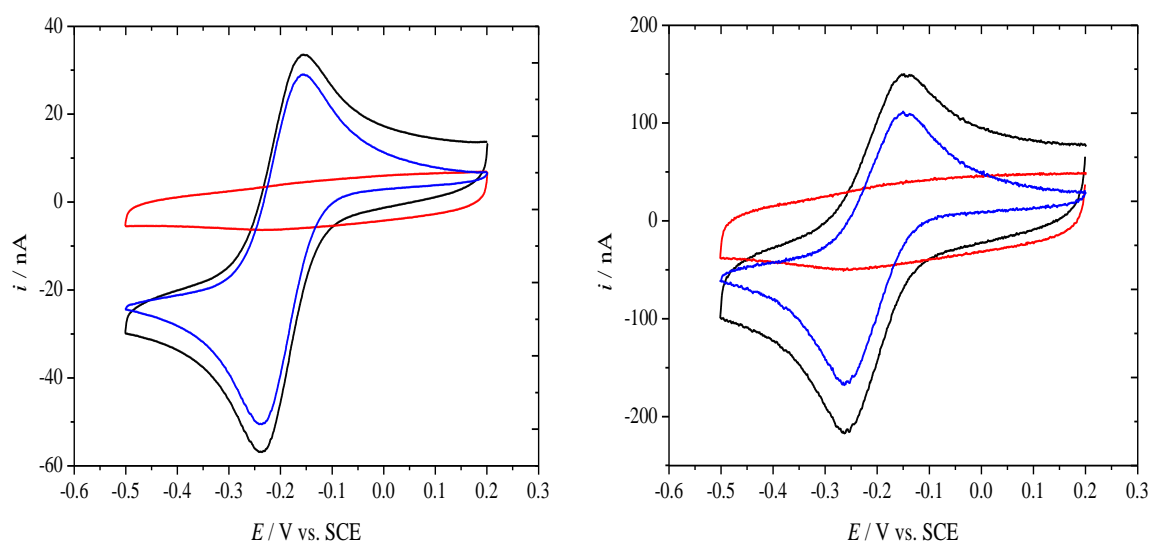
Figure 3.3 FSV in 2.5 mM $Ru(NH_3)_6Cl_3$ in 0.5 M KCl solution (deoxygenated with argon), using SCE as a reference electrode, Au microdisc (25 μm Ø) as a working electrode, a Pt mesh CE at 10 V s^{-1} (left) and 100 V s^{-1} (right) at room temperature. Recorded CV in black, background subtracted CV in blue and background CV in red.

The background response at gold electrode shows the typical featureless CV reflecting surface processes (double layer charging has a negligible contribution at this sweep rate). Unlike Pt, surface processes like hydrogen adsorption/desorption do not take place at gold surface, but oxide formation/stripping still occurs. Therefore, the background subtracted response for the reduction of ruthenium is better discriminated from surface process at Au electrodes than platinum ones.

3.2 Potential step experiments in hexaammineruthenium (III) chloride solution

3.2.1 Au microelectrodes

The steady state voltammogram for the reduction of the ruthenium complex ion in KCl was run at slow scan rate to check the response of the electrode and measure the limiting current. Figure 3.5 shows a well-defined plateau for the maximum rate of the diffusion of ruthenium species with little hysteresis between the forward and backward scans. Then the potential step experiments were carried out. The potential was stepped from the region, where no reaction is taking place to various potential values along the reduction wave. The chronoamperogram was recorded three times at each potential. From the averaged current transient output, the current was sampled at various fixed times. The reconstructed voltammograms at different time regimes were plotted and compared to the theoretical current (Shoup-Szabo equation) modified to account for the potential, Equation 3.2 in Section 3.5 for a diffusion controlled process. The parameters used to obtain the theoretical expression were $D= 7.1\times10^{-6}$ cm^{2}s^{-1}, $c^{\infty} = 2.5\times10^{-6}$ mol cm^{-3}, $E_{1/2} = -0.15$ V and $a = 12.5\times10^{-4}$ cm.

The choice of Au for ruthenium hexaammine reduction was due to the absence of the hydrogen adsorption/desorption at this surface. Therefore the reconstructed voltammograms are not expected to be affected by background surface processes provided the start potential is such that the Au electrode is free from oxide. Only the capacitance of the electrode should affect the overall currents at very short timescales.
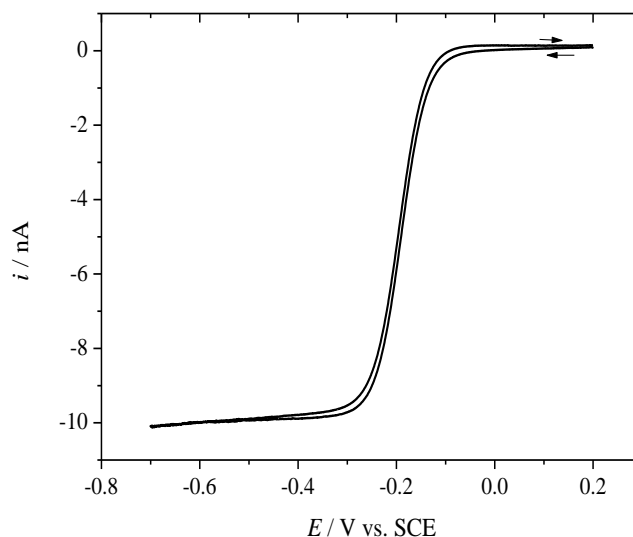
Figure 3.4 Steady state CV in 2.5 mM Ru(NH$_3$)$_6$Cl$_3$ in 0.5 M KCl solution (deoxygenated with argon) before potential step experiments, using SCE as a reference electrode, Au microdisc (25 µm Ø) as a working electrode, and a Pt mesh CE, at 10 mV s^{-1} at room temperature.

The shape of the sampled current voltammograms shows a pseudo steady state plateau in accordance with the modified Shoup and Szabo equation. The current at the plateau increases with the decrease of the sampling time as expected. It can be seen from Figure 3.5 that the reconstructed voltammograms (without any background subtraction but normalised by the diffusion controlled current expected for the corresponding sampling times) are in good agreement with theory for long time scales 500, 200, 100, 50 ms and 20 ms. However, the reconstructed voltammograms at timescales shorter than that show deviations from the theory that could not be explained by the contribution of the capacitance of the electrode since from our calculation it is over in microseconds.
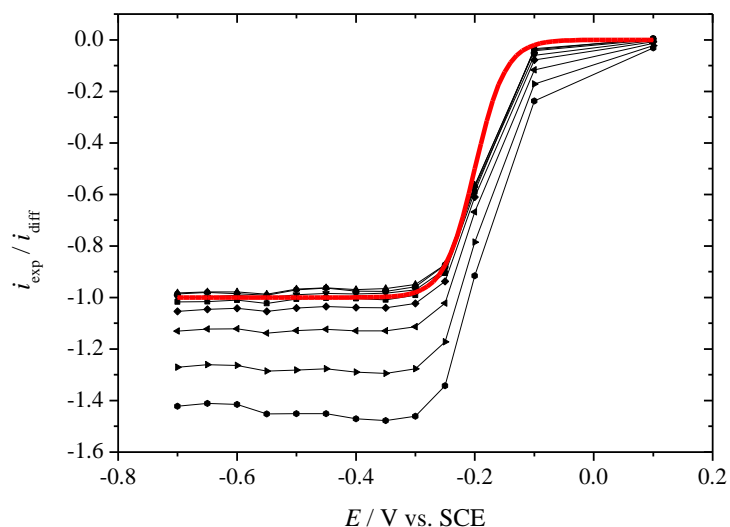
Figure 3.5 Normalised reconstructed voltammograms in 2.5 mM Ru(NH$_3$)$_6$Cl$_3$ in 0.5 M KCl solution (deoxygenated with argon) extracted from the potential step experiments, using SCE as a reference electrode, Au microdisc (25 µm Ø) as a working electrode and Pt mesh as CE, at room temperature. Red solid line represents theory (modified Shoup-Szabo Equation, equation 3.2) whereas lines with symbols represent experimental (with no background subtracted) reconstructed voltammograms. From top to bottom sampling times: 500, 200, 100, 50, 20, 10, 5 and 3 ms. No preconditioning or pretreatment was carried out, except the polishing of the electrode at the beginning of the experiment. The parameters used in the calculations of the theoretical values are: D= 7.1x10^{-6} cm^{2}s^{-1}, a=1.25x10^{-3} cm, i_{lim}=8.56 nA and $E_{1/2}$= -0.15 V at 25°C.

Figure 3.6 shows the reconstructed background voltammograms at different timescales when the potential was stepped from 0.1 V to targeted potential values in KCl solution degassed with argon. For a given timescale the sampled current voltammogram shows a current almost independent of potential within the potential window. This current clearly increases with shorter sampling times. This increase cannot be ascribed to the charging current for those timescales.
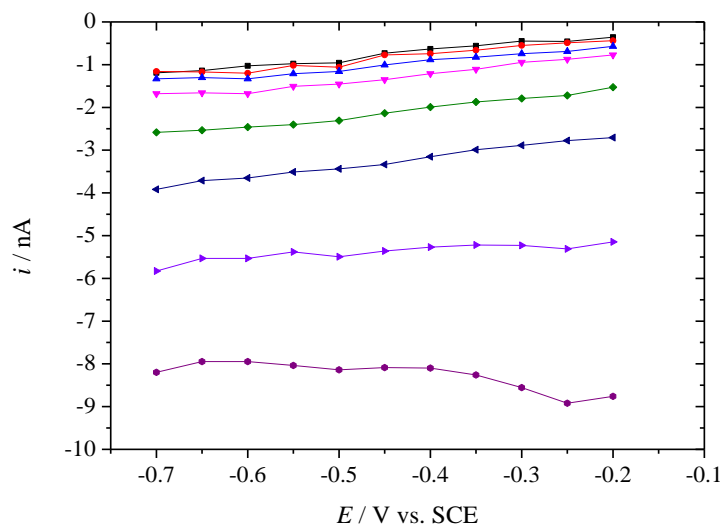
Figure 3.6 Reconstructed voltammograms in 0.5 M KCl solution (deoxygenated with argon) extracted from the potential step experiments, using SCE as a reference electrode, Au microdisc (25 μm Ø) as a working electrode and Pt mesh as CE at room temperature. From top to bottom sampling times: 500, 200, 100, 50, 20, 10, 5 and 3 ms. No preconditioning or pretreatment was carried out, except the polishing of the electrode at the beginning of the experiment.

It can be seen clearly from Figure 3.5, that the experimental data fit well with theory at long timescales, producing a constant current over the potential range from 0.3 V till -0.7 V particularly 500, 200, 100, 50 and 20 ms even though no background subtraction was needed. However, a deviation from theoretical current values suggested the necessity for background subtraction for short timescales (less than 20 ms). From Figure 3.7, a good fit was found at 10 ms, just after background subtraction. Surprisingly, this technique did not work with times shorter and longer than 10 ms. Figure 3.8 shows the responses of the gold electrode in ruthenium hexaammine before and after applying potential step experiments.

It was not clear whether the cathode material has any effect on the overall sampled current in this experiment. The fit between the experimental data and theory at short times is not as good as those at long timescales; this is unlikely due to the capacitance of the electrode or the condition of the electrode (roughening effect). In the next section similar experiments are reported for a Pt microelectrode to investigate the same model system using potential step experiments.
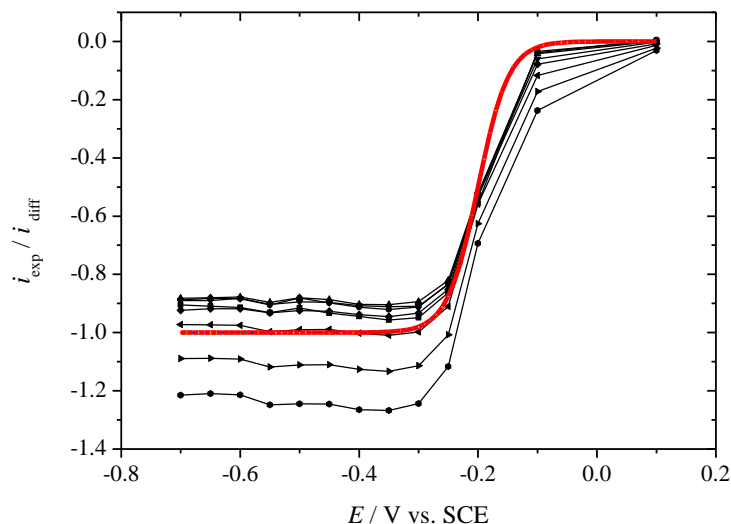
Figure 3.7 Normalised background subtracted reconstructed voltammograms in 2.5 mM Ru(NH$_3$)$_6$Cl$_3$ in 0.5 M KCl solution (deoxygenated with argon) extracted from the potential step experiments, using SCE as a reference electrode, Au microdisc (25 µm Ø) as a working electrode and Pt mesh as CE, at room temperature. Red solid line represents theory, equation 3.2, whereas lines with symbols represent the background subtracted experimental reconstructed voltammograms. From top to bottom sampling times: 500, 200, 100, 50, 20, 10, 5 and 3 ms. No preconditioning or pretreatment was carried out, except the polishing of the electrode at the beginning of the experiment. The parameters used in the calculation of the theoretical values are: D= 7.1x10^{-6} cm^2 s^{-1}, a=1.25x10^{-3} cm, i_{lim}=8.56 nA and $E_{1/2}$= -0.15 V at 25°C.
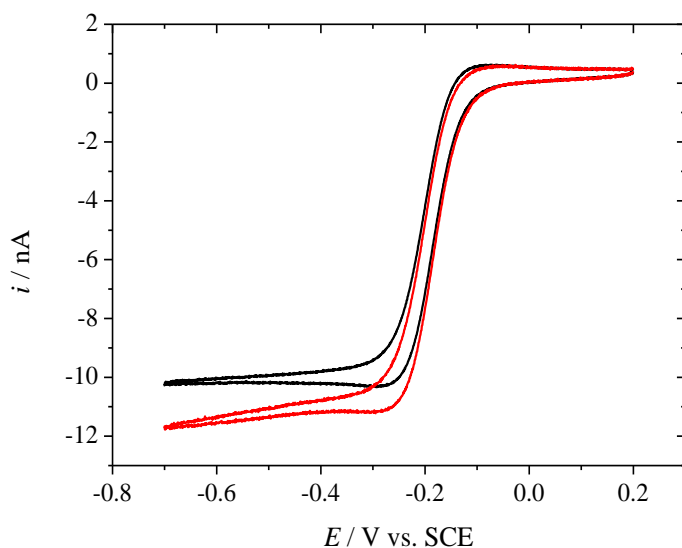
Figure 3.8 CV in 2.5 mM Ru(NH$_3$)$_6$Cl$_3$ in 0.5 M KCl solution (deoxygenated with argon) before (black line) and after (red line) applying a series of potential step experiments, using SCE as a reference electrode, Au microdisc (25 µm Ø) as a working electrode, and a Pt mesh CE, at 100 mV s^{-1} at room temperature.

3.2.2 Pt microelectrodes

The potential step experiments were conducted at Pt microelectrodes to investigate the reduction of the ruthenium complex. 5 mM $Ru(NH_3)_6Cl_3$ in 0.5 M KCl (deoxygenated with argon) was used. The steady state voltammograms were recorded before and after the application of potential step experiments. Figure 3.9 shows the responses obtained; there was a decrease in limiting current, presumably due to normal reproducibility and slight change in temperature during the course of the experiment which could have affected the diffusion coefficient of redox species and subsequently the limiting current value. Any roughening of the electrode during the sampled current voltammograms would not affect the steady state voltammograms.
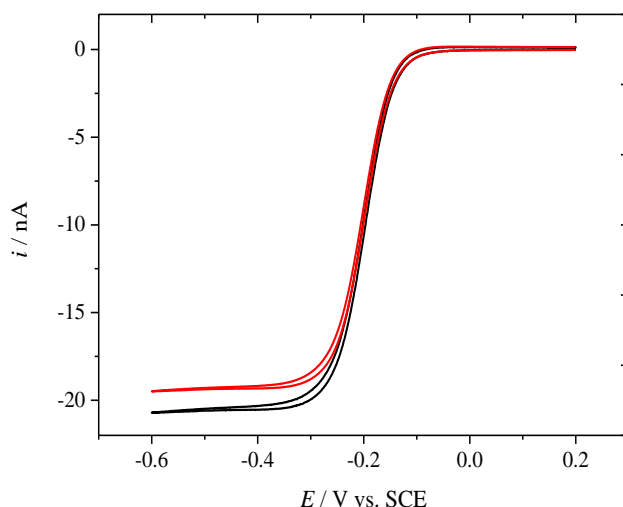
Figure 3.9 CVs in 5 mM $Ru(NH_3)_6Cl_3$ in 0.5 M KCl solution (deoxygenated with argon) before (red line) and after (black line) potential step experiments, using SCE as a reference electrode, Pt microdisc (25 μm Ø) as a working electrode, at 10 mV s^{-1} and Pt mesh as CE; at room temperature.

The potential was stepped from 0.2 V to various targeted potentials along the reduction wave of the ruthenium complex ion. For each potential the potential step experiment was repeated 10 times and the reproducibility was assessed. Figure 3.10 shows the variation between runs and the reproducibility between the results for 10 measurements at -0.6 V (diffusion controlled region). Except for the 1st transient which stands out, it is clear that a good agreement between successive experiments was achieved up to 10 ms; before this time the current was affected by the response time of the current amplifier.

Sampled current voltammograms were reconstructed with a 25 μm diameter Pt disc in 5 mM $Ru(NH_3)_6Cl_3$ + 0.5 M KCl from a series of potential steps (stepping from +0.2 V vs. SCE to the

59

target potential) and presented in Figure 3.11. It should be mentioned that no preconditioning was applied before the potential step experiments. The average current was calculated and no background subtraction was done. A significant contribution of the background processes to overall current was seen in the potential region from -0.3 till -0.6 V.
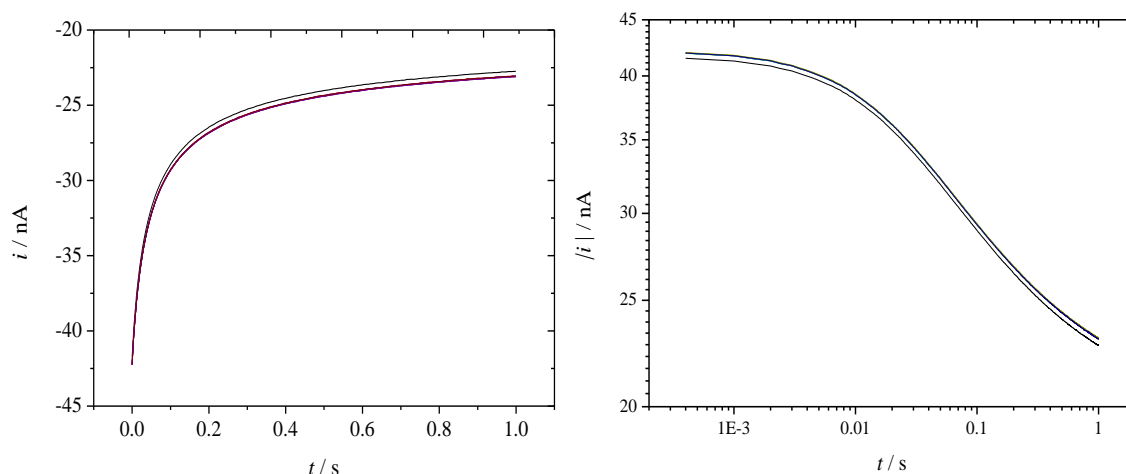
Figure 3.10 Ten consecutive current transients at -0.6 V in 5 mM $Ru(NH_3)_6Cl_3$ in 0.5 M KCl solution (deoxygenated with argon) using SCE as a reference electrode, Pt microdisc (25 μm Ø) as a working electrode and Pt mesh as CE at room temperature. The plot on the right is for the same data.

An alternative approach was used for fitting a theoretical CV. Fitting a theoretical CV to describe the obtained current is appropriate provided the theoretical expression is valid. The alternative approach is only valid in the plateau region and makes no assumption about the shape of the voltammogram but it is still convenient to plot the theoretical CV. By normalising the sampled current voltammograms in Figure 3.12 by the diffusion controlled current calculated with the Mahon & Oldham equation [18], n_{app} could be obtained from the plateau region. Clearly, normalised SCVs follow the theoretical predictions for sampling times down to 100 ms. However, they systematically produce values larger than one in the plateau region for sampling times shorter than 100 ms. This is presumably due to the current from the background processes, e.g. the adsorption of hydrogen.

Therefore, a conditioning waveform should be applied to minimise or eliminate the effect of the background and surface processes on the measured current. A new Normal Pulse Voltammetry (NPV) waveform was applied to the working electrode and is the subject of the next section.
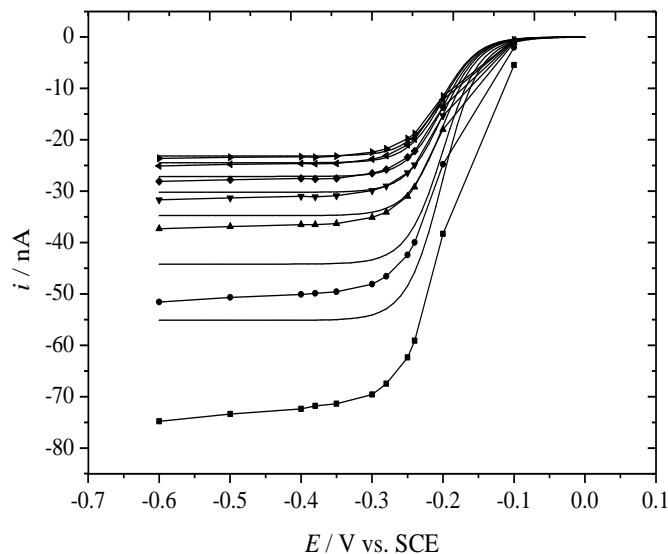
Figure 3.11 Reconstructed voltammograms in 5 mM $Ru(NH_3)_6Cl_3$ in 0.5 M KCl solution (deoxygenated with argon) extracted from series of potential step experiments, after stepping from +0.2 V vs. SCE to the target potential, using SCE as a reference electrode, Pt microdisc (25 µm Ø) as a working electrode and Pt mesh as CE, at different timescales at room temperature. Theoretical CVs (solid lines) drawn from Equation 3.2 with $D=8.3\times10^{-6}$ cm^2 s^{-1}, $a=12.5$ µm, $c^\infty=5$ mM, $E_0=-0.2$ V. From top to bottom sampling times are: 500, 200, 100, 50, 20, 10, 5 and 3 ms.
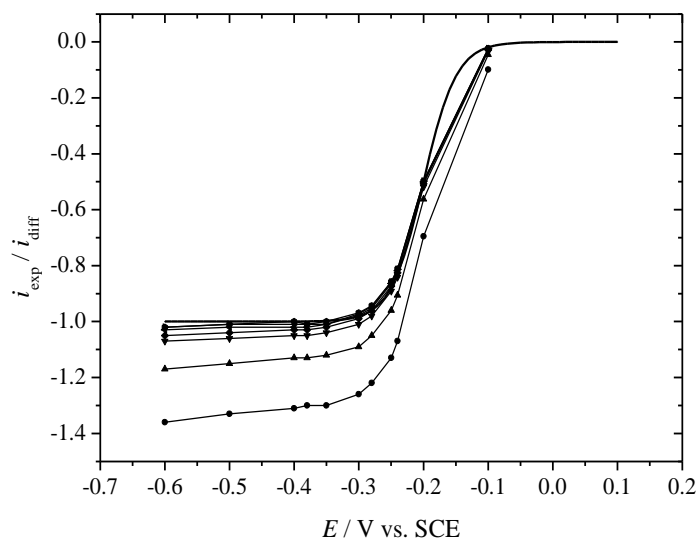
Figure 3.12 Normalised sampled current voltammograms (symbols) for the data shown in Figure 3.12. Theoretical CV (solid line) drawn from Equation 3.2 using the following parameters $D=8.3\times10^{-6}$ cm^2 s^{-1}, $a=12.5$ µm, $c^\infty=5$ mM, $E_0=-0.2$ V. By normalising the experimental current at the plateau by the diffusion controlled current, the number of electron involved (n_{app}) could be obtained and read from the vertical axis of the plot.

3.3 NPV in hexaammineruthenium (III) chloride solution

Some parameters should be chosen before commencing any NPV experiments such as the direction of the scan and E_{base}. Basically the E_{base} value was chosen in the region where no current flows (before the start of the reduction of ruthenium complex ion). Therefore $E_{base} = +0.3$ V (vs SCE) was selected from the steady state CV (Figure 3.13). The direction of scan was decided to be from negative to positive potential after accomplishing some preliminary experiments (shown in the next chapter) to observe the difference in response in either direction (negative to positive or positive to negative sweeps). The waiting time between pulses should be sufficiently long to restore the initial concentration of the species at the electrode surface before the next pulse to establish zero or negligible current [118]. It was suggested that the waiting time should be five to ten times the pulse time [118].
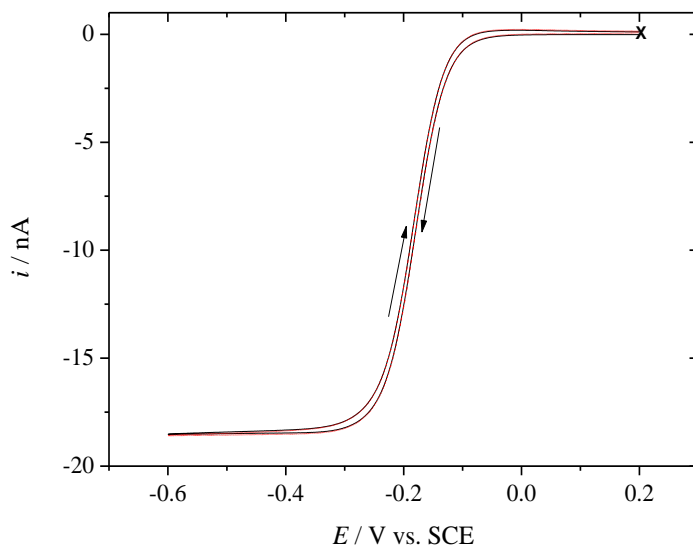
Figure 3.13 Steady state CV in 5 mM Ru(NH$_3$)$_6$Cl$_3$ in 0.5 M KCl solution (deoxygenated with argon) before (solid line) and after (dashed line) normal pulse experiments, using SCE as a reference electrode, Pt microdisc (25 µm Ø) as a working electrode, Pt mesh as a CE at 2 mV s^{-1} at room temperature.

Purposely, steady state linear sweep voltammograms were recorded before and after NPV experiments to assess the condition of the electrode before and after applying this waveform. Figure 3.13 shows that the current response for the reduction of hexaammineruthenium (III) complex ion was the same before and after the NPV experiment. Ideally no difference should be observed since we would not expect a change of surface condition to affect a diffusion controlled process at 2 mV s^{-1}.

The normal pulse voltammetric curves obtained for the reduction of hexaammineruthenium(III) chloride at a platinum microelectrode are shown in Figures 3.14, 3.15 and 3.16 for the range of pulse times 0.003, 0.005, 0.05, 0.02, 0.01, 0.5, 0.2 and 0.1 s and interval time 1 s. As mentioned earlier, pulses of such short duration could be applied because of the very low electrode capacitance [119].
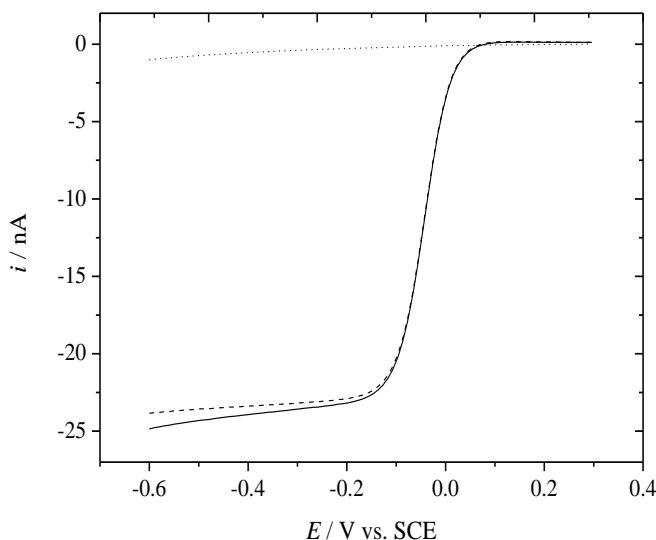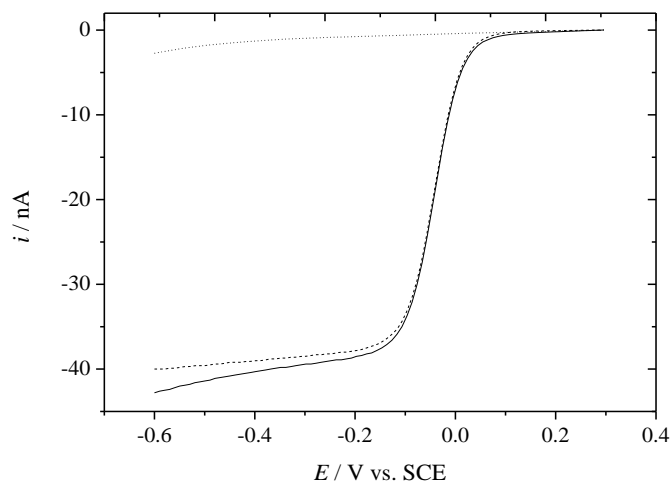

Figure 3.14 NPV in 5 mM Ru(NH$_3$)$_6$Cl$_3$ in 0.5 M KCl solution, background (0.5 M KCl) and corrected NPV (background subtracted), deoxygenated with argon at pulse time = 500 ms and potential increment of 10 mV, using SCE as a reference electrode, Pt microdisc (25 μm Ø) as a working electrode, Pt mesh as a CE at room temperature, background current (……..), corrected current (-------) and uncorrected current (_____).

The NPV was performed in presence and absence of hexaammineruthenium (III) chloride to assess the voltammetric response of the bare electrode. The current response of the background NPV curve is small and increases slightly at the end of the curve in Figure 3.14. At the longest pulse time (500 ms) the magnitude of the background current is low (few nA) and leads to very small difference between the subtracted pseudo steady state voltammogram and the original experimental steady state current; the corrected voltammogram shows a very clear sigmoidal shape.

As the pulse time becomes shorter, 50 ms in Figure 3.15, the magnitude of the background current observed becomes larger and as a result there is a significant difference between the background subtracted CV and un-subtracted experimental one. The background subtracted voltammogram shows a reasonable plateau down to -0.45 V. Below this potential, the subtraction produces a

smaller limiting current. We do not have an explanation for this observation. However, it is possibly the rapid reaction for adsorption of hydrogen which involves more active sites for the reaction to occur in absence of the ruthenium complex ion than in its presence. This background effect takes on a more important role as we pulse to shorter times as shown in Figure 3.16. Therefore, the subtraction is not appropriate since the processes in the background alone and the background with redox species are not the same.

Figure 3.15 NPV in 5 mM Ru(NH$_3$)$_6$Cl$_3$ in 0.5 M KCl solution, background (0.5 M KCl) and corrected NPV (background subtracted), deoxygenated with argon at pulse time = 50 ms and pulse increment of 10 mV, using SCE as a reference electrode, Pt microdisc (25 μm Ø) as a working electrode, Pt mesh as a CE at room temperature, background current (……..), corrected current (-------) and uncorrected current (_____).
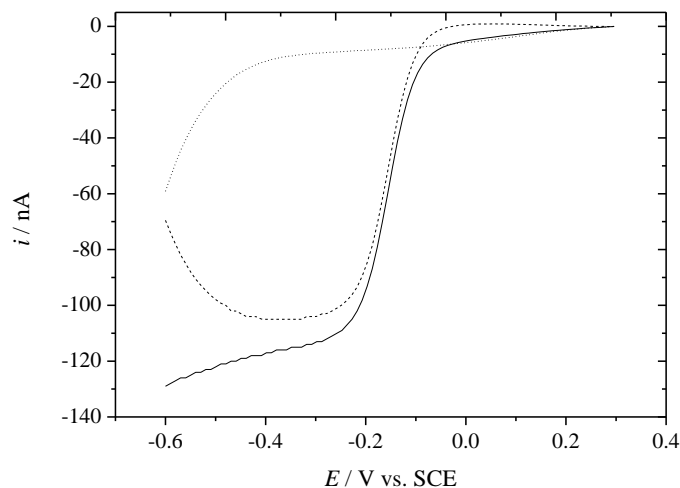
Figure 3.16 NPV in 5 mM Ru(NH$_3$)$_6$Cl$_3$ in 0.5 M KCl solution, background (0.5 M KCl) and corrected NPV (background subtracted), deoxygenated with argon at pulse time = 3 ms and pulse increment of 10 mV, using SCE as a reference electrode, Pt microdisc (25 μm Ø) as a working electrode, Pt mesh as a CE at room temperature, background current (……..), corrected current (-------) and uncorrected current (_____).

At the pulsing time of 3 ms, there is a huge background current compared to the actual NPV with Ru(NH$_3$)$_6^{3+}$, (~ 40 nA at -0.6 V) and the subtraction is clearly not appropriate.   By comparing three time scales 500 ms, 50 ms and 3 ms, we can conclude that the effect of the background becomes more important and possibly the surface process plays an important role as the time scales become shorter. This behaviour can be attributed to surface processes as suggested by the voltammogram in KCl, Figure 3.17 particularly those processes taking place in the potential range where the ruthenium complex ion reduces such as the oxide reduction and the beginning of hydrogen adsorption. At 200 mV s^{-1}, roughly equivalent to a pulse duration of 0.1 s similar background currents to those observed in Figure 3.16 and 3.15 (~4 nA) are seen.
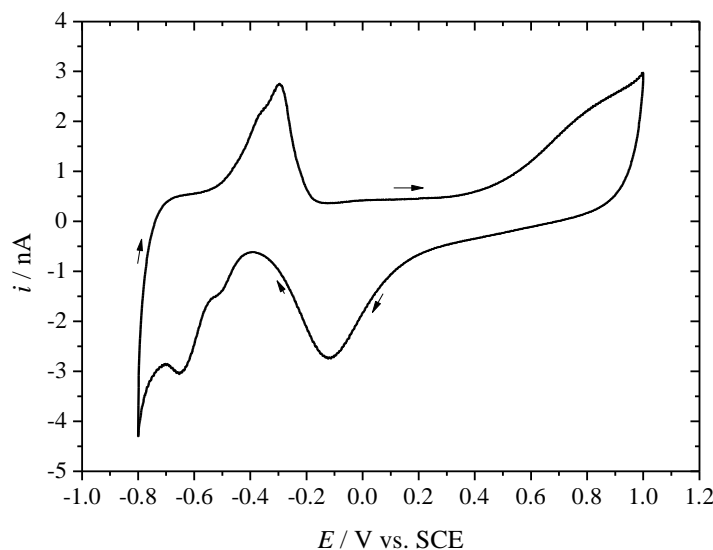
Figure 3.17 Stable cyclic voltammogram, in argon degassed aqueous 0.5 M KCl at 200 mV s^{-1}, after 10 cycles using 25 μm Ø Pt microdisc electrode as working electrode, SCE as RE and Pt mesh as a CE; recorded at room temperature.

By employing the Tomeš criterion of reversibility and the following equation

$$E = E_{1/2} + \frac{RT}{nF} \ln\left\{\frac{i_{\lim} - i}{i}\right\}$$
Equation 3.1

where $E_{1/2}$ is the half wave potential, i , $i_{\lim}$ are the current at any potential and limiting current, n is the number of electrons involved, F is the Faraday constant, T the temperature (K) and R is the gas constant, 8.314 J K^{-1} mol^{-1}, it was found that the reduction of Ru(NH$_3$)$_6^{3+}$ was reversible at all time scales considered.

65

Table 3.1 Different pulse times (τ) used in NPV experiments, corresponding background subtracted experimental pseudo steady state currents, $E_{1/4}$, $E_{3/4}$ and $E_{3/4}$-$E_{1/4}$. All potentials are with respect to the SCE.

τ / s	0.5	0.2	0.1	0.05	0.02	0.01	0.005	0.003
i_{lim}/ nA	- 21.8	- 25.7	- 30.2	- 36.8	- 49.7	- 63.1	- 80.9	- 99.1
$E_{1/4}$/ V	- 0.217	-0.217	-0.217	-0.217	-0.217	- 0.217	- 0.217	-0.217
$E_{1/4}$/ V	- 0.157	-0.157	-0.157	-0.157	-0.157	- 0.157	- 0.157	-0.157
$E_{3/4}$-$E_{1/4}$/ V	-0.060	-0.060	-0.060	-0.060	-0.060	-0.060	-0.060	-0.060

In Table 3.1, $E_{1/4}$ and $E_{3/4}$ are identical at all τ because the NPV is recorded with 10 mV increments. i_{lim} was measured at the plateau, at -0.45 V. The applicability of Equation 1 (Shoup-Szabo Equation) for chronoamperometry at stationary disc microelectrodes was checked using the reduction of $Ru(NH_3)_6Cl_3$ (in KCl) at platinum microelectrodes. By using the Shoup-Szabo Equation, we can estimate the number of electrons involved in the reduction at different time scales, as shown in Table 3.2. The calculated n_{app} are obtained by dividing the experimental current by the theoretical current (Shoup-Szabo values) on the plateau at different time scales. This can give us an indication of the efficiency of this technique to acquire data free from background or capacitive current. Since the reduction of $Ru(NH_3)_6^{3+/2+}$ is a fast one electron outer sphere process, the expected value of electrons should be one electron at all time scales.

The application of this technique to the one electron reduction of $Ru(NH_3)_6^{3+}$ was not as successful as expected. The results shown in Figures 3.14, 3.15 and 3.16 above presented the *i-E* curves derived from NPV experiments at different time regimes. These and others recorded for a range of pulse times were analysed to determine n_{app}. The value of the diffusion coefficient used in the theoretical current calculation was 7.4×10^{-6} cm^2 s^{-1}.

Table 3.2 Different pulse times (τ) used in NPV experiments, the corresponding background subtracted experimental pseudo steady state current (i_{lim}) and the number of electrons involved (n_{app}), using Shoup-Szabo equation ($D = 7.4 \times 10^{-6}$ cm^2 s^{-1}) and background substracted current to obtain n_{app} for the reduction of $Ru(NH_3)_6^{3+}$.

τ / s	0.5	0.2	0.1	0.05	0.02	0.01	0.005	0.003
i_{lim}/ nA	- 21.8	- 25.7	- 30.2	- 36.8	- 49.7	- 63.1	- 80.9	- 99.1
n_{app}	0.9	0.9	1.0	1.0	1.1	1.1	1.1	1.1

From the findings obtained for n_{app} for the $Ru(NH_3)_6^{3+}$ reduction, Table 3.2, where the limiting current was measured at -0.45 V, we observe a trend in the calculated n_{app}. There is a systematic

variation in the number of electrons involved; within 10%, which indicates that there is still a problematic issue with this technique, despite the background subtraction.

In Figure 3.18 the results shown in Table 3.2 have been plotted against $(t_{pulse})^{-1/2}$ and are compared with the expected diffusion controlled current calculated with $n=1$, $D = 7.4 \times 10^{-6}$ cm^2 s^{-1}, $c^\infty = 5 \times 10^{-6}$ mol s^{-1} and $a = 12.5 \times 10^{-4}$ cm. The figure clearly shows that the pseudo limiting current recorded from the background subtracted NPV voltammograms is systematically larger than the expected diffusion controlled current.
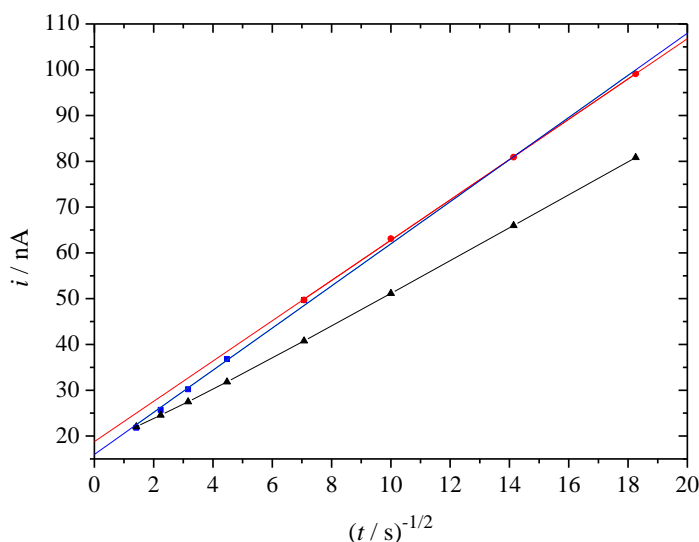
Figure 3.18 Relationship between limiting current and $t_{pulse}^{-1/2}$ extracted from background subtracted NPV experiments run in argon degassed aqueous 5 mM Ru(NH$_3$)$_6$Cl$_3$ in 0.5 M KCl using 25 μm Ø Pt microdisc electrode as working electrode recorded at room temperature. The black line represents experimental data whereas the red and the blue lines are for the Mahon-Oldman theoretical current and background subtracted experimental respectively.

3.4 Application of a conditioning waveform

In Figure 3.19, a sawtooth waveform is shown. Preconditioning sweeps include sweeping from the onset of oxide formation potential + 0.3 V as in step 1, 3 and 5 to – 0.7 V, a potential that removes the oxide previously formed and promotes hydrogen adsorption as in step 2, 4 and 6. The sweep rate used for positive and negative sweep directions was 500 mV s^{-1}. This sweep rate was chosen to be comparable to that used for conventional voltammetry in acid; no attempt was made to optimize this sweep rate in terms of its effects on the conditioning. This is repeated several times and then the electrode is allowed to rest at a potential of 0 V (10 s) as in step 7, where there is no

formation of oxide and no hydrogen left on the electrode. Finally, this is followed by a 0.5 s step to a given potential within the potential range of interest, (as in step 8). In order to construct a sampled current voltammogram, the whole waveform is repeated without changing any of the parameters except the potential of the final step. It should be emphasised that the designed waveform is in fact NPV with conditioning procedures embedded between each step. Hence the current transient sampled at high frequency (typically one data point every 0.1 ms) throughout the duration of the last step produces a chronoamperogram. For each potential of interest, the whole waveform was repeated ten times and the current transient was taken as an average of the ten measurements. These were therefore recorded without any treatment of the electrode other than that provided by the sweeps/rest/step waveform before each step. The averaged amperometric current (last step in the applied waveform) measured at each potential was then sampled at different fixed times. The voltammograms were reconstructed at fixed times along the wave from -0.7 V to 0.3 V and compared with theory. By employing the conditioning waveform, the electrode should be in a pristine condition; every point of the voltammogram is recorded under the same conditions and the order with which the potential steps are performed (equivalent to the direction of the scan in NPV) no longer matters. The resting potential was chosen to be held in the double layer region to ensure a complete reduction of any surface oxide, the desorption of hydrogen and no consumption of the ruthenium complex.
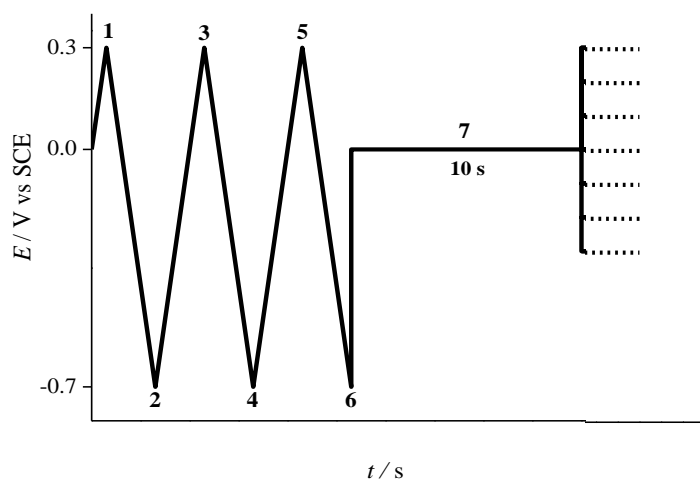
Figure 3.19 The conditioning waveform used includes sweeps and steps to acquire the current transient and construct a sampled current voltammogram. Sweeps 1-6 (at 500 mV s^{-1}) are for preconditioning, step 7 for resting and step 8 for measuring. The dashed square indicates where the current is extracted to reconstruct voltammograms.

In order to assess the efficiency of the conditioning sawtooth waveform and its effect on the background current it was applied to the reduction of the ruthenium hexaammine complex. Since it undergoes a fast one electron transfer process the analysis of the reconstructed voltammograms should yield n_{app} equal to 1 at all sampling times; any deviation from this should reflect the role of additional processes. Current transients at different potentials along the reduction wave of $[Ru(NH_3)_6]^{3+}$ in KCl system were recorded after applying the sawtooth waveform. Three separate current transients were analysed: the total current transient ($[Ru(NH_3)_6]Cl_3$ / KCl system), the background (degassed KCl electrolyte) current transient and the background subtracted transient current (faradaic current of $[Ru(NH_3)_6]Cl_3$ only).

Throughout this work, all experiments were recorded using a 25 μm diameter Pt microdisc microelectrode. In Figure 3.20, the potential was scanned between 0.2 V and -0.6 V, forward and backward at 10 mV s^{-1} to record the reduction of $[Ru(NH_3)_6]^{3+}$ to $[Ru(NH_3)_6]^{2+}$ before and after applying the conditioning waveform described earlier (Figure 3.19). One can notice almost similar responses in scans between the two curves presented, before and after application of the conditioning waveform. The response obtained after applying the whole measurement results in no hysteresis between forward and backward scans, but it was found that a slight increase in limiting current occurred after applying the conditioning waveform. That might be due to not maintaining the temperature exactly at 25ºC during the recording of all the chronoamperograms for the different potentials. It is well known that the diffusion coefficient of the redox couples and subsequently the limiting current depend on temperature.
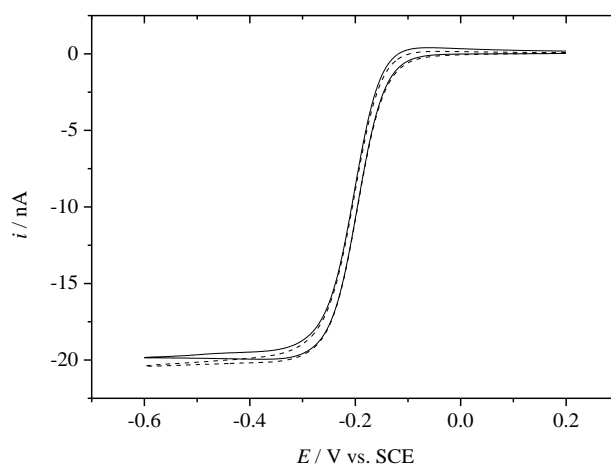
Figure 3.20 Steady state voltammograms recorded at 10 mV s^{-1} at a 25 μm Pt microdisc microelectrode at 25˚C in argon degassed 5 mM Ru(NH$_3$)$_6$Cl$_3$/ 0.5 M KCl before (solid line) and after (dashed line) applying the sawtooth preconditioning waveform. A Pt mesh acts as a counter electrode.

Also, another voltammetric study in 0.5 M KCl background (electrolyte) was carried out until a reproducible voltammogram of the expected form was recorded, as shown in Figure 3.21. Then, application of the conditioning waveform under the same experimental conditions of that for [Ru(NH$_3$)$_6$]Cl$_3$ / KCl system was performed as it was described previously (Figure 3.19). The similarity in responses before and after application of the conditioning waveform is clear. Although the whole applied conditioning waveform was repeated 10 times for each measurement, there was no evidence of roughening (e.g. increased peak heights) at the electrode surface in this experiment.
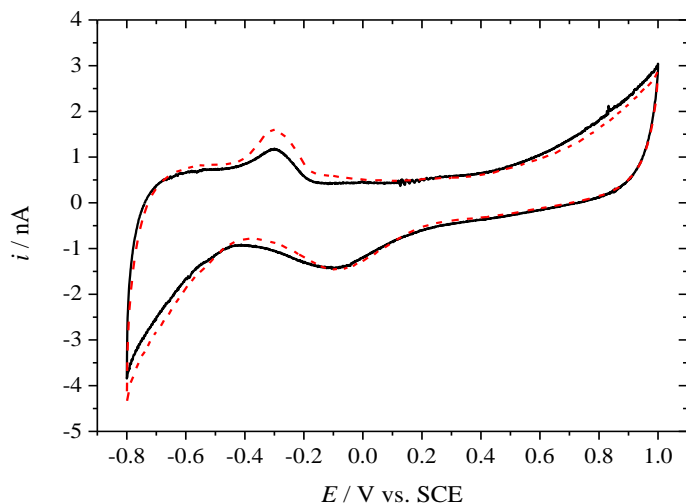
Figure 3.21 Cyclic voltammograms at 200 mV s^{-1} in argon degassed 0.5 M KCl before (solid black line) and after (dashed red line) applying the sawtooth conditioning waveform. A Pt mesh acted as a counter electrode and a 25 μm diameter Pt microdisc as a working electrode.

3.5 Sampled current voltammograms

The waveform shown in Figure 3.19 was used and sampled current voltammograms for both the [Ru(NH$_3$)$_6$]Cl$_3$ / KCl system and the background (KCl degassed electrolyte) were reconstructed. The reduction wave for [Ru(NH$_3$)$_6$]$^{3+}$ system was reconstructed by recording the transient current with an acquisition rate of 0.0001 s (step 8 in the sawtooth waveform shown in Figure 3.19) at different measuring potentials between -0.7 V and +0.3 V at fixed times. Figure 3.22 shows the ruthenium complex reduction voltammograms reconstructed at the following sampling times, 0.003, 0.005, 0.01, 0.02, 0.05, 0.1, 0.2 and 0.5 s. It is clear that the amperometric current obtained

in the last measuring step depends on the measuring potential. At -0.6 V the mass transport limitation of ruthenium hexaammine takes place, as observed with steady state voltammetry at 2 mV s^{-1}, Figure 3.13). As time becomes shorter, the wave becomes slanted for potentials below -0.5 V and the current increases. This is probably due to some surface process like the adsorption of hydrogen which occurs below -0.5 V as shown in Figure 3.17.
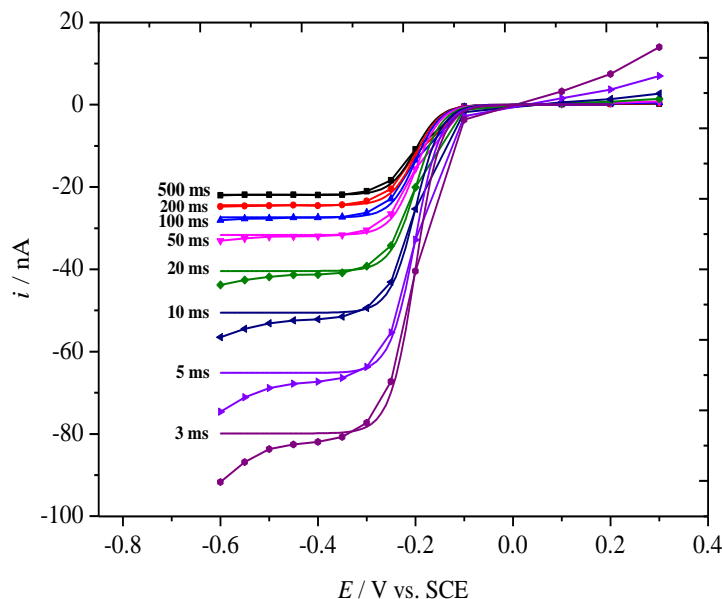
Figure 3.22 Theoretical and experimental sampled current voltammograms at fixed sampling times extracted from amperometric transients (step 8) at different potentials after applying the sawtooth waveform (sweeps from 0.3 V to -0.7 V), followed by a 10 s resting step at 0 V; 5 mM Ru(NH$_3$)$_6$Cl$_3$ / 0.5 M KCl at 25 μm diameter Pt microdisc. No background current has been subtracted. The theoretical currents were calculated with Equation 3.2 and $n=1$, $D = 8.2 \times 10^{-6}$ cm^2 s^{-1}, $c^\infty = 5 \times 10^{-6}$ mol cm^{-3} and $a = 12.5 \times 10^{-4}$ cm.

As this system involves the transfer of one electron during its reduction, the calculated number of electrons involved should be one over the time scales considered. As before, n_{app} was estimated by dividing the current sampled at each potential with the theoretical diffusion controlled current for the particular sampling time and potential calculated with the modified Shoup-Szabo equation – Equation 3.2.

$$i = 4nFDc^{\infty *}a \left\{ \begin{array}{l} 0.7854 + 0.4431\left(\dfrac{D_A t}{a^2}\right)^{-1/2} \\ + 0.2146\exp\left[-0.3912\left(\dfrac{D_A t}{a^2}\right)^{-1/2}\right] \end{array} \right\} * \dfrac{1}{1+\exp(\dfrac{nF}{RT} * (E_{1/2} - E))} \qquad \text{Equation 3.2}$$

F is the Faraday constant, D and c^∞ are the diffusion coefficient and the bulk concentration of the species, respectively, a is the radius of the disk electrode, t is the sampling time, E is the potential to where the electrode was stepped and $E_{1/2}$ is the half wave potential for the reduction wave. The parameters used were $D = 8.2\times10^{-6}$ cm^2 s^{-1} at 298 K [120], $c^\infty = 5\times10^{-6}$ mol cm^{-3}, $a = 12.5\times10^{-4}$ cm, $n = 1$ and t is various times such as 0.003, 0.005, 0.01, 0.02, 0.05, 0.1, 0.2 and 0.5 s.

Compared with the previously used techniques (potential step experiments and NPV), it is clear that the conditioning waveform has significantly improved the chronoamperometric response of the microdisc. Figure 3.22 shows there is very good agreement between experiment and theory down to 10 ms. However, despite using the preconditioning waveform before recording the chronoamperometric transients, some background current still contributed to the reduction current and could be responsible for the deviation between theory and experimental transients. Therefore, correcting reconstructed voltammograms by subtracting the background current from the total may be more efficient in discriminating any extra current especially at short times, when the effect of the background current is significant. However, Figure 3.23 shows that background subtraction produces worse results than with the reconditioning waveform alone. This is particularly the case for very short times where the background subtracted current is well below the expected theoretical value. Basically, even the subtraction of the current transients recorded in absence of the ruthenium complex does not improve agreement with the theory, Figure 3.23. This again suggests that the rates of the background processes in presence of the ruthenium complex are lower than those in absence of the complex. It is worth recalling that the sampling times chosen, 500, 200, 100, 50, 20, 10, 2 and 1 ms respectively correspond to 0.05, 0.13, 0.26, 0.51, 1.3, 2.6, 13 and 26 V s^{-1} when using voltammetry. For these rather low scan rates the reduction of the ruthenium complex is known to be diffusion controlled.
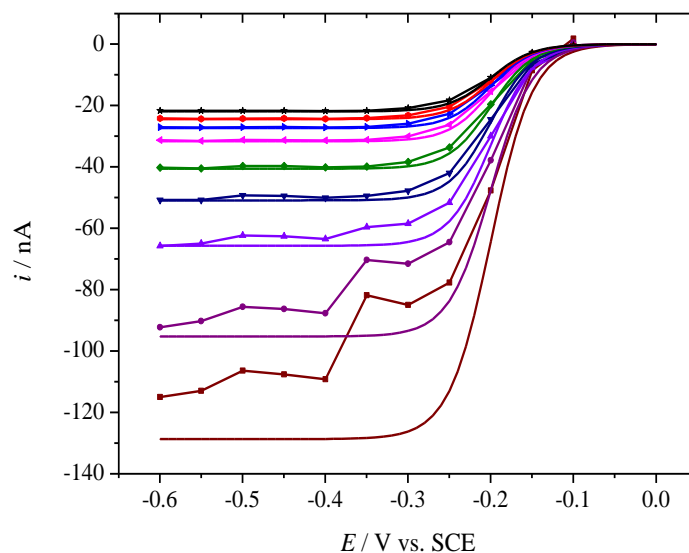
Figure 3.23 Theoretical and experimental background subtracted sampled current voltammograms for the reduction of ruthenium complex ion (5 mM in 0.5 M KCl) at different fixed times extracted from amperometric transients at different potentials after applying a sawtooth conditioning waveform (sweeps from 0.3 V to -0.7 V), followed by a 10 s resting step at 0 V. From top to bottom sampling times are 500 (black), 200, 100, 50, 20, 10, 5, 2 and 1 ms (brown).

Figure 3.24 shows a comparison of current transients obtained at E= -0.6 V on the plateau for the ruthenium complex reduction. The figure presents the average of ten current transients against the theoretical transient (this time calculated with the Mahon Oldham Equation- Equation 1.2), the background subtracted transient, and the background alone current. It clearly shows that good agreement between the current is obtained down to 1 ms sampling time.

To clarify the effect of the conditioning waveform on the response obtained, normalised sampled current voltammograms were plotted in Figure 3.25. Normalisation was obtained by dividing the experimental sampled currents for each potential by the theoretical diffusion controlled current. Interestingly, all normalised sampled current voltammograms at various timescales collapse onto the theoretical curve. This agreement is still reasonable up to 1 ms timescale. This is a remarkable improvement in contrast with the normalised voltammograms recorded without preconditioning waveform, Figure 3.12. Again, this result is much better than the data with background subtraction. Clearly, the normalised SCVs reflect the marked effect of the conditioning waveform in achieving a clean surface. It can be seen that all timescales SCVs superimposed onto the theoretical curve except for 1 ms sampling time.
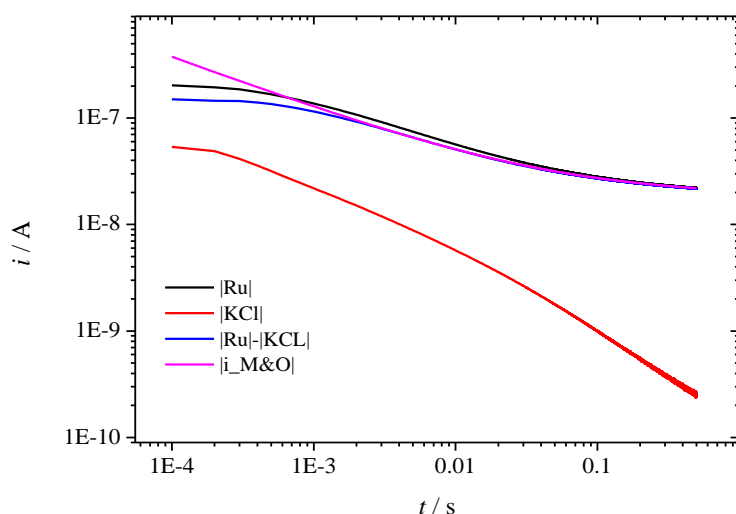
Figure 3.24 Average of 10 current transients at -0.6 V (vs SCE) in 5 mM ruthenium hexaammine in 0.5 M KCl after applying a sawtooth conditioning waveform (sweeps from 0.3 V to -0.7 V), followed by a 10 s resting step at 0 V. In each case the absolute value of the currents is plotted. The parameters used for theory were $D = 8.2 \times 10^{-6}$ cm^2 s^{-1} at 298 K [120], $c^{\infty} = 5 \times 10^{-6}$ mol cm^{-3}, a = 12.5$\times 10^{-4}$ cm, $n = 1$.
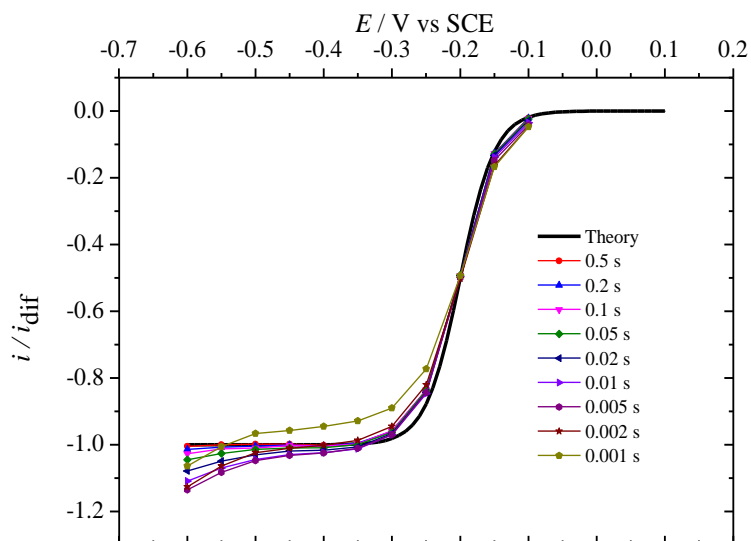
Figure 3.25 Normalised sampled current voltammograms (symbols) recorded with the preconditioning waveform. Theoretical CV (solid line) drawn from Mahon-Oldham equation using the following parameters $n=1$, $D=7.35 \times 10^{-6}$ cm^2 s^{-1}, a=12.5 µm, c^{∞}=5 mM, E_0=−0.2 V. No subtraction of the background (argon degassed KCl) transients was done. The vertical axis could be read as n_{app}, since the experimental plateau current at different timescales was normalised by the diffusion controlled current for n=1.

74

3.6 Conclusion

The reduction of the ruthenium hexaammine cation was chosen as a model system due to its fast kinetics and similarity in the potential window as the ORR. Many techniques were employed to investigate its reduction at short time scales. Voltammetry for the reduction of the ruthenium complex showed an increase in peak current with the scan rate and of the magnitude of the background current. There was a deviation from the expected relationship between square root of the scan rate and the cathodic peak for the reduction of ruthenium complex ion at fast measurements. The reason for that is unknown.

Potential step experiments with no pretreatment were applied; there was a clear trend in the plateau current moving away from the theory. Even when normalising the experimental current at different sampling times by the diffusion controlled current, sampled current voltammograms did not collapse onto one curve, indicating the effect of the condition of the electrode surface. NPV was then applied with various sampling times and a trend in the increase of the number of electrons involved in the reaction was seen; this is presumably due to some surface processes taking place at the same potential range as the reduction of ruthenium complex ion such as the adsorption of hydrogen and the reduction of platinum. In this case, the background subtraction was reasonably efficient.

Therefore a conditioning waveform was applied which includes preconditioning sweeps, resting and measuring step. The conditioning and measuring procedure was repeated 10 times for each potential and the averaged current transient was sampled at fixed timescales. The reconstructed current response for the ruthenium reduction is in a good agreement with theory down to 2 ms sampling times and indicates the ability of the applied waveform in conditioning the electrode without any need for background subtraction. The calculated number of electrons involved was one at all timescales. By normalising the pseudo steady stated current at different timescales by the diffusion controlled current, a collapse of all sampled current voltammograms onto the theoretical one was seen.

Since the applied conditioning waveform works well with a model system, such as ruthenium hexaammine reduction and produces a sampled currents in agreement with theory and $n_{app} = 1$ at all timescales, the experimental approach and data analysis presented in this chapter were used to investigate the ORR. The results of these investigations are presented in the next chapter.

Chapter 4

Transient studies of the oxygen reduction reaction

4 Overview

This chapter considers the ORR on platinum and gold microdisc electrodes. The electrochemical reduction of molecular oxygen is studied using different techniques: voltammetry, amperometry, conditioning waveform coupled with potential single step or double potential steps and Electrochemical Quartz Crystal Microbalance (EQCM). The same strategy as for the ruthenium hexaammine system is applied to the ORR investigations. In particular, sampled current voltammograms are used to determine n_{app} as a function of time and to assess the efficiency of the conditioning waveform. Different electrolytes are considered to probe the effects of anions adsorption during the reduction of oxygen.

4.1 Voltammetry in chloride solutions

Oxygen reduction was investigated by cyclic voltammetry in solutions containing 0.5 M aqueous NaCl with 25 μm diameter Pt microdisc electrodes and scanning at 200 mV s^{-1} between -0.85 V and 1.1 V (vs. SCE). The solution was deoxygenated with argon and a series of background voltammograms (absence of O_2 species) was recorded. The solution was then bubbled with compressed air and the voltammograms for the ORR wave recorded. A typical stable response recorded after approximately ten cycles for both aerated and argon degassed solution is shown in Figure 4.1 for NaCl and 4.2 for KCl. As noticed by Sotiropoulos [12], the repetitive potential cycling of Pt microelectrodes in neutral, unbuffered solutions of NaCl (or KCl) shows markedly different hydrogen adsorption/desorption regions in presence and absence of oxygen as shown in Figure 4.1 and 4.2 [12]. In absence of oxygen the hydrogen desorption peaks occur at more positive potentials than in presence of oxygen. The hydrogen adsorption peaks are also affected

but to a lesser extent. Similarly the Pt oxide reduction peaks is shifted to more negative potentials in presence of oxygen. These observations are consistent with changes in the local pH as if the reduction of oxygen was buffering the solution close to the electrode at a pH slightly more alkaline than that of the bulk solutions. This is expected in the potential region where the ORR occurs because the reaction consumes H^+ and produces OH^-. See ref [38] for an SECM study of the PH changes that accompany redox processes at the surface of a Pt electrode.

In general, the voltammograms in KCl are similar to those in NaCl for both aerated and deoxygenated cases. The hydrogen adsorption/desorption peaks are not as pronounced as those in acid, this effect is possibly due to the blockage by chloride ions which adsorb over most of the potential window [60].

In both NaCl and KCl the aerated solutions show that the reduction of oxygen occurs in the same potential region as that for the platinum oxide reduction in degassed solution. Clearly the reduction of the oxide will affect ORR mechanism because the electrode surface will change from being oxide covered to oxide free during the course of the oxygen reduction. A special conditioning waveform needs to be designed to eliminate the oxide stripping process during the ORR.

The cathodic reduction of oxygen in neutral sodium chloride and potassium chloride solutions was also investigated by cyclic voltammetry at low scan rate. A stable and typical voltammetric response obtained after 5 – 10 full cycles is shown in Figure 4.3. A well-formed reduction wave in air-saturated aqueous solution of 0.5 M NaCl was observed and a well-defined limiting current plateau was obtained. The response shown was recorded at 10 mV s^{-1}, after the electrode had been pretreated as described in section 2.3 (Chapter 2). In KCl, the ORR voltammogram is similar although the H$_2$ evolution occurs at slightly more negative potential than in NaCl.

While a well-defined diffusion limited current is easily obtained, one can observe that unlike for purely diffusion controlled reactions such as the reduction of hexaammineruthenium (III) chloride (Chapter 2 - Figure 2.5) the forward and reverse scans cross in two places along the O$_2$ reduction waves in Figure 4.3. These correspond to the crossings seen in Figure 4.1b. Clearly, the hysteresis between forward and backward sweeps reflects the evolution of the electrode surface and suggests that the ORR occurs on different surfaces during the voltammogram. As demonstrated by Sotiropoulos [12], the number of cross-overs and the hysteresis between the scans reflect the

sensitivity of oxygen reduction to the surface state of the platinum electrode. The sensitivity results from the initial step of oxygen adsorption and from the presence of adsorbed reaction intermediates. Our results agree with Sotiropoulos's explanation for the same steady state CV in 0.5 M KCl / NaCl regarding the role of major factors such as scan rate and potential limits for the observed voltammetric behaviour [12]. Some authors suggested that the cross-over is attributed to the place exchange of atoms in the oxidised metals.
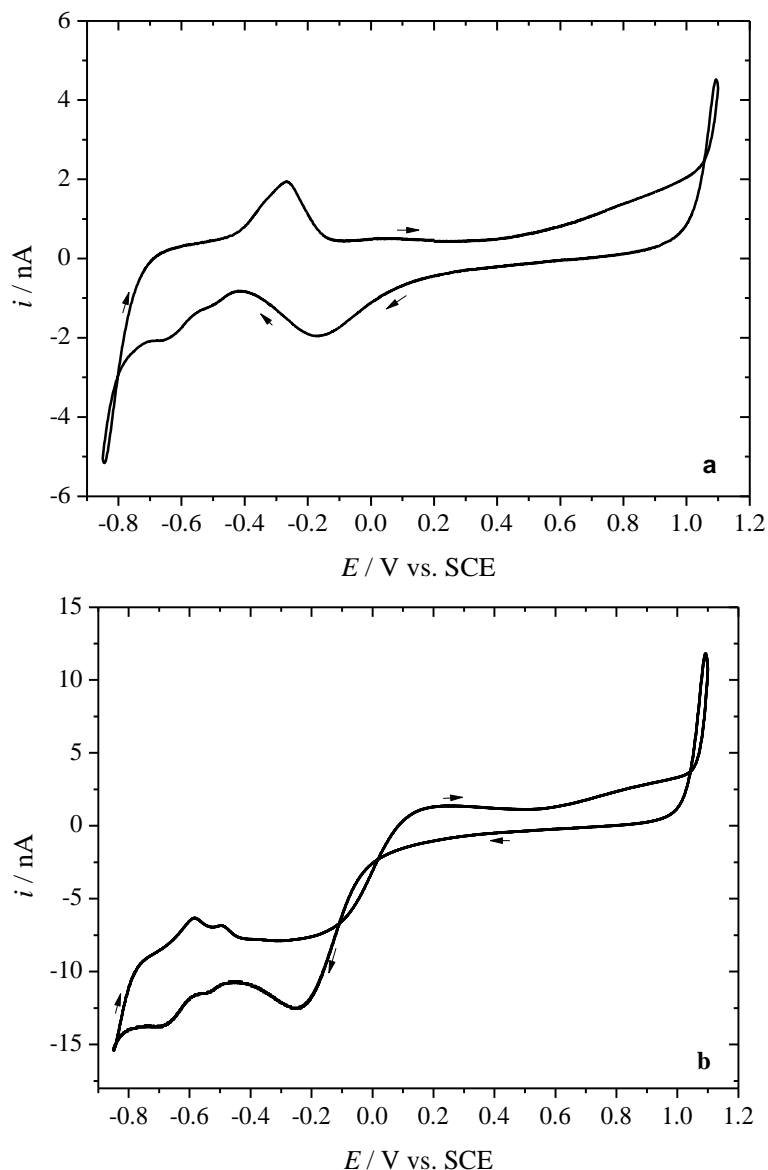
Figure 4.1 Stable cyclic voltammograms, in a) deoxygenated (with argon) and b) air saturated aqueous 0.5 M NaCl at 200 mV s^{-1}, after 5 cycles using a 25 μm diameter Pt microdisc electrode as working electrode and recorded at room temperature.
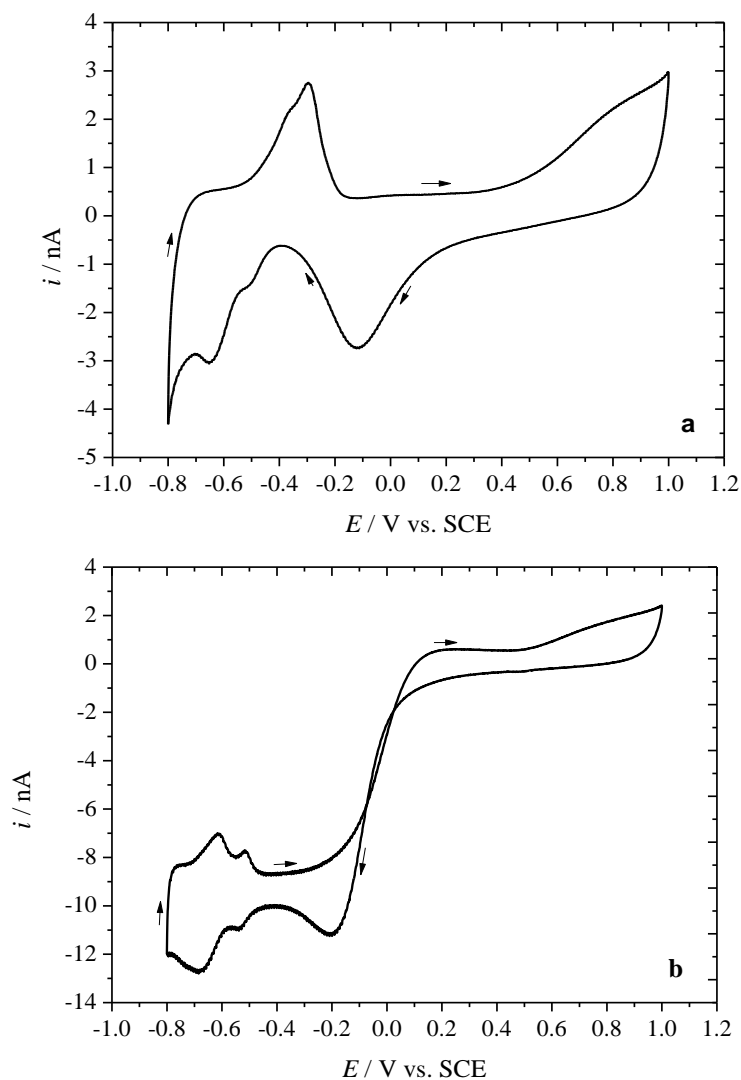
Figure 4.2 Stable cyclic voltammograms, in a) argon degassed and b) aerated aqueous 0.5 M KCl at 200 mV s^{-1}, after 10 cycles using a 25 μm diameter Pt microdisc electrode as working electrode and recorded at room temperature.
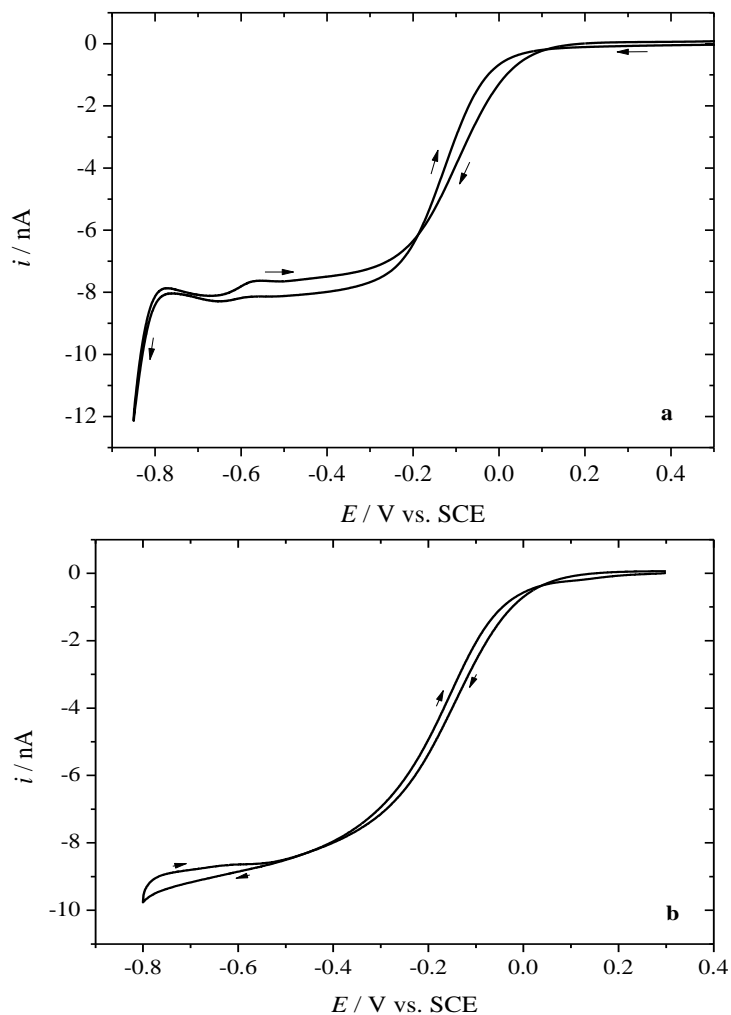
Figure 4.3 Stable steady state voltammograms in aerated aqueous 0.5 M NaCl (a) and 0.5 M KCl (b), using a 25 μm Ø Pt microdisc electrode as working electrode and respectively recorded at 10 mV s^{-1} and 20 mV s^{-1} at 25ºC.

4.2 Cyclic voltammetry of the background (argon degassed KCl)

This section investigates the background surface processes as a function of scan rates in absence of O$_2$, using cyclic voltammetry. Voltammograms were recorded in argon degassed 0.5 M KCl using a PGSTAT30 Autolab (Eco-Chemie, Utrecht, The Netherlands) with an analog ramp generator. An ADC 750 module was coupled with the scan generator to achieve high speed

measurements. Linear CVs are shown in Figures 4.4. Since the current is normalized by the scan rate, it is expected that all peaks should have the same height. At low scan rates, while the peak position barely changes, the normalized heights were found to vary with scan rates, in particular for the oxide reduction and hydrogen adsorption peaks. At large sweep rates, there are considerable shifts in peak position for hydrogen desorption; this is possibly due to changes in surface in pH. These observations agree with Pletcher and Sotiropoulos findings [101]. But the most striking feature is the variation of peak heights with scan rates shown in Figure 4.4. Above 2 V s^{-1}, the peak currents become smaller than expected from the normal linear relationship observed at lower sweep rates. On voltammograms recorded at higher scan rates (up to 10 kV s^{-1}) it was not possible to distinguish the peak currents for the surface processes from the double layer charging current. We have no explanation for these observations and have not found relevant articles for high speed voltammetry of platinum electrodes in neutral aqueous media.
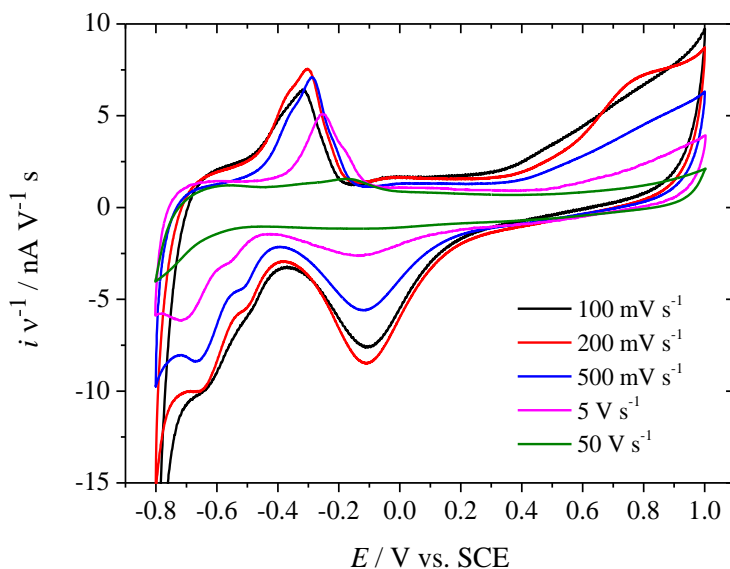
Figure 4.4 Normalised linear cyclic voltammograms at a 25 μm diameter Pt microdisc electrode in 0.5 M KCl (purged with argon) recorded at different scan rates, at room temperature.
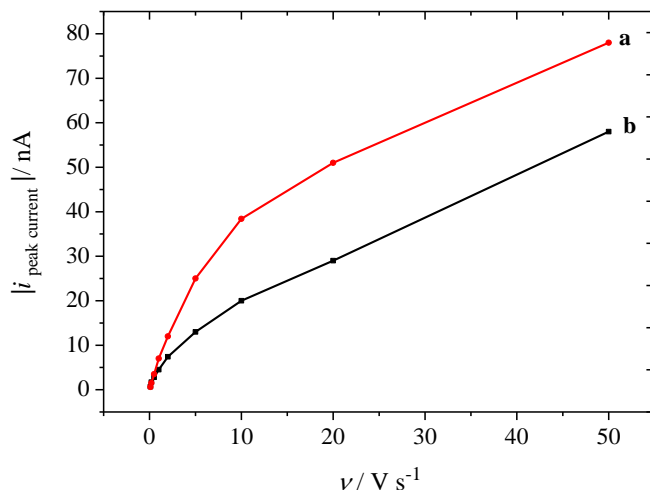
Figure 4.5 Plots of the peak currents for a) H desorption and b) Pt oxide reduction against the potential sweep rate recorded on a 25 μm diameter Pt disc electrode in 0.5 M KCl, argon purged. Data taken from Figure 4.4.

4.3 ORR investigations

4.3.1 Potential step experiments at Pt electrode

Similar to the ruthenium hexaammine system (Chapter 3), a chronoamperometric technique was employed to study the ORR at Pt microdisc. A series of potential step experiments was applied to investigate the ORR and the background (absence of oxygen species). No pretreatments were done except polishing the electrode at the beginning of the experiments to start with a fresh surface. The potential was stepped from 0 V (where no current flows) to various potentials along the ORR wave. The average of three amperometric responses was calculated for each potential considered. Then the current was sampled at various time scales and the sampled current voltammograms were reconstructed and plotted for the ORR raw data and the background (absence of oxygen species) as shown in Figure 4.6.

Figure 4.6a clearly shows that even in absence of O_2 large currents are obtained at short times. The magnitude of these currents is comparable to the faradaic currents due to oxygen reduction for the same sampling times. In presence of O_2, the reconstructed voltammograms present defined sigmoidal shapes. As expected the oxygen reduction currents increase with shorter sampling times but the waves appear more drawn out, therefore indicating the irreversibility of the ORR. Below - 0.6 V the increase in current seen at short times is attributed to the adsorption of hydrogen.
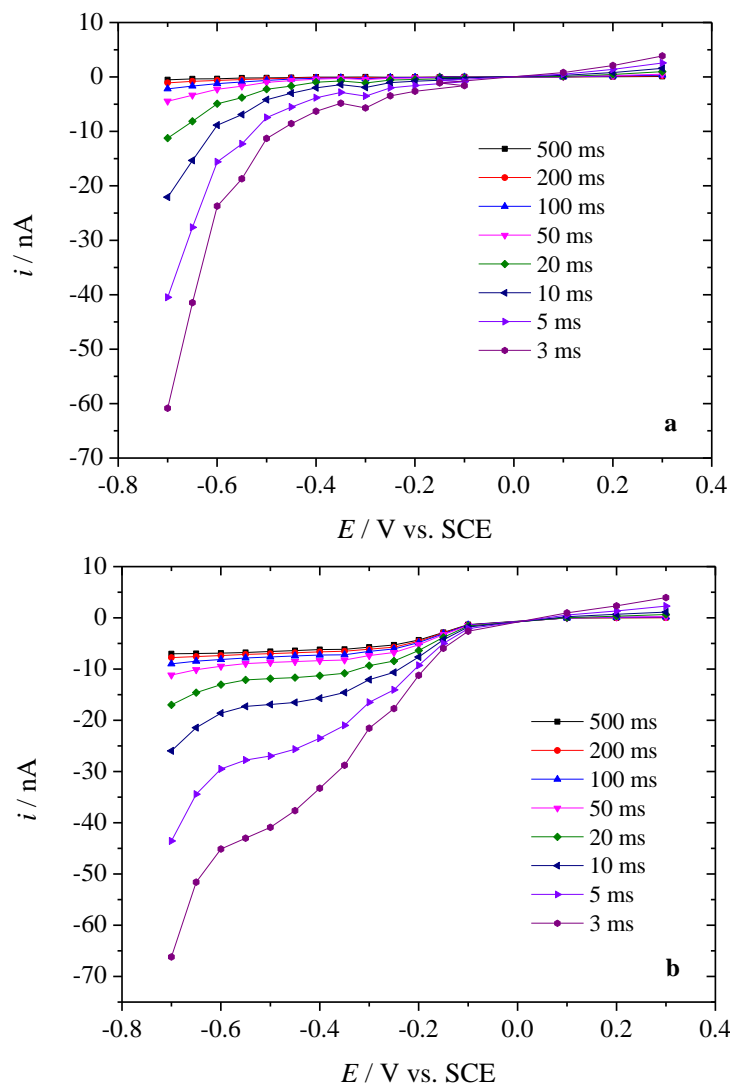
Figure 4.6 Reconstructed sampled current voltammograms recorded in 0.5 M KCl in absence a) and presence b) of O_2 with 25 μm diameter Pt disc, a Pt mesh counter electrode and SCE reference electrode. The chronoamperograms were obtained by stepping from 0 V to selected potentials along the ORR wave. The sampling times are shown in the legend 500, 200, 100, 50, 20, 10, 5 and 3 ms. No pretreatment or preconditioning was carried out except the polishing of the electrode at the beginning of the experiment.

The sampled current voltammograms shown in Figure 4.6 were normalised by dividing all current values with the diffusion controlled theoretical current calculated from Equation 1.2 using n=1, D = 2.2x10^{-7} cm s^{-1}, c^{∞} = 2.2x10^{-5} mol cm^{-3}, a = 12.5 μm and t equal to the relevant sampling time. The normalised sampled current voltammograms are shown in Figure 4.7. Since the currents are effectively time normalised the vertical axis can be considered as the value for n_{app}, the apparent

number of electrons for the reaction. At long sampling times n_{app} approximates 3 in an agreement with the value determined by Sosna using steady state measurements [11]. However at short sampling times n_{app} is much larger than expected.

In view of the dependence of n_{app} on the steady state mass transfer coefficient at microdisc [23, 39] and rotating disc electrodes [39] we would have expected n_{app} to decrease from the value found at steady state (~3.3 for a 25 µm diameter disc, [11]) to 2 as the transient mass transfer coefficient increased at shorter sampling times. This increase in the number of electrons with shorter sampling times must reflect an additional faradaic process, presumably from species adsorbed on the electrode.
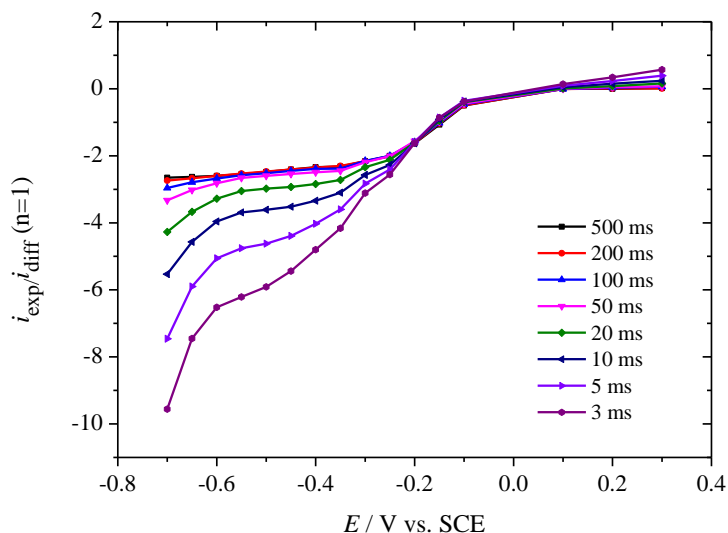
Figure 4.7 Normalised reconstructed sampled current voltammograms for the ORR in 0.5 M KCl. The working electrode is a Pt 25 µm diameter and the counter electrode is Pt mesh. $E_{start}= 0$ V. No pretreatment or preconditioning was carried out except the polishing of the electrode at the beginning of the experiment. The diffusion controlled theoretical current was calculated with Equation 1.2 using $n=1$, $D = 2.2 \times 10^{-7}$ cm s^{-1}, $c^{\infty} = 2.2 \times 10^{-5}$ mol cm^{-3}, $a = 12.5$ µm and t equal to the relevant sampling time. The sampling times are shown in the legend.

The following section focuses on an alternative approach, Normal Pulse Voltammetry, to allow preconditioning of the electrode before each measurement.

4.3.2   Normal Pulse Voltammetry (NPV)

The NPV technique was employed to create pseudo stationary voltammograms in a more automated way than sampled current voltammetry and to determine conditions for a good cleaning

waveform for the ORR investigation. The values of the electrode potentials selected for the normal pulse experiments were in the range -0.8 to 1 V, and the electrode was tested between these potentials to assess the kinetics of the reduction of oxygen in 0.5 M KCl. Figure 4.8 shows a typical NPV waveform where a sequence of potentials is applied to the electrode and the current is measured at the end of each pulse.
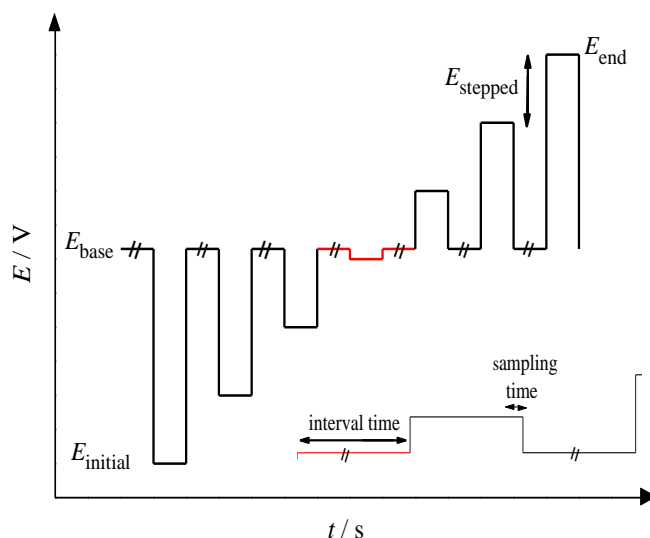

Figure 4.8 Schematic of a typical NPV waveform.

4.3.2.1 Effect of E_{base}

The influence of a range of experimental parameters such as E_{base}, the potential applied before each pulse was assessed. In order to obtain minimal background signals and maximum measured current output, E_{base} (also known as rest potential) should be chosen carefully in NPV. E_{base} is chosen to be where no signal is expected for the redox system. Hence the zero current is expected at this potential. Several trials were undertaken to assess the best E_{base} to be chosen for 0.5 M KCl. Ideally E_{base} should be such that no oxide is formed or reduced. At this potential, the history of the electrode should remain the same before each measurement to obtain a background free current response at each measuring potential.

Figures 4.9, 4.10 and 4.11 show different possibilities to record the NPV voltammogram depending on E_{base} and the initial scan direction. Choosing E_{base} to be -0.8 V was not as successful as the electrode was left with some hydrogen on it. Similarly, choosing $E_{base} = 1$ V left the electrode with some oxide coverage. Therefore, E_{base} was chosen within a narrow window in the

double layer region to have an oxide-free and hydrogen-free electrode all the time. After some trials with different base potentials decision was made to select E_{base} = +0.3 V. Figures 4.12a and 4.12b show the magnitude of the responses of both the background and the faradic currents at different time scales.
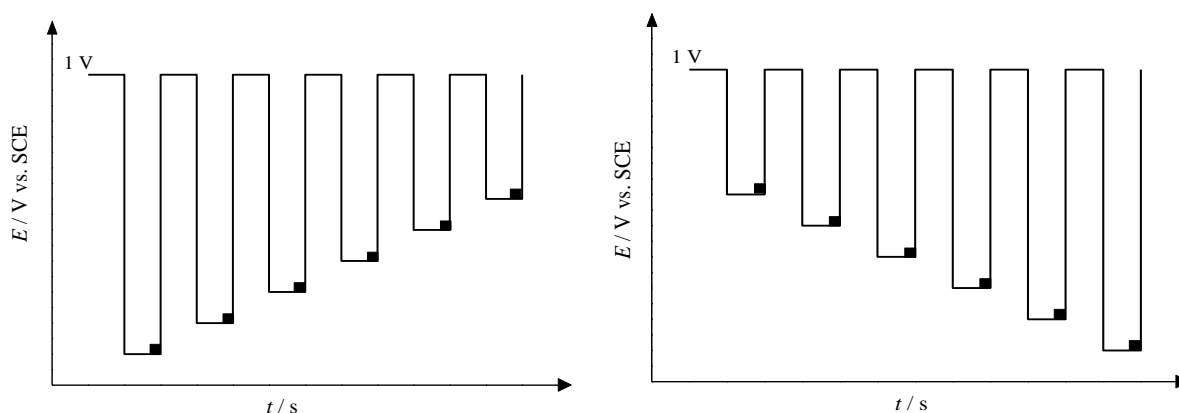
Figure 4.9 A NPV waveform starting at E_{base} = 1 V. Increasing (left) and decreasing potentials (right). Such a waveform would mean the electrode always start with an oxide layer. On the left the oxide layer would be removed by the first pulse and rebuilt at the next rest. On the right the oxide layer would build up with each pulse until the pulse potential is negative enough to reduce the oxide. The two scan directions would produce different normal pulse voltammograms. The black square indicates when the current is sampled.
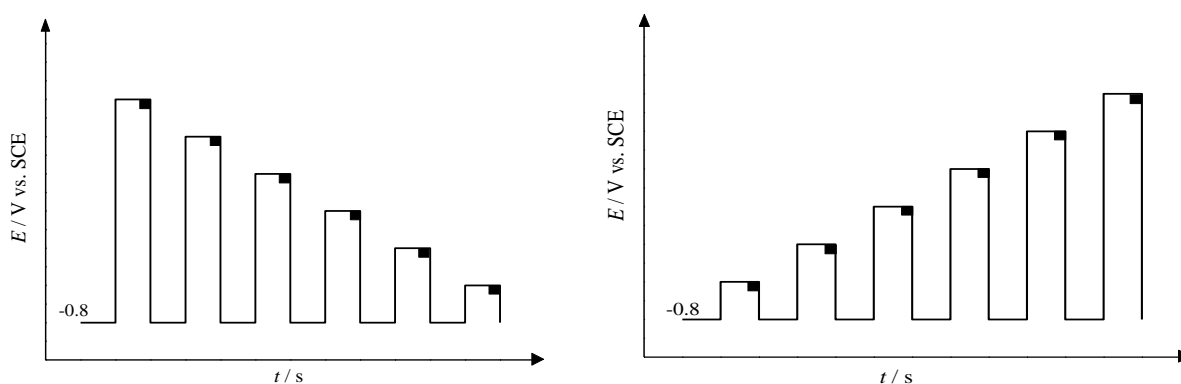
Figure 4.10 A NPV waveform starting at E_{base} = -0.8 V. Decreasing (left) and increasing potentials (right). In these cases the electrode is always covered with a layer of adsorbed hydrogen. In this case the two NPVs should be similar since no oxide build up is possible.
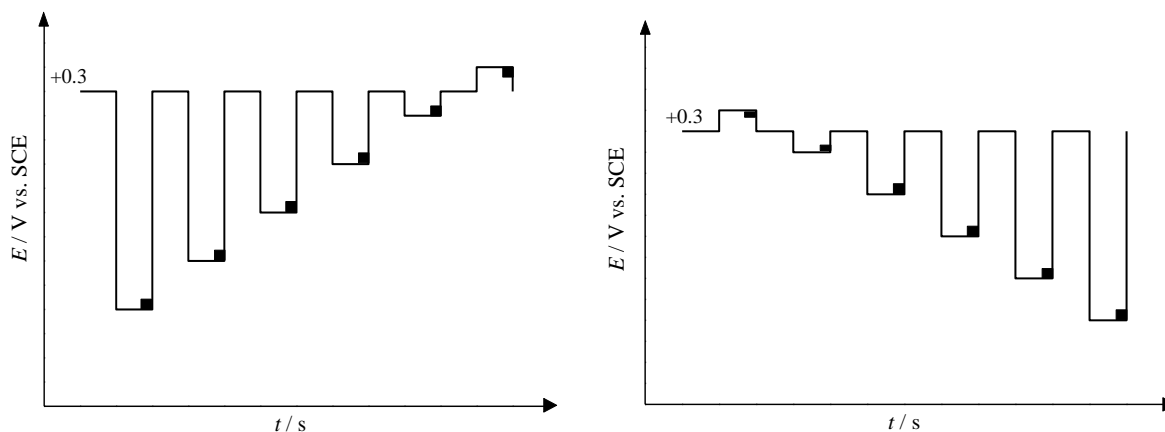
Figure 4.11 A NPV waveform starting at $E_{\textbf{base}}$ = +0.3 V. Increasing (left) and decreasing potentials (right). Here the rest potential is chosen to produce a low oxide coverage to recondition the electrode but prevent oxide build up.

Interestingly, we have found using NPV that the response to sweeps from negative to positive potentials (E_{base} =0.3 V, $E_{initial}$ = -0.8 V and E_{end} = 1 V) is better than that from positive to negative potentials (E_{base} =0.3 V, $E_{initial}$ = 1 V and E_{end} = -0.8 V) as shown in Figure 4.12. This can be related to the effect of the positive potential limit. The hysteresis between the negative and the positive scan decreases as the positive limit is lowered, i.e. as the amount of oxide on the electrode surface decreases. At 0.3 V E_{base} is not able to remove oxide from the electrode surface thus it is important to record the NPV starting from –0.8 V. The oxide formed on the electrode when starting the scan at +1.0 V is present until its reduction circa -0.285 V in Figure 4.12a.
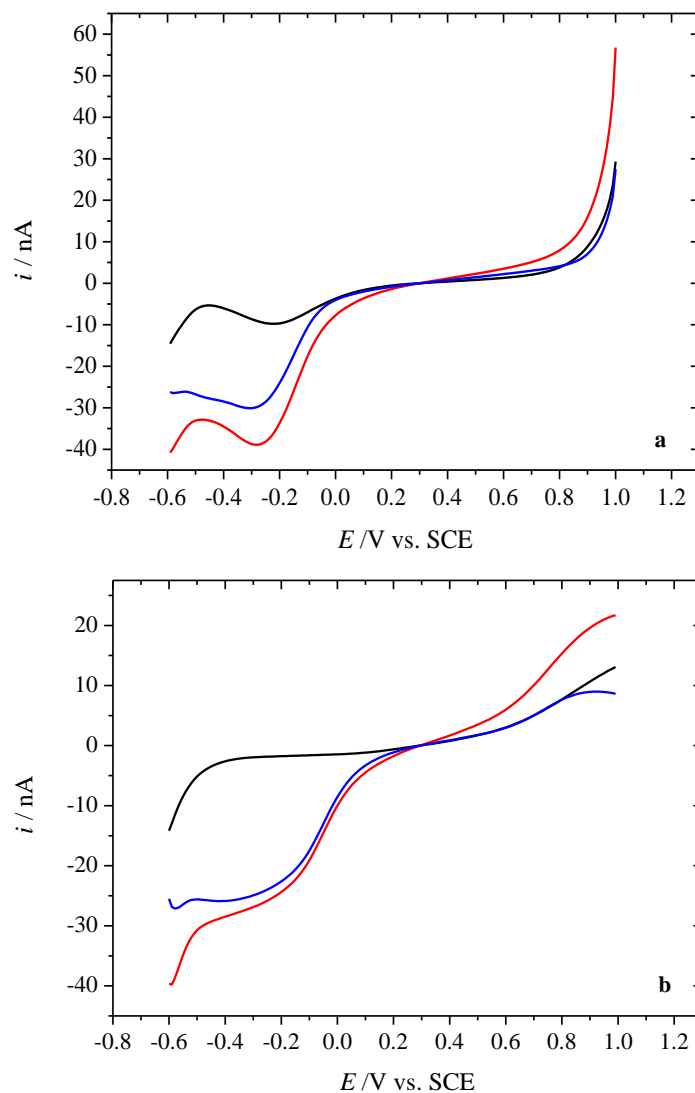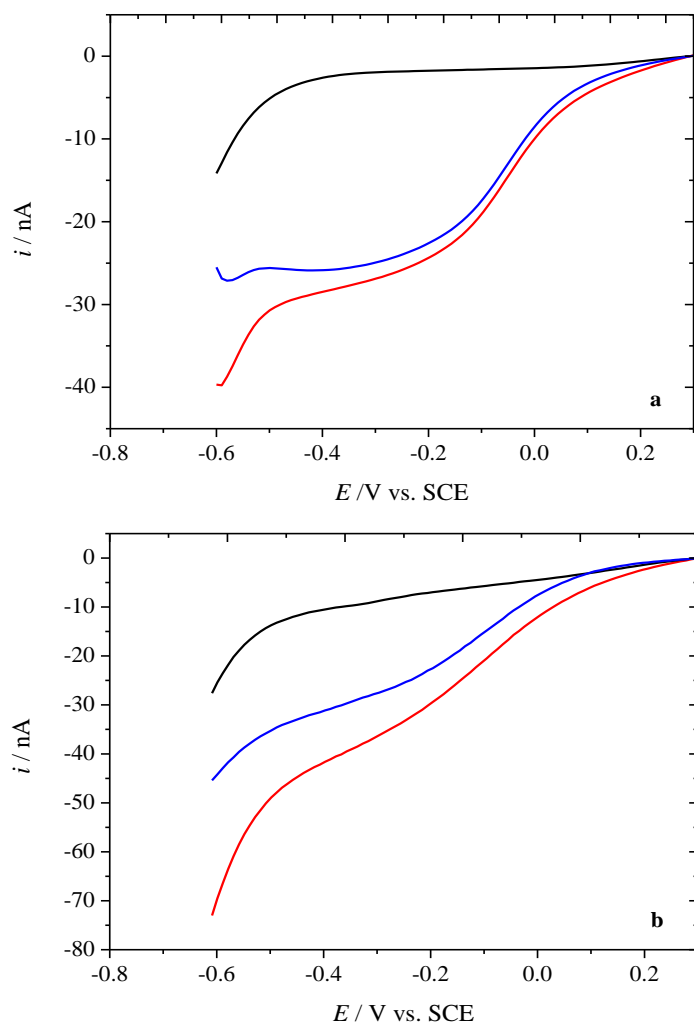
Figure 4.12 Comparison between NPVs for the reduction of oxygen on 25 μm diameter microdisc electrode in 0.5 M KCl, background current (black), background corrected current (blue) and raw ORR current (red), pulse time = 10 ms, when a) sweeping from positive to negative potential, b) sweeping from negative to positive potential, $E_{base} = 0.3$ V at room temperature.

A cyclic voltammogram was recorded in the same solution before and after the pulse technique employed to ensure no roughening of the electrode had taken place. This is shown in Figure 4.13 where it can be seen, that the current responses were the same before and after the NPV experiments; this means the surface of the electrode has not been roughened using this technique in this experiment.
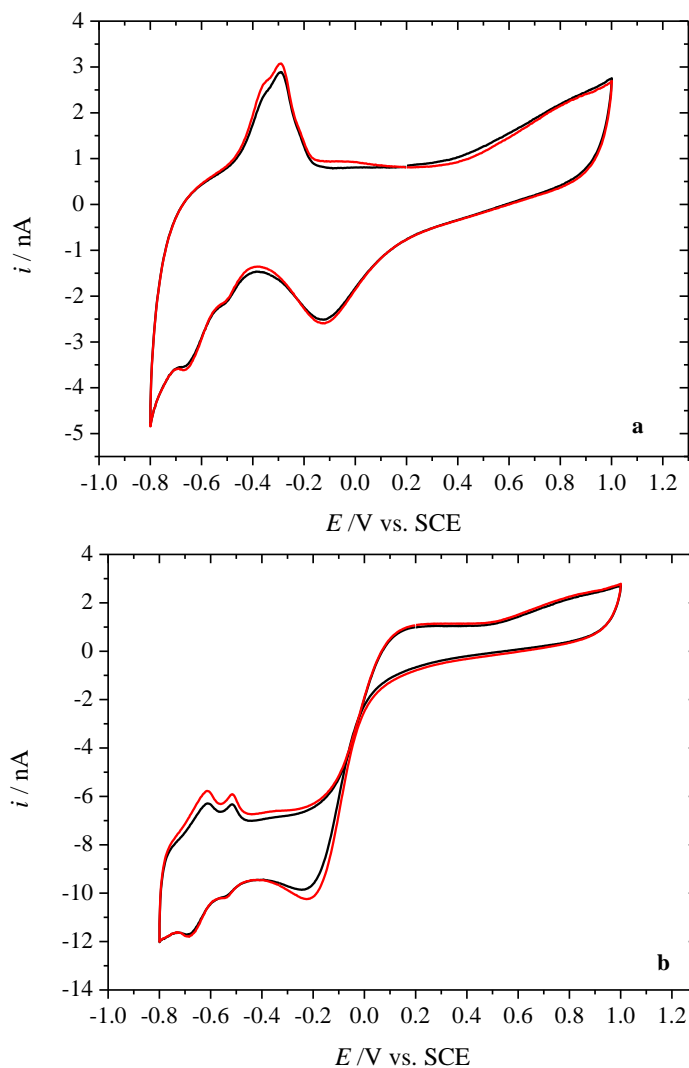
Figure 4.13 Stable cyclic voltammograms (10th cycle) of a) deoxygenated and b) aerated aqueous 0.5 M KCl, at 200 mV s^{-1}, using 25 μm Ø Pt microdisc electrode as working electrode recorded at room temperature, black line for CVs before NPV and red line for CVs after NPV.

From the previous findings of the effect of the sweeping direction on the current response for ORR, the decision was made to choose the sweep from negative to positive potentials. Figure 4.14 shows typical voltammograms recorded for different pulse duration for the ORR in aerated KCl solution, the background and the background subtracted current potential plots. In presence of oxygen the normal pulse voltammograms show a clear sigmoidal shape analogous to that seen with sampled current voltammetry. Background subtraction appears to work well down to 10 ms pulse duration. Below this background subtraction does not yield a flat ORR plateau thus suggesting the surface processes are running at different rates in presence and absence of oxygen.

Alternatively these processes may be different in each case. Below -0.5 V the NPVs show a marked increase in current presumably corresponding to hydrogen adsorption. At 3 ms pulse duration the shape of the ORR wave appears more drawn out than at 10 ms, thus again indicating the apparent irreversibility of the ORR.

Figure 4.14 NPV for the reduction of oxygen on 25 μm diameter microdisc electrode in 0.5 M KCl, background current (black), corrected current (blue) and aerated current (red), pulse times are a) 10 ms and b) 3 ms; sweeping from negative to positive potential, E_{base} = 0.3 V at room temperature.

Due to the effect of surface condition on the current response for ORR, it is necessary to find a way where the surface should be the same before each measurement. Since it is well known that the adsorption behaviour for some species can interfere with the actual measurement, a cleaning procedure should be applied. The occurrence of ORR is observed in a potential region where both

hydrogen adsorption and oxide stripping take place. This could involve a fraction of electroactive area at the electrode. A short time their dominance could cause distortion of the ORR current transient. Therefore, a potential waveform was designed to minimise hydrogen and oxide coverage. Experiments were performed in 0.5 M KCl solution with a specially designed NPV waveform to include two other potentials, an upper cleaning potential, a lower cleaning potential, a rest potential and finally the potential for measuring the signal.

4.3.3   Development of a sweeping conditioning waveform

In Figure 4.15, a sawtooth waveform is shown. Preconditioning sweeps include sweeping at 500 mV s^{-1} to the onset of oxide formation potential + 0.3 V as in sweeps 1, 3 and 5 then to – 0.7 V the potential that removes the oxide formed and adsorb any hydrogen as in sweeps 2, 4 and 6. This is followed by a rest at 0 V (10 s) as in step 7, where there is no formation of oxide and no hydrogen left on the electrode. Finally, this is followed by a 0.5 s step to a particular potential (step 8) within the range of interest. To construct a sampled current voltammogram the whole waveform is repeated, each time for a different value of the potential in the last step. Overall the sawtooth waveform aims to recondition the electrode by taking it through the following sequence: form oxide, remove oxide & adsorb hydrogen, desorb hydrogen & allow O_2 to recover, then step to record current. The current transient was taken as an average of 10 measurements recorded without any treatment of the electrode other than that provided by the waveform shown in Figure 4.15.
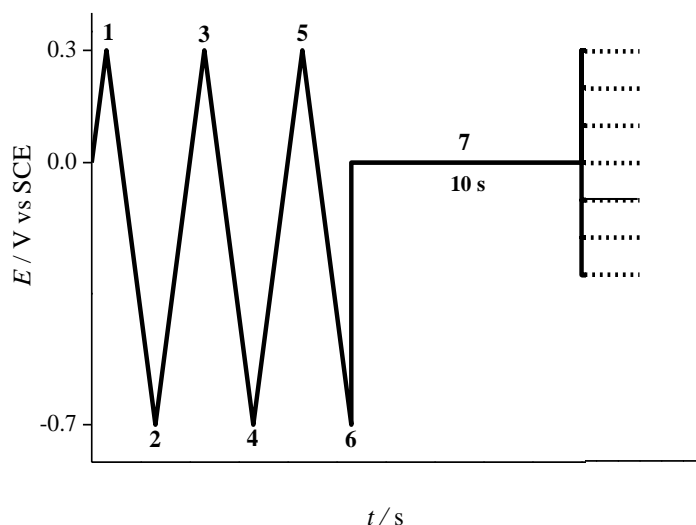
Figure 4.15 Conditioning waveform used to acquire the current transient and construct sampled current voltammograms. Sweeps 1-6 (at 500 mV s^{-1}) are for preconditioning, step 7 for resting and step 8 for measuring. The solid line shows the waveform for one experiment at one potential; the dotted lines indicate the changes made to the waveform to record the current for other potentials and reconstruct the SCV.

The chronoamperometric response and sampled current voltammograms for the reduction of Ru(NH$_3$)$_6^{3+}$ were reported in Chapter 3. This complex ion undergoes a relatively fast one electron reduction in the same potential window as for the reduction of oxygen; its chronoamperometry at short times should therefore be affected by the same surface processes. The results presented in Chapter 3 clearly showed the ability of the conditioning waveform shown in Figure 4.15 to reduce the background effect and prepare a clean electrode free from oxide or adsorbed hydrogen.

When applied to the ORR the conditioning waveform shown in Figure 4.15 produces well-formed sigmoidal sampled current voltammograms with flatter plateaux than those observed previously, e.g. with NPV. The waves are slanted, once again revealing a surprisingly slow kinetics, the plateau currents increase with shorter sampling times and a sharp increase in current appears below -0.6 V. Overall these observations are consistent with the results obtained with the other methods however flat plateaux are obtained despite the absence of background subtraction. Those results and those obtained for Ru(NH$_3$)$_6^{3+}$ reduction indicate the effectiveness of the sweeping conditioning waveform in producing "clean" sampled current voltammograms devoid of distortion from parallel surface processes. The increase in plateau currents with shorter sampling times is however puzzling. The time normalised sampled current voltammograms shown in Figure 4.16 clearly show that the apparent number of electron (as read from the vertical axis) increases way above the maximum 4 electrons expected for the ORR. At long times n_{app} is consistent with that obtained with steady state methods. The increase with shorter sampling times is also consistent

with the observed results reported previously with different waveforms and with NPVs. The reason for this is unknown. It was demonstrated that the presence of chloride inhibits the kinetics of ORR but not the pathway [60]. This pathway via H_2O_2 formation has been proven even in chloride media. The Pt sites availability for breaking the O-O bond is reduced as a result of strong adsorption of chloride to Pt electrode. However a slower kinetics due to chloride adsorption does not explain why the number of apparent electrons increases at shorter sampling times. This increase can only reflect extra Faradaic current from a reducible species.

The sweeping conditioning waveform performed very well for $Ru(NH_3)_6^{3+}$ reduction in the same potential down to 3 ms sampling times. For the ORR the waveform produces flat plateaux on the sampled current voltammograms without requiring background subtraction. Yet the trend in n_{app} with sampling times is contrary to expectations (n_{app} was expected to decrease from 4 to 2 with shorter sampling times). Furthermore the increase in n_{app} appears with moderately long sampling times, e.g. at 100 ms n_{app} is already larger than 4.
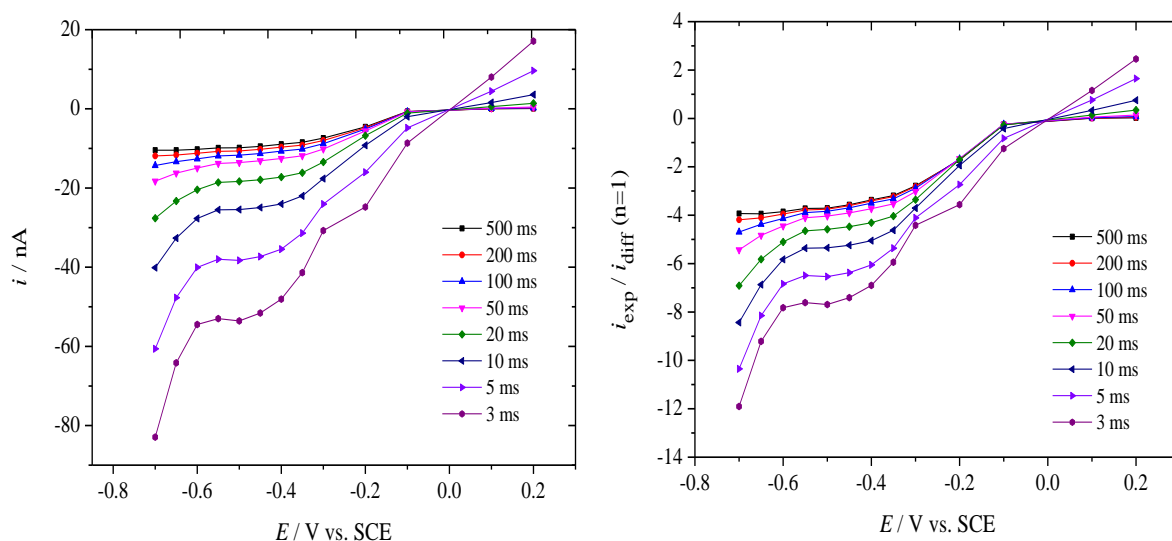
Figure 4.16 Sampled current voltammograms (left) and time normalized sampled current voltammograms (right) for the different sampling times considered. The chronoamperograms used to reconstruct the sampled current voltammograms were acquired in aerated 0.5 M KCl with the waveform shown in Figure 4.15, with 25 μm diameter Pt disc, a Pt mesh counter electrode and SCE reference electrode. The normalisation was performed by dividing the experimental currents with the theoretical diffusion controlled current for a microdisc, Equation 1.2, with $n=1$, $D = 2.2 \times 10^{-5}$ cm s^{-1}, $c^\infty = 2.2 \times 10^{-5}$ mol cm^{-3}, $a = 12.5$ μm and t the corresponding sampling times. The sampled current voltammograms shown were not background subtracted.

Attempts to subtract the background current from the measured faradaic current of ORR were not successful. The reason for this is ascribed to the fact that hydrogen adsorption/desorption take place at different potentials; desorption does not occur at the same potential in presence and absence of O_2 due to difference in the local pH in argon degassed and open air KCl solution. The shift in hydrogen adsorption/desorption peaks in argon degassed solution is controlled by the electrochemistry of Pt itself which determines the pH conditions (Figure 4.2). However, in presence of air a fairly reversible hydrogen adsorption/ desorption processes can be observed. That can be attributed to the OH^- generated during ORR, which changes the local pH conditions. Therefore, the following reactions take place in an alkaline local pH [101].

The experiments with ruthenium hexaammine validated the experimental approach, in particular the conditioning waveform, and the approach taken to analyse the data. The unexpected trend in n_{app} for the ORR cannot therefore be due to the experimental or analytical approach. Instead it must reflect a difference in background processes during the two reactions on a Faradaic process specific to the ORR and only seen at that times.

A clear question remains, could some remaining oxide at the electrode play a role in adding extra current to the measurement? The conditioning waveform was then modified to test for the presence of any oxide present after the conditioning procedures. The results of these experiments are presented in the next section.

4.3.4   Conditioning sweeping waveform and stripping experiment

In this section we address the possibility that a potential oxide coverage is formed during the resting step. If this was the case the transient recorded during step 8 in the waveform would have a contribution from the reduction of this oxide coverage. This could account for some of the current seen in the reconstructed voltammograms for the ORR response at short timescales. In order to investigate the effect of the conditioning waveform in obtaining an electrode free of oxide, step 8 was performed by a triangle sweep as shown in Figure 4.17. If any oxide is still present on the electrode after the preconditioning procedure, the sweep from the resting potential towards negative potentials should strip the oxide and produce a reduction peak while a return sweep should show peaks for hydrogen desorption.
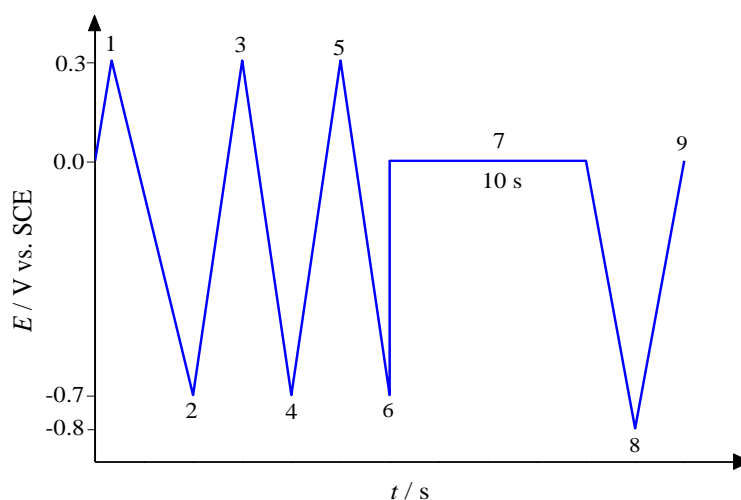
Figure 4.17 Schematic of the waveform used to assess whether oxide formed during the rest (step 7).

Figure 4.18 presents the results of the experiments carried out in deaerated 0.5 M KCl with a 25 μm diameter Pt disc. The upper cleaning potential for steps 1, 3 and 5 was set at +0.6 V in Figure 4.18a and +0.3 V in Figure 4.18b. Neither figure shows an oxide reduction peak thus indicating that the rest period (step 7) does not promote the formation of oxide coverage. This therefore rules out the reduction of oxide as the source of extra current in the sampled current voltammograms for the ORR. However Figure 4.18 shows that the hydrogen adsorption and desorption peaks systematically decrease with subsequent experiments. This could be interpreted as a decrease in electroactive area but complete cyclic voltammograms recorded before and after the series of experiments show no change in the electroactive area, Figure 4.19, thus ruling out electrode roughing. Thus Figure 4.18 must reflect a decrease in the activity of the surface, maybe due to a reorganization of the active sites. The choice of $E_{upper-cleaning} = 0.6$ V was indicated by the improved stability of the steady state current for ORR reported by Sosna *et al* [11].

Figure 4.18 reflected the absence of oxide peak; however, an oxide or hydroxide layer could still be present after the application of the designed waveform as there is evidence in the literature that once formed, Pt–O is possibly not totally reduced during the cathodic sweep. Additionally, the Pt oxide was reported to exist over the potential range up to hydrogen adsorption according to Jacob *et al* [121]. The hypothesis of the remaining of some oxide on the surface after applying the conditioning waveform seems to be invalid according to the results shown in Figure 4.18, although the possibility of place exchange reconstruction process was reported by several investigators [102, 122]. The reconstructing of the Pt surface upon potential cycling has been

95

reported [77]. It was found, using the EQCM technique, that not all the β-oxide was reduced during cycling while holding the potential enabled the complete film reduction. This in turn results in extra cathodic charge.

Assuming a monolayer of OH desorbs from a 25 micron diameter disc with a typical roughness factor of 3 and taking 210 μC cm^{-2} as the typical charge for a monolayer, the corresponding charge equals ~3 nC. The integration of the chronoamperometric response over 500 ms for a step to -0.45 V *vs*. SCE in degassed 0.5 M KCl gives circa 0.23 nC . This is clearly a tiny fraction of a monolayer and cannot be responsible for the extra current observed during the ORR. However it is possible that the nature and amount of oxide remaining on the electrode is different in presence of dissolved oxygen.
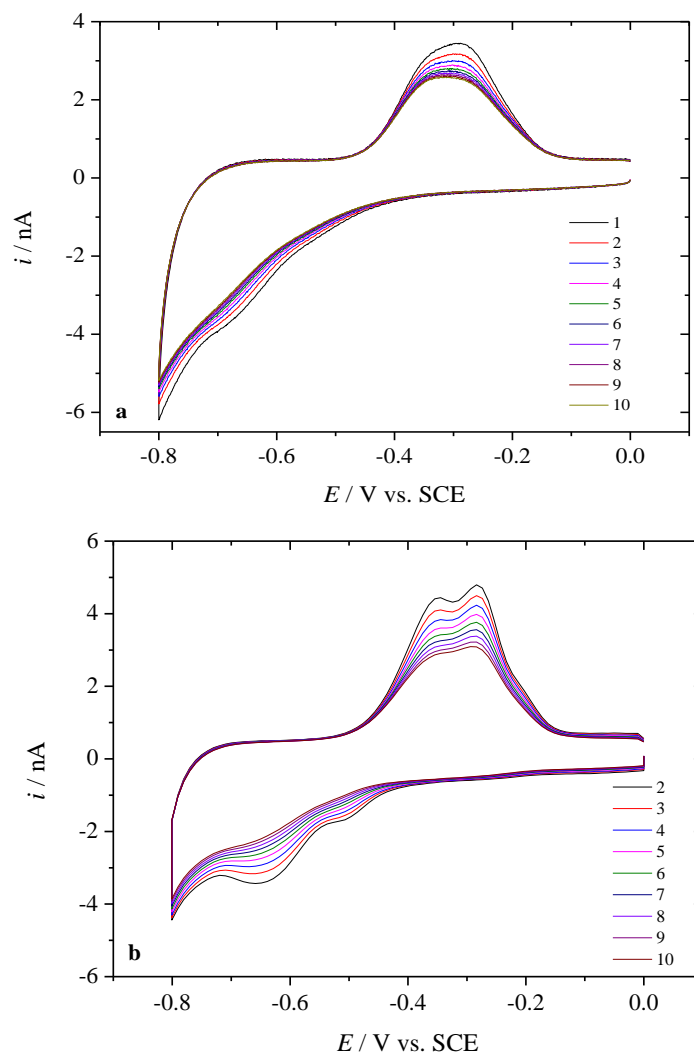
Figure 4.18 Cycling voltammograms recorded with the sweeps (events 8 and 9) in the waveform shown in Figure 4.17. $\nu = 500$ mV s^{-1}, 25 μm diameter Pt disc, a Pt mesh counter electrode, SCE reference electrode, room temperature, argon purged 0.5 M KCl. $E_{rest} = 0$ V, $E_{upper\ cleaning} = +0.6$ V (a) and +0.3 V (b). The waveform was repeated ten times, and the voltammogram recorded for each repeat is indicated in the legend.
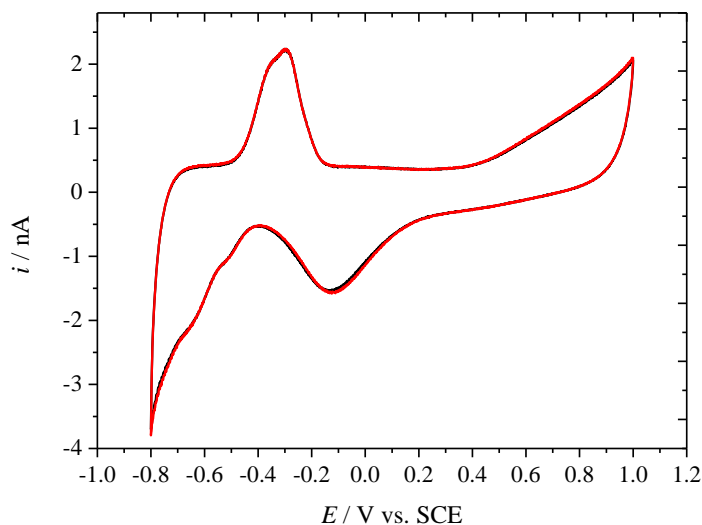
Figure 4.19 Stable cyclic voltammograms, in deoxygenated (with argon) aqueous 0.5 M KCl at 200 mV s^{-1}, using 25 μm Ø Pt microdisc electrode as working electrode recorded before (black line) and after (red line) applying the stripping waveform shown in Figure 4.16 with $E_{\text{upper-cleaning}}$ = 0.6 V at room temperature.

While these observations of the effect of the conditioning waveform in excluding oxide from the electrode surface are of interest they do not explain the observed behaviour of molecular oxygen reduction at Pt microelectrode on the sampled current voltammograms. Hence further investigation is necessary. Attempts to improve the ORR amperometry by increasing the number of cleaning preconditioning sweeps in the applied waveform are presented in the next section.

4.3.5 Conditioning waveform (increasing the number of conditioning sweeps)

In further experiments attempting to completely minimise the contribution from extra processes to the amperometric ORR response, the number of conditioning sweeps was increased by adding one extra cycle to the waveform as shown in Figure 4.20. Note that the upper cleaning potential is now set at +0.6 V in view of the improvement in stability observed in Figure 4.18. The effects of the prolonged cycling are discussed and illustrated below.

98
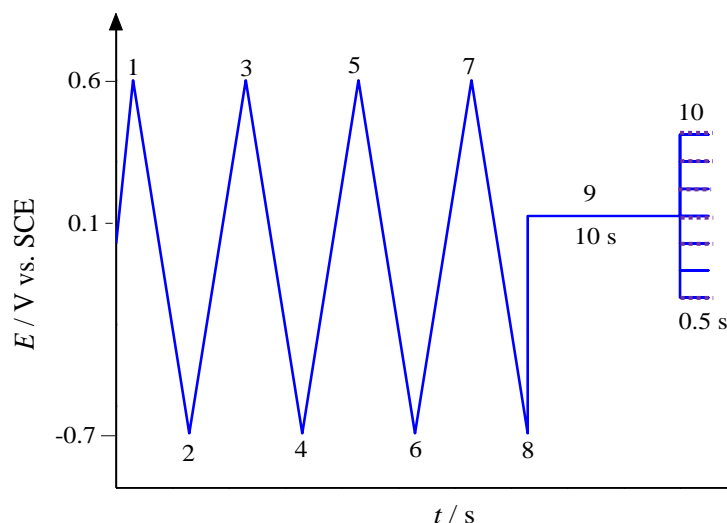
Figure 4.20 Conditioning waveform used to acquire the current transient and construct sampled current voltammograms. Sweeps 1-8 (at 500 mV s^{-1}) are for preconditioning, step 9 for resting and step 10 for measuring. The solid line shows the waveform for one experiment at one potential; the dotted lines indicate the changes made to the waveform to record the current for other potentials and reconstruct the SCV.

To assess the variation in ORR amperometric current (step 10 in the conditioning waveform) at different potentials, ten measurements have been plotted together as a log-log plot. The reproducibility at -0.4 V was calculated from 10 measurements and Figure 4.21 presents the data for the measured amperometric response after including two extra preconditioning sweeps in the conditioning applied waveform. It is clear that there was very good agreement between measurements down to 1 ms.

Then the experiments were repeated for a range of potentials within the ORR region; the corresponding reconstructed normalized voltammograms are shown in Figure 4.22. Still the same behavior (as found in previous sections) was seen. At long time scales, the ORR wave involves just over 3 electrons in agreement with the value measured in the steady state [11]. However as the sampling times become shorter n_{app} increases to an unreasonable value. For short sampling times a sudden drop in current was observed below -0.3 V. This occurred for all ten experiments and is, so far unexplained. The ten experiments were repeated with a large platinum microdisc, 50 μm, to see whether a similar trend of n_{app} with sampling time is observed.
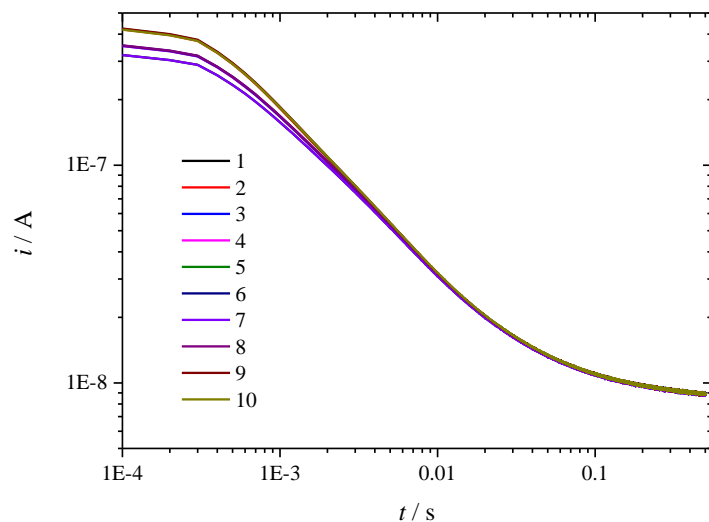
Figure 4.21 Log-log plot for ten current transients at -0.4 V (vs. SCE), in aerated 0.5 M KCl, using a 25 μm Ø Pt microdisc electrode as working electrode and recorded at 25°C after applying the conditioning waveform shown in Figure 4.20.
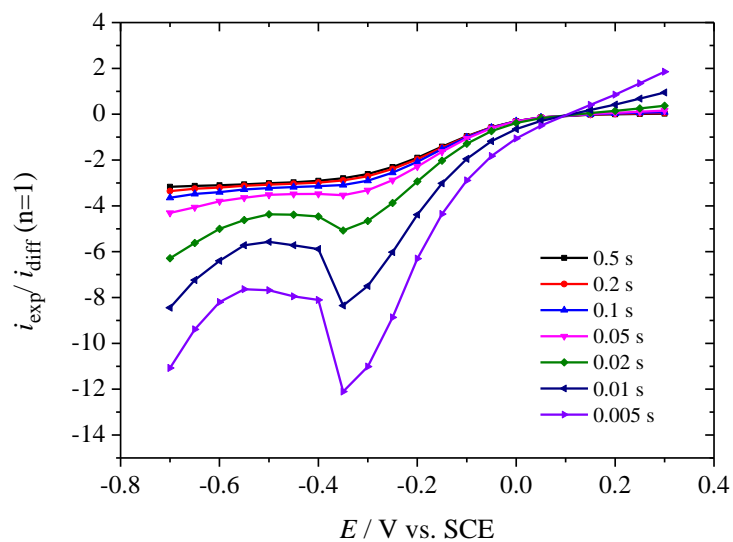

Figure 4.22 Normalised reconstructed voltammograms recorded after applying the waveform shown in Figure 4.20 at a Pt microdisc (25 μm diameter) in 0.5 M KCl at 25 °C. SCE served as a RE and Pt mesh as a CE. The normalised voltammograms were obtained by dividing the average of ten experimental currents with the theoretical current for a 1 electron diffusion controlled process calculated with the Mahon & Oldham equation taking $n = 1$, $D = 2.2 \times 10^{-5}$ cm^2 s^{-1}, c^∞ =2.2x10^{-7} mol cm^{-3}, and $a = 12.5 \times 10^{-4}$ cm. The sampling times are shown on the plot.

The ORR was therefore explored at a 50 μm diameter Pt microdisc in 0.5 M KCl solution. The reproducibility of ten consecutive current transients at -0.4 V was very good down to 1 ms sampling time, similarly to the data obtained at a 25 μm diameter disc. The closeness of ten runs

reflects the improvement in the measured amperometric current upon the application of the conditioning waveform. Figure 4.23 shows the data for reproducibility test. As observed with the smaller disc, the sampled current voltammograms show clear sigmoidal waves with well-defined plateaus for all sampling times. The experimental currents were time normalised by dividing with the theoretical diffusion controlled current for the relevant sampling times. The results shown in Figure 4.24 once again indicate that the apparent number of electrons increases with shorter sampling times. At long timescale the number of electron reached that for steady state conditions 3.6, while at short times it increased to circa 8. Interestingly, the range of n_{app} obtained with the bigger electrode is smaller than that obtained with the larger electrode. Those results therefore indicate that the time dependence of n_{app} is specific to the ORR (since no such dependence was found for the reduction of ruthenium complex) but somewhat dependent on the microelectrode radius with a strange dependence seen with smaller electrodes.
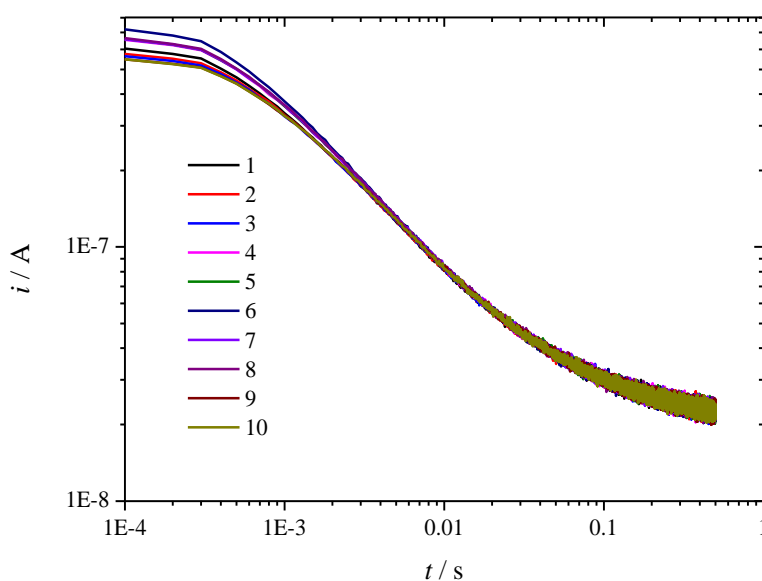
Figure 4.23 Log-log plot for the averaged current transients at -0.4 V (*vs*. SCE), after applying the waveform shown in Figure 4.20 at 50 μm Ø Pt microdisc electrode as working electrode in aerated 0.5 M KCl at 25°C.
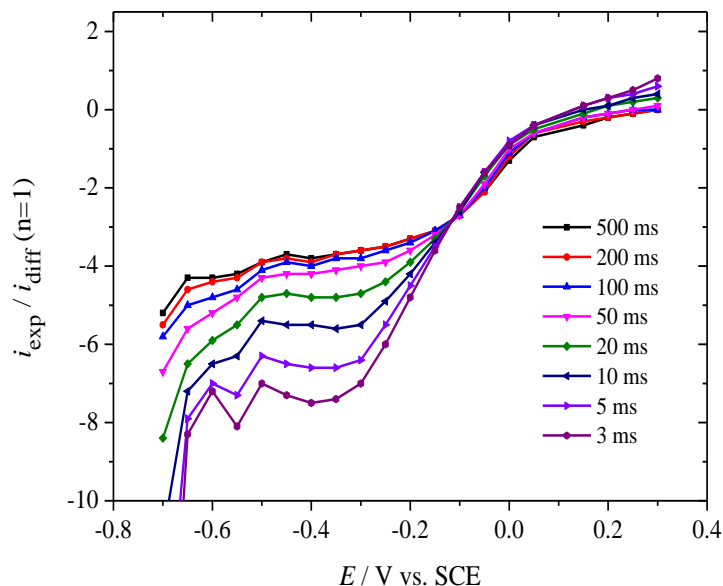
Figure 4.24 Normalised reconstructed voltammograms at different timescales recorded after applying the conditioning waveform shown in Figure 4.20 at a Pt microdisc (50 μm diameter) in 0.5 M KCl at 25 °C. SCE served as a RE. The normalised voltammograms were obtained by dividing the experimental currents with the theoretical current for a 1 electron diffusion controlled process calculated with the Mahon and Oldham equation (Equation 1.2) taking $n = 1$, $D = 2.2 \times 10^{-5}$ cm^2 s^{-1}, $c^\infty = 2.2 \times 10^{-7}$ mol cm^{-3}, and $a = 25 \times 10^{-4}$ cm. Sampling times are shown on the plot. Each data point is the average of ten experiments.

The next section considers the possibility that the extra current comes from the re-plating of Pt dissolved during the cleaning procedure.

4.3.6   Investigation of the dissolution and re-plating of Pt

The discrepancies between the experimental and theoretical currents in the reconstructed sampled current voltammograms suggest another effect at short time scales. The extra current observed at short times may reflect the re-deposition of Pt possibly dissolved when cleaning the electrode in the conditioning waveform. Pt is known to dissolve under high frequency potentiostatic cycling (or stepping) in chloride media [123]. Indeed a solution of HCl, CaCl$_2$ and water is often used to etch Pt to produce recessed microdiscs and STM tips [61]. Under these conditions, platinum chloride complexes form; one possible reaction is shown below. By means of XPS analysis, the presence of such metal hydroxochloro chloride in oxide film on Pt was proven.
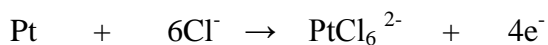
Pt   +   6Cl$^-$ →   PtCl$_6$$^{2-}$ +   4e$^-$

102

Two approaches were explored to determine whether Pt was dissolving during cleaning and re-plating during the ORR measuring step. The first is based on double potential step chronocoulmetry, the second microgravimetry with an electrochemical quartz crystal microbalance (EQCM).

4.3.6.1 Investigation of Pt dissolution and re-plating by double potential chronocoulometry

The purpose of this study was to apply a conditioning waveform with a double potential step at a 25 μm diameter Pt disc to assess any processes (e.g metal dissolution during the conditioning followed by plating during the ORR) taking place in parallel with the ORR in 0.5 M KCl. Figure 4.25 illustrates the design of the employed waveform. The time in the first potential step (8 in Figure 4.25) was varied to be 500, 10 and 1 ms while the time in the second potential step (9 in Figure 4.25) was kept at 1 s. The chronoamperograms in steps 8 and 9 were then integrated to calculate the charge passed under each event.

Figure 4.25 Schematic of the conditioning waveform and double potential step experiments used to investigate the charge passed and assess whether Pt dissolved and re-plated. Sweep rate 500 mV s^{-1}, $t_7 = 10$ s and t_8 is varied.

Three values were considered for the rest potential, E_{rest}, 0, 0.1 and 0.2 V vs SCE to see wether it affected the charge passed in the step 8. The potential for step 8 was set on the ORR plateau at -0.4 V vs SCE. Another set of experiments was conducted when stepping to -0.5 V vs SCE but the results are not included in this thesis. The lower cleaning potential was set at -0.7 V as previously and the upper cleaning potential was set at + 0.3 V to minimise the extent of Pt dissolution. Table

4.1 summarises the results of the double potential step chronocoulometric experiments for $E_{measure}$ = -0.4 V vs SCE.

A systematic trend in Q_8: Q_8 (0 V) < Q_8 (0.1 V) < Q_8 (0.2 V) cannot be due to the consumption of more oxygen but to the reduction of oxide with more being formed the more positive is the rest potential. It could also be that more Pt is being dissolved at E_{rest} and re-plated in the 1st step.

Table 4.1 Charges found when integrating the chronoamperograms in the double potential step experiments. t_8 is the duration of step 8 (in all cases the measuring potential in step 8 was set at -0.4 V vs. SCE *i.e* on the plateau for oxygen reduction). i_{rest} (t_7) is the rest current observed at the end of the rest period. Q_8 and Q_9 are respectively the charges for step 8 and 9 in the waveform shown in Figure 4.25. The WE was 25 μm diameter Pt disc, CE a Pt mesh and the RE a SCE. The solution was aerated 0.5 KCl at 25ºC.

E_{rest} / V	t_8 / s	i_{rest} (t_7) / A	Q_8 / C	Q_9 / C
0	0.5	-7.02 x 10^{-10}	-5.57 x10^{-9}	2.25 x10^{-10}
	0.01	-7.45 x 10^{-10}	-5.96 x10^{-10}	5.41 x10^{-10}
	0.001	-7.45 x10^{-10}	-1.79 x10^{-10}	8.38 x10^{-10}
0.1	0.5	-5.55 x10^{-10}	-6.13 x10^{-9}	4.52 x10^{-10}
	0.01	-5.856 x10^{-10}	-5.17 x10^{-10}	6.39 x10^{-10}
	0.001	-5.92 x10^{-10}	-1.53 x10^{-10}	7.79 x10^{-10}
0.2	0.5	-2.47 x10^{-10}	-6.5 x10^{-9}	4.93 x10^{-10}
	0.01	-2.72 x10^{-10}	-6.12 x10^{-10}	1.46 x10^{-11}
	0.001	-2.56x10^{-10}	-2.48 x10^{-10}	1.84 x10^{-10}

Table 4.1 also shows the rest current recorded just before step 8 for each rest potential. The negative values recorded prompted us to record a series of SCVs for ORR using +0.1 V as a rest. A set of sample current voltammograms was recorded with the waveform shown in Figure 4.25 with E_{rest} =0.1 V and $E_{upper\ cleaning}$ = +0.6 V *vs*. SCE. The complete waveform was repeated ten times and the sampled currents were averaged. They were normalised by dividing with the theoretical diffusion controlled current calculated with the Mahon and Oldham equation using n=1, D = 2.2x10^{-5} cm^2 s^{-1}, c^{∞} =2.2x10^{-7} mol cm^{-3}, a = 12.5x10^{-4} cm and the relevant sampling times.

Once again we see n_{app} (the vertical axis) increasing from circa 3.6 at long times to unexpectedly large values at short times. Also, a sudden drop in the plateau current appears below -0.3 V *vs*. SCE; this is thought to relate to the charge in current sensitivity on the instrument.
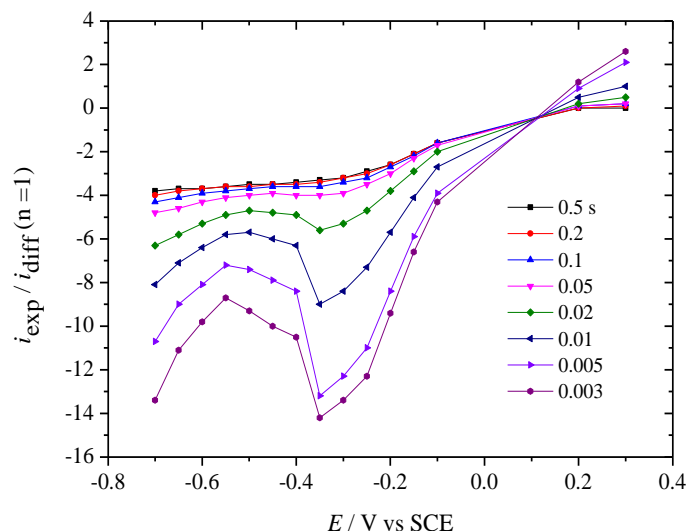

Figure 4.26 Normalised reconstructed voltammograms after applying the conditioning waveform shown in Figure 4.15 at a Pt microdisc (25 µm diameter radius) in 0.5 M KCl at 25°C. SCE served as a RE and Pt mesh as a CE. The normalised voltammograms were obtained by dividing the experimental currents with the theoretical current for a 1 electron diffusion controlled process calculated with the Mahon & Oldham equation taking $n = 1$, $D = 2.2 \times 10^{-5}$ cm^2 s^{-1}, $c^\infty = 2.2 \times 10^{-7}$ mol cm^{-3}, and $a = 12.5 \times 10^{-4}$ cm. Sensitivity 100 nA when $E \leq -0.4$ V and 10 nA when $E \geq -0.35$ V.

The next subsection investigates whether the waveform promoted the dissolution and re-plating of Pt.

4.3.6.2 Investigation of Pt dissolution and re-plating by EQCM

Our previous results imply that there is another source for the extra current seen in the SCVs of ORR. One question is whether the Pt is dissolved to create Pt-Cl complexes and re-deposited which could account for extra current. The dissolution of Pt has been studied at high frequency using the electrochemical quartz crystal microbalance (EQCM) [58] and we used the same approach here to assess whether the extra current observed during the ORR was related to Pt re-deposition from Pt chloride complexes formed during the application of the conditioning waveform. The inhibitory nature of chloride ions to the catalytic oxidation of H_2O_2 was reported using microelectrodes and RDE [124]. Many workers have found that there is a decrease in the

rate of H_2O_2 oxidation in presence of chloride ions. The formation of a $PtCl_2$ film on the electrode surface is thought to be responsible for that [124]. The variation of pH in HCl indicated the formation of platinum chloride complex in a previous study [123]. The formation of Pt(II) or Pt(IV) species on platinum electrodes was found to be affected by the adsorption of chloride ions [124].

The additional current could come from the re-deposition of Pt since it could be electroplated during the last step of the waveform. To study and investigate this issue, the EQCM was used to monitor the changes in the mass of the electrodeposited Pt/Au substrate during the applied conditioning waveform.

The experimental configuration was as follows: The gold quartz crystal (1 cm diameter) was first placed in a Teflon holder at the base of the main compartment (which is sandwiched between two rubber O-rings) to serve as the working electrode, where it was in contact with the electrolyte. The electrodeposition of Pt onto the Au electrode was carried out in 0.04 M $H_2PtCl_2.xH_2O$ solution, degassed with argon using the Chrono method (interval time >0.1 s) and a μAutolab equipped with a QCM 200 (Quartz Crystal Microbalance Digital Controller) and QCM25, 5MHz Crystal Oscillator. The charge passed to deposit the Pt was -1.16 C. The applied potential for electrodeposition was -1 V (600 s) *vs*. SCE. The corresponding current transient is displayed in Figure 4.27.
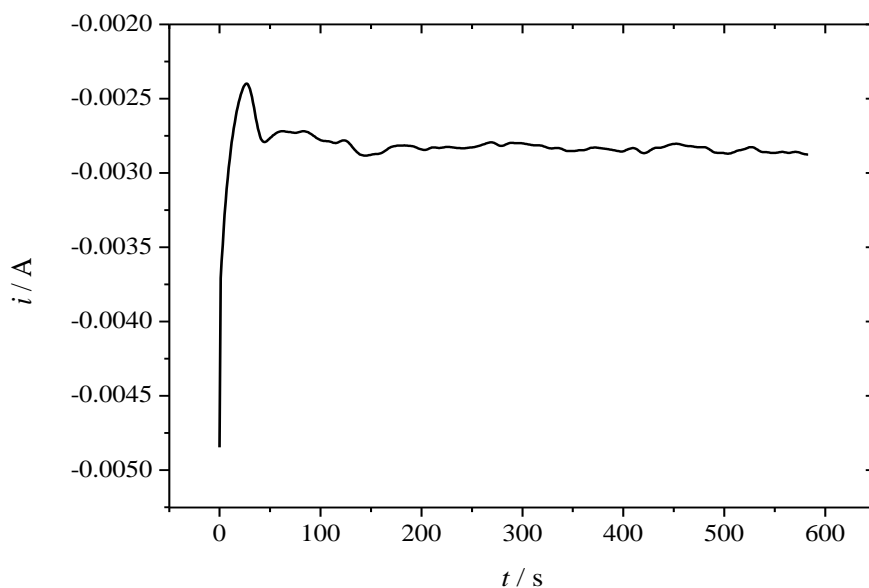

Figure 4.27 Current transient for the deposition of Pt onto a Au quartz crystal. The solution was 0.04 M $H_2PtCl_2.xH_2O$. Electrode geometric area is 1.37 cm^2.

106

The current transient shown in Fig. 4.27 is characteristic of a nucleation and growth electrodeposition process. The Pt(IV) ion undergoes a two-step reduction process. The Pt film deposited appeared clear under visual observation. The charge deposited during the electrodeposition of Pt at Au quartz = 1.163 C and the corresponding charge density = 0.85 C cm^{-2}. In order to obtain the roughness factor, the integrated area of the hydrogen desorption region seen in the acid CV was calculated. The roughness factor was found to be ~109.

The deposition of Pt (thickness in nm) has attracted the attention of many researchers. Some tried to investigate ORR on electrodeposited Pt films (1-50 nm) electrodes and they observed a slight influence of the deposited thickness on the kinetics [125].

An acid CV and accompanying EQCM response (in 1 M H_2SO_4) recorded at 20 mV s^{-1} after Pt deposition are shown in Figure 4.28. The deposited platinum has similar surface characteristics to that of polycrystalline Pt electrode. Due to the expected small changes in mass, the scale was selected to be 200 Hz / V. The frequency output was 10 kHz / V. To convert from a frequency change to a mass change, Equation (4.1) was used. To limit the magnitude of the current due to the large quartz electrode, small scan rates, 20 mV s^{-1} were applied. The mass response was recorded simultaneously with the CV. The mass response shows a considerable slope in the double layer region (probably associated with the adsorption of HSO_4^- and water molecules as was reported by many investigators) and a continuous mass increase in the oxide region was seen. A decrease in mass follows the reduction of oxide in the backward scan, according to Shimazu and Kita [126]. A mass increase was observed in the hydrogen region in the positive-going scan.
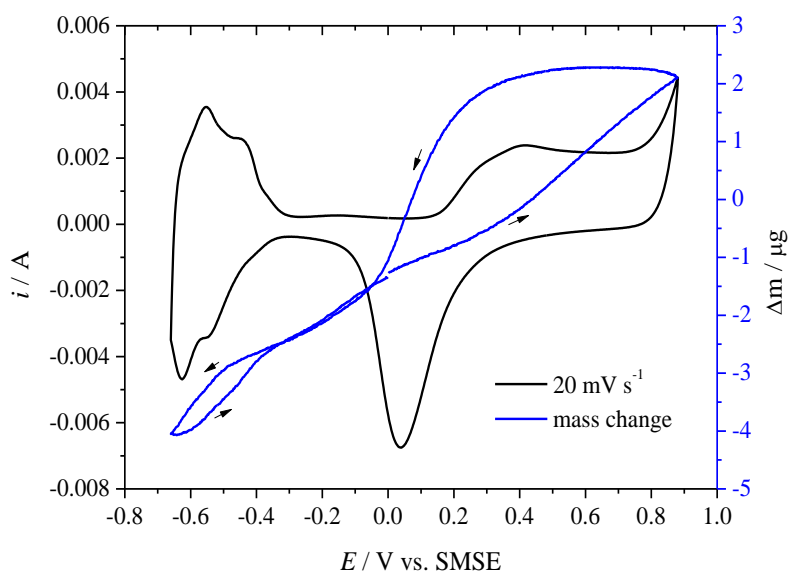
Figure 4.28 CV and corresponding mass response in argon degassed 1 M H_2SO_4 at 20 mV s^{-1} at platinum deposited onto gold on quartz. Electrode geometric area = 1.37 cm^2. Arrows on the mass response indicate the direction of the scan.

In order to calculate mass changes, the following equation was used.

$$\Delta f = C_F \times \Delta m$$

Equation 4.1

C_f is the sensitivity factor, 56.6 Hz µg^{-1} cm^2 is the sensitivity of the 5 MHz at-cut quartz crystal at room temperature and Δf is the change in frequency and Δm is the change in mass.

However for Electrode Electroactive area = 1.37 cm^2, the change in mass is calculated according to the following equation.

$$\Delta m = \frac{\Delta f}{1000} \times \frac{200}{-56.6}$$

Equation 4.2

The obtained mass change is 5.8773x10^{-4} g.

Then the Pt on the Au quartz crystal was used for observing any changes in mass during the application of the conditioning waveform for the ORR system. By combining the voltammetric response with the simultaneous mass response it should be possible to assess whether Pt is dissolved and re-deposited and also whether the electroactive area is changing.

To contrast the data presented for chloride electrolyte, the same experiment was run in perchlorate solution. This experiment was the key to understand the behaviour of ORR at short times in solutions other than chloride. The presence of trace amount of chloride (as a product of the reduction of perchlorate) with various oxygen species (the product of the reaction between chloride and H_2O_2, the intermediate in ORR) with their own redox processes could be another problem to consider. However this hypothesis can be neglected since the SCVs for ruthenium reduction do not show any of the previously mentioned complications.

Difficulties were encountered in this experiment to determine the cause for the decrease in mass during the measuring step in the applied conditioning waveform.

To find the molar mass of the adsorbing substance, the following equation was used

$$\Delta M = \frac{\Delta q \times M}{nF}$$

Equation 4.3

ΔM is the change in mass, Δq is the charge, m is the mass, n is the number of electron involved and F is Faraday constant.

Figure 4.29 The waveform (10 cycles shown) and corresponding current transients for ORR in 0.5 M KCl at -0.4 V *vs.* SCE on platinum deposited onto the gold on quartz EQCM crystal. Electrode geometric area =1.37 cm^2. Sweep rate is 500 mV s^{-1}.
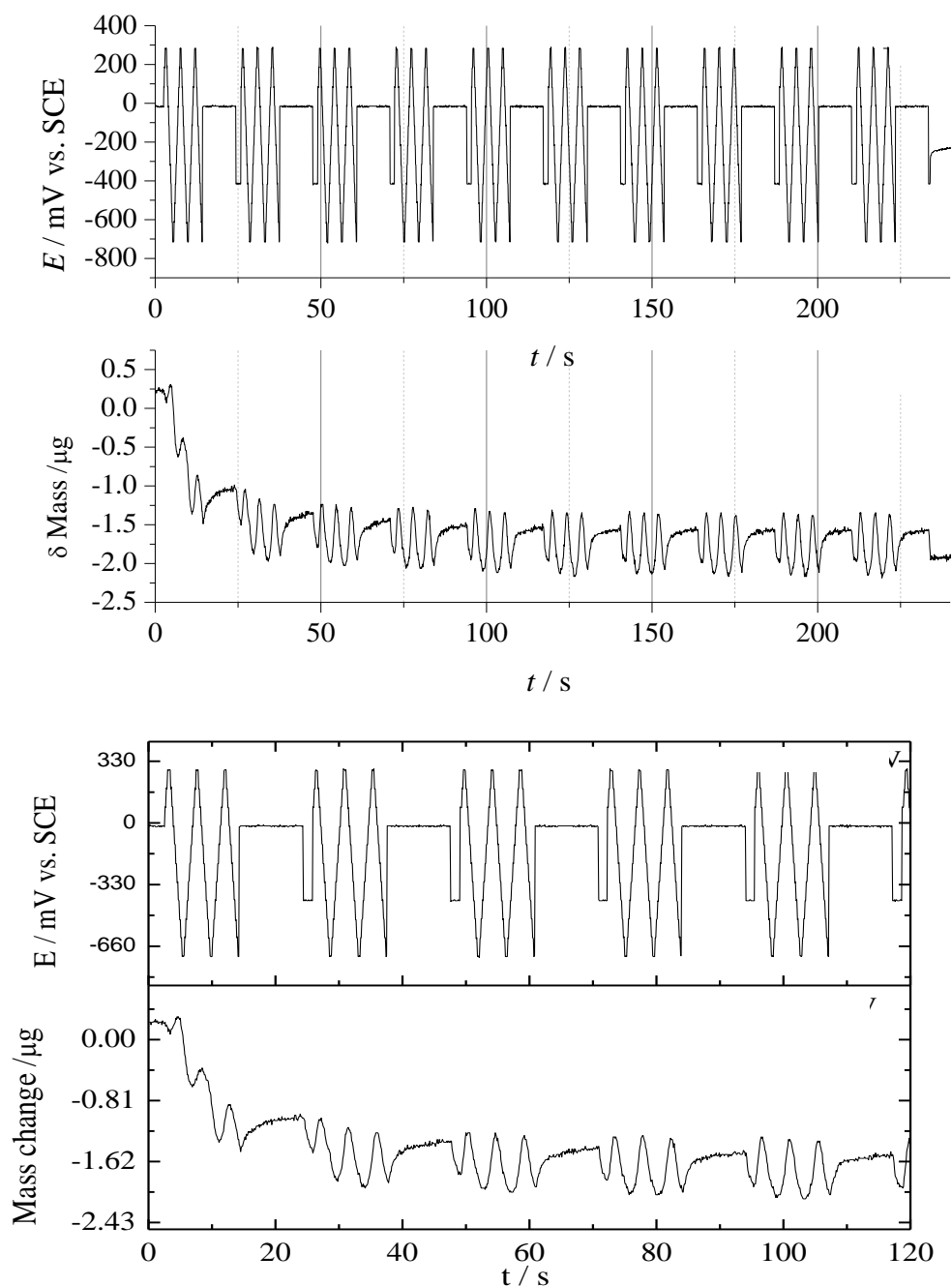
Figure 4.30 The waveform (10 cycles) and corresponding mass changes for ORR in 0.5 M KCl at -0.4 V *vs.* SCE on platinum deposited onto the gold on quartz EQCM crystal. Electrode geometric area =1.37 cm^2. Sweep rate is 500 mV s^{-1}. The lower figure is a zoom on the first 2 min recorded.

The results are shown in Figures 4.30 and 4.31. The mass changes were recorded during ten consecutive waveforms. Interestingly the mass changes became reproducible after two waveforms. For a given waveform the mass increases when sweeping towards the upper cleaning potential,

decreases when sweeping towards the lower cleaning potential, slightly increases during the rest period and decreases during the measuring step at -0.4 V. These observations are consistent with a build-up of oxide when sweeping towards the upper cleaning potential, the removal of oxide during sweeping towards lower cleaning potential, slight build-up of oxide when at rest, even at 0 V *vs*. SCE, and removal of this oxide during the measuring step as shown in section 4.24. However, no oxide stripping peak was observed when running stripping voltammograms after the rest period. The two experiments are however difficult to compare because the stripping experiments were recorded with a 25 μm diameter disc with a typical roughness factor of 3 whereas the EQCM experiments are performed with 1.37 cm^2 with roughness factor of 109.

EQCM experiments in perchlorate, Figure 4.32, show similar trends as in chloride, although the mass build up observed during the rest period appears a lot larger. The gradual loss of mass with the first two waveforms is unexplained.

Analysis of the main transients reveals that the first mass decrease seen during the potential step after the rest depends on potential, -0.5 μg for a step at -0.4 V and -0.16 μg for a step to -0.1 V (see Figure 4.31). The fact that the mass decreases during the step indicates that a layer or a fraction of a layer is removed during the step. This therefore rules out the hypothesis of Pt being plated during the step since the plating of Pt would lead to a mass increase.
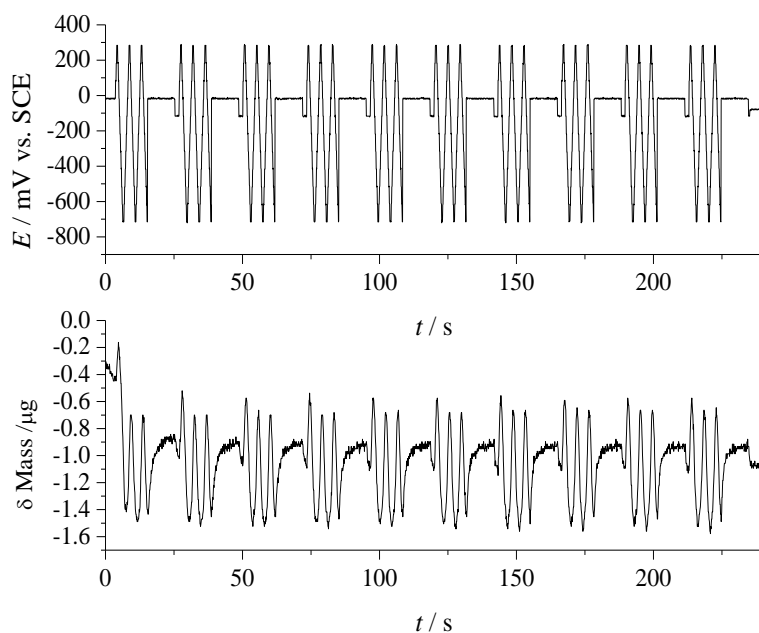

Figure 4.31 The waveform (10 cycles) and corresponding mass changes for ORR in 0.5 M KCl with -0.1 V *vs*. SCE on platinum deposited onto the gold on quartz EQCM crystal. Electrode geometric area =1.37 cm^2. Sweep rate is 500 mV s^{-1}.

Applying Equation 4.3 to a 25 microns diameter disc electrode (R_f=3), the corresponding charge = 9.7 x 10^{-11} C and the question raised here is whether it is equivalent to the extra charge seen during the potential step (7.89 x 10^{-10} C)?

Although this number is big once considering what has been observed during the last step of the sequence, it is still a realistic quantity considering the assumptions made during the calculation. It is therefore reasonable to interpret the observed mass charge as corresponding to the desorption of a fraction of monolayer of adsorbed anions.

Assuming a monolayer of chloride adsorbs and desorbs from the same sites as H, a charge of 210 μC cm^{-2} would be involved. Taking into account the roughness factor (109) the corresponding charge would be ~0.03 C (210x10^{-6} C cm^{-2} *1.37 cm^2 * 109) and the corresponding mass change would be ~ 11 μg (210x10^{-6} C cm^{-2} * 1.37 cm^2 * 109 / 96485 C mol^{-1} * 35 g mol^{-1}). This is less than one order of magnitude larger than any of the mass changes observed with the EQCM and therefore reasonable considering the assumptions made in the calculation.

Looking at Figure 4.32, where the mass changes were recorded in perchlorate solution, the mass loss appears to be important at the beginning then the mass stabilizes, although it goes up and down during the waveform. It should be noted that in ClO_4^- the initial mass loss is slightly smaller than in Cl^-.
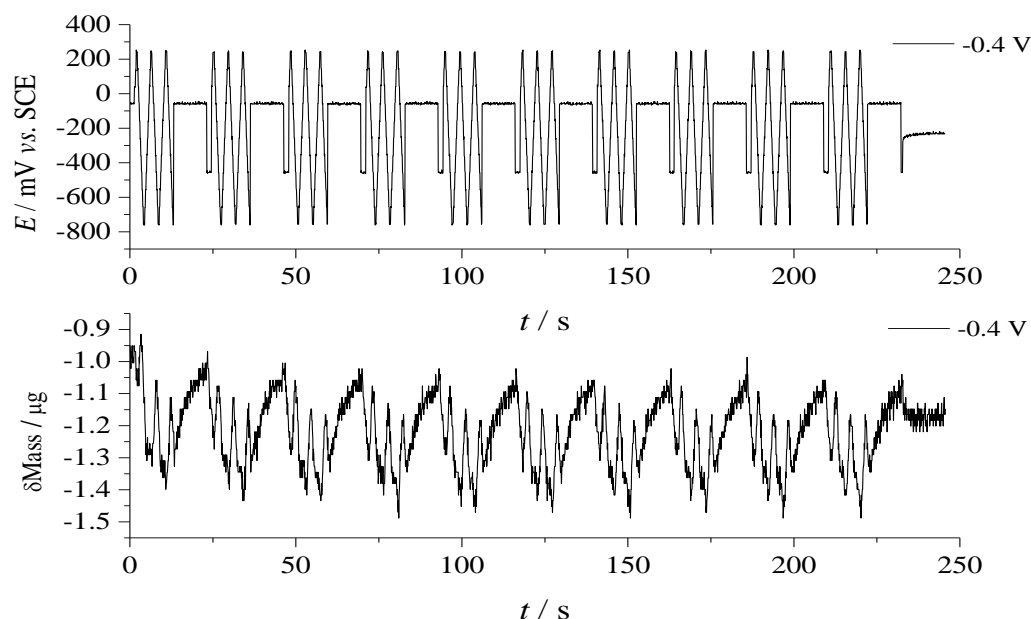
Figure 4.30 The waveform (10 cycles) and corresponding mass changes in 0.5 M $KClO_4$ at -0.4V as a measuring potential (*vs*. SCE) at platinum deposited onto gold quartz. Electrode geometric area =1.37 cm^2.

The Pt dissolution was seen, using EQCM, during the repeated β-oxide (amorphous) reduction cycles and Pt was re-deposited at negative potential in the work carried out by Birss *et al* [127]. The combination of Inductively Coupled Plasma Mass Spectroscopy (ICP-Mass) analysis and Atomic Force Microscopy (AFM) images confirmed the mass loss as a result of Pt dissolution in chloride containing electrolyte [58]. The dissolution of Pt depends on the concentration of chloride. With as low as 100 ppm chloride concentration, there was a significant Pt dissolution rate. Hence it would be expected that a large dissolution will take place with 0.5 M KCl and re-deposition could be hindered due to the overpotential needed to drive the reduction reaction for chloride complex. A similar observation was made by other investigators when sweeping in a negative potential direction, resulting in deposition of Pt atoms. Most importantly, our findings show additional charge which we do not believe is due to a re-deposition phenomenon. Quantitative estimations of the amount of Pt undergoing dissolution seemed to be small, and it was not possible to identify the dissolution products. Furthermore, the experiment done in ClO_4^-, i.e. in absence of Cl^-, shows the mass changing in sync with the waveform. As Pt is not expected to dissolve in ClO_4^- the above experiments seem to rule out the dissolution / deposition of Pt during the ORR in Cl^- or ClO_4^- media.

114

The specific adsorption of perchlorate ions on Pt was recently proven, using EQCM technique and ATR- FTIR spectroscopy [47]. The mass increased markedly in presence of oxygen species compared with its absence in recent study. Additionally, the ORR current and mass decreased gradually with time. They attributed this to the adsorbed oxygen species on Pt-EQCM under diffusion controlled region [47]. However our data in Figures 4.31 and 4.32 are still not clear towards the dissolution behaviour of Pt and more investigations should be done.

So far, the data for the reconstructed SCVs have shown unexpected results. Calculations predict that the current is unlikely to be due to the charging of the double layer. It is possible the observed behaviour could arise from adsorbates, although the adsorption would mean fewer active sites for the redox species of interest. In particular, the shape of reconstructed voltammograms for the electroreduction of oxygen could be understood in terms of strong effect arising from the adsorption of chloride. Since the presence of the adsorbed species will also influence the results obtained, trials were therefore attempted in different non-chloride electrolytes. This is the subject of the next section.

4.3.7   Sampled current voltammetry for ORR in other electrolytes
4.3.7.1 NaOH

It was reported previously that the ORR is sensitive to the supporting electrolyte. To establish the role of different species in the reduction mechanism when performing sampled current voltammetry, further experiments were carried out. Zhang *et al* found that the ORR is a quasi-reversible diffusion-controlled reaction at polycrystalline Pt electrode in NaOH [128]. Therefore, the ORR was investigated in a NaOH solution to examine whether making the reaction more ideal would help the interpretation of the transient ORR response. Experiments in NaOH solutions were run and the calomel reference electrode was separated in the electrochemical cell with a frit to minimise the leakage of chloride. It should also be noticed that the diffusion coefficient and concentration of O_2 will be different from those in KCl solution.

Steady state voltammetry was recorded and a typical voltammogram is presented in Figure 4.33. Additionally, the reduction of Pt oxide in 0.1 M NaOH electrolyte was not complete until the H_2 adsorption region as it was found for alkaline electrolyte [129].
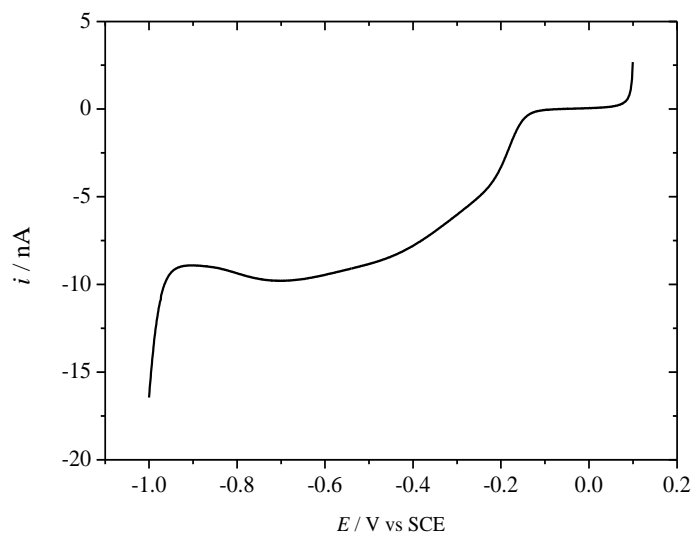
Figure 4.33 Stable steady state voltammogram in aerated aqueous 0.5 M NaOH, using 25 μm Ø Pt microdisc electrode as working electrode recorded at 10 mV s^{-1} at 25 °C.

The potential programme of the conditioning waveform was then modified as a result of noticeable shift in ORR in NaOH. The preconditioning procedures were set to be from 0.3 to -0.7 V while the resting potential 0 V and the current was measured along the ORR wave at different targeted potentials. Figure 4.34 represents SCVs for ORR. An extensive region for the maximum rates of the reduction of oxygen (pseudo steady state plateau) was observed.

Figure 4.31 Reconstructed voltammograms normalised by Mahon and Oldham theory after applying the conditioning waveform (sweeps at 500 mV /s: 0.1_-0.9_0.1_-0.9_0.1_-0.9 V; step (10 s): -0.1 V) at a Pt microdisc (25 μm diameter radius) in 0.5 M NaOH at 25 °C. SCE served as a RE and Pt mesh as a CE. The parameters used to normalise the experimental currents were: c^∞ =2.29x10^{-07} mol cm^{-3}, D_{O2}=2.45x10^{-05} cm^2 s^{-1}, $E_{1/2}$ =-0.3 V and a = 12.5x10^{-4} cm.
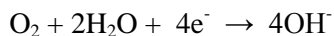
Looking at Figure 4.34, the n_{app} obtained is larger than expected. This would suggest that the process is not related to chloride.

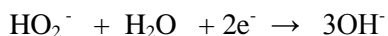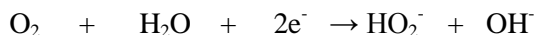The overall mechanism of ORR in alkaline solution is depicted below.

$k_1\ (4e^-)$

k_b $\quad k_5\ (2e^-)$ $\quad k_3(2e^-)$

O_2 $\quad O_2$ $\quad OH_2^-$ surface $\quad OH^-$
bulk $\quad$ surface

k_4 $\quad k_5$

OH_2^- bulk

Scheme 4.1 Mechanism of ORR in alkaline solution[26]

In neutral and alkaline conditions, the direct reduction of O_2 produces OH^- as follows
$$O_2 + 2H_2O + 4e^- \rightarrow 4OH^-$$
while the indirect four-electron reduction produces OH^- as follows
$$O_2 + H_2O + 2e^- \rightarrow HO_2^- + OH^-$$
$$HO_2^- + H_2O + 2e^- \rightarrow 3OH^-$$

Using a channel flow double electrode (CFDE) it was possible for (HO_2^-) which is generated by the reduction of O_2 on the working electrode in NaOH solution to be detected with the collecting electrode [103]. Additionally, using EIS technique confirmed the detection of HO_2^- as an intermediate during ORR at Pt electrode [103]. In the frequency domain examined by EIS, there was an evidence of the involvement of the intermediate of HO_2^- in indirect four-electron reduction showing inductive behaviour [103].

Some studies reported [128]on the differences between ORR in both NaCl and NaOH under mass transport control (using convective RDE experiment). In the case of NaOH, a well-formed reduction of oxygen was seen at different rotation rates with a shift in $E_{1/2}$ compared to the experiment conducting in NaCl.

Another electrolyte composition was tested under transient conditions for ORR to see whether less weakly adsorbed perchlorate species could make a difference to the obtained SCVs data for ORR. The following section outlines the findings for ORR in sodium perchlorate solution.

4.3.7.2 Perchlorate

Due to the low adsorbability of perchlorate ions compared to Cl^- and OH^- ions at noble metals, a perchlorate electrolyte was used to avoid the effect from specifically adsorbed ions on the response of ORR when applying the conditioning.

In Figure 4.35, a cyclic voltammogramm was run at 200 mV s^{-1} in aerated NaClO$_4$ solution to investigate the absence of chloride ion on the voltammogram and on the reconstructed voltammograms since the adsorption of perchlorate is weaker than that of chloride ion [46]. One clear observation is the similarity of the voltammograms in both NaCl and NaClO$_4$; this confirms that the effect of anion adsorption was negligible. Comparing with similar experiments in NaCl and KCl, Figures 4.1 and 4.2, it can be seen that the presence of perchlorate anions shifts the oxide formation region to more positive potentials and slightly compresses the hydrogen oxidation due to the blocking of Pt sites. The adsorption of perchlorate anions leads to a decrease of the ORR rate [47].
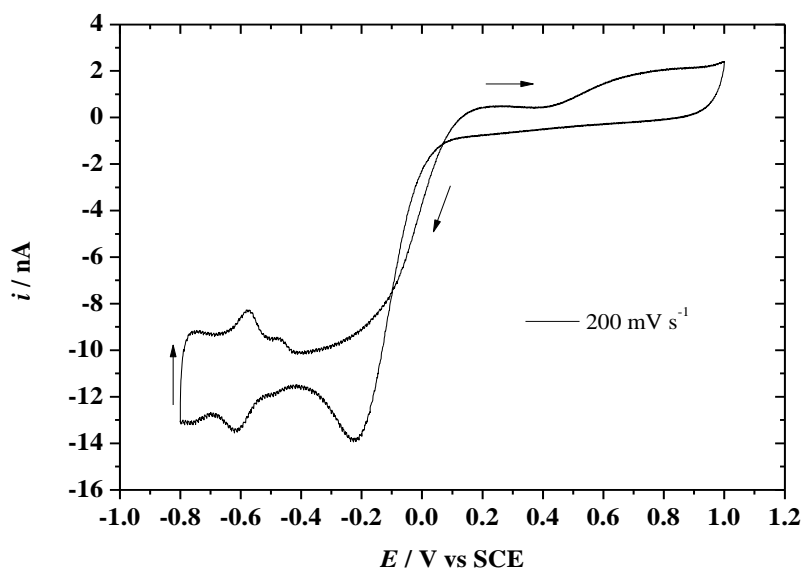

Figure 4.32 Stable cyclic voltammogram, in aerated aqueous 0.5 M NaClO$_4$ at 200 mV s^{-1}, after 10 cycles using a 25 μm Ø Pt microdisc electrode as working electrode recorded at room temperature.

The ORR was then investigated under steady state conditions. Figure 4.36 shows the recorded electroreduction of oxygen steady state at low scan rate. A well-defined wave was observed and an extended plateau region was seen when compared to the ORR wave in KCl solution.
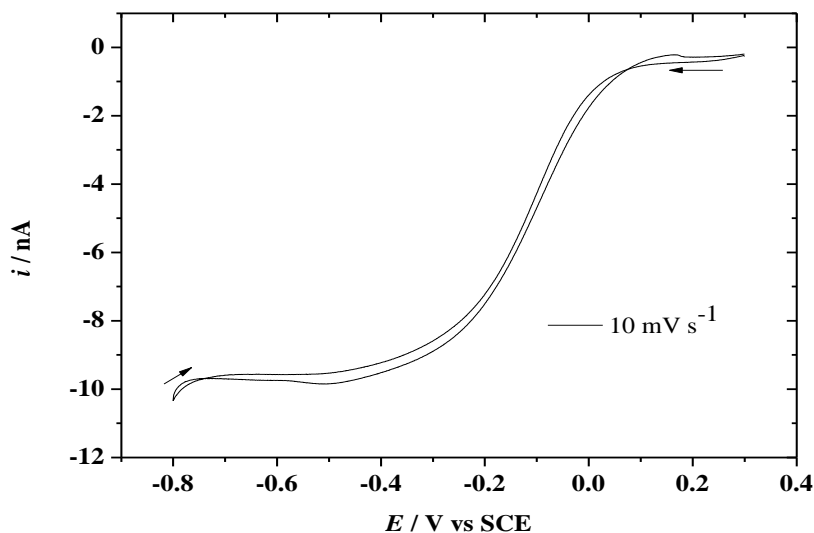

Figure 4.33 Stable steady state voltammogram in aerated aqueous 0.5 M NaClO$_4$ at 10 mV s^{-1}, using 25 μm Ø Pt microdisc electrode as working electrode recorded at 25°C.

However, the question raised here is whether this electrolyte is chloride free or not? In order to minimise the effect of diffusion of chloride from the reference electrode (SCE), a special frit was used to slow down the leakage of chloride ion. However, the experiments carried out in NaClO$_4$ solution could suffer from the presence of chloride as impurity or from the slow reduction of perchlorate to form chloride anions which can cause complications, such as poor reproducibility as reported in methanol oxidation studies at platinum electrode [130]. A marked reduction of perchlorate was observed at Ru and Ir electrodes. Furthermore, it is known to undergo reduction catalytically and electrocatalytically on Pt black powder. However, this reduction can be blocked by adsorbed hydrogen through competitive adsorption with the reacting species as seen in current transient data in presence of HClO$_4$ and H$_2$SO$_4$.

The conditioning waveform was applied to investigate the ORR in $NaClO_4$ solution. The upper cleaning potential was kept at 0.3 V, and from this point the potential was scanned to -0.7 V, holding for 10 s at 0 V, and finally measuring for 0.5 s at various potentials along the wave for ORR. The parameters used to generate the theoretical voltammograms with equation 1.2 were as follows: $D = 2.2 \times 10^{-5}$ cm s^{-1}, $c^{\infty} = 2.2 \times 10^{-7}$ mol cm^{-3}, $i_{lim} = 8.41$ nA and $E_{1/2} = -0.1$ V at 298 K. Again, n_{app} involved in the reaction seemed to increase as the sampling time decreased as shown in Figure 4.37. Once again n_{app} is seen to reach unexpectedly large values at very short sampling times. The work done by Jovancicevic *et al* [131] showed the deviation of experimental currents from theoretical at times shorter than 0.5 s for buffered borrate solutions.

Figure 4.34 Reconstructed voltammograms normalised by Mahon and Oldham theory after applying the conditioning waveform (sweeps at 500 mV /s: 0.6_-0.7_0.6_-0.7_0.6_-0.7_0.6_-0.7 V; 10 s rest at 0.1 V) at a Pt microdisc (25 μm diameter) in 0.5 M $NaClO_4$ at 25°C. SCE served as a RE. The parameters used to normalise the experimental currents were: $c^{\infty} = 2.29 \times 10^{-7}$ mol cm^{-3}, $D_{O2} = 2.45 \times 10^{-5}$ cm^2 s^{-1} and $a = 12.5 \times 10^{-4}$ cm. Sampling times were as follows: 500, 200,100, 50, 20, 10, 5 and 3 ms (from top to bottom).

The presence of chloride as a product of the reduction of perchlorate could affect this investigation. The reduction of perchlorate to chloride is as follows.

$$ClO_4^- + 8H^+ + 8e^- \rightarrow Cl^- + 4H_2O$$
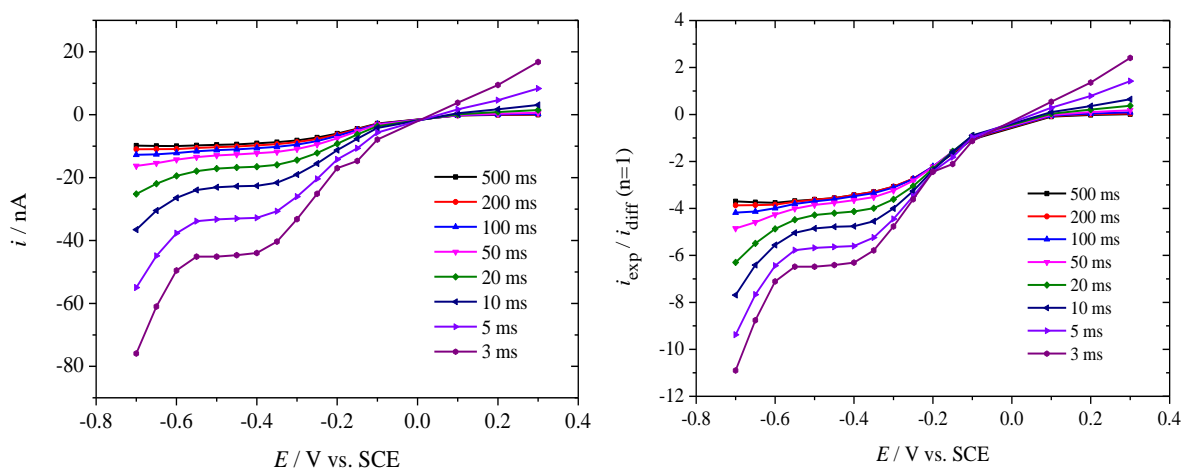
It is well known that the product of the reduction reaction, chloride ion, acts as inhibitor for many reactions including ORR. Previous investigations were performed to probe the effect of milimolar amounts of chloride on the recorded CV for perchlorate solution [51]. Bearing in mind that the adsorption strength of ions affects the activity of reduction of oxygen, the surface sensitivity decreases in respect to anions in the order $ClO_4^- > HSO_4^- > Cl^-$. Although the presence of either

chloride or sulphate ion -which can adsorb on the surface - inhibits the kinetics of the reduction, it does not affect the pathway of the reaction [60].

Overall, the ORR in both NaOH and $NaClO_4$ followed the same behaviour. The rate determining step for ORR in both NaCl and $NaClO_4$ was the same first order in oxygen adsorption [51]. However the kinetics was different. There was an observable cathodic shift in ORR in $NaClO_4$ compared to chloride containing solution; this is presumably not due to chloride adsorption since the CV in case of chloride contamination would give the same CV as in KCl or NaCl. ORR is controlled to a large degree by adsorption / desorption and Pt surface exhibits oxidation / reduction at potentials similar to that of the ORR. It was reported previously that chloride containing electrolyte tends to generate more peroxide than perchlorate under the same pH [51]. However, the findings showed that the response for the reconstructed voltammograms for ORR did not depend on the tested electrolyte, since the same behaviour of irreversibility and slanted waves for ORR was seen in KCl, NaOH and $NaClO_4$ solutions.

4.4 Conclusion

The reduction of O_2 at Au and Pt was explored extensively in this chapter. It showed significantly different responses due to various factors. In particular surface processes caused considerable difficulty in obtaining a response free of any adsorption complication. The interpretation of the results when investigating the n_{app} involved in the reaction as a function of time was found to be really difficult at very short times.

Background subtraction was not really effective in this work. The reason for this behaviour is attributed to the fact that hydrogen adsorption/desorption take place at different potentials and to different extends in presence and absence of oxygen. Based on the results of the experiments, this effect depends on the redox species, although both molecular oxygen and $Ru(NH_3)_6^{3+}$ reduction showed similar current deviation in the hydride adsorption region at short timescales, however, the background surface processes in case of the ruthenium complex reduction are believed to be suppressed by the conditioning waveform we developed.

The conditioning waveform worked well for the reduction of ruthenium complex, hence validating the approach. It minimised the background processes and it was possible to get very well defined sampled current voltammograms even at 3 ms. The basis of this conclusion was shown when comparing the reconstructed voltammograms of ruthenium and ORR, after applying a conditioning waveform. When applied to ORR, it was no longer possible to fit the reconstructed voltammograms at all timescales with one n_{app} value. Instead, it was necessary to increase n_{app} values as the sampling time was shortened. This was not a problem with the methodology; it is a feature of the ORR at very short time.

There was a large faradaic signal from an unknown source under the current experimental conditions; therefore, some further experiments were tried. The signal dependency on the adsorbed ion was investigated, showing almost similar behaviour of extra current for reduced oxygen species. There was a considerable difficulty to determine the source of the increase in mass in the measuring step of the conditioning waveform. The possibility likely to explain the increase in current seemed not to be related to the adsorption of anions as the behaviour of ORR in different solution compositions such as chloride, hydroxide and perchlorate containing electrolytes was almost the same.

It was important to investigate whether the increase in the signal described above was caused by a displacement of chloride and for this purpose and in order to elucidate the cause of these

observations, the conditioning waveform was modified to include double potential step experiments in order to detect the source of the extra current. An increase in charge was clearly seen as the timescale was shortened. This also allowed tuning the resting potential in the applied conditioning waveform.

The nature of ORR mechanism at short time regimes is still open to question. Was it governed by the dissolution of Pt? EQCM results indicate a decrease in mass during the ORR measuring step after the electrode was subjected to the conditioning waveform. This therefore suggests that possible plating of Pt dissolved during the cleaning sequence is not the cause of the extra current seen at short times. The next chapter sheds light on the investigation of ORR at coated electrodes.

Chapter 5

Development of coatings to protect the microelectrodes for oxygen sensing and dopamine detection

5 Overview

Chapter five introduces the development of inorganic and organic coatings for the protection of both platinum (Pt) and carbon fibre (CF) microdisc electrodes. This is basically another way to modify the electrode to minimise the interferences instead of designing a cleaning waveform (as it was mentioned in chapter 3). The modified electrodes would then be used to investigate the ORR for example in a biological medium in presence of dopamine. Therefore, different coated electrodes are considered to study the reduction of oxygen in presence of dopamine. The chapter also presents results for the preparation and characterisation of the different coatings and their use in voltammetric and chronoamperometric experiments.

Chemically Modified Electrodes

Chemically modified electrodes (CMEs) have attracted great attention as important analytical tools to be used for the electrochemical determination of various analytes. The modification of the electrodes results in efficient detection of electroactive biomolecules while excluding major interferences. Generally, exploiting the use of inorganic and organic materials for the modification of electrodes surface has been of common interest for many researchers, particularly with polymer-modified electrodes (PMEs) [132]. Electropolymerization is a good approach to prepare PMEs in which adjusting electrochemical parameters can help control film thickness, permeation

and charge transport characteristics. PMEs are advantageous in the detection of analytes as they exhibit some key properties such as selectivity, sensitivity and homogeneity in electrochemical deposition, in addition to strong adherence to electrode surface and chemical stability of the film [4-5].

Numerous efforts have been paid to the search for the best coatings for the oxygen reduction reaction. A survey of the literature reveals that modification of electrode for electrocatalytic reduction of O_2 was studied at Pt dispersed on poly(1,2 diaminobenzene) films [133], Pt/polyaniline [134] and Au-polyaniline porous nanocomposites [135]. These coatings, in particular conducting polymers have been used for specific applications in various fields such as fuel cells, biosensors, electroanalysis, and electrocatalysis. Interestingly; they offer plenty of advantages in enhancing the electrocatalytic activity towards the ORR [133].

5.1 Deposition of poly (phenylene oxide) film at microelectrodes

The new surface was firstly prepared with a poly(phenylene oxide) (PPO) coating. This material is well known to be a very attractive candidate as protective coating [136]. 50 mM phenol as a monomer in 0.1 M sodium phosphate buffer (pH=7) was used for the deposition. The deposition procedures were carried out either by cyclic voltammetry or double potential steps experiment. For cyclic voltammetry (Figure 5.1), the working electrode was scanned between 0.2 V and 0.9 V till achieving a straight line with no response. The first scan reflects the oxidation of phenol to poly(phenylene oxide) at around 0.6 V at a 50 µm Ø Pt electrode while the subsequent scans show a decay in current. In contrast the CF is not showing a sharp oxidation peak compared to the Pt substrate. However, a similar decrease in current is seen after the first scan. The double potential step deposition was accomplished by applying the following potential step regime: 0.0 V (20 s), +0.9 V (8 min) and 0.0 V (20 s) (potentials measured vs. SCE). After modification the electrodes were washed with distilled water and capped with a plastic pipette to protect the coated electrode.
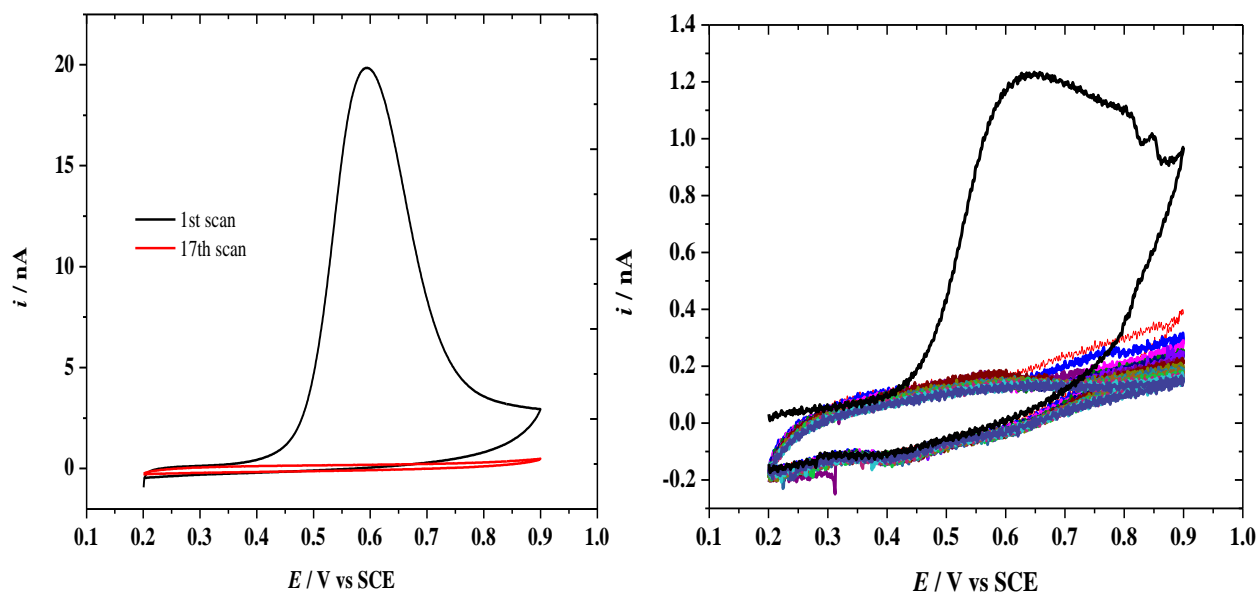
Figure 5.1 Cyclic voltammograms for deposition of a poly (phenylene oxide) film on 50 μm Ø Pt (left) and 7 μm Ø CF (right) microdisc working electrodes in 50 mM phenol and 0.1 M sodium phosphate buffer (pH=7.0) at 50 mV s^{-1} at 25 °C under deoxygenated conditions. Black line in both plots is for the first scan of the deposition. Different coloured lines in the right plot show consecutive scans.

Phenol was chosen as a monomer for the deposition and electropolymerization [137] is reported to proceed according to the following scheme.
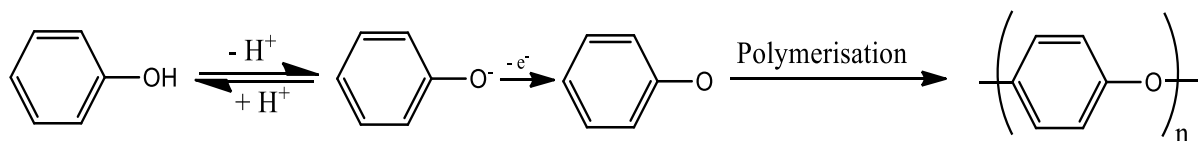
Scheme 5.1 The electrooxidation processes of phenol.

Basically, from Scheme 5.1, it could be said that under electropolymerization of phenol, productions of *para-* coupling of phenolate radicals occur by oxidation of the phenylate anion. In subsequent reactions oligomers are produced and, finally, poly(phenylene oxide) films are polymerized on the surface of the electrode creating an insulating layer at the electrode surface and causing the current to fall.

There have been some reports investigating the use of this polymer for various applications. According to the work done by Bartlett *et al.* a thin layer film with a matrix of glucose oxidase (GOx) with a thickness of nanometer (25 mM phenol, sweep range of 0.00–0.95 V vs. SCE) was

126

deposited at Pt electrodes for sensing glucose concentrations towards the fabrication of glucose biosensors [136].

Characterisation of poly (phenylene oxide) film

The permselective behaviour of the polymer coating was studied in this work. To address the selectivity demand of the coated electrode toward redox species, experiments in positively and negatively charged ions was accomplished. Characterisation of the film, deposited on the electrode was done by probing it with a negatively charge ferro/ ferri-cyanide complex ion. The electrochemistry of this ion shows no response (Figure 5.2), which means the success in depositing the film and in rejecting the interferences from negatively charged species, such as ascorbate. The presence of non-electroactive polymer layers facilitates the production of a selective electrode that allows certain molecules like the ruthenium hexaammine ion (Figure 5.3), dopamine or oxygen to reach the surface of the electrode.
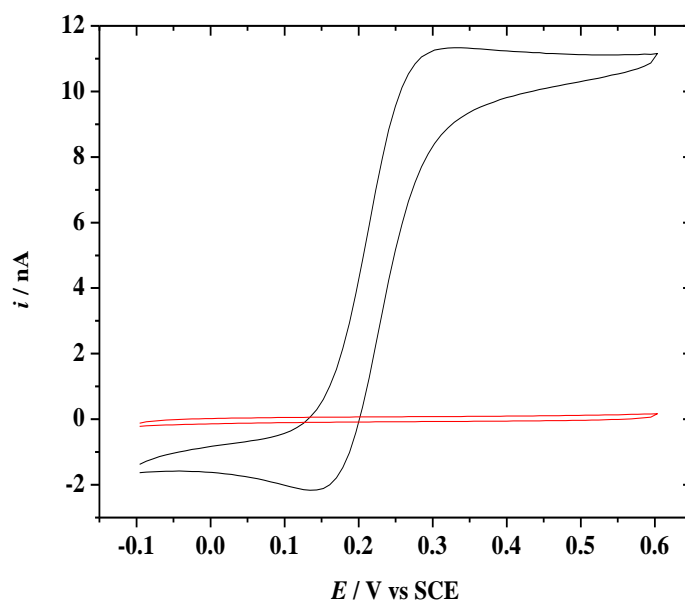
Figure 5.2 Cyclic voltammograms (first cycle) for oxidation of 5 mM ferro to ferricyanide in 0.5 M Na_2SO_4 system at 200 mV s^{-1}. The red line represents the electrode with poly (phenylene oxide) film on it and the black line the bare 25 μm Ø Pt microdisc working electrode. The coating was deposited in 50 mM phenol and in 0.1 M sodium phosphate buffer (pH=7.0) at 50 mV s^{-1}, recorded at 25ºC.
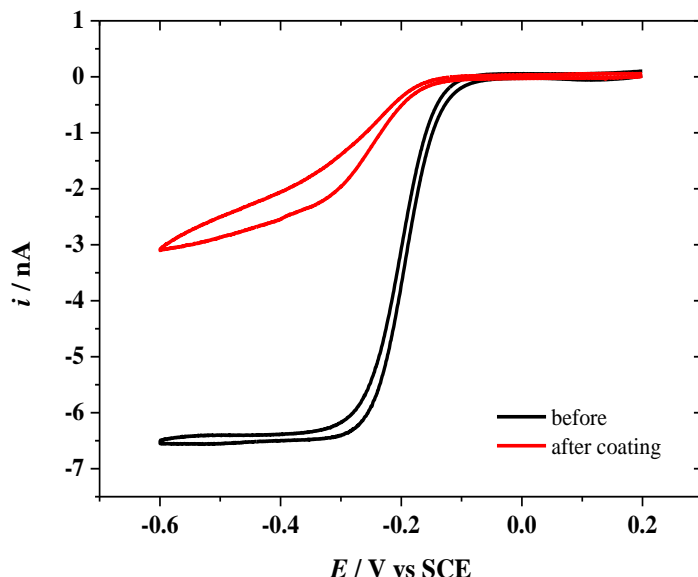
Figure 5.3 Cyclic voltammograms (1st cycle) for reduction of 5 mM ruthenium hexaaammine at 10 mV s^{-1} in 0.5 M KCl system and 25 ºC. The red line represents the electrode with a poly (phenylene oxide) film on it, and the black line the bare 7 μm Ø CF microdisc. The coating was deposited in 50 mM phenol and in 0.1 M sodium phosphate buffer (pH=7.0) at 50 mV s^{-1}.

Investigation of ORR

In order to address the sensitivity of this coating towards ORR, the experiment was run in chloride solution in presence (Figures 5.5 to 5.7) and absence of oxygen species (Figures 5.4 to 5.6). The response was little affected by the presence of the coating. The surface processes such as hydrogen adsorption/desorption and oxide adsorption/stripping were still pronounced on the voltammogram. For the electrode with 25 μm Ø, it seems the adherence of the coating to the surface was weak and the film could be lost easily. This might be due to the local pH change occurring during the reduction of oxygen. Considering Figures 5.5 to 5.7 the presence of the coating does not appear to affect the ORR response; the response is almost identical to that at bare electrodes with no suppression of the adsorption and desorption of hydrogen and oxygen atoms. The magnitude of the peaks is unchanged, suggesting the electroactive area remains unchanged despite the coating. This may suggest that a film of water sits on the electrode beneath the film.
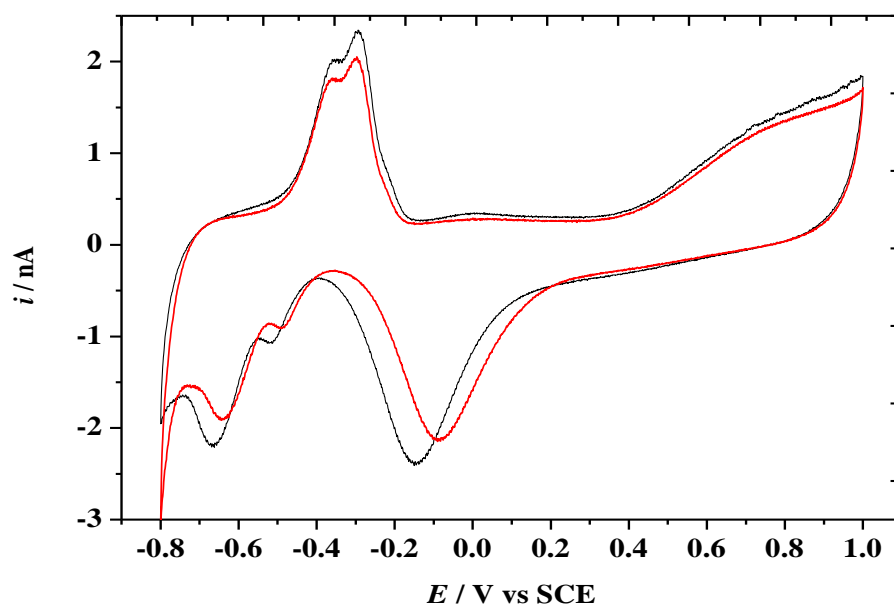
Figure 5.4 Stable cyclic voltammograms, in argon degassed aqueous 0.5 M KCl at 200 mV s^{-1}, using bare (black line) and poly (phenylene oxide) coated (red line) 25 µm Ø Pt microdisc electrodes; recorded at 25 ºC.
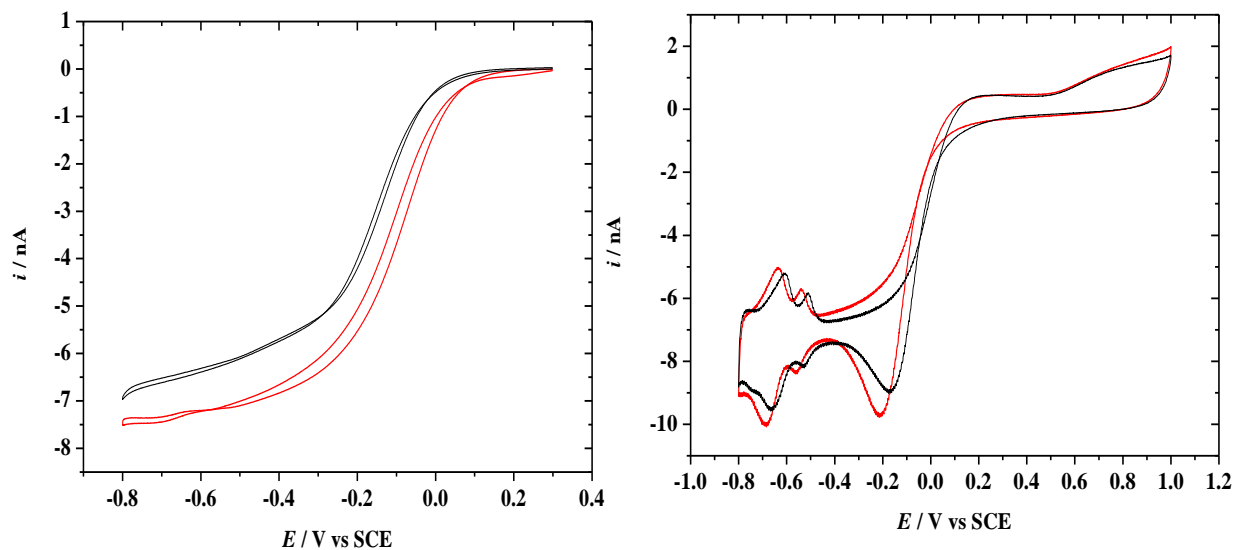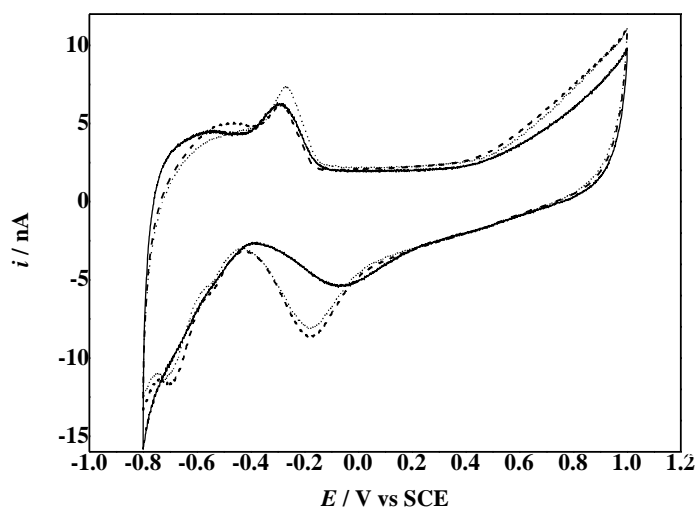

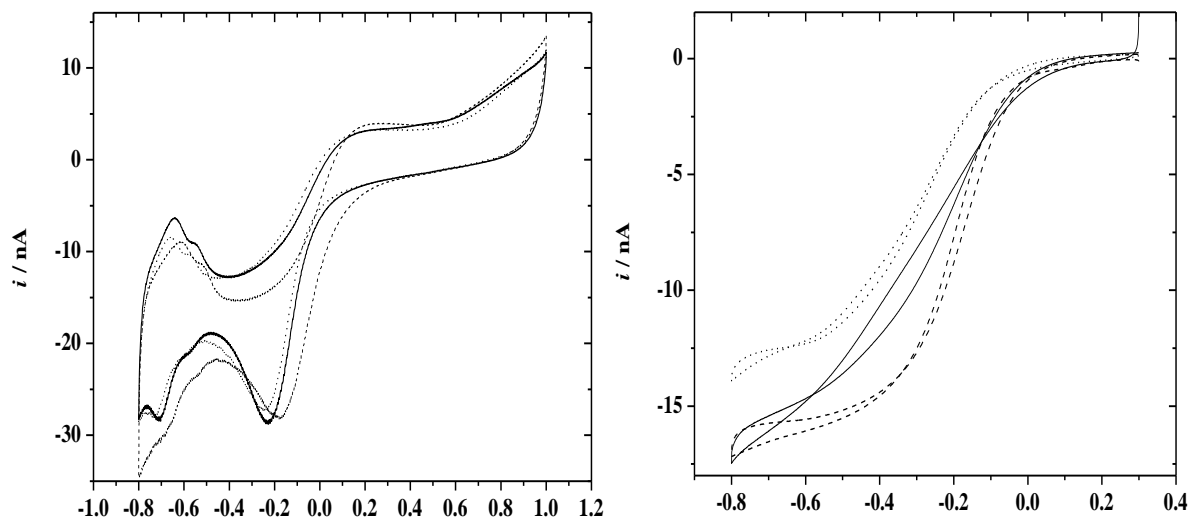**Figure 5.5** Stable cyclic voltammograms, in aerated aqueous 0.5 M KCl at 200 and 10 mV s^{-1}, using bare(black line) and poly (phenylene oxide) coated (red line) 25 µm Ø Pt microdisc electrode (dashed line); recorded at 25 ºC.

Figure 5.6 Stable cyclic voltammograms, in argon degassed aqueous 0.5 M KCl at 200 mV s^{-1}, using bare (solid line) and poly (phenlyene oxide) coated 50 µm Ø Pt microdisc electrode (dashed line for coating using CV and dotted line for coating using double potential step); recorded at 25 °C.

Figure 5.7 Stable $E/V\,vs\,SCE$ cyclic voltammograms, in aerated $E/V\,vs\,SCE$ aqueous 0.5 M KCl at 200 and 20 mV s^{-1}, using bare (solid line) and poly (phenlyene oxide) coated 50 µm Ø Pt microdisc electrode (dashed line for coating using CV and dotted line for coating using double potential step); recorded at 25°C.

130

This film is sensitive to pH changes and has been used as a pH sensor [136]. When employing it for ORR investigations, the background current (absence of oxygen species) is lowered significantly. In the next section we investigate the reduction of oxygen in presence of dopamine with PPO modified Pt electrodes.

Reduction of oxygen and oxidation of dopamine at poly(phenylene oxide) coated electrodes

The aim of the use of the coated electrode for the simultaneous determination of both ORR and dopamine is to promote these two desired reactions and prevent any fouling of the electrode. It was found that an electropolymerized non-conducting film is advantageous in exhibiting selectivity towards interfering species.
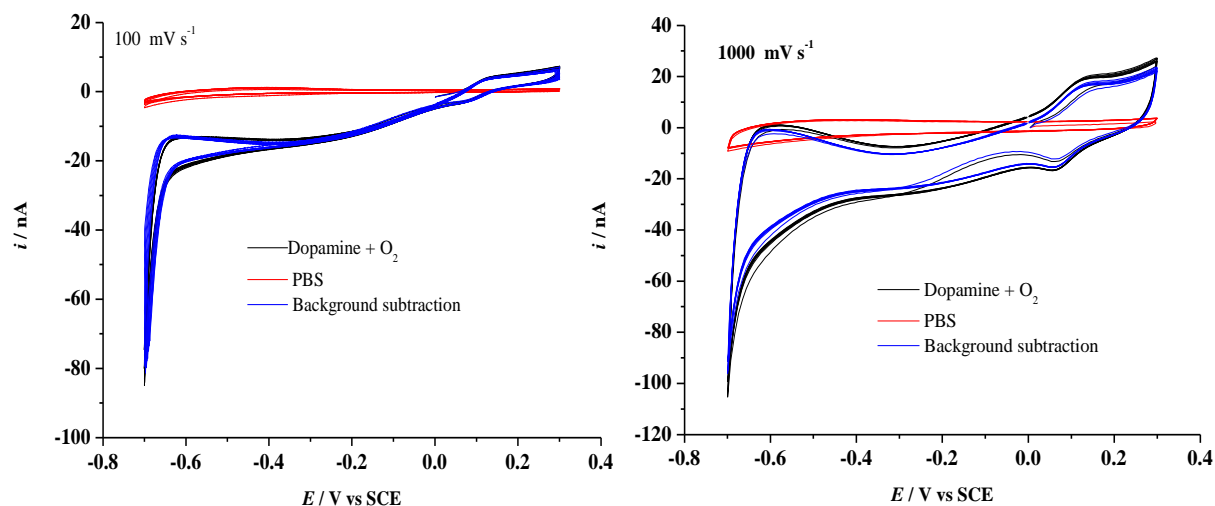
Figure 5.8 Eight cyclic voltammograms, in Ar purged 0.1 M PBS electrolyte (red), aerated 10^{-4} mM dopamine + 0.1 M PBS (black), and background subtracted (blue) at poly(phenylene oxide) coated 50 μm Ø Pt microdisc electrode, recorded at 37º C.

The dopamine was detectable at the modified Pt electrode (Figure 5.8). However, the signal for ORR was not as good as that for dopamine oxidation. The onset of hydrogen evolution was more positive compared with its position at uncoated electrode. The signal for dopamine oxidation was enhanced while the reduction of oxygen showed a clear wave compared with that at bare electrode (see appendices). This film has influence on the signal for the redox species under study. It could be concluded that this treatment of the electrode allows the simultaneous measurement of dopamine and reduced oxygen.

131

5.2 Deposition of polypyrrole film at microelectrodes

Another membrane material was used in this study. The pyrrole was purified by distillation before undertaking any eletropolymerisation experiment. The electropolymerisation was driven by the oxidation of pyrrole. The experiment was run at room temperature. In the first scan, a broad anodic peak was observed. It was followed by a steady decrease in the current passed with each scan, which is indicative of the build-up of an insulating polymer film due to sweeping to high positive potential (1.8 V vs SCE), (Figure 5.9). A similar shape of voltammogram was previously reported [138]. The peak current drops significantly with each scan until it reaches a minimum value. This indicates that a compact and nonconductive film is formed which blocks the access of the monomer to the electrode surface.
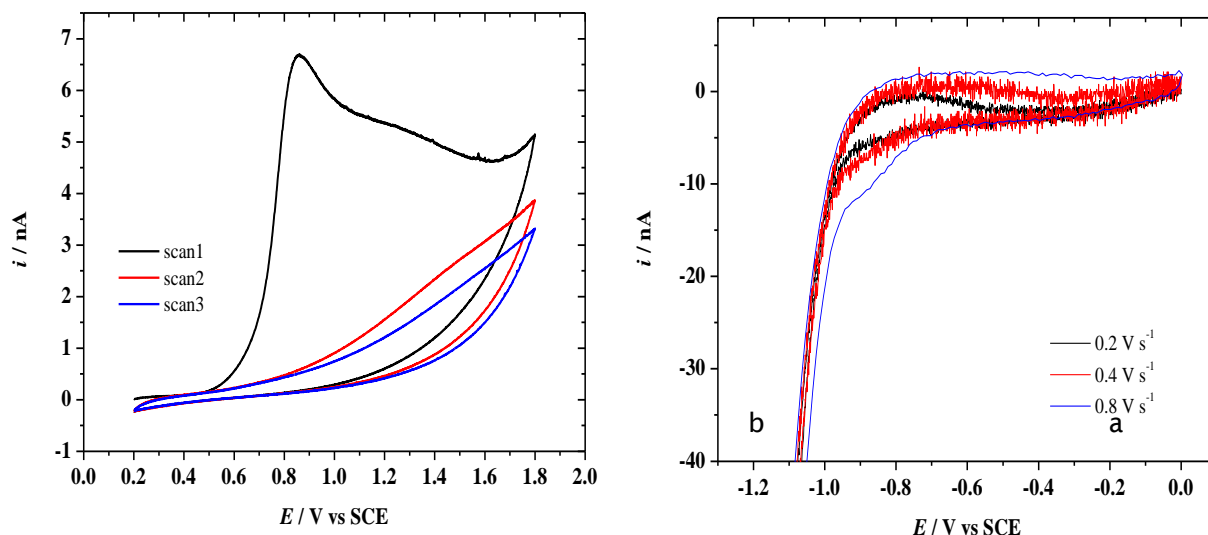

Figure 5.9 Cyclic voltammograms (three cycles) for the deposition of a polypyrrole film on a 25 μm Ø Pt microdisc electrode recorded at room temperature in 50 mM pyrrole and 0.2 M K_2SO_4 at 100 mV s^{-1} (a), and in 0.2 M K_2SO_4 to dope the coated electrode (b). A Pt mesh serves as a CE.

The behaviour seen during the electropolymerisation could be explained in terms of the fact that polypyrrole (PPy) is a positively charged conducting polymer (Figure 5.10). Upon overoxidation, it loses its conductivity and charge. XPS and FT-IR revealed that the overoxidation results in addition of carbonyl and carboxylic groups [139]. These groups are beneficial in attracting dopamine cations and rejecting ascorbate anions since the carbonyl groups create strong electrostatic interactions with dopamine and other cations.
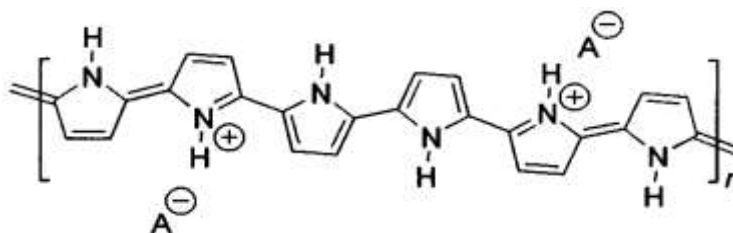
Figure 5.10 The structure of oxidised conducting (PPy).

It is well known that Overoxidised Polypyrrole (OPPy) is an electronegative polymer. The incorporation of amounts of negatively charged groups in the polymer backbone during overoxidation is responsible for the anion exclusion behaviour of the film. Overoxidation was accomplished by placing the polypyrrole coated electrode in 0.2 M K_2SO_4 and cycling at different scan rates to dope it (see Figure 5.9 (b). The background CV (in 0.2 M K_2SO_4 electrolyte) shows featureless profile with only hydrogen evolution at the negative potential side.
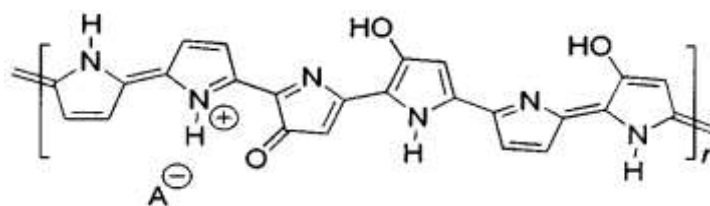
Figure 5.11 The structure of Overoxidised polypyrrole (OPPy).

The main characteristics of the OPPy (see Figure 5.11) films are that the PPy polymer is dedoped, i.e. the anions are expelled from the polymer, and some carbonyl groups are formed in β-position of the pyrrole rings [9–13] yielding disruption of the conjugation. Thus, repulsive interactions can be expected between anions and the carbonyl groups of the OPPy film, which have high-electron density. The OPPy is then produced as a result of PPy reaction with hydroxyl radicals.

Overoxidation of polypyrrole (PPy) films has been studied with the aim of controlling their permeability towards ionic species in solution. During overoxidation electron-rich groups are introduced onto pyrrole units, and the conducting polymer is converted into an ion exchange polymer. Differences in permeability are obtained by varying the component of the electrolyte solution in which the overoxidation of PPy is carried out. The exclusion of anionic species offers substantial improvement in the selectivity of voltammetric determination of cationic species.

Prevention of electrode fouling due to protein and surfactant adsorption is observed in the case of overoxidized PPy film coated electrodes in previous study.

The SEM technique was employed to examine the morphology of the deposited film on the electrode as it can be seen in Figure 5.12. The morphology of the film is similar to that reported in [140]. Some applications for this kind of modification are glucose [141] and H_2O_2 [142] sensor as the overoxidized polypyrrole was found to be a best candidate.

Characterisation of polypyrrole film

This film was characterised visually and chemically. The film was tested in some redox species like ruthenium complex ion and ferrocyanide complex ion. Figure 5.12 displays the difference in the response at bare and OPPy coated Pt electrodes. The permselectivity was probed with both negatively and positively charged redox species. In both cases the film led to a decrease in limiting current. The film seems to affect the rate of diffusion of the species under study, resulting in less limiting current. This may be due to the species membrane partition coefficient and to their molecular diffusion coefficient within the film [143]. It was demonstrated that the slow response times due to the diffusion of the species through this membrane was some of the merits it possesses [142].

According to some work in literature, the polymerisation of pyrrole and its overoxidation can be repeated several times to reduce the pinholes sufficiently to suppress the response for ferrocyanide [142]. The ratio in the decrease in limiting current for two probes, ferrocyanide oxidation and ruthenium reduction at OPPy coated electrode and bare electrode is not the same. Also, there are some agreements in literature regarding the extensive interfacial polymer growth formed from water [139] which suggest that the morphology could be affected by water which is trapped within the polymer chains. The OPPy is a membrane that possesses size exclusion property towards the tested probe. Therefore the ferrocyanide and ruthenium ions may be partially blocked to different extent due to their size and this could result in lower limiting currents. To obtain a uniformly thick film, the overoxidization step could last for hours [144].

This film was previously characterised using EIS technique [145]. Also, XPS was used to verify the presence of thin conducting polypyrrole (PPy) and non-conducting oxidised polypyrrole (OPPy) film [139]. Both were reported to show porosity.
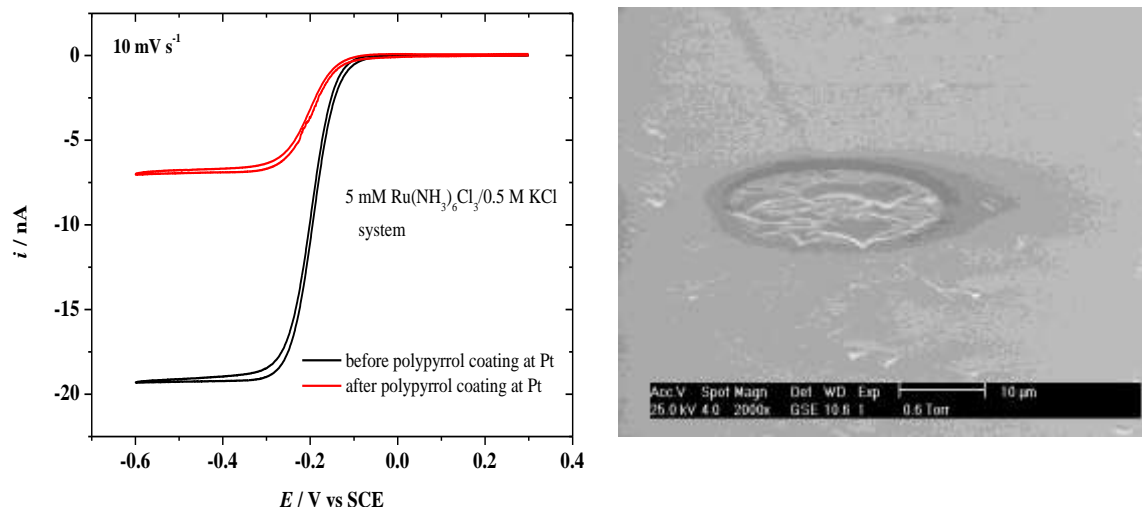
134

Figure 5.12 Cyclic voltammograms (1st cycle) for the reduction of 5 mM $Ru(NH_3)_6^{3+}$ to $Ru(NH_3)_6^{2+}$ in 0.5 M KCl (left) at 25 ºC. The red line represents the electrode with polypyrrole film on it and the black line the bare 25 μm Ø Pt microdisc electrode. The deposition of the electrode was accomplished in 50 mM pyrrole and in 0.2 M K_2SO_4 at 50 mV s^{-1}. The picture on the right shows the SEM for the polypyrrole coated electrode. The scale bar represents 10 μm.

Investigation of polypyrrole film

Further tests of the OPPy coating were carried out in presence of oxygen and observations were made on its effect on the limiting current for the ORR.

The film produced was thick enough to be seen on SEM images but its thickness appeared non-uniform. When compared with bare electrodes, the limiting current is smaller when the electrode is coated and this is consistent with previous observations (previous section), Figure 5.13.
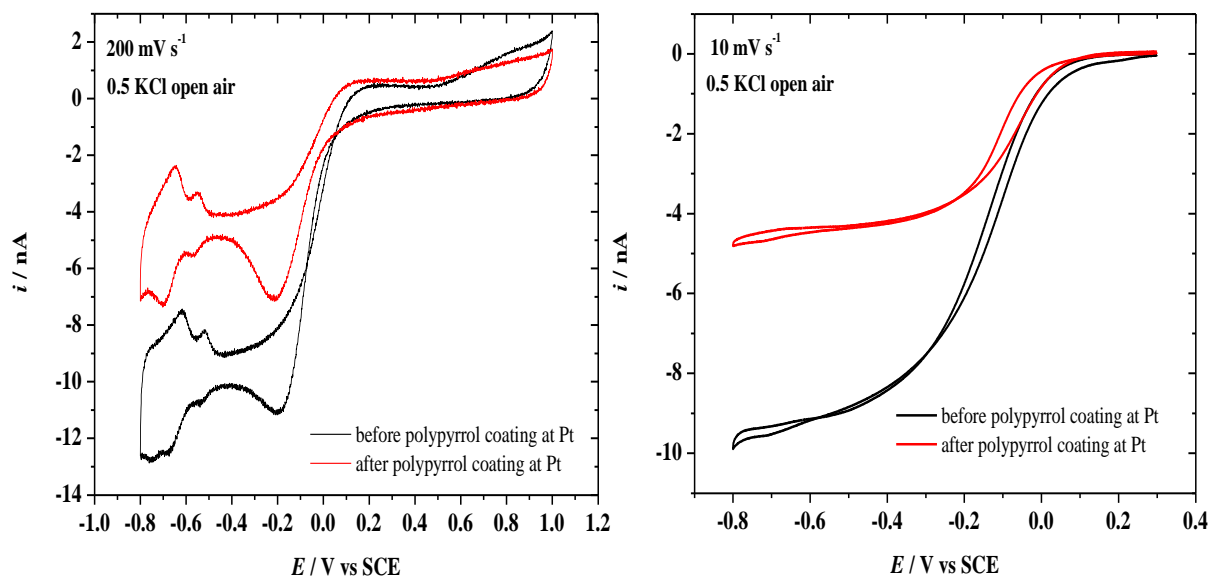
Figure 5.13 Stable cyclic voltammograms, in aerated aqueous 0.5 M KCl at 200 and 10 mV s^{-1}, using bare (black line) and polypyrrole coated (red line) 25 µm Ø Pt microdisc electrode, recorded at 25 ℃.

According to previous study of PPy for ORR investigation at dispersed Pt electrode, it was found that n_{app} is affected by pH [29]. In addition, polypyrrole with various thicknesses was used for pH potentiometric measurements when coated at GC electrode [146]. This protective barrier affects the ORR limiting current but to a different extent compared to the limiting currents for ruthenium and ferrocyanide redox species (CV is not shown).

In absence of O$_2$, the surface processes response decreases in presence of the film, Figure 5.14. But in presence of oxygen, figure 5.13 (left), the hydrogen adsorption/desorption peaks do not seem affected by the presence of the PPY film on the Pt electrode.
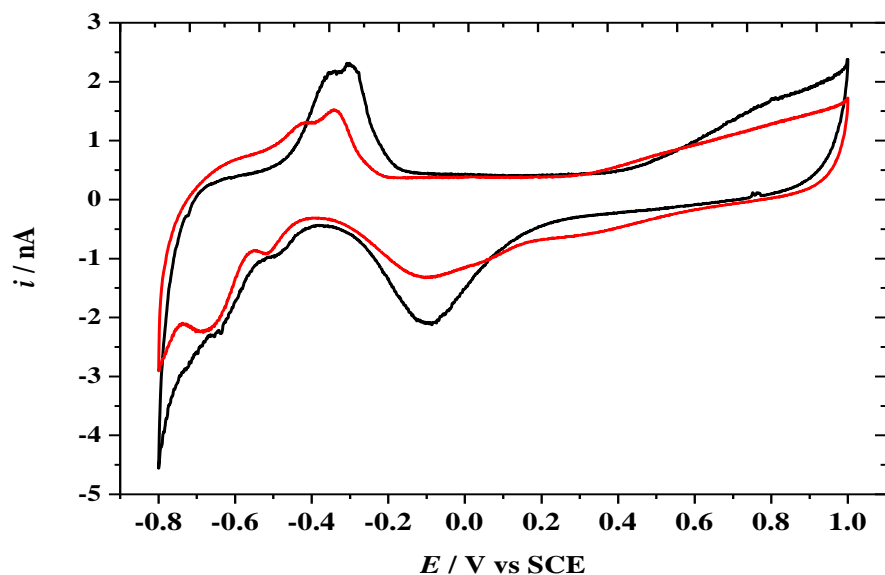
Figure 5.14 Stable cyclic voltammograms, in argon degassed aqueous 0.5 M KCl at 200 mV s^{-1}, using bare (black line) and polypyrrole coated (red) 25 µm Ø Pt microdisc electrode, recorded at 25 ºC.

Applied conditioning waveform at polypyrrole coated Pt electrode

The combination of the presence of coating and the application of conditioning waveform was tried in this work to calculate the number of electrons involved in the ORR. Reconstructed SCVs are shown in Figure 5.15. The pyrrole film is not preventing the ORR but it seems to promote a process which hinders the ORR between -0.4 and -0.6 V (*vs* SCE), particularly at short sampling times.
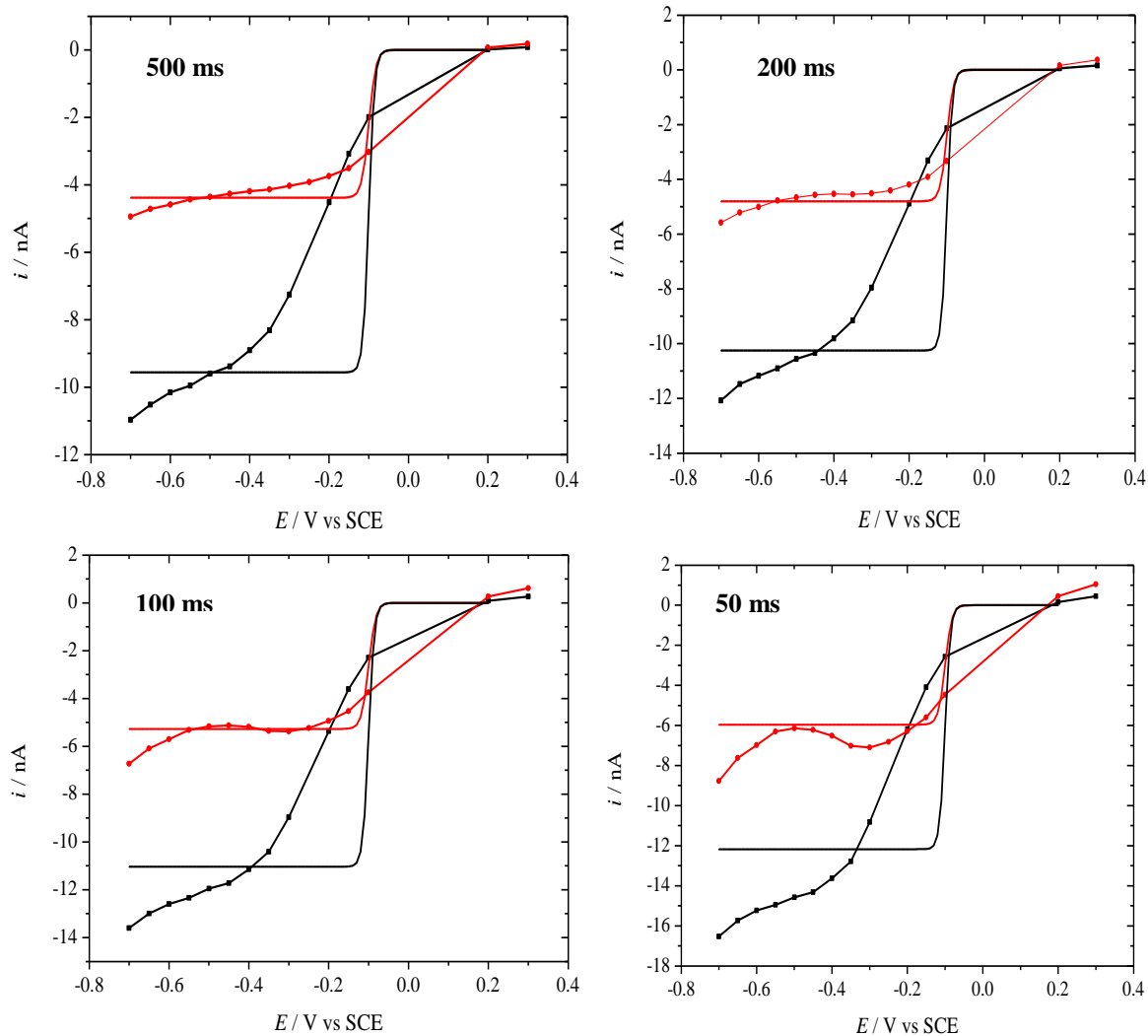
Figure 5.15 Reconstructed voltammograms, in aerated aqueous 0.5 M KCl at different sampling times 500, 200, 100 and 50 ms compared with theory (solid lines), using bare (black) and polypyrrole coated (red) 25 μm Ø Pt microdisc electrode, recorded at 25 ºC. The applied conditioning waveform is as follows: Sweeps (500 mV / s) from 0.6 V to -0.7, 0.6, -0.7, 0.6 and -0.7 V then step (10 s) to 0.1 V and step (0.5 s) to the potential of interest within the ORR wave. The parameters used for the theoretical curves are the following: for bare electrode $D = 2.2 \times 10^{-5}$ cm^2 s^{-1}, $c = 2.2 \times 10^{-7}$ mol cm^{-3}, $n_{app} = 3.6$ and $E_{1/2} = -0.1$ V at 298 K and for coated electrode as follows $D = 1.2 \times 10^{-5}$ cm^2 s^{-1}, $c = 2.2 \times 10^{-7}$ mol cm^{-3}, $n_{app} = 2.9$ and $E_{1/2} = -0.1$ V at 298 K.

The reconstructed voltammograms for the reduction of oxygen at different timescales are presented in Figure 5.15. The limiting current for the oxygen reduction is roughly halved in presence of the polypyrrole coating. The film leads to a flatter plateau for the ORR.The process which makes the plateau dips occurs at more positive potentials as the sampling time gets shorter. Also that process is stronger in presence of film than in absence. The effect of the polypyrrole film on the limiting current for oxygen reduction was demonstrated in the study by Jakobs *et al*. [147].

5.3 Deposition of diazonium derivatives film

Investigation of diazonium BOC derivatives film

Covalent attachment to the electrode as another method for modification of the electrode was carried out. The electrochemical reduction of Boc-protected $NHCH_2C_6H_4$ diazonium salt was performed. Boc stands for tert-butyl carbamate and is a commonly used protecting group for amine groups which is easily removed in a later step with strong acid. It was reported [148] that the reproducibility of this type of modification as well as its stability for long term storage is very good [149]. Below is the chemical structure of the diazonium salt (Figure 5.16).
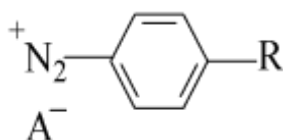

Figure 5.16 General chemical structures of aryl diazonium salts. R stands for functional groups (organic or organometallic substituents) and A⁻ is the counter anion.

This coating was accomplished at both 25 µm Ø Pt and 7 µm Ø CF microdisc electrodes. A weighed amount of $C_6H_4CH_2NHBoc$ (5 mM) was added to anhydrous acetonitrile (CH_3CN), in the dark, under deoxygenated atmosphere. The presence of atmospheric oxygen has been found to promote the formation of disordered multilayers [150]. Therefore, substituted diazonium salt was stored in dark in tightly capped vials in the fridge prior to use.

One of the issues with this kind of coating is the probability of the formation of multilayers [150]. The shape of the voltammogram for the deposition in terms of broadening effect of the reduction peak suggests the formation of thicker layer corresponding to several monolayers. After coating the electrode was transferred to acetonitrile solution and was soaked for a while to remove any residual diazonium salt.
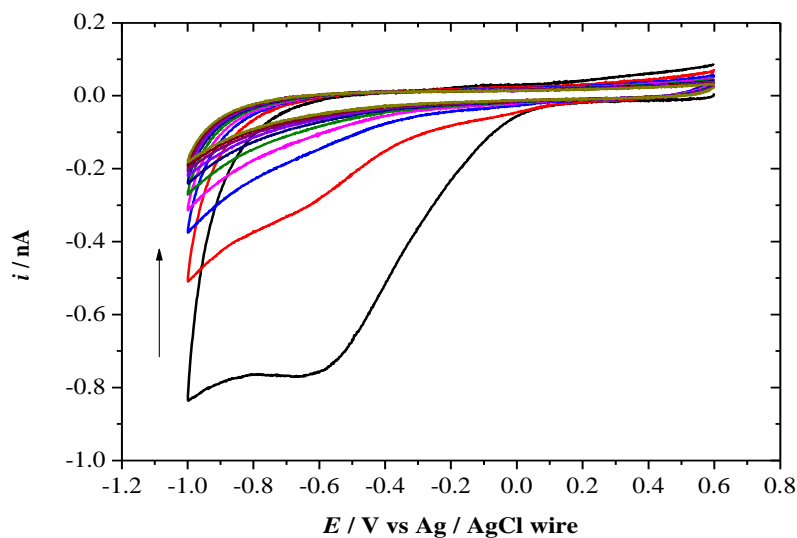
Figure 5.17 Cyclic voltammograms for the deposition of poly 4-(N-Boc-aminomethyl) benzene diazonium tetrafluoroborate salt film in acetonitrile with 0.1 M TBATFA at 25 μm Ø Pt microdisc electrode at 50 mV s^{-1}, 10 cycles recorded at 25 °C.

From Figure 5.17, when the deposition was carried out at Pt microelectrodes, a small current was seen for the reduction peak (around -0.8 nA). This coating was used recently in many applications, some involving microelectrodes [151].

At both Pt and CF substrates, the deposition of substituted diazonium salt shows a broad reduction peak that corresponds to one electron transfer [150] in the first scan. The consecutive scans show a decline in the current suggesting the blockage of the surface by the deposited organic layer.

Some applications with this coating were done at carbon materials, such as Glassy Carbon, GC. Also, *p*-phenylacetate diazonium film at CF was reported to be beneficial for dopamine sensing. Here, in the presented work, the CF electrode was exploited to test the properties of this coating. The recorded deposition cycle shown in Figure 5.18 was done at CF electrode. However, when this data is compared with those for Pt electrode, one can notice that the current for CF should be less than that for the reduction of the polymer at Pt electrode since the radius is lower. It can be concluded that the reduction is much harder to proceed at CF substrate.
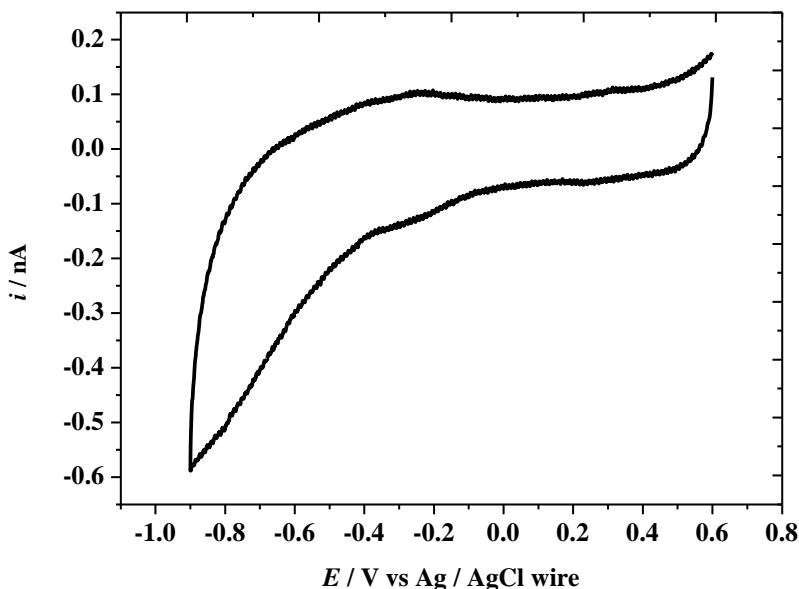
Figure 5.18 Cyclic voltammogram for the deposition of 4-(N-Boc-aminomethyl) benzene diazonium tetrafluoroborate salt film in acetonitrile with 0.1 M TBATFA at 7 μm Ø CF microdisc electrode at 50 mV s^{-1}, 10 cycles were recorded and the last scan is shown at 25°C.

The corresponding reaction for the reduction 4-(N-Boc-aminomethyl) benzene diazonium tetrafluoroborate salt is shown below[150].
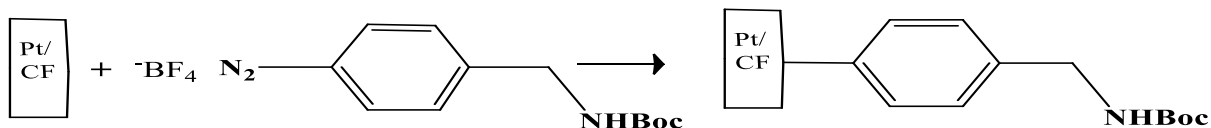
Scheme 5.2 Electrochemical immobilisation of $C_6H_4CH_2NHBoc$ on the CF and Pt surface (potential range from 0.6 to -1.0 V *vs* Ag/AgCl) in CH_3CN solvent [150].

There are two steps to form 4-(N-Boc-aminomethyl) benzene diazonium tetrafluoroborate salt. First, Boc protection of the amino group in the benzylic position yielding 97% takes place, followed by formation of the diazonium salt with 86% yield [150].

The reduction of the ruthenium hexaamine complex on the modified electrode is shown in Figure 5.19. The shape for the reduction was distorted at both coated electrodes Pt and CF. In the case of Pt, the current was very small compared with the bare electrode, suggesting the blockage of the positive ions. The same treatment was carried out at a CF electrode and the distorted reduction voltammogram shows again the lower current after coating compared with the bare electrode. This

blocking property was seen also for negatively charged ferrocyanide ion oxidation at carbon fibre, Figure 5.20, and is consistent with previous study [152].
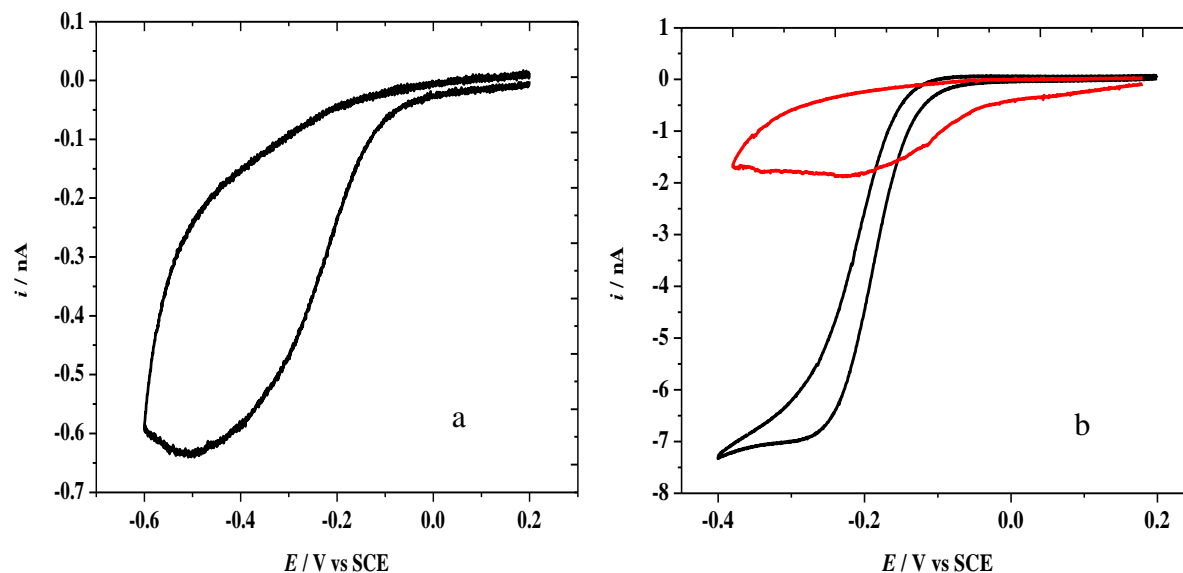

Figure 5.19 Cyclic voltammograms (first cycle) for the reduction of 5 mM mM $Ru(NH_3)_6^{3+}$ in 0.5 M KCl system. a) on a 25 µm Ø Pt   microdisc electrode coated with poly 4-(N-Boc-aminomethyl) benzene diazonium tetrafluoroborate; b) the red line represents the CF electrode coated with poly 4-(N-Boc-aminomethyl) benzene diazonium tetrafluoroborate and the black line the bare 7 µm Ø CF; at 10 mV s^{-1}.   Voltammograms   recorded at 25 ℃.
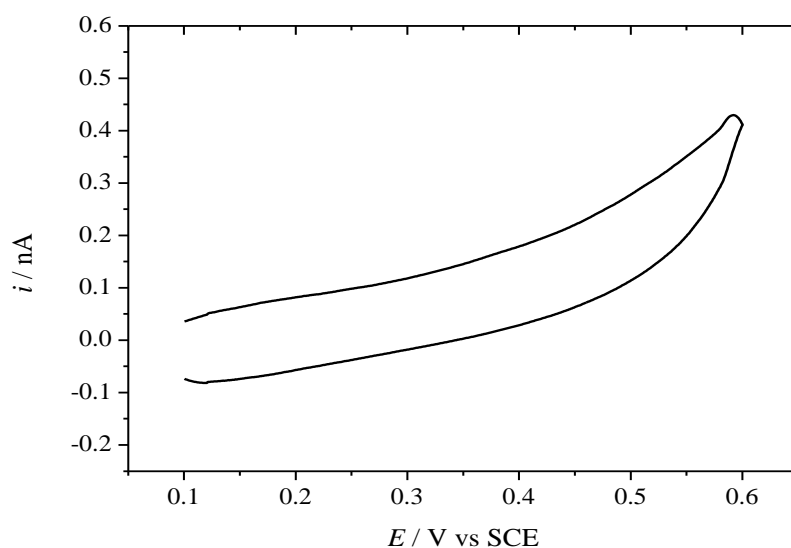

Figure 5.20 Cyclic voltammogram for the oxidation of 5 mM ferro cyanide complex ion in 0.5 M KCl after attachment of poly 4-(N-Boc-aminomethyl) benzene diazonium tetrafluoroborate to a carbon fibre electrode (7 µm Ø) at 10 mV s^{-1}.

ORR investigations at BOC-diazonium coated electrode

The coated Pt electrode was used to run voltammetry in KCl solution to investigate the ORR. The obtained data shows that this film is not affecting the ORR; the limiting current is almost the same as that at a bare electrode with one crossover between forward and backward voltammograms. The surface processes were present as well, although under deoxygenated conditions it seems that the film suppresses the hydrogen adsorption/ desorption to some extent. The electroactive area of the surface is reduced, suggesting less availability of active sites for adsorption reaction. Figures 5.21 and 5.22 illustrate all these observations.
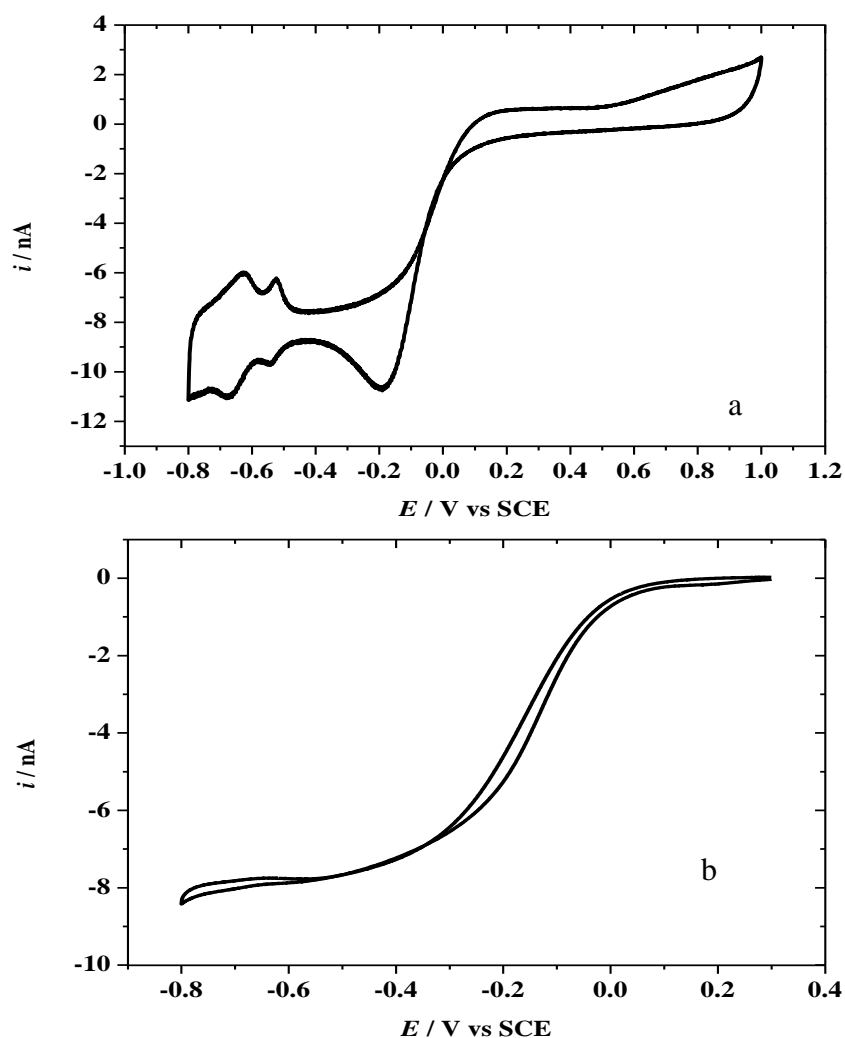

Figure 5.21 Stable cyclic voltammograms, in aerated aqueous 0.5 M KCl at (a) 200 and (b) 10 mV s^{-1}, using a 25 µm Ø Pt microdisc electrode with deposited poly 4-(N-Boc-aminomethyl) benzene diazonium tetrafluoroborate film. Voltammograms recorded at 25 ºC.

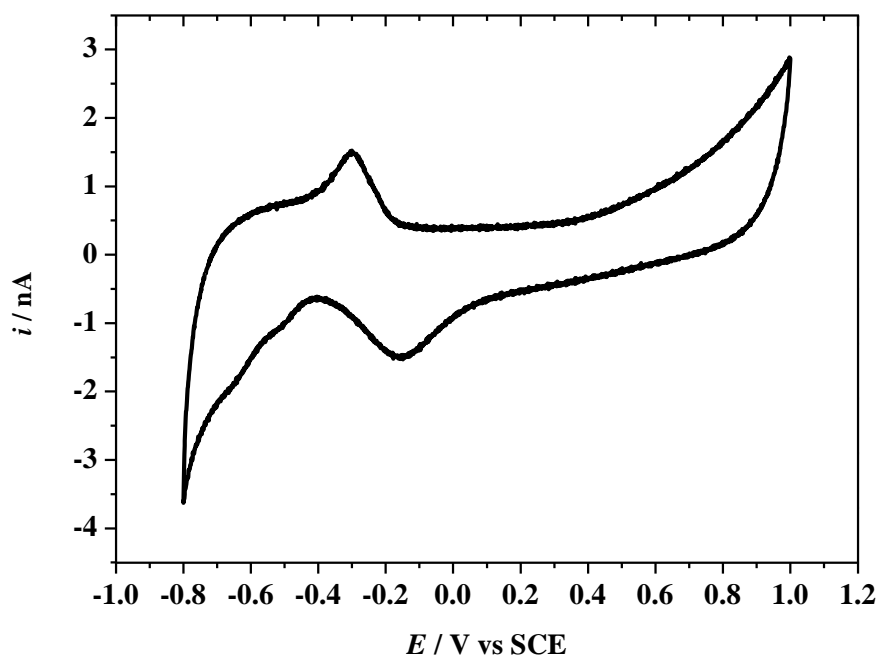**Figure 5.22** Stable cyclic voltammogram recorded at 25 ℃ in argon degassed aqueous 0.5 M KCl at 200 mV s^{-1}, using a 25 μm Ø Pt microdisc electrode with deposited poly 4-(N-Boc-aminomethyl) benzene diazonium tetrafluoroborate film .

To discuss the role of coating at different substrates in the response of redox couple reactions, ORR and dopamine measurement were conducted.

ORR and dopamine oxidation at BOC-diazonium coated microelectrodes

The simultaneous measurements of ORR and dopamine oxidation at different scan rates at both coated CF and Pt microdisc electrodes were recorded. Although the wave for ORR was well-defined, the detection of dopamine was not, Figure 5.23. The dopamine oxidation signal was not resolved clearly at Pt electrode and was really difficult to detect at a coated CF microdisc electrode (not shown).
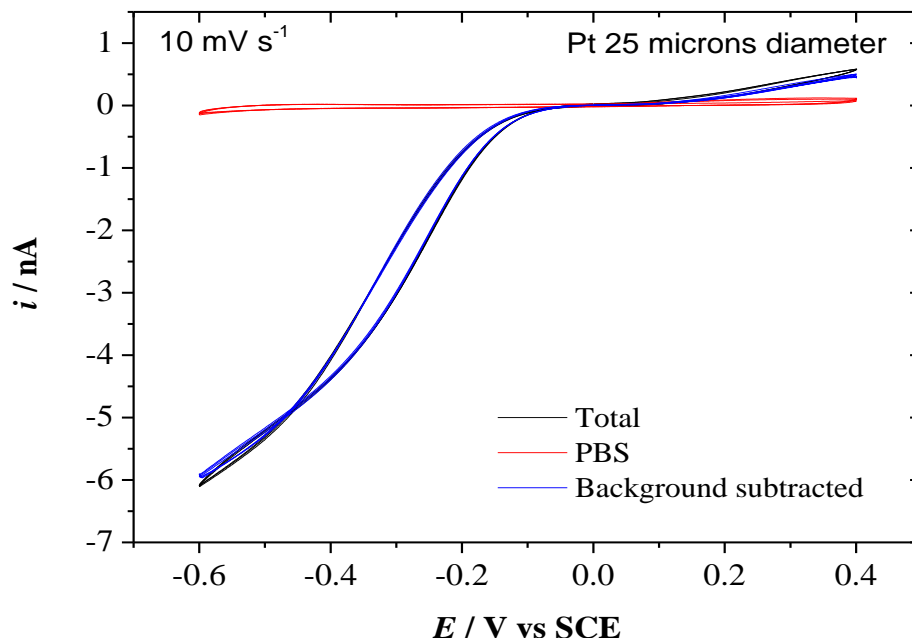
144

Figure 5.23 Eight cyclic voltammograms at 10 mV s^{-1}, in PBS electrolyte, 10 μL of (10 ml of 10 mM) Dopamine + PBS and background subtracted with a poly 4-(N-Boc-aminomethyl) benzene diazonium tetrafluoroborate film on a 25 μm Ø Pt microdisc electrode, recorded at 37ºC.

Investigation of COOH derivatives diazonium film

A specific substituent (e.g –COOH) was attached to the electrode surface. One of the difficulties of this kind of attachment is the availability of diazonium salts with suitable functional groups (-COOH- diazonium), therefore a synthesis procedure was followed. A similar treatment of Boc-diazonium deposition was tried with different derivatives of diazonium salt in 0.1 M TBTFA and acetonitrile as the solvent. Under exactly the same condition as it was done with Boc-diazonium coating as shown in the previous section, carboxylic diazonium tetrafluoroborate coating was achieved at CF and Pt microdisc electrodes as shown in Figure 5.24. As for the work with the previous Boc-diazonium salt electrochemical procedure, a nitrogen atmosphere was kept and blanketed over the solution during the course of the experiment.

In this kind of coating, attachment of carboxylic group to the electrode surface was proposed. The obtained voltammograms for both substrates Pt and CF show the expected shape (Figure 5.24). However, the start of the reduction wave was rapid compared to those data for poly 4-(N-Boc-aminomethyl) benzene diazonium tetrafluoroborate coating. This might be due to the presence of trace of water in the system which changes the resistance of the solution and subsequently the

145

applied potential. Also, it was suggested that the presence of water can lead to the formation of multilayer on the electrode [152].
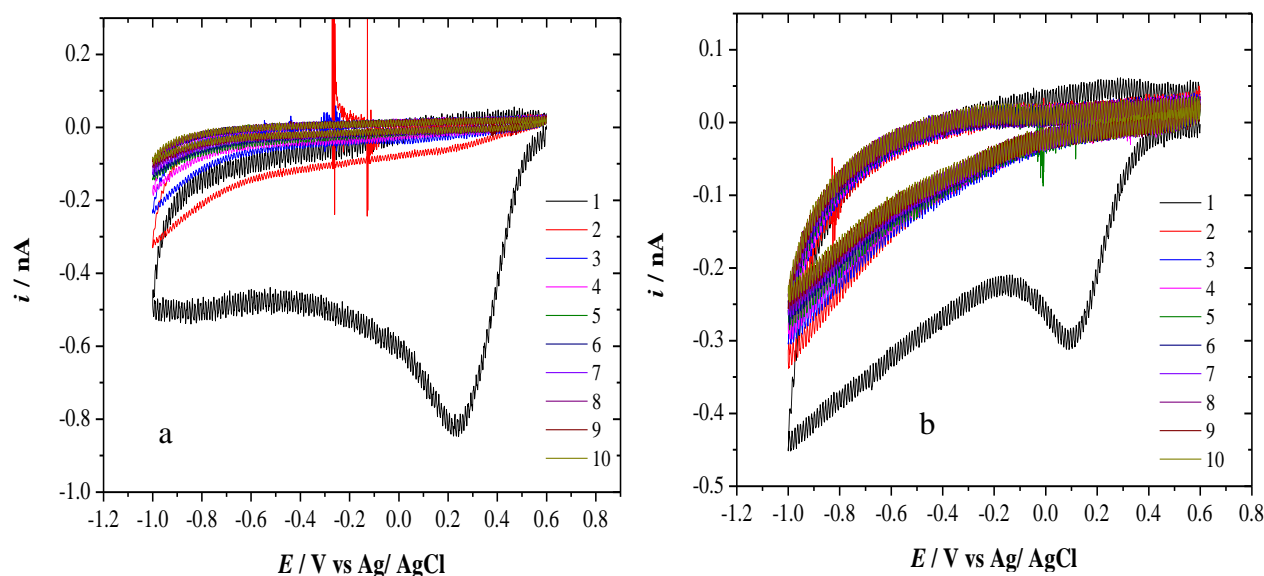

Figure 5.24 Cyclic voltammograms for the deposition of COOH diazoniumtetrafluoroborae salt film in acetonitrile with 0.1 M TBATFA at 7 μm Ø CF (a) and 25 μm Ø Pt (b) microdisc electrode as working electrode at 50 mV s-1, 10 cycles recorded at 25ºC.

It is clearly seen from Figure 5.25 that the response for reduction of ruthenium at both coated Pt and CF electrodes shows a normal behavior, similar in both the shape and the limiting current as those at bare electrodes. The hysteresis at coated CF electrode is within the experimental errors.

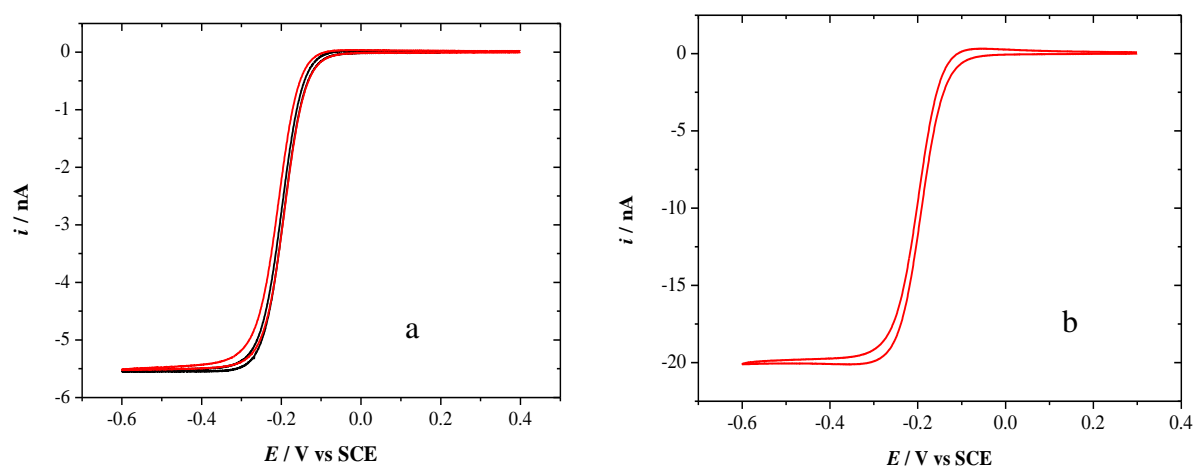**Figure 5.25** Cyclic voltammograms (first cycle) for the reduction of 5 mM $Ru(NH_3)_6^{3+}$ in 0.5 M KCl. The red line represents 7 μm CF (a) and 25 μm Ø Pt (b) microdisc electrodes coated with COOH-diazonium-tetrafluoroborate salt film and the black line represents the response at the bare 7 μm CF, at 10 mV s^{-1}, recorded at 25ºC.
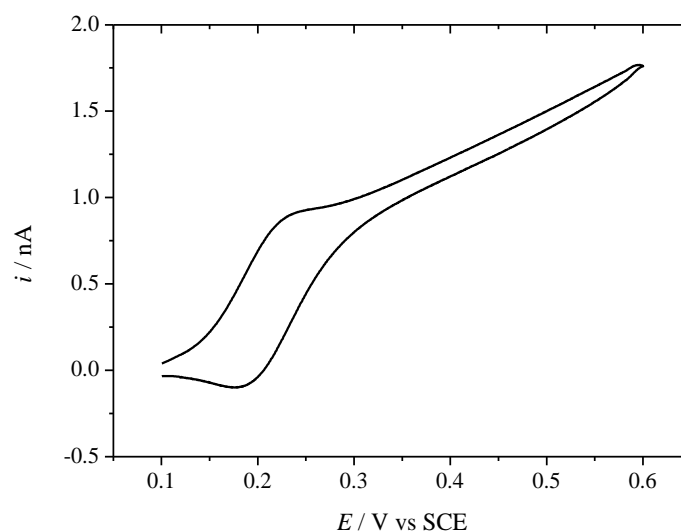
Figure 5.26 Cyclic voltammogram for the oxidation of 5 mM ferrocyanide in 0.5 M KCl after modification of a carbon fibre electrode (7 μm Ø) with a COOH-diazoniumtetrafluoroborate film at 10 mV s^{-1}.

There is a clear oxidation wave at 0.2 V with a significant current coming from another process at more positive potentials when the coated electrode was tested in ferrocyanide complex ion solution (see Figure 5.26).

ORR investigations at COOH-diazonium coated electrode

The coated electrode was then used for ORR investigations. Despite the coating, the ORR signal is very much the same. Figure 5.27 shows the obtained response for ORR at high and low scan rates.
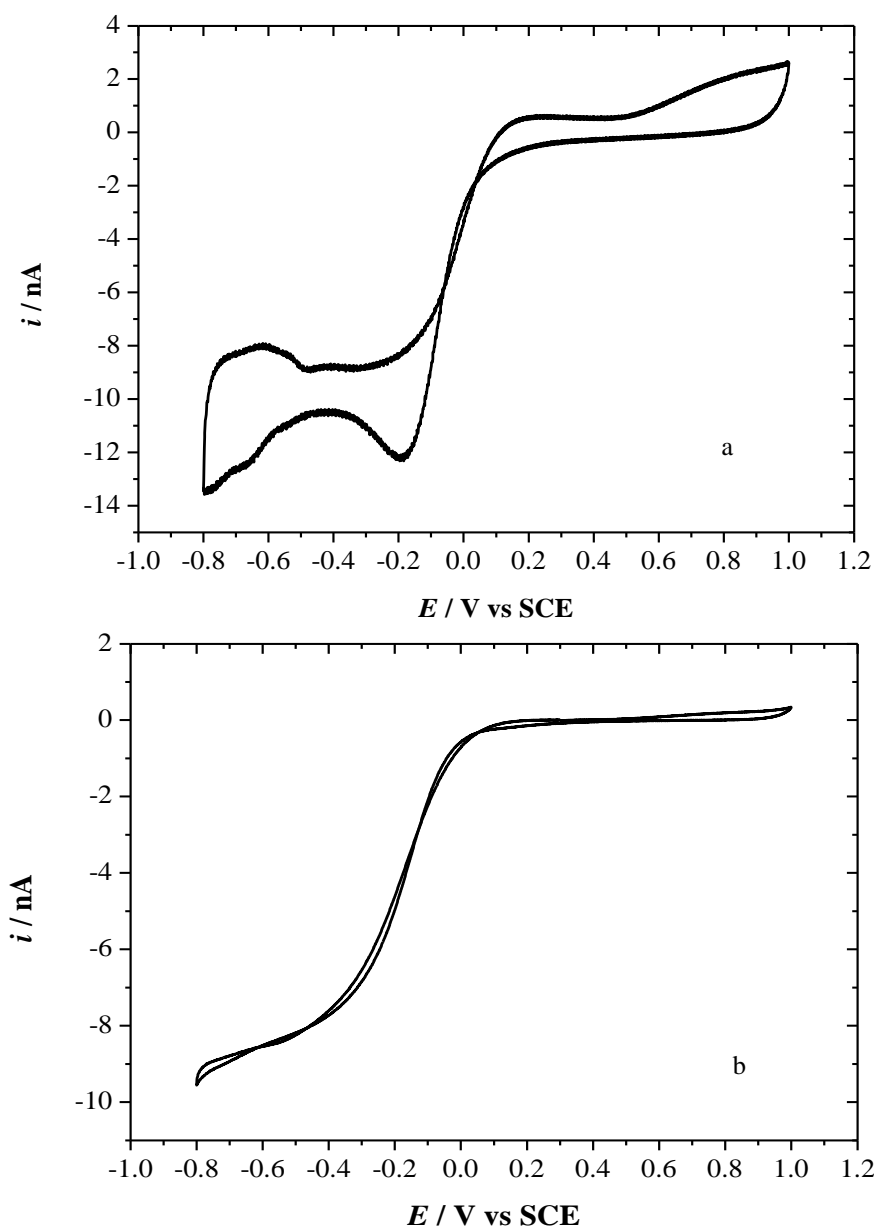
Figure 5.27 Stable cyclic voltammograms, in aerated aqueous 0.5 M KCl at 200 and 10 mV s^{-1}, recorded with a COOH-diazonium tetrafluoroborate modified 25 μm Ø Pt microdisc electrode at 25 °C.
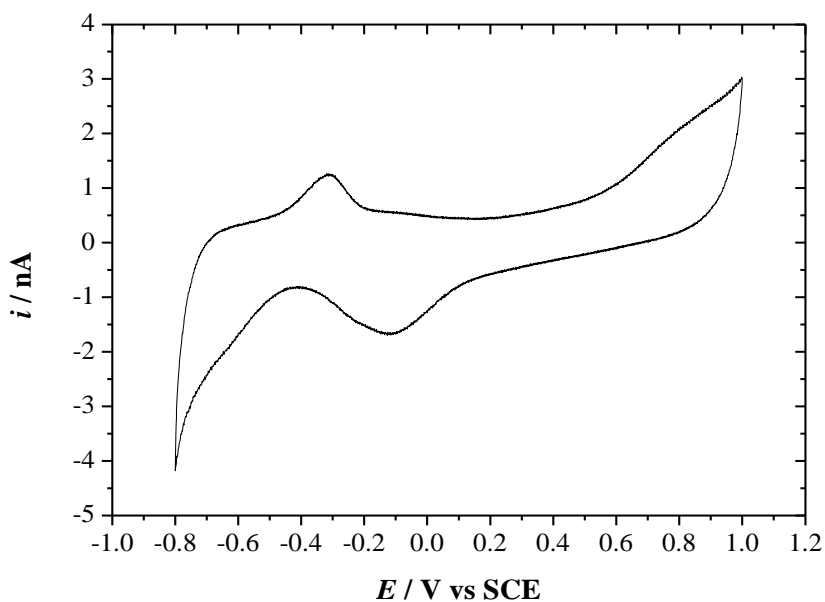
Figure 5.28 Stable cyclic voltammogram, in argon degassed aqueous 0.5 M KCl at 200 mV s^{-1}, recorded with a COOH-diazonium tetrafluoroborate salt modified 25 μm Ø Pt microdisc electrode at 25 ℃.

In absence of O_2, Figure 5.28, the voltammetric response is in agreement with the voltammogram obtained at the bare electrode.

5.4 Deposition of polyaniline (PANI) film

The work was extended to be done with another coating, polyaniline. Close inspection of the literature reveals a variety of approaches for PANI modification, with different advantages and merits according to the aimed application. Some applications for PANI were for gas sensors [153] and H_2O_2 sensing [134]. Electropolymerisation was carried out in 0.2 M aniline (which was passed through a silicagel column for purification and was stored in the fridge afterwards) in 1 M H_2SO_4 under anaerobic condition. The film thickness is expected to be more than 0.3 μm (under acidic conditions). Some reports suggested the film thickness after 20 cycles to be 0.4 μm. It was known that the thickness of the film increases as a result of the increase in number of scans. PANI film growth was electrochemically prepared (through electropolymerisation process) under the same conditions (25 ℃, argon degassed aniline solution in acidic electrolyte) for Pt and CF electrodes. Below is the chemical structure of poly(aniline).
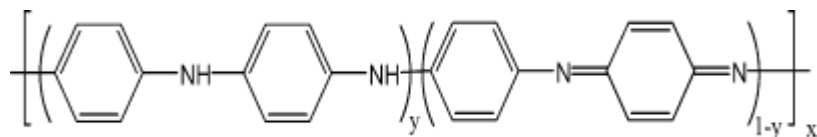
Figure 5.29 General structure of polyaniline.

In Figure 5.30, the oxidation of aniline exhibited a complicated mechanism since it involves three oxidation states, L(leucoemeraldine), E(emeraldine) and P(pernigraniline). On the first scan, the electropolymerisation was initiated from zero current (-0.2 V), which increased narrowly and sharply at around 0.2 V and producing a loop which is more likely due to the nucleation on the electrode surface. To control the film stability at microelectrode, a slow scan rate was applied. Different deposition CV signatures are seen at Pt and CF substrates (Figure 5.30). Some degradation products (e.g. benzoquinone) resulted from the decomposition of PANI which was observed as a pair of redox peaks [154].
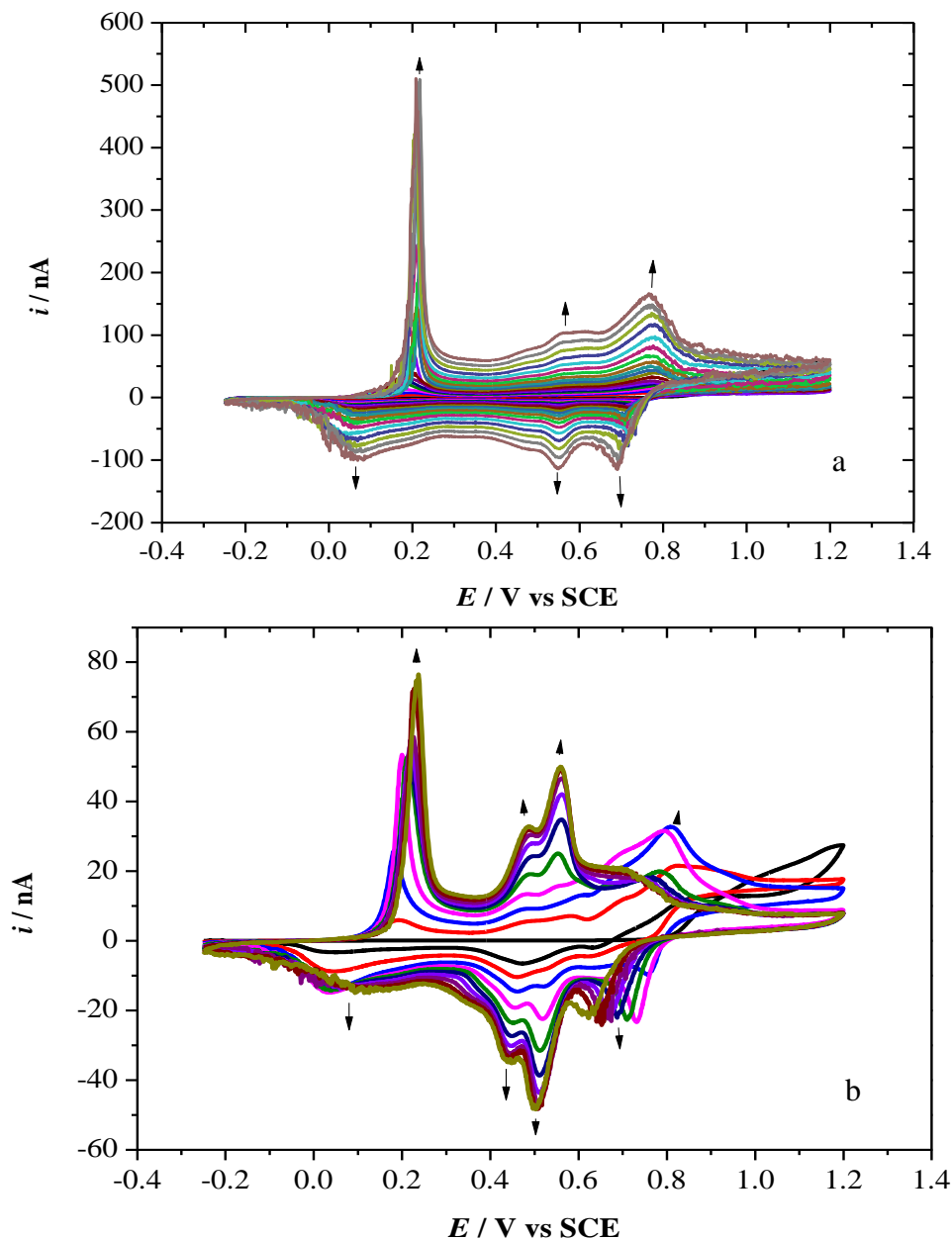
Figure 5.30 Cyclic voltammograms for the deposition of a polyaniline film from 0.2 M aniline in 1 M H_2SO_4 at 25 μm Ø Pt (a) and 7 μm Ø CF (b) microdisc electrodes at 50 mV s^{-1}, 30 cycles recorded at 25 °C. Arrows indicate the evolving of the various peaks with the consecutive scans.

As the scan goes further till 1.2 V (*vs* SCE), the peaks correspond to the oxidation state for the fully oxidized and ends with insulating P form. Almost similar characteristic CV for the deposition of PANI was achieved previously [154]. Bartlett *et al* used an insulating PANI deposited at Pt needle microelectrodes by incorporating the negatively charged sulfonate or carboxylic groups to form a composite film to detect the oxidation of ascorbate [155]. It was pointed out in their work the difficulty to obtain a reproducible coating at microelectrodes.

The deposition of PANI at CF electrodes showed different patterns due to the absence of oxide layer (unlike Pt) which in turn promote rapid growth of the PANI film [154]. Additionally, more hydrolysis products incorporate compared with Pt electrode [154]. The strength of aniline adsorption to CF should be stronger than to Pt due to the competition between aniline and hydrogen to adsorb at Pt electrode [154].

Ruthenium hexaamine reduction was then investigated at the coated electrodes. Figure 5.33 shows that the response reflected the chemistry of aniline at the electrode. The triple oxidation and reduction of aniline could be seen on the voltammograms and the peak currents increase with the increase in the number of cycles. However, these features disappeared after the third scan at coated Pt for unknown reason. Due to the role of H_2O in the hydrolysis of PANI film, therefore, this film might be subject to protonation and the formation of degradation products [154]. In neutral conditions this conductive film has been known to be subjected to deprotonation [155].
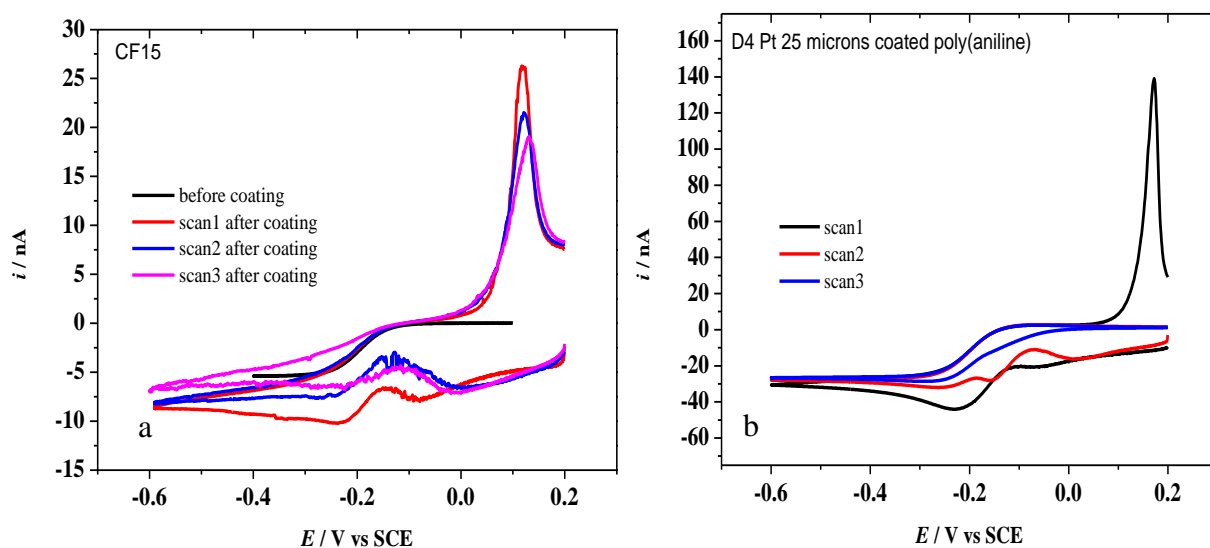
Figure 5.31 Cyclic voltammograms (3 cycles) for the reduction of 5 mM Ru(NH$_4$)$^{3+}$ in 0.5 M KCl at 10 mV s^{-1}, at polyaniline coated electrode at 25 μm Ø Pt and 7 μm CF microdisc electrode as working, at 25 °C .
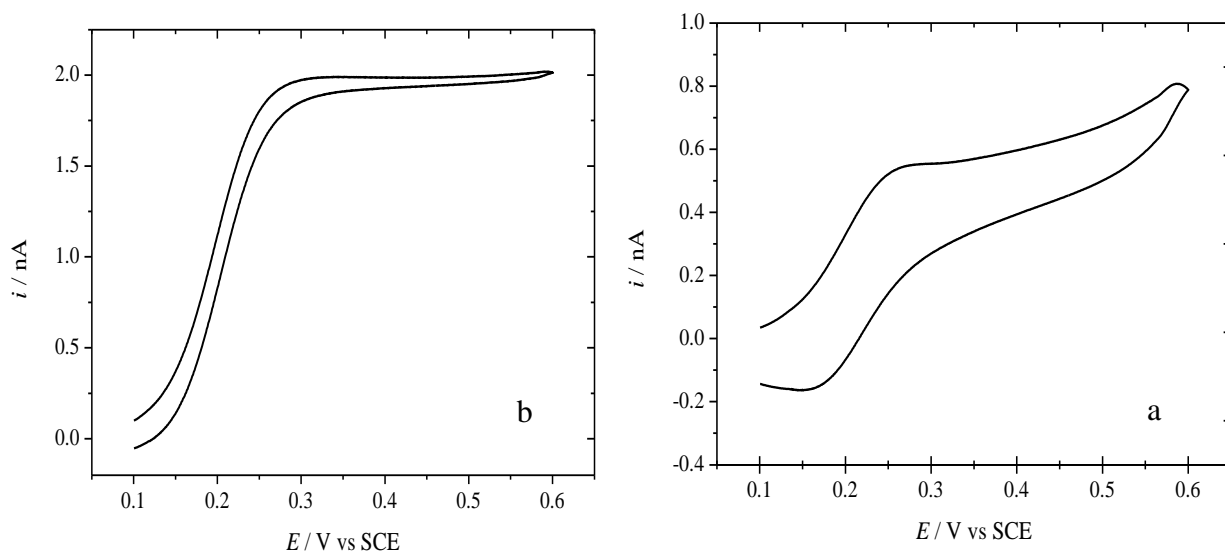
Figure 5.32 Cyclic voltammograms for oxidation of 5 mM Ferrocyanide in 0.5 M KCl after coating both (b) Pt 25 μm Ø and (a) carbon fibre 7 μm Ø electrodes with a polyaniline film.

At CF electrode, referring to Figure 5.31, the chemistry of polyaniline was observed and again almost the same reduction current as at bare electrode was seen after coating with polyaniline, but with large hysteresis, probably due to a thicker film. A residual of electrochemical activity of

polyaniline line were clearly shown as peaks. The coated electrodes were tested for the oxidation of ferrocyanide; it showed almost no response compared to coated Pt which showed a significant decrease in the oxidation steady state current (2 nA relative to 16 nA at the bare Pt electrode), Figure 5.32. This in turn reflects the presence of a thick film at the electrode surface.

ORR investigations at polyaniline coated electrode

The latter experiments describe the ORR at polyaniline coated Pt. A close inspection into the voltammograms in KCl solution (Figure 5.33) reveals all the characteristic features typical of the redox processes at Pt electrodes. However, the chemistry of aniline was missing. The reason for that is unknown. The ORR response was lower in current, and this might be due to the presence of a thick film of polyaniline as a previous report in demonstrated that the higher catalytic activity is accompanied with low thickness of PANI [156]. The steady state voltammograms at slow scan rate for ORR show greater hysteresis between forward and backward scans. It is clear that the diffusion of oxygen species that undergoes reduction is slow to reach the underlying substrate surface and this observation is consistent with previous report on the effect of PANI on the rate of ORR at GC electrode [156]. Previous investigation pointed out the chemisorption of molecular oxygen at the polyaniline surface which appears to facilitate the reduction of oxygen. The hindrance effect of PANI towards ORR was observed at PANI/GC electrode in basic media [135]. Interestingly, the ORR was found to affect the oxidation state of PANI [134].
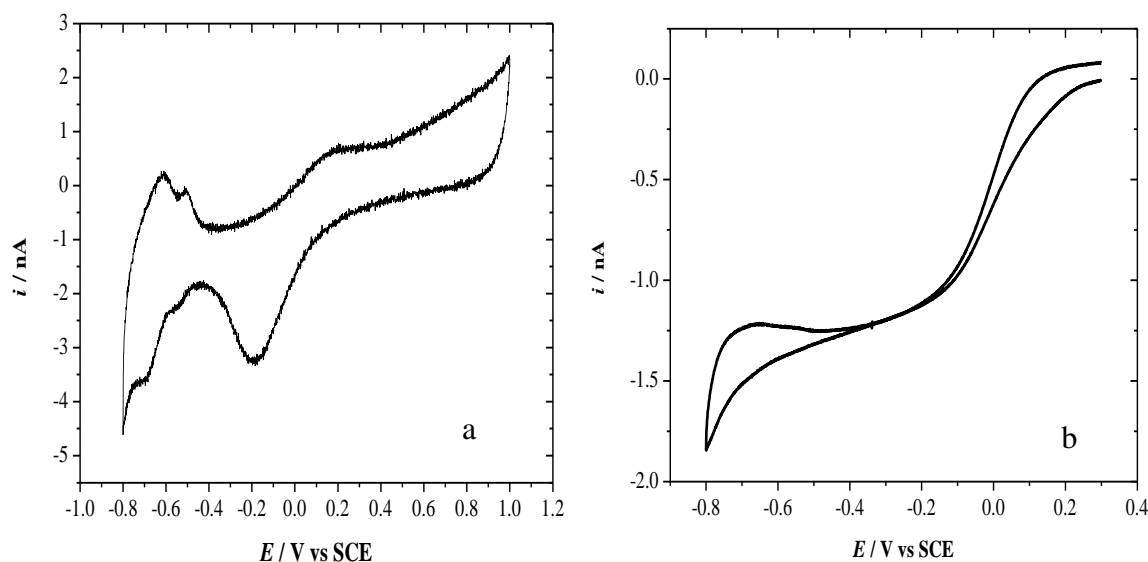

Figure 5.33 Stable cyclic voltammograms, in aerated aqueous 0.5 M KCl at 200 mV s^{-1} (a) and 10 mV /s (b) recorded with a polyaniline coated 25 μm Ø Pt microdisc electrode at 25 ºC.

The voltammogram in absence of oxygen species was very strange (see Figure 5.34). Due to the complexity of this film (the number of oxidation and reduction reactions taking place on the electrode surface during the deposition of the film and after), it is not worth paying more attention to the background signal. It is worth mentioning that a previous report indicated the effect of conductive PANI on the suppression of the background processes at Pt electrode [134].
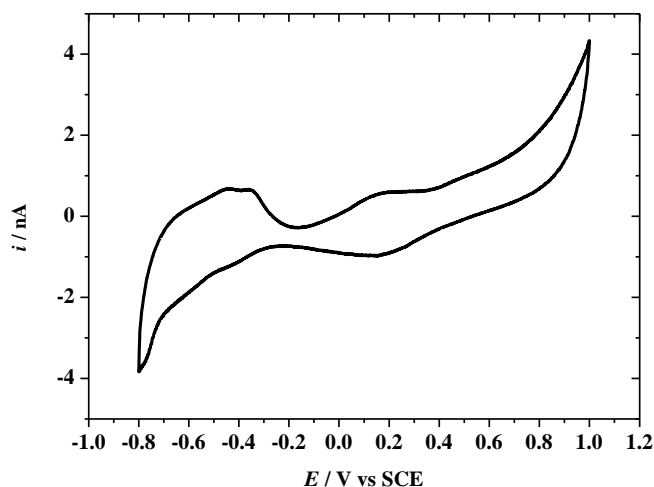
Figure 5.34 Stable cyclic voltammogram, in argon degassed aqueous 0.5 M KCl at 200 mV s^{-1}, recorded with a polyaniline coated 25 μm Ø Pt microdisc electrode at 25 ºC.

5.5 The amperometric responses for the electroreduction of O_2 at coated electrodes

To gain more information about the effect of the coatings at the electrode surface on the ORR, current transients were recorded in each case. The shape of the amperometric response reflects how easy / difficult it is for ORR to occur. The coating can alter the catalytic properties of the electrode towards the ORR.

The analysis is here based on comparing the current transients for the ORR recorded with the modified electrodes, Figure 5.35. There is a considerable alteration in the ORR behaviour, when coating the electrode with polypyrrole. ORR is not entirely blocked using this film, although the limiting current was decreased, similar to CV data. The shape of the current transient for ORR is markedly different.
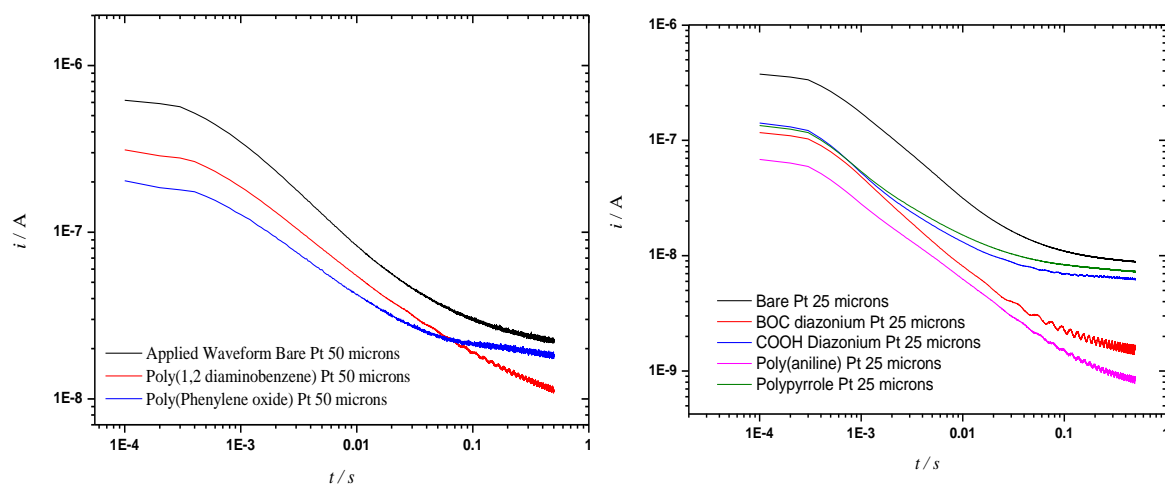
Figure 5.35 Log-log current transients of some selected coated electrodes (right plot- without applying any conditioning waveform) and left plot for electrode subjected to conditioning waveform for O_2 electroreduction signal in aerated 0.5 M KCl. The applied conditioning waveform is as follows: Sweeps at 500 mV / s from 0.6 to-0.7 to 0.6 to -0.7 to 0.6 and -0.7 then step (10 s) to 0.1 V and step (0.5 s) to -0.4 V.

More reproducible electrode surface was obtained when using the conditioning waveform at bare electrode rather than coated electrodes (without any conditioning waveform), Figure 5.36. The conclusion drawn here is that the effect of the conditioning waveform in generating reproducible data exceeds that obtained when just using an electrode modified with a coating.
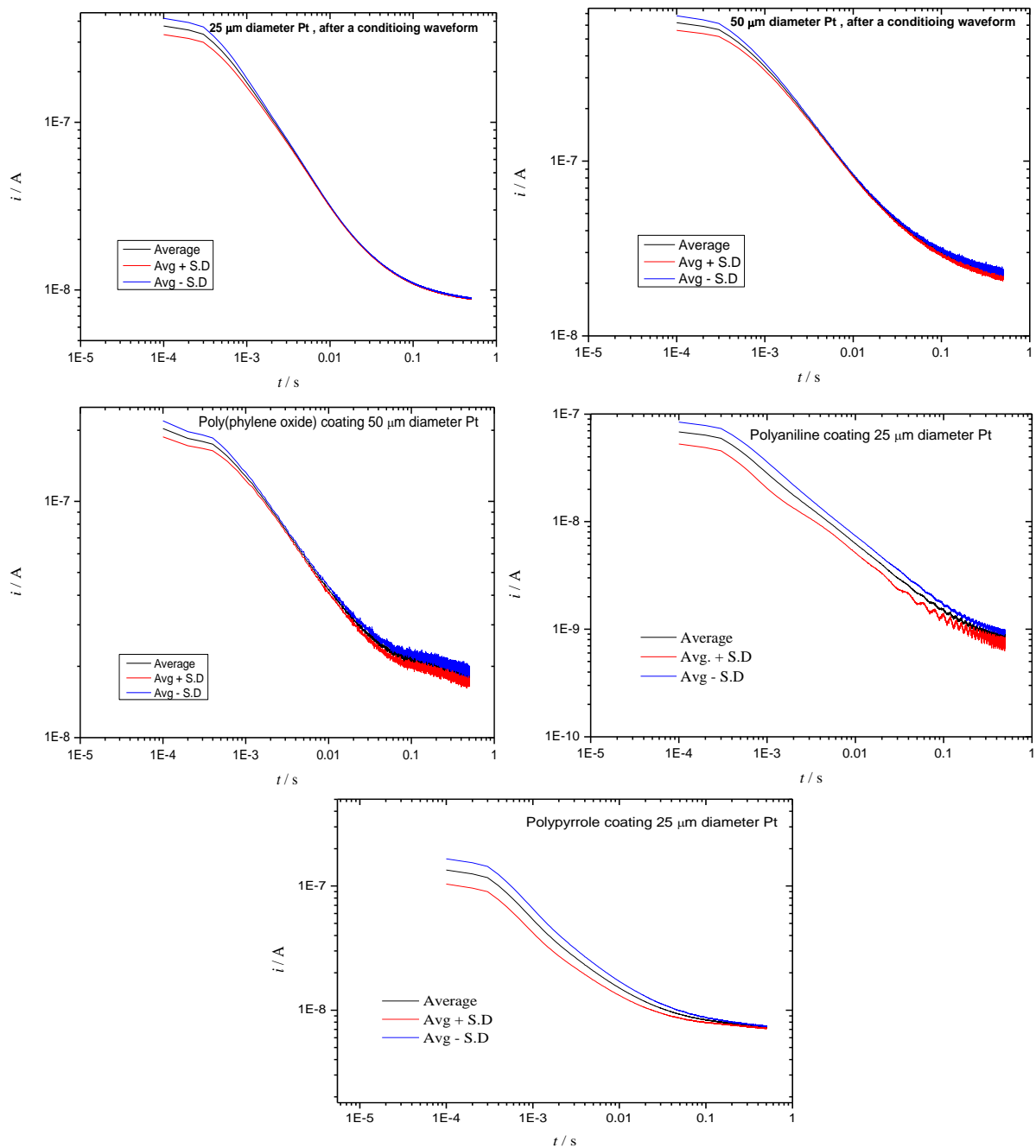
Figure 5.36 The reproducibility test of O_2 electroreduction signal in 0.5 M KCl at some selected coated electrodes and when applying a conditioning waveform at coated electrodes. The applied conditioning waveform is as follows: Sweeps (500 mV / s): from 0.6 to -0.7, 0.6, -0.7, 0.6, and -0.7 V, step (10 s) to 0.1 V, then step (0.5 s) to the potential of interest within the ORR wave at 298 K.

Comparing three different coatings, Figure 5.36, poly(phenylene oxide), polypyrrole and polyaniline, poly (phenylene oxide) was the most stable film to obtain similar reproducible data for O_2 reduction signal.

5.6 Conclusion

This chapter provides some examples of how the variation of surface composition can alter the electrocatalytic properties of Pt and CF electrodes towards the ORR and dopamine oxidation. Various types of modifications show advantages and limitations in measuring the redox species under study.

Based on these preliminary investigations, coated Pt electrode in most cases is better as a catalyst for detecting dopamine and oxygen.

The data obtained also showed the better reproducibility of the response for the electroreduction of oxygen when applying the conditioning waveform at the bare electrode rather than using coatings (without any conditioning waveform) at the Pt electrode. Polypyrrole and poly(phyenlene) coatings are the best two coatings for the coxidation of dopamine species and to obtain a reproducible surface for the amperometric response of oxygen.

Electrodes covalently modified with substituted diazonium salts can be used for further chemical modification. This in turn suggests the ability to tune the property of the modified electrode to be used for many applications like dopamine and other neurotransmitter determinations.

Voltammetric investigations in biological media encounter the problem of interferences. Adsorption of protein molecules is another difficulty in the measurement. For the tried coatings the electrochemically modified electrodes can be used then to test the ability to prevent protein adsorption at the electrode. The stability of the electrode is another issue which needs to be taken into account and the trials for prolonging the use of the coated electrodes are some targets that need to be achieved in further work.

Although this study is of a preliminary nature, future work should include testing the effect of the film in excluding interferences such as ascorbic acid, the use of needle type microelectrodes in real samples and assessing the ability of the coated film in reducing protein adsorption.

Chapter 6

Conclusion and future work

After the successful development of a steady state sensor for dissolved oxygen reported by Sosna *et al*, the work presented in this thesis extended the investigation of the ORR to transient conditions. This led to the development of specific experimental and analytical procedures which make it possible to investigate the ORR in biological systems and oceanographic environment.

Starting with model systems like ferrocene oxidation, the fast scan voltammetry was employed. There was an increase in the peak separation with scan rates, possibly due to the slow electron transfer effects. The redox system was also used to validate the instrumentation and parameters for sampled current voltammetry. No pretreatment was carried out in this case. A good agreement between the reconstructed voltammograms and the theoretical curves at various time regimes was obtained.

The reduction of the ruthenium hexaammine cation was chosen as a model system due to its fast kinetics and similarity in the potential window with the ORR. Many techniques were employed to investigate its reduction at short time scales. Voltammetry showed an increase in peak current with the scan rate and of the magnitude of the background current. Potential steps experiment without any pretreatment before the measurement were carried out. There was a systematic trend in the increase of the number of electron involved, although it is supposed to be one at all timescales. The condition of the electrode surface was thought to be the reason behind that. This led to the development of a specific conditioning and measuring potentiostatic waveform.

Two important targets were met in designing a conditioning waveform. First, a reproducible surface was maintained. Second, the magnitude of the background effect was minimised. The successful waveform consists of preconditioning sweeps, a resting step and a measuring step. The upper and lower cleaning potentials were chosen carefully to respectively form and reduce a small amount of oxide. The resting potential was chosen to allow the ruthenium ion complex to re-establish. The whole waveform was repeated 10 times for each measurement and the average measured current transient was sampled at fixed timescales. At sampling times down to 3 ms the good agreement between theory and experimental data indicates the ability of the applied waveform in conditioning the electrode without any need for background subtraction. The calculated number of electrons involved was one at all timescales. By normalising the pseudo steady stated current by the diffusion controlled current at different timescales, a collapse of all sampled current voltammograms onto the theoretical one was seen.

The ORR was then investigated. The specific effect of some variables like the electrode material and size, electrolyte, scan rates, rest potential and upper and lower potential limits were systematically studied for background CVs and ORR CVs. The effect of the electrode material and media on the ORR response was addressed in this work. Referring to data in Chapter 5 the Pt electrode was chosen for transient studies in saline solution. Hydroxide, chloride and perchlorate anions were tested with conventional cyclic voltammetry and SCV; there were not much difference towards the ORR and in all cases the SCVs reflected an additional current in the recorded oxygen signal.

All the methods used, potential steps, NPV, SCV, under the conditions presented, show a similar trend where the apparent number of electrons involved in ORR increases with shorter timescales. The shape of reconstructed sampled current voltammograms could be understood in terms of the increase of the irreversibility of the reaction at short time scales. The similar trend of the increase in n_{app} with the shorter timescales was seen when using bigger size electrode. Also, the increase in the number of sweeps for preconditioning procedures in the conditioning waveform was beneficial to obtain a reproducible data. Hence, the stability of ORR signal might be achieved either by increasing the preconditioning sweeps or possibly their scan rates.

Attempts to elucidate the source of the additional current were undertaken. A waveform where the final potential step was replaced with sweeps from and back to the resting potential was applied to test the presence of any residual oxide during the conditioning procedures. It was clear from the voltammograms obtained after applying this waveform that no oxide is left on the electrode after the conditioning sweeps and rest. Subsequently, a new waveform where the last two sweeps were replaced with double potential steps was used to investigate the amount of charge remaining after the measuring step; it was found that the magnitude of the charge is minimal and that it increased with the increase in the sample time. Using this technique the obtained results may reflect a displacement of chlorides from the surface. A more sensitive technique, EQCM, was tried. It made possible the detection of mass changes during the application of the conditioning and measuring waveform. There was a clear difference in the mass incorporated during the measuring step in two different solutions KCl and KClO4 . However, no evidence that is attributed to the dissolution and redeposition of Pt.

Although the ORR investigation in biological samples is of preliminary nature, some success in simultaneous determination of oxygen and dopamine was accomplished. Different types of coatings were tried: polymer layers, permeseclective polymers and covalently attached monolayers. They differ in their properties towards redox species. Modified electrodes were tried for the study of dopamine oxidation and oxygen reduction. Polypyrrole, poly(phylene oxide), polyaniline, poly(1,2 diaminobenzene), BOC-diazonium and COOH-diazonium films were tried. They were electrochemically deposited on the microelectrode then characterised by voltammetry for with different redox species. The ferrocyanide anion and ruthenium hexaammine cation complexes were used for this purpose. Some problems were noted such as the breakdown of the insulating layer with poly(1,2 DAB) coatings. It was observed that some coatings adhered better to larger microdiscs. It was not possible to produce an identical thickness for all the coatings so comparison could not be systematic. For future work the formation of uniform thickness membrane is of great important to achieve a good response in addition to strong adhesion to the surface.

The possibility of using this sensor with an appropriate coating for the simultaneous determination of oxygen and neurotransmitter in the field of biological application was demonstrated. It remains to be seen whether these coatings prevent the adsorption of proteins on the electrode surface and thus alleviate electrode fouling. Thus the tried coatings should be examined to test their ability to reduce this adsorption effect.

This study underlined the importance of applying a conditioning waveform instead of a coating to obtain reproducible data but the long term stability of the electrode performance when a coating is present is another area that should be investigated.

Chapter 7

References

1. Pletcher, D., *A First Course in Electrode Processes, The Electrochemical Consultancy*. 1991, Romsey: Chichester, UK.
2. Wang, J., *Analytical electrochemistry*. 2006: Vch Verlagsgesellschaft Mbh.
3. Howell, J.O. and R.M. Wightman, *Ultrafast voltammetry and voltammetry in highly resistive solutions with microvoltammetric electrodes*. Analytical Chemistry, 1984. **56**(3): p. 524-529.
4. Denuault, G., *Microelectrodes*. Chemistry and Industry, 1996(18): p. 678-80.
5. Zoski, Cynthia G., *Ultramicroelectrodes: Design, Fabrication, and Characterization*. Electroanalysis, 2002. **14**(15-16): p. 1041-1051.
6. Montenegro, M., M. Queirós, and J. Daschbach, *Microelectrodes: theory and applications*. 1991: Kluwer Academic Publishers.
7. Štulik, K., et al., *Microelectrodes. Definitions, characterization, and applications*. Pure Appl. Chem, 2000. **72**(8): p. 1483-1492.
8. Wightman, R.M., *Microvoltammetric electrodes*. Analytical Chemistry, 1981. **53**(9): p. 1125A-1134A.
9. Basha, C. and L. Rajendran, *Theories of Ultramicrodisc Electrodes: Review article*. Int. J. Electrochem. Sci, 2006. **1**: p. 268-282.
10. Reimers, C.E., *Applications of Microelectrodes to Problems in Chemical Oceanography*. Chemical Reviews, 2007. **107**(2): p. 590-600.
11. Sosna, M., *Oxygen reduction at microelectrodes: application to the dissolved oxygen sensor for in situ oceanographic measurements*. 2006: University of Southampton.
12. Sotiropoulos, S., *Ph.D. Thesis*. 1994 University of Southampton: Southampton.
13. Brett, C., A. Brett, and A. Brett, *Electrochemistry: principles, methods, and applications*. 1993: Oxford University Press Oxford.
14. Greef, R., et al., *Instrumental methods in electrochemistry*. 1985: Ellis Horwood Chichester.
15. Lu, R. and a.T. Yu, *Fabrication and evaluation of an oxygen microelectrode applicable to environmental engineering and science*. Journal of Environmental Engineering and Science 2002. **1** (3): p. 225-235
16. Shoup, D. and A. Szabo, *Chronoamperometric current at finite disk electrodes*. Journal of Electroanalytical Chemistry, 1982. **140**(2): p. 237-245.
17. Aoki, K. and J. Osteryoung, *Diffusion-controlled current at the stationary finite disk electrode: Theory*. Journal of Electroanalytical Chemistry, 1981. **122**: p. 19-35.
18. Mahon, P.J. and K.B. Oldham, *Diffusion-controlled chronoamperometry at a disk electrode*. Analytical Chemistry, 2005. **77**(18): p. 6100-6101.
19. Aoki, K. and J. Osteryoung, *Diffusion controlled current at a stationary finite disk electrode: Experiment*. Journal of Electroanalytical Chemistry, 1981. **125**(2): p. 315-320.
20. Ikeuchi, H. and M. Kanakubo, *Determination of diffusion coefficients of the electrode reaction products by the double potential step chronoamperometry at small disk electrodes*. Journal of Electroanalytical Chemistry, 2000. **493**(1-2): p. 93-99.

21. Denuault, G., M.V. Mirkin, and A.J. Bard, *Direct determination of diffusion coefficients by chronoamperometry at microdisk electrodes.* Journal of Electroanalytical Chemistry, 1991. **308**(1-2): p. 27-38.

22. Sosna, M., et al., *Field assessment of a new membrane-free microelectrode dissolved oxygen sensor for water column profiling.* Limnology and Oceanography-Methods, 2008. **6**: p. 180-189.

23. Sosna, M., et al., *Development of a reliable microelectrode dissolved oxygen sensor.* Sensors and Actuators B: Chemical, 2007. **123**(1): p. 344-351.

24. Zhang, T. and A.B. Anderson, *Oxygen reduction on platinum electrodes in base: Theoretical study.* Electrochimica Acta, 2007. **53**(2): p. 982-989.

25. Markovi, N.M., et al., *Oxygen Reduction Reaction on Pt and Pt Bimetallic Surfaces: A Selective Review.* Fuel Cells, 2001. **1**(2): p. 105-116.

26. Wroblowa, H.S., P. Yen Chi, and G. Razumney, *Electroreduction of oxygen: A new mechanistic criterion.* Journal of Electroanalytical Chemistry, 1976. **69**(2): p. 195-201.

27. Hutton, L., et al., *Amperometric Oxygen Sensor Based on a Platinum Nanoparticle-Modified Polycrystalline Boron Doped Diamond Disk Electrode.* Analytical Chemistry, 2008. **81**(3): p. 1023-1032.

28. Vukmirovic, M.B., et al., *Platinum monolayer electrocatalysts for oxygen reduction.* Electrochimica Acta, 2007. **52**(6): p. 2257-2263.

29. Huang, J., et al., *Application of a platinum dual-disk microelectrode to measurement of the electron transfer number of dioxygen reduction.* Journal of Electroanalytical Chemistry, 1997. **433**(1-2): p. 33-39.

30. Birkin, P.R., J.M. Elliott, and Y.E. Watson, *Electrochemical reduction of oxygen on mesoporous platinum microelectrodes.* Chemical Communications, 2000(17): p. 1693-1694.

31. Kucernak, A. and J. Jiang, *Mesoporous platinum as a catalyst for oxygen electroreduction and methanol electrooxidation.* Chemical Engineering Journal, 2003. **93**(1): p. 81-90.

32. Sleightholme, A., et al., *Nafion Film-Templated Platinum Electrodes for Oxygen Reduction.* Electrocatalysis, 2010. **1**(1): p. 22-27.

33. Bauer, A., et al., *Liquid Crystalline Phase Templated Platinum Catalyst for Oxygen Reduction.* Journal of The Electrochemical Society, 2009. **156**(10): p. B1169-B1174.

34. Jiang, S.P.C., C. Q.; Tseung, A. C. C.,, J. Electrochem. Soc., 1991. **138**: p. 3599.

35. Miyata, Y. and S. Asakura, *Oxygen reduction reaction at rust free iron surface in neutral unbuffered chloride solutions.* Corrosion Science, 2002. **44**(3): p. 589-602.

36. King, F., M.J. Quinn, and C.D. Litke, *Oxygen reduction on copper in neutral NaCl solution.* Journal of Electroanalytical Chemistry, 1995. **385**(1): p. 45-55.

37. Pletcher, D. and S. Sotiropoulos, *Cathodic reduction of oxygen in water and media of low ionic strength.* Journal of the Chemical Society, Faraday Transactions 1995. **91**(3): p. 457 - 462.

38. Yang, Y.-F. and G. Denuault, *Scanning electrochemical microscopy (SECM): Study of the formation and reduction of oxides on platinum electrode surfaces in Na_2SO_4 solution (pH = 7).* Journal of Electroanalytical Chemistry, 1998. **443**(2): p. 273-282.

39. Pletcher, D. and S. Sotiropoulos, *A study of cathodic oxygen reduction at platinum using microelectrodes.* Journal of Electroanalytical Chemistry, 1993. **356**(1-2): p. 109-119.

40. Pletcher, D. and S. Sotiropoulos, *Cathodic reduction of oxygen in water and media of low ionic strength.* Journal of the Chemical Society, Faraday Transactions, 1995. **91**(3): p. 457-462.

41. Franaszczuk, K. and J. Sobkowski, *The voltammetry of platinized platinum electrodes in aqueous Na_2SO_4.* Journal of Electroanalytical Chemistry, 1989. **261**(1): p. 223-227.

42. Gasana, E., et al., *Influence of changes of platinum electrode surface condition on the kinetics of the oxidation of sodium dithionite and sulfite in alkaline solution.* Electrochemistry Communications, 2000. **2**(10): p. 727-732.

43. Caruana, D.J. and J.V. Bannister, *Surface properties of fractured and polished platinum microelectrodes.* Journal of Electroanalytical Chemistry, 1997. **424**(1-2): p. 197-205.

44. Santos, M.C., D.W. Miwa, and S.A.S. Machado, *Study of anion adsorption on polycrystalline Pt by electrochemical quartz crystal microbalance.* Electrochemistry Communications, 2000. **2**(10): p. 692-696.

45. Zolfaghari, A., B.E. Conway, and G. Jerkiewicz, *Elucidation of the effects of competitive adsorption of Cl-and Br- ions on the initial stages of Pt surface oxidation by means of electrochemical nanogravimetry.* Electrochimica Acta, 2002. **47**(8): p. 1173-1187.

46. Tripkovic, D.V., et al., *The role of anions in surface electrochemistry.* Faraday Discussions, 2009. **140**: p. 25-40.

47. Omura, J., et al., *Electrochemical Quartz Crystal Microbalance Analysis of the Oxygen Reduction Reaction on Pt-Based Electrodes. Part 1: Effect of Adsorbed Anions on the Oxygen Reduction Activities of Pt in HF, HClO4, and H2SO4 Solutions.* Langmuir, 2011. **27**(10): p. 6464-6470.

48. Lei, H.-W., H. Uchida, and M. Watanabe, *Electrochemical Quartz Crystal Microbalance Study of Halide Adsorption and Concomitant Change of Surface Excess of Water on Highly Ordered Au(111).* Langmuir, 1997. **13**(13): p. 3523-3528.

49. Thomas, S., et al., *Specific adsorption of a bisulfate anion on a Pt (111) electrode. Ultrahigh vacuum spectroscopic and cyclic voltammetric study.* The Journal of Physical Chemistry, 1996. **100**(28): p. 11726-11735.

50. Gilman, S., *Studies of Anion Adsorption on Platinum by the Multipulse Potentiodynamic (M.p.p.) Method. II. Chloride and Phosphate Desorption and Equilibrium Surface Concentrations at Constant Potential1.* The Journal of Physical Chemistry, 1964. **68**(8): p. 2112-2119.

51. Kaska, S.M., S. Sarangapani, and J. Giner, *Oxygen Reduction on Platinum in Borate-Buffered Saline Solutions.* Journal of The Electrochemical Society, 1989. **136**(1): p. 75-83.

52. Chiu, Y.-C. and M.A. Genshaw, *Study of anion adsorption of platinum by ellipsometry.* The Journal of Physical Chemistry, 1969. **73**(11): p. 3571-3577.

53. Orts, J.M., et al., *Potentiostatic charge displacement by exchanging adsorbed species on Pt(111) electrodes—acidic electrolytes with specific anion adsorption.* Electrochimica Acta, 1994. **39**(11-12): p. 1519-1524.

54. Lucas, C.A., N.M. Markovic-acute, and P.N. Ross, *Adsorption of halide anions at the Pt(111)-solution interfacestudied by in situ surface x-ray scattering.* Physical Review B, 1997. **55**(12): p. 7964-7971.

55. Horányi, G. and G. Vértes, *Study of the adsorption of chloride ions in the course of electrosorption of copper on platinized platinum electrodes.* Journal of electroanalytical chemistry and interfacial electrochemistry, 1973. **45**(2): p. 295-299.

56. Li, N. and J. Lipkowski, *Chronocoulometric studies of chloride adsorption at the Pt(111) electrode surface.* Journal of Electroanalytical Chemistry, 2000. **491**(1-2): p. 95-102.

57. Patil, R., V.A. Juvekar, and V.M. Naik, *Oxidation of Chloride Ion on Platinum Electrode: Dynamics of Electrode Passivation and its Effect on Oxidation Kinetics.* Industrial & Engineering Chemistry Research, 2011: p. null-null.

58. Yadav, A.P., A. Nishikata, and T. Tsuru, *Effect of halogen ions on platinum dissolution under potential cycling in 0.5 M H2SO4 solution.* Electrochimica Acta, 2007. **52**(26): p. 7444-7452.

59. Zoski, C.G., *Handbook of Electrochemistry.* 2007, Burlington, MA: Elsevier.

60. Stamenkovic, V., N. M. Markovic, and P.N. Ross, *Structure-relationships in electrocatalysis: oxygen reduction and hydrogen oxidation reactions on Pt(111) and*

Pt(100) in solutions containing chloride ions. Journal of Electroanalytical Chemistry, 2001. **500**(1-2): p. 44-51.

61. Zoski, C.G., B. Liu, and A.J. Bard, *Scanning Electrochemical Microscopy: Theory and Characterization of Electrodes of Finite Conical Geometry.* Analytical Chemistry, 2004. **76**(13): p. 3646-3654.

62. Li, H., et al., *Chloride contamination effects on proton exchange membrane fuel cell performance and durability.* Journal of Power Sources, 2011. **196**(15): p. 6249-6255.

63. Li, Y., et al., *The electrochemical reduction reaction of dissolved oxygen on Q235 carbon steel in alkaline solution containing chloride ions.* Journal of Solid State Electrochemistry, 2010. **14**(9): p. 1667-1673.

64. Imabayashi, S.-i., et al., *Effects of Atmospheric Trace Species on the Oxygen Reduction Reaction and the Production of Hydrogen Peroxide.* ECS Transactions, 2008. **16**(2): p. 925-930.

65. Schmidt, T.J., et al., *The oxygen reduction reaction on a Pt/carbon fuel cell catalyst in the presence of chloride anions.* Journal of Electroanalytical Chemistry, 2001. **508**(1-2): p. 41-47.

66. Van Muylder, J.P., M, *In Atlas of Electrochemical Equilibria in Aqueous Solutions.* 1974, New York: Pourbaix, M., Ed.; NACE International.

67. Shimazu, K. and H. Kita, *In situ measurements of water adsorption on a platinum electrode by an electrochemical quartz crystal microbalance.* Journal of Electroanalytical Chemistry, 1992. **341**(1-2): p. 361-367.

68. Reddy, J.O.B.a.A.K.N., *Modern Electrochemistry.* 1970, London: Plenum.

69. Pletcher, D. and S. Sotiropoulos, *Towards a microelectrode sensor for the determination of oxygen in waters.* Analytica Chimica Acta, 1996. **322**(1-2): p. 83-90.

70. Wilde, C.P., et al., *The influence of adsorbed hydrogen and extended cycling on the EQCM response of electrodeposited Pt electrodes.* Electrochimica Acta, 2000. **45**(22-23): p. 3649-3658.

71. Markovic, N.M., et al., *Oxygen reduction reaction on Pt(111): effects of bromide.* J. Electroanal. Chem., 1999. **467**(1-2): p. 157-163.

72. Markovic, N.M., H.A. Gasteiger, and P.N. Ross, *Oxygen Reduction on Platinum Low-Index Single-Crystal Surfaces in Sulfuric Acid Solution: Rotating Ring-Pt(hkl) Disk Studies.* The Journal of Physical Chemistry, 1995. **99**(11): p. 3411-3415.

73. Johnson, D.C. and S. Bruckenstein, *Effect of passivation of platinum electrodes on oxygen reduction in 1.0M sulfuric acid.* Analytical Chemistry, 1971. **43**(10): p. 1313-1316.

74. Nørskov, J.K., et al., *Origin of the Overpotential for Oxygen Reduction at a Fuel-Cell Cathode.* The Journal of Physical Chemistry B, 2004. **108**(46): p. 17886-17892.

75. Gerischer.H, R.G.a. in *Z.Physicc.Chem.* 1956. Frankfurt.

76. Bianchi, G. and G. Caprioglio, *Influence of surface preparation of platinum electrodes on cathodic processes of hydrogen peroxide.* Electrochimica Acta, 1959. **1**(1): p. 18-21.

77. Jerkiewicz, G., et al., *Surface-oxide growth at platinum electrodes in aqueous H2SO4: Reexamination of its mechanism through combined cyclic-voltammetry, electrochemical quartz-crystal nanobalance, and Auger electron spectroscopy measurements.* Electrochimica Acta, 2004. **49**(9-10): p. 1451-1459.

78. Tindall, G.W., S.H. Cadle, and S. Bruckenstein, *Inhibition of the reduction of oxygen at a platinum electrode by the deposition of a monolayer of copper at underpotential.* Journal of the American Chemical Society, 1969. **91**(8): p. 2119-2120.

79. LaCourse, W.R., D.A. Mead, and D.C. Johnson, *Anion-exchange separation of carbohydrates with pulsed amperometric detection using a pH-selective reference electrode.* Analytical Chemistry, 1990. **62**(2): p. 220-224.

80. Chen, S. and A. Kucernak, *Electrocatalysis under Conditions of High Mass Transport Rate: Oxygen Reduction on Single Submicrometer-Sized Pt Particles Supported on Carbon.* The Journal of Physical Chemistry B, 2004. **108**(10): p. 3262-3276.

81. Morita, K. and Y. Shimizu, *Microhole array for oxygen electrode.* Analytical Chemistry, 1989. **61**(2): p. 159-162.

82. Braun, R.D., et al., *Comparison of tumor and normal tissue oxygen tension measurements using OxyLite or microelectrodes in rodents.* American Journal of Physiology - Heart and Circulatory Physiology, 2001. **280**(6): p. H2533-H2544.

83. Atkinson, M.J., *Fast-Response Oxygen Sensor for a Free-Fall CTD.* Limnology and Oceanography, 1988. **33**(1): p. 141-145.

84. Amatore, C., et al., *Difference between Ultramicroelectrodes and Microelectrodes: Influence of Natural Convection.* Analytical Chemistry, 2010. **82**(16): p. 6933-6939.

85. Rychen, P.G., J.; Santoli, R. *Electrochemical Self-Cleaning & Self Calibrating Microdisk Array*. in *The 56th Annual Meeting of the International Society of Electrochemistry*. 2005. Busan, Korea

86. Atkinson, M.J., et al., *A micro-hole potentiostatic oxygen sensor for oceanic CTDs.* Deep Sea Research Part I: Oceanographic Research Papers, 1995. **42**(5): p. 761-771.

87. Lee, J.-H., et al., *Needle-type dissolved oxygen microelectrode array sensors for in situ measurements.* Sensors and Actuators B: Chemical, 2007. **128**(1): p. 179-185.

88. Gust, G., et al., *On the velocity sensitivity (stirring effect) of polarographic oxygen microelectrodes.* Netherlands Journal of Sea Research, 1987. **21**(4): p. 255-263.

89. Prien, R., et al. *Development and first results of a new fast response microelectrode DO-sensor*. in *Oceans 2005 - Europe*. 2005.

90. Whitfield, M. and D. Jagner, *Marine electrochemistry: a practical introduction*. 1981: John Wiley & Sons.

91. Winkler, L.W., *Die Bestimmung des im Wasser gelösten Sauerstoffes.* Berichte der deutschen chemischen Gesellschaft, 1888. **21**(2): p. 2843-2854.

92. Baumgartl, H. and D. Lubbers, *Microcoaxial needle sensor for polarographic measurement of local O2 pressure in the cellular range of living tissue. Its construction and properties.* Polarographic oxygen sensors: aquatic and physiological applications. Springer, Berlin Heidelberg New York, 1983: p. 37-65.

93. Gnaiger, E.F., H., Eds, *Polarographic oxygen sensors: aquatic and physiological applications*. 1983, the University of Michigan: Springer-Verlag.

94. Karagounis, V., L. Lun, and C.-C. Liu, *A Thick-Film Multiple Component Cathode Three-Electrode Oxygen Sensor.* Biomedical Engineering, IEEE Transactions on, 1986. **BME-33**(2): p. 108-112.

95. Revsbech, N.P., *An oxygen microsensor with a guard cathode.* Limnology and Oceanography, 1989: p. 474-478.

96. Hitchman, M., *Measurement of dissolved oxygen.* John Wiley and Sons, New York N. Y. 1978. 255, 1978.

97. Wittkampf, M., et al., *Silicon thin film sensor for measurement of dissolved oxygen.* Sensors and Actuators B: Chemical, 1997. **43**(1–3): p. 40-44.

98. Tengberg, A., et al., *Evaluation of a lifetime-based optode to measure oxygen in aquatic systems.* Limnology and Oceanography: Methods, 2006. **4**(7-17).

99. Preidel, W., et al., *A new principle for an electrochemical oxygen sensor.* Sensors and Actuators B: Chemical, 1995. **28**(1): p. 71-74.

100. Brendel, P.J. and G.W. Luther, III, *Development of a Gold Amalgam Voltammetric Microelectrode for the Determination of Dissolved Fe, Mn, O2, and S(-II) in Porewaters of Marine and Freshwater Sediments.* Environmental Science & Technology, 1995. **29**(3): p. 751-761.

101. Pletcher, D. and S. Sotiropoulos, *Hydrogen adsorption-desorption and oxide formation-reduction on polycrystalline platinum in unbuffered aqueous solutions.* Journal of the Chemical Society, Faraday Transactions, 1994. **90**(24): p. 3663-3668.

102. Bondarenko, A.S., et al., *The Pt(111)/Electrolyte Interface under Oxygen Reduction Reaction Conditions: An Electrochemical Impedance Spectroscopy Study.* Langmuir, 2011. **27**(5): p. 2058-2066.

103. Itagaki, M., et al., *Electroreduction mechanism of oxygen investigated by electrochemical impedance spectroscopy.* Journal of Electroanalytical Chemistry, 2003. **557**: p. 59-73.

104. WIPF, D., *Fast-scan cyclic voltammetry at ultramicroelectrodes* 1989, Indiana University.

105. Wipf, D.O. and R.M. Wightman, *Submicrosecond measurements with cyclic voltammetry.* Analytical Chemistry, 1988. **60**(22): p. 2460-2464.

106. Amatore, C., C. Lefrou, and F. Pflüger, *On-line compensation of ohmic drop in submicrosecond time resolved cyclic voltammetry at ultramicroelectrodes.* J. Electroanal. Chem., 1989. **270**(1-2): p. 43-59.

107. Wipf, D.O., et al., *Fast-scan cyclic voltammetry as a method to measure rapid heterogeneous electron-transfer kinetics.* Analytical Chemistry, 1988. **60**(4): p. 306-310.

108. Wightman, R.M. and D.O. Wipf, *High-speed cyclic voltammetry.* Accounts of Chemical Research, 1990. **23**(3): p. 64-70.

109. Guo, Z.-Y., X.-Q. Lin, and Z.-X. Deng, *Undistorted cyclic voltammograms at scan rates up to 2.5 MV.s−1 through positive feedback compensation of Ohmic drop.* Chinese Journal of Chemistry, 2004. **22**(9): p. 913-919.

110. Amatore, C., E. Maisonhaute, and G. Simonneau, *Ohmic drop compensation in cyclic voltammetry at scan rates in the megavolt per second range: access to nanometric diffusion layers via transient electrochemistry.* Journal of Electroanalytical Chemistry, 2000. **486**(2): p. 141-155.

111. Beriet, C. and D. Pletcher, *A further microelectrode study of the influence of electrolyte concentration on the kinetics of redox couples.* Journal of Electroanalytical Chemistry, 1994. **375**(1-2): p. 213-218.

112. Hsueh, C., et al., *Surface and kinetic enhancement of selectivity and sensitivity in analysis with fast scan voltammetry at scan rates above 1000 V/s.* Analytica Chimica Acta, 1997. **349**(1-3): p. 67-76.

113. Wipf, D.O., A.C. Michael, and R.M. Wightman, *Microdisk electrodes : Part II. Fast-scan cyclic voltammetry with very small electrodes.* J. Electroanal. Chem., 1989. **269**(1): p. 15-25.

114. Gennett, T. and M.J. Weaver, *Reliability of standard rate constants for rapid electrochemical reactions.* Analytical Chemistry, 1984. **56**(8): p. 1444-1448.

115. Marken, F., J.C. Eklund, and R.G. Compton, *Voltammetry in the presence of ultrasound: Can ultrasound modify heterogeneous electron transfer kinetics?* Journal of Electroanalytical Chemistry, 1995. **395**(1-2): p. 335-339.

116. Aoki, K., et al., *Linear Sweep Voltammetry at Very Small Stationary Disk Electrodes.* Journal of Electroanalytical Chemistry, 1984. **171**(1-2): p. 219-230.

117. Aoki, K., et al., *Linear sweep voltammetry at very small stationary disk electrodes.* Journal of electroanalytical chemistry and interfacial electrochemistry, 1984. **171**(1-2): p. 219-230.

118. Lin, S., et al., *Normal and reverse pulse voltammetry at microdisk electrodes.* Analytical Chemistry, 1988. **60**(11): p. 1135-1141.

119. Hepel, T. and J. Osteryoung, *Chronoamperometric transients at the stationary disk microelectrode.* The Journal of Physical Chemistry, 1982. **86**(8): p. 1406-1411.

120. Banks, C.E., N.V. Rees, and R.G. Compton, *Sonoelectrochemistry in acoustically emulsified media.* Journal of Electroanalytical Chemistry, 2002. **535**(1-2): p. 41-47.

121. Keith, J.A. and T. Jacob, *Theoretical Studies of Potential-Dependent and Competing Mechanisms of the Electrocatalytic Oxygen Reduction Reaction on Pt(111).* Angewandte Chemie International Edition, 2010. **49**(49): p. 9521-9525.

122. Alsabet, M., M. Grden, and G. Jerkiewicz, *Comprehensive study of the growth of thin oxide layers on Pt electrodes under well-defined temperature, potential, and time conditions.* Journal of Electroanalytical Chemistry, 2006. **589**(1): p. 120-127.

123. Benke, G. and W. Gnot, *The electrochemical dissolution of platinum.* Hydrometallurgy, 2002. **64**(3): p. 205-218.

124. Hall, S.B., E.A. Khudaish, and A.L. Hart, *Electrochemical oxidation of hydrogen peroxide at platinum electrodes. Part V: inhibition by chloride.* Electrochimica Acta, 2000. **45**(21): p. 3573-3579.

125. Tammeveski, K., et al., *Electrochemical reduction of oxygen on thin-film Pt electrodes in 0.1 M KOH.* Electrochimica Acta, 1997. **42**(5): p. 893-897.

126. Shimazu, K. and H. Kita, *In situ measurements of water adsorption on a platinum electrode by an electrochemical quartz crystal microbalance* J. Electroanal. Chem., 1992. **341**: p. 361.

127. Birss, V.I., M. Chang, and J. Segal, *Platinum oxide film formation—reduction: an in-situ mass measurement study.* Journal of Electroanalytical Chemistry, 1993. **355**(1–2): p. 181-191.

128. Jin, W., et al., *Comparison of the Oxygen Reduction Reaction between NaOH and KOH Solutions on a Pt Electrode: The Electrolyte-Dependent Effect.* The Journal of Physical Chemistry B, 2010. **114**(19): p. 6542-6548.

129. Striebel, K.A., F.R. McLarnon, and E.J. Cairns, *ChemInform Abstract: Oxygen Reduction of Pt in Aqueous K2CO3 and KOH.* ChemInform, 1991. **22**(2): p. no-no.

130. Herrero, E., K. Franaszczuk, and A. Wieckowski, *Electrochemistry of Methanol at Low Index Crystal Planes of Platinum: An Integrated Voltammetric and Chronoamperometric Study.* The Journal of Physical Chemistry, 1994. **98**(19): p. 5074-5083.

131. Jovancicevic, V., P. Zelenay, and B.R. Scharifker, *The transport properties of oxygen in aqueous borate solutions.* Electrochimica Acta, 1987. **32**(11): p. 1553-1555.

132. Bard, A.J., *Chemical modification of electrodes.* Journal of Chemical Education, 1983. **60**(4): p. 302.

133. Li, Y., et al., *Investigation of Oxygen- and Hydrogen Peroxide-Reduction on Platinum Particles Dispersed on Poly(o-phenylenediamine) Film Modified Glassy Carbon Electrodes.* Electroanalysis, 1998. **10**(10): p. 671-676.

134. Gu, Y. and C.C. Chen, *Eliminating the Interference of Oxygen for Sensing Hydrogen Peroxide with the Polyaniline Modified Electrode.* Sensors, 2008. **8**(12): p. 8237-8247.

135. Song, J., et al., *Tunable activity in electrochemical reduction of oxygen by gold–polyaniline porous nanocomposites.* Journal of Solid State Electrochemistry, 2010. **14**(10): p. 1915-1922.

136. Bartlett, P.N., P. Tebbutt, and C.H. Tyrrell, *Electrochemical immobilization of enzymes. 3. Immobilization of glucose oxidase in thin films of electrochemically polymerized phenols.* Analytical Chemistry, 1992. **64**(2): p. 138-142.

137. Yuqing, M., C. Jianrong, and W. Xiaohua, *Using electropolymerized non-conducting polymers to develop enzyme amperometric biosensors.* Trends in Biotechnology, 2004. **22**(5): p. 227-231.

138. Pihel, K., Q.D. Walker, and R.M. Wightman, *Overoxidized polypyrrole-coated carbon fiber microelectrodes for dopamine measurements with fast-scan cyclic voltammetry.* Analytical Chemistry, 1996. **68**(13): p. 2084-2089.

139. Jaramillo, A., et al., *XPS characterization of nanosized overoxidized polypyrrole films on graphite electrodes.* Analyst, 1999. **124**(8): p. 1215-1221.
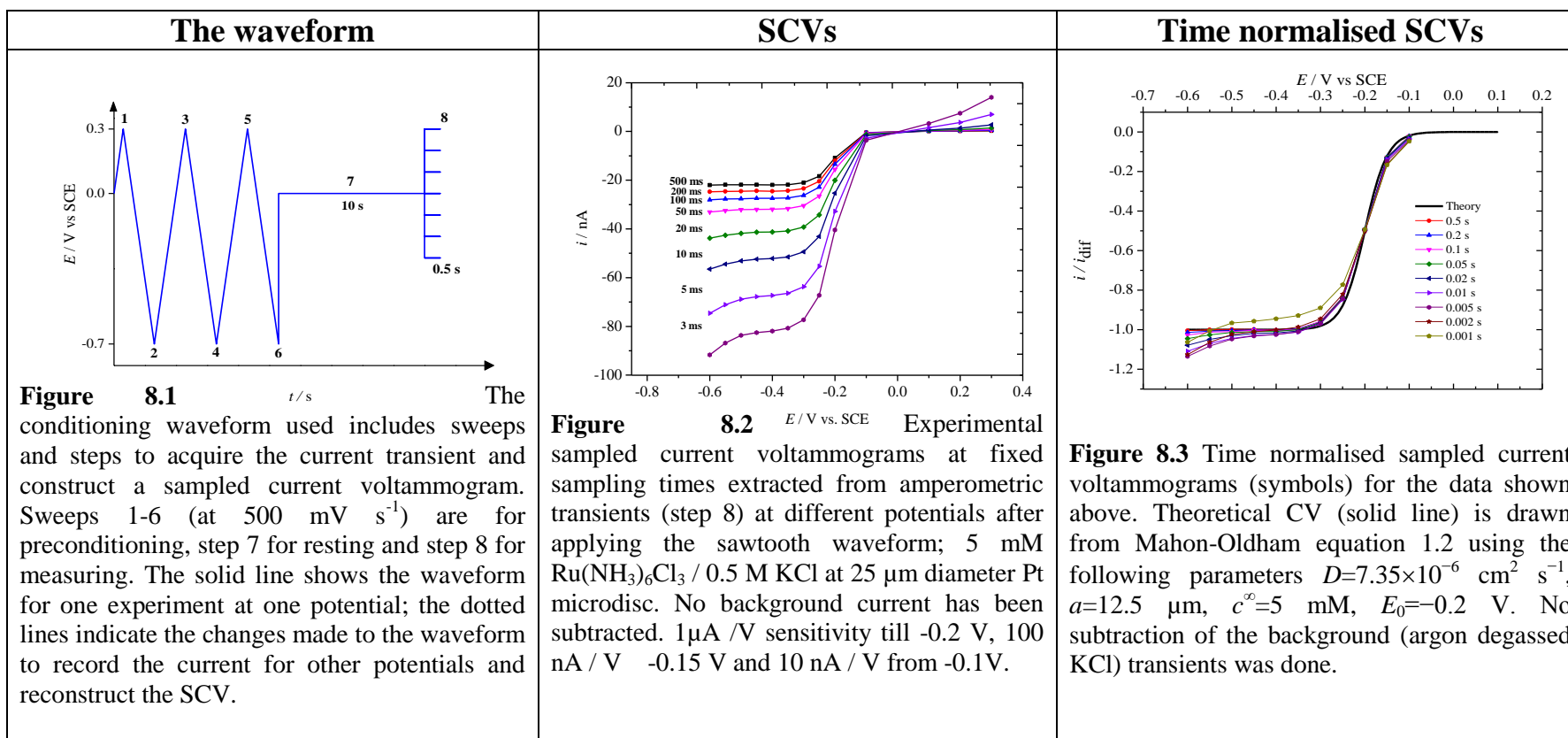
140. Chen, X., et al., *The stability of polypyrrole and its composites.* Journal of Materials Science, 1997. **32**(6): p. 1515-1518.

141. Li, Q., et al., *Interference free platinum wire glucose biosensors based on covering nonconductive substituted heteropolypyrrole film.* Analytical Letters, 1998. **31**(6): p. 937-948.

142. Debiemme-Chouvy, C., *A very thin overoxidized polypyrrole membrane as coating for fast time response and selective H_2O_2 amperometric sensor.* Biosensors and Bioelectronics, 2010. **25**(11): p. 2454-2457.

143. Witkowski, A. and A. Brajter-Toth, *Overoxidized polypyrrole films: a model for the design of permselective electrodes.* Analytical Chemistry, 1992. **64**(6): p. 635-641.

144. Debiemme-Chouvy, C. and M. Gallois, *Characterization of a very thin overoxidized polypyrrole membrane: application to H_2O_2 determination.* Surface and Interface Analysis, 2010. **42**(6-7): p. 1144-1147.

145. Sluijs, M.J., A. Underhill, and B. Zaba, *Electrochemistry of polypyrrole films.* Journal of Physics D: Applied Physics, 1987. **20**: p. 1411.

146. Shiu, K.K., F.Y. Song, and K.W. Lau, *Effects of polymer thickness on the potentiometric pH responses of polypyrrole modified glassy carbon electrodes.* Journal of Electroanalytical Chemistry, 1999. **476**(2): p. 109-117.

147. Jakobs, R., L. Janssen, and E. Barendrecht, *Oxygen reduction at polypyrrole electrodes-II. Experimental results.* Electrochimica Acta, 1985. **30**(11): p. 1433-1439.

148. Downard, A.J., A.D. Roddick, and A.M. Bond, *Covalent modification of carbon electrodes for voltammetric differentiation of dopamine and ascorbic acid.* Analytica Chimica Acta, 1995. **317**(1–3): p. 303-310.

149. Chrétien, J.-M., et al., *Covalent Tethering of Organic Functionality to the Surface of Glassy Carbon Electrodes by Using Electrochemical and Solid-Phase Synthesis Methodologies.* Chemistry – A European Journal, 2008. **14**(8): p. 2548-2556.

150. Chrétien, J.M., et al., *Covalent Tethering of Organic Functionality to the Surface of Glassy Carbon Electrodes by Using Electrochemical and Solid-Phase Synthesis Methodologies.* Chemistry-A European Journal, 2008. **14**(8): p. 2548-2556.

151. Downard, A.J., A.D. Roddick, and A.M. Bond, *Covalent modification of carbon electrodes for voltammetric differentiation of dopamine and ascorbic acid.* Analytica Chimica Acta, 1995. **317**(1-3): p. 303-310.

152. Stewart, M.P., et al., *Direct covalent grafting of conjugated molecules onto Si, GaAs, and Pd surfaces from aryldiazonium salts.* Journal of the American Chemical Society, 2004. **126**(1): p. 370-378.

153. Nicolas-Debarnot, D. and F. Poncin-Epaillard, *Polyaniline as a new sensitive layer for gas sensors.* Analytica Chimica Acta, 2003. **475**(1-2): p. 1-15.

154. Dinh, H.N. and V.I. Birss, *Effect of Substrate on Polyaniline Film Properties A Cyclic Voltammetry and Impedance Study.* Journal of The Electrochemical Society, 2000. **147**: p. 3775.

155. Bonastre, A. and P. Bartlett, *Electrodeposition of PANi films on platinum needle type microelectrodes. Application to the oxidation of ascorbate in human plasma.* Analytica Chimica Acta, 2010. **676**(1-2): p. 1-8.

156. Barsukov, V., et al., *Catalytic activity of polyaniline in the molecular oxygen reduction: its nature and mechanism.* Russian Journal of Electrochemistry, 2004. **40**(11): p. 1170-1173.

157. Zhou, D.-M., H.-X. Ju, and H.-Y. Chen, *Catalytic oxidation of dopamine at a microdisk platinum electrode modified by electrodeposition of nickel hexacyanoferrate and Nafion®.* Journal of Electroanalytical Chemistry, 1996. **408**(1–2): p. 219-223.
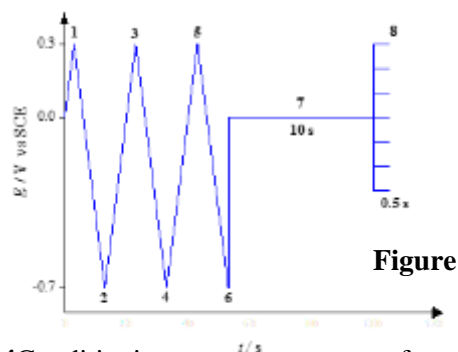
158.	Lane, R.F. and A.T. Hubbard, *Differential double pulse voltammetry at chemically modified platinum electrodes for in vivo determination of catechol amines.* Analytical Chemistry, 1976. **48**(9): p. 1287-1293.

159.	Strein, T.G. and A.G. Ewing, *Characterization of small noble metal microelectrodes by voltammetry and energy-dispersive x-ray analysis.* Analytical Chemistry, 1993. **65**(9): p. 1203-1209.

160.	Keithley, R.B., et al., *Higher sensitivity dopamine measurements with faster-scan cyclic voltammetry.* Analytical Chemistry, 2011.

161.	Xiao, Y., et al., *Highly sensitive and selective method to detect dopamine in the presence of ascorbic acid by a new polymeric composite film.* Analytical Biochemistry, 2007. **371**(2): p. 229-237.

162.	Ates, M., et al., *Carbon fiber microelectrodes electrocoated with polycarbazole and poly(carbazole-co- p -tolylsulfonyl pyrrole) films for the detection of dopamine in presence of ascorbic acid.* Mikrochimica Acta, 2008. **160**(1): p. 247-251.

163.	Jeong, H. and S. Jeon, *Determination of Dopamine in the Presence of Ascorbic Acid by Nafion and Single-Walled Carbon Nanotube Film Modified on Carbon Fiber Microelectrode.* Sensors, 2008. **8**(11): p. 6924-6935.

164.	Wightman, R.M., L.J. May, and A.C. Michael, *Detection of Dopamine Dynamics in the Brain.* Analytical Chemistry, 1988. **60**(13): p. 769A-793A.

165.	Hočevar, S.B., et al., *Carbon nanotube modified microelectrode for enhanced voltammetric detection of dopamine in the presence of ascorbate.* Electroanalysis, 2005. **17**(5-6): p. 417-422.

166.	Kishida, K.T., et al., *Sub-Second Dopamine Detection in Human Striatum.* PloS one, 2011. **6**(8): p. e23291.

167.	Adams, K.L., et al., *Highly Sensitive Detection of Exocytotic Dopamine Release Using a Gold-Nanoparticle-Network Microelectrode.* Analytical Chemistry, 2010. **83**(3): p. 920-927.

168.	Yixin, S. and S. Fu Wang, *Simultaneous Determination of Dopamine and Ascorbic Acid at a Triazole Self-Assembled Monolayer-Modified Gold Electrode.* Microchimica Acta, 2006. **154**(1): p. 115-121.

169.	Liu, T., M. Li, and Q. Li, *Electroanalysis of dopamine at a gold electrode modified with N-acetylcysteine self-assembled monolayer.* Talanta, 2004. **63**(4): p. 1053-1059.

170.	Zachek, M.K., et al., *Electrochemical dopamine detection: Comparing gold and carbon fiber microelectrodes using background subtracted fast scan cyclic voltammetry.* Journal of Electroanalytical Chemistry, 2008. **614**(1-2): p. 113-120.

171.	Budai, D., *Carbon Fiber-based Microelectrodes and Microbiosensors*. Intelligent and Biosensors. 2010.

172.	Kovach, P.M., M.R. Deakin, and R.M. Wightman, *Electrochemistry at partially blocked carbon fiber microcylinder electrodes.* The Journal of Physical Chemistry, 1986. **90**(19): p. 4612-4617.

173.	Zachek, M.K., et al., *Electrochemical dopamine detection: Comparing gold and carbon fiber microelectrodes using background subtracted fast scan cyclic voltammetry.* Journal of Electroanalytical Chemistry, 2008. **614**(1–2): p. 113-120.

Chapter 8

Appendices

Ruthenium hexaammine system: Below figures describe the conditioning waveforms to acquire the current transients and constructing SCVs which are normalised by diffusion controlled current.

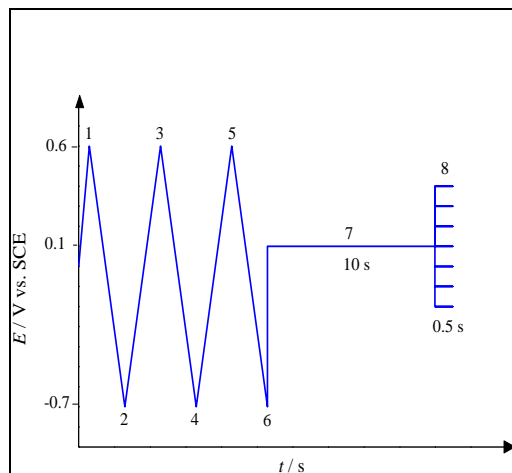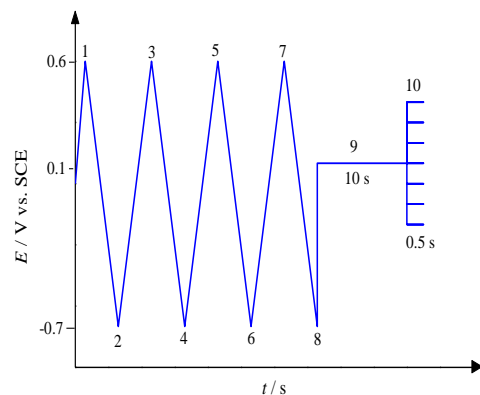| The waveform	SCVs	Time normalised SCVs
Figure 8.1 The conditioning waveform used includes sweeps and steps to acquire the current transient and construct a sampled current voltammogram. Sweeps 1-6 (at 500 mV s^{-1}) are for preconditioning, step 7 for resting and step 8 for measuring. The solid line shows the waveform for one experiment at one potential; the dotted lines indicate the changes made to the waveform to record the current for other potentials and reconstruct the SCV.	**Figure 8.2** Experimental sampled current voltammograms at fixed sampling times extracted from amperometric transients (step 8) at different potentials after applying the sawtooth waveform; 5 mM Ru(NH$_3$)$_6$Cl$_3$ / 0.5 M KCl at 25 μm diameter Pt microdisc. No background current has been subtracted. 1μA /V sensitivity till -0.2 V, 100 nA / V -0.15 V and 10 nA / V from -0.1V.	**Figure 8.3** Time normalised sampled current voltammograms (symbols) for the data shown above. Theoretical CV (solid line) is drawn from Mahon-Oldham equation 1.2 using the following parameters D=7.35×10^{-6} cm^2 s^{-1}, a=12.5 μm, c^{∞}=5 mM, E_0=−0.2 V. No subtraction of the background (argon degassed KCl) transients was done.

173

8.4 Conditioning waveform used to acquire the current transient and construct sampled current voltammograms. Sweeps 1-6 (at 500 mV s^{-1}) are for preconditioning, step 7 for resting and step 8 for measuring. The solid line shows the waveform for one experiment at one potential; the dotted lines indicate the changes made to the waveform to record the current for other potentials and reconstruct the SCV.

Figure 8.5 Sampled current voltammograms for the different sampling times considered. The chronoamperograms used to reconstruct the sampled current voltammograms were acquired in aerated 0.5 M KCl with the waveform shown in Figure 8.4, with a 25 µm diameter Pt disc, a Pt mesh counter electrode and SCE reference electrode. 100 nA /V sensitivity till -0.15 V, 10 nA / V from -0.1V. Each data point is the average of ten experiments.
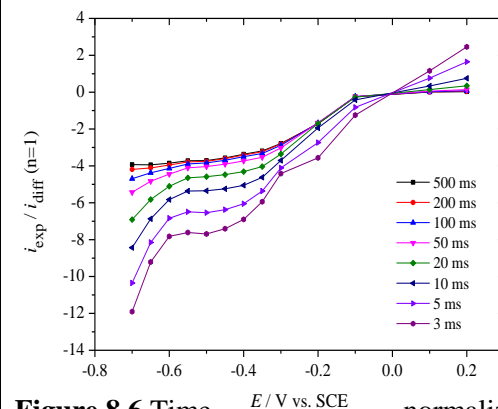
Figure 8.6 Time normalized sampled current voltammograms for the data shown in Figure 4.16 left. The normalisation was performed by dividing the experimental currents with the theoretical diffusion controlled current for a microdisc, Mahon and Oldham Equation 1.2, with n=1, $D = 2.2 \times 10^{-5}$ cm^2 s^{-1}, $c^\infty = 2.2 \times 10^{-5}$ mol cm^{-3}, $a = 12.5$ µm and t the corresponding sampling times. The sampled current voltammograms shown were not background subtracted.

Figure 8.7 Conditioning waveform used to acquire the current transient and construct sampled current voltammograms. Sweeps 1-6 (at 500 mV s^{-1}) are for preconditioning, step 7 for resting and step 8 for measuring. The solid line shows the waveform for one experiment at one potential; the dotted lines indicate the changes made to the waveform to record the current for other potentials and reconstruct the SCV.
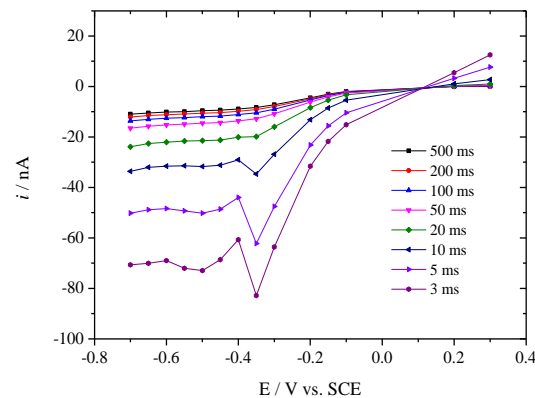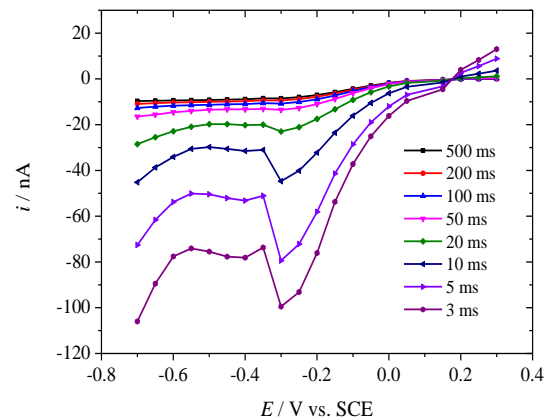
Figure 8.8 Sampled current voltammograms for the different sampling times considered. The chronoamperograms used to reconstruct the sampled current voltammograms were acquired in aerated 0.5 M KCl with the waveform shown in Figure 4.7, with 25 μm diameter Pt disc, a Pt mesh counter electrode and SCE reference electrode. 100 nA /V sensitivity till -0.4 V, 10 nA / V from -0.35V. Each data point is the average of ten experiments.
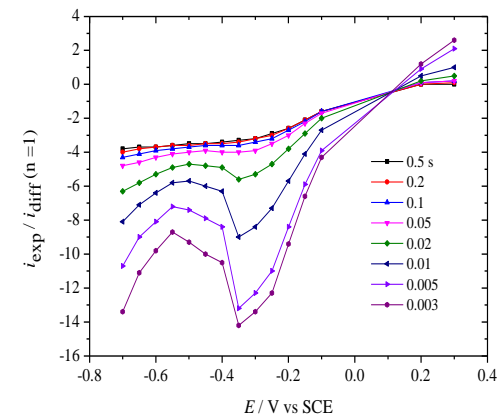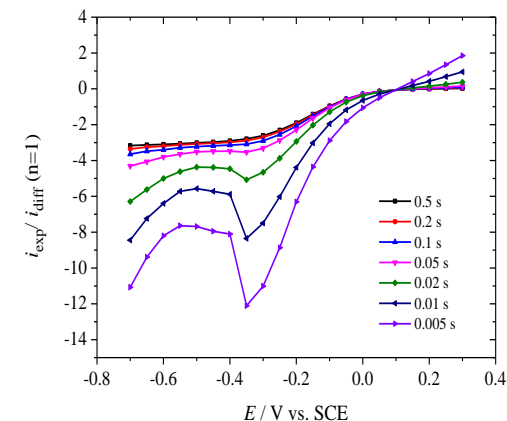
Figure 8.9 Time normalised sampled current voltammograms for the data shown. The normalised voltammograms were obtained by dividing the experimental currents with the theoretical current for a 1 electron diffusion controlled process calculated with the Mahon and Oldham equation 1.2 taking $n = 1$, $D = 2.2 \times 10^{-5}$ cm^2 s^{-1}, $c^{\infty} = 2.2 \times 10^{-7}$ mol cm^{-3}, and $a = 12.5 \times 10^{-4}$ cm.
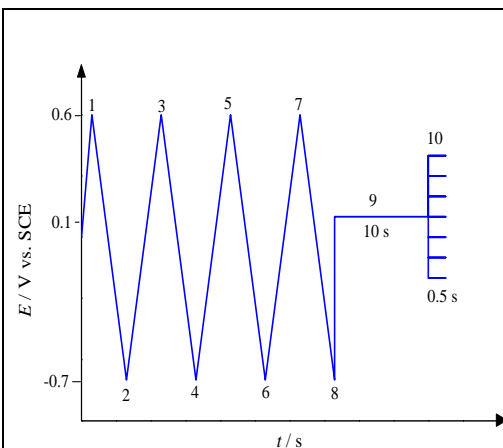
Figure 8.10 Conditioning waveform used to acquire the current transient and construct sampled current voltammograms. Sweeps 1-8 (at 500 mV s^{-1}) are for preconditioning, step 9 for resting and step 10 for measuring. The solid line shows the waveform for one experiment at one potential; the dotted lines indicate the changes made to the waveform to record the current for other potentials and reconstruct the SCV.
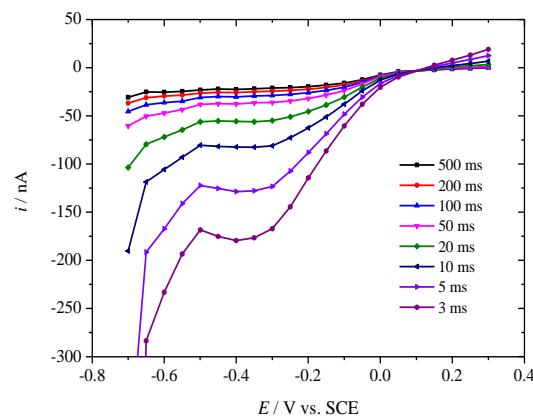

Figure 8.11 Sampled current voltammograms for the different sampling times considered. The chronoamperograms used to reconstruct the sampled current voltammograms were acquired in aerated 0.5 M KCl with the waveform shown in Figure 8.10, with 25 μm diameter Pt disc, a Pt mesh counter electrode and SCE reference electrode. Senstivity: 100 nA / V till -0.4 V and 10 nA / V from -0.35 V. Each data point is the average of ten experiments.
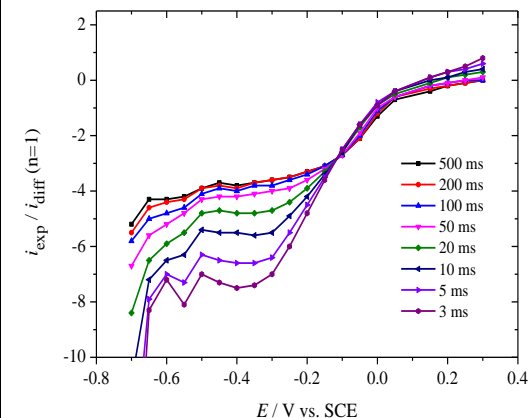

Figure 8.12 Time normalised sampled current voltammograms for the data shown. The normalised voltammograms were obtained by dividing the experimental currents with the theoretical current for a 1 electron diffusion controlled process calculated with the Mahon and Oldham equation 1.2 taking $n = 1$, $D = 2.2 \times 10^{-5}$ cm^2 s^{-1}, $c^{\infty} = 2.2 \times 10^{-7}$ mol cm^{-3}, and $a = 12.5 \times 10^{-4}$ cm.
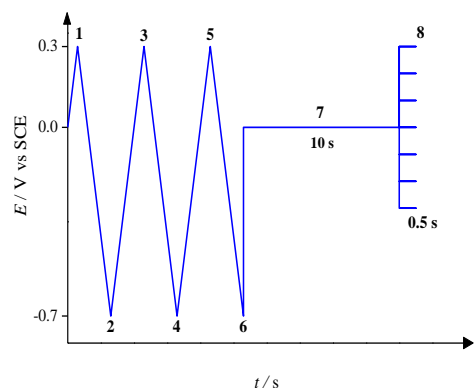
176

Figure 8.13 Conditioning waveform used to acquire the current transient and construct sampled current voltammograms. Sweeps 1-8 (at 500 mV s^{-1}) are for preconditioning, step 9 for resting and step 10 for measuring. The solid line shows the waveform for one experiment at one potential; the dotted lines indicate the changes made to the waveform to record the current for other potentials and reconstruct the SCV.
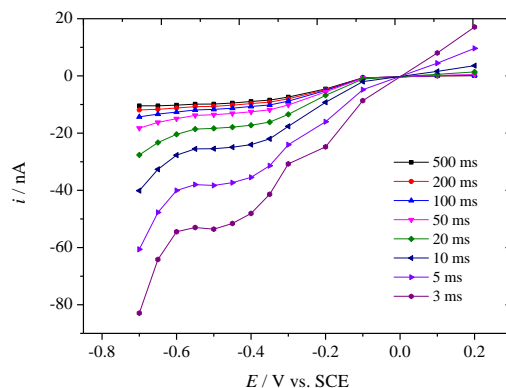
Figure 8.14 Sampled current voltammograms at different timescales recorded after applying the conditioning waveform shown in Figure 4.20 at a Pt microdisc (50 μm diameter) in 0.5 M KCl at 25 °C. SCE served as a RE. Each data point is the average of ten experiments. Sensitivity 1μA /V till -0.5 V AND 100 nA. Each data point is the average of ten experiments.

Figure 8.15 Time normalised sampled current voltammograms for the data shown. The normalised voltammograms were obtained by dividing the experimental currents with the theoretical current for a 1 electron diffusion controlled process calculated with the Mahon and Oldham Equation 1.2 taking $n = 1$, $D = 2.2 \times 10^{-5}$ cm^2 s^{-1}, $c^{\infty} = 2.2 \times 10^{-7}$ mol cm^{-3}, and $a = 25 \times 10^{-4}$ cm.

177

ORR in 0.5 M KCl: Below figures describe the conditioning waveforms to acquire the current transients and constructing SCVs which are normalised by diffusion controlled current.
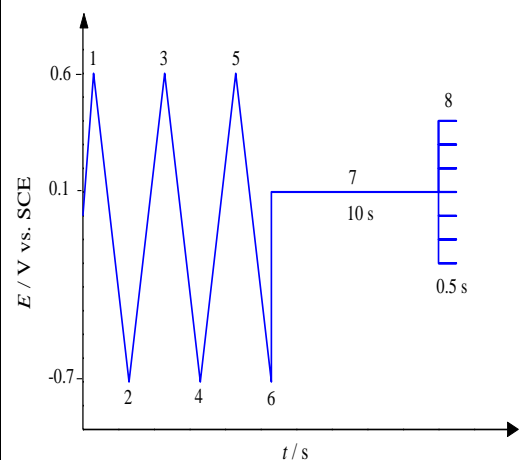

Figure 8.16 Conditioning waveform used to acquire the current transient and construct sampled current voltammograms. Sweeps 1-6 (at 500 mV s^{-1}) are for preconditioning, step 7 for resting and step 8 for measuring. The solid line shows the waveform for one experiment at one potential; the dotted lines indicate the changes made to the waveform to record the current for other potentials and reconstruct the SCV.
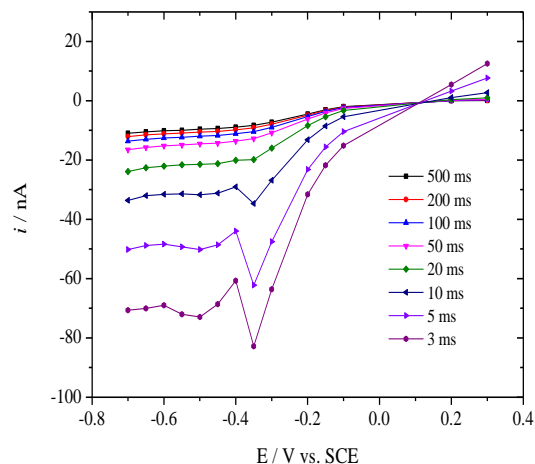
Figure 8.17 Sampled current voltammograms for the different sampling times considered. The chronoamperograms used to reconstruct the sampled current voltammograms were acquired in aerated 0.5 M KCl with the waveform shown in Figure 4.15, with a 25 μm diameter Pt disc, a Pt mesh counter electrode and SCE reference electrode. 100 nA /V sensitivity till -0.15 V, 10 nA / V from -0.1V. Each data point is the average of ten experiments.
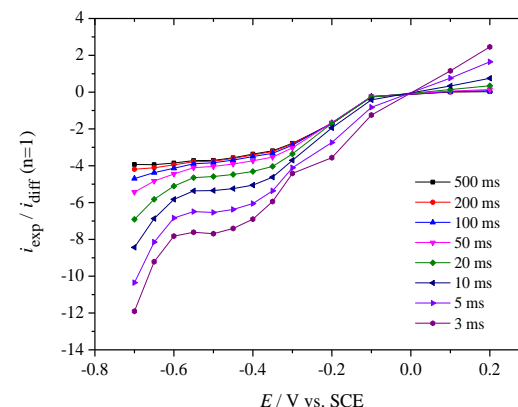
Figure 8.18 Time normalized sampled current voltammograms for the data shown in Figure 4.16 left. The normalisation was performed by dividing the experimental currents with the theoretical diffusion controlled current for a microdisc, Mahon and Oldham Equation 1.2, with n=1, D = 2.2x10^{-5} cm^2 s^{-1}, c^{∞} = 2.2x10^{-5} mol cm^{-3}, a = 12.5 μm and t the corresponding sampling times. The sampled current voltammograms shown were not background subtracted.

Figure 8.19 Conditioning waveform used to acquire the current transient and construct sampled current voltammograms. Sweeps 1-6 (at 500 mV s^{-1}) are for preconditioning, step 7 for resting and step 8 for measuring. The solid line shows the waveform for one experiment at one potential; the dotted lines indicate the changes made to the waveform to record the current for other potentials and reconstruct the SCV.

Figure 8.20 Sampled current voltammograms for the different sampling times considered. The chronoamperograms used to reconstruct the sampled current voltammograms were acquired in aerated 0.5 M KCl with the waveform shown in Figure 4.15, with 25 μm diameter Pt disc, a Pt mesh counter electrode and SCE reference electrode. 100 nA /V sensitivity till -0.4 V, 10 nA / V from -0.35V. Each data point is the average of ten experiments.
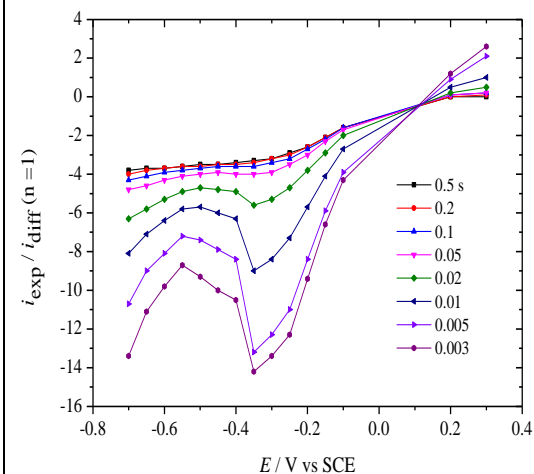
Figure 4.21 Time normalised sampled current voltammograms for the data shown. The normalised voltammograms were obtained by dividing the experimental currents with the theoretical current for a 1 electron diffusion controlled process calculated with the Mahon and Oldham equation 1.2 taking $n = 1$, $D = 2.2 \times 10^{-5}$ cm^2 s^{-1}, $c^{\infty} = 2.2 \times 10^{-7}$ mol cm^{-3}, and $a = 12.5 \times 10^{-4}$ cm.
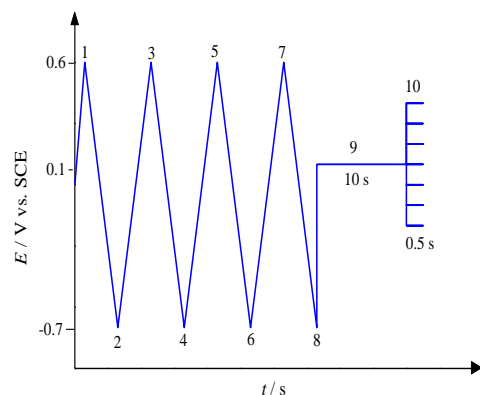
Figure 8.22 Conditioning waveform used to acquire the current transient and construct sampled current voltammograms. Sweeps 1-8 (at 500 mV s^{-1}) are for preconditioning, step 9 for resting and step 10 for measuring. The solid line shows the waveform for one experiment at one potential; the dotted lines indicate the changes made to the waveform to record the current for other potentials and reconstruct the SCV.
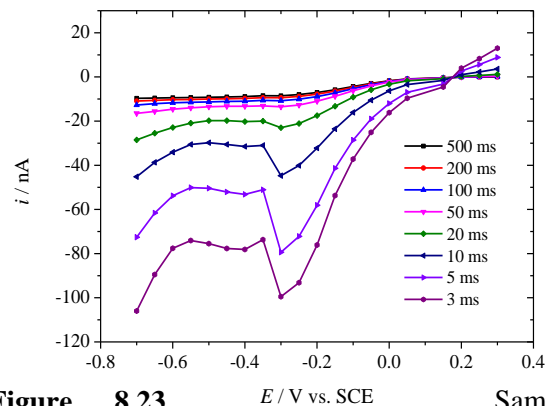

Figure 8.23 Sampled current voltammograms for the different sampling times considered. The chronoamperograms used to reconstruct the sampled current voltammograms were acquired in aerated 0.5 M KCl with the waveform shown in Figure 4.15, with 25 μm diameter Pt disc, a Pt mesh counter electrode and SCE reference electrode. Senstivity: 100 nA / V till -0.4 V and 10 nA / V from -0.35 V. Each data point is the average of ten experiments.
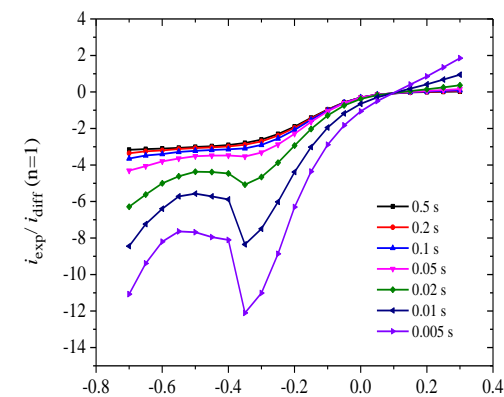

Figure 8.24 Sampled current voltammograms at different timescales recorded after applying the conditioning waveform shown in Figure 4.20 at a Pt microdisc (50 μm diameter) in 0.5 M KCl at 25 °C. SCE served as a RE. The normalised voltammograms were obtained by dividing the experimental currents with the theoretical current for a 1 electron diffusion controlled process calculated with the Mahon and Oldham Equation 1.2 taking $n = 1$, $D = 2.2 \times 10^{-5}$ cm^2 s^{-1}, $c^\infty = 2.2 \times 10^{-7}$ mol cm^{-3}, and $a = 25 \times 10^{-4}$ cm.
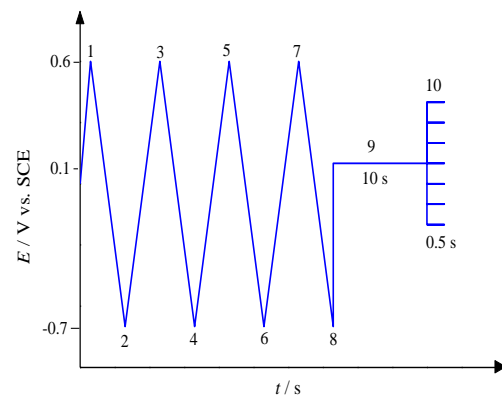
Figure 8.25 Conditioning waveform used to acquire the current transient and construct sampled current voltammograms. Sweeps 1-8 (at 500 mV s^{-1}) are for preconditioning, step 9 for resting and step 10 for measuring. The solid line shows the waveform for one experiment at one potential; the dotted lines indicate the changes made to the waveform to record the current for other potentials and reconstruct the SCV.
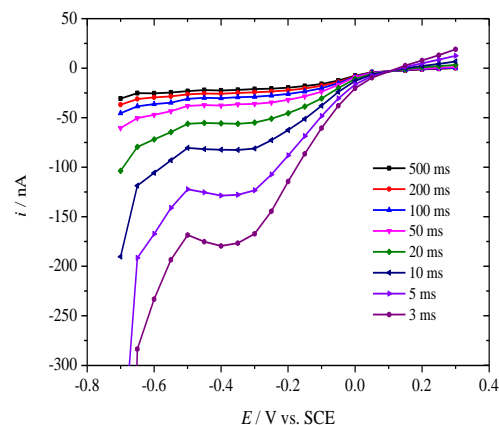

Figure 8.26 Sampled current voltammograms at different timescales recorded after applying the conditioning waveform shown in Figure 4.20 at a Pt microdisc (50 µm diameter) in 0.5 M KCl at 25 °C. SCE served as a RE. Each data point is the average of ten experiments. Sensitivity 1µA /V till -0.5 V AND 100 nA. Each data point is the average of ten experiments.

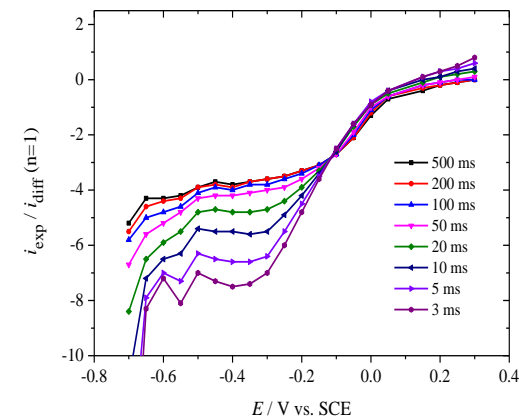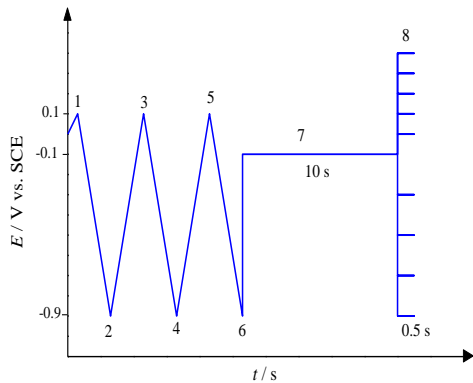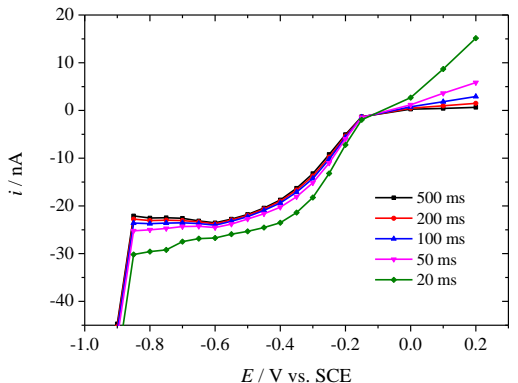**Figure 8.27** Time normalised sampled current voltammograms for the data shown. The normalised voltammograms were obtained by dividing the experimental currents with the theoretical current for a 1 electron diffusion controlled process calculated with the Mahon and Oldham Equation 1.2 taking $n = 1$, $D = 2.2 \times 10^{-5}$ cm^2 s^{-1}, $c^{\infty} = 2.2 \times 10^{-7}$ mol cm^{-3}, and $a = 25 \times 10^{-4}$ cm.

ORR in 0.5 M NaOH: Below figures describe the conditioning waveforms to acquire the current transients and constructing SCVs which are normalised by diffusion controlled current.

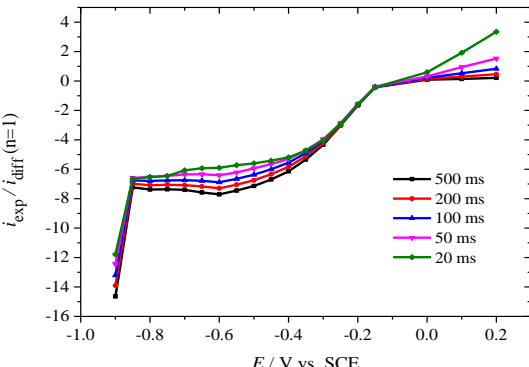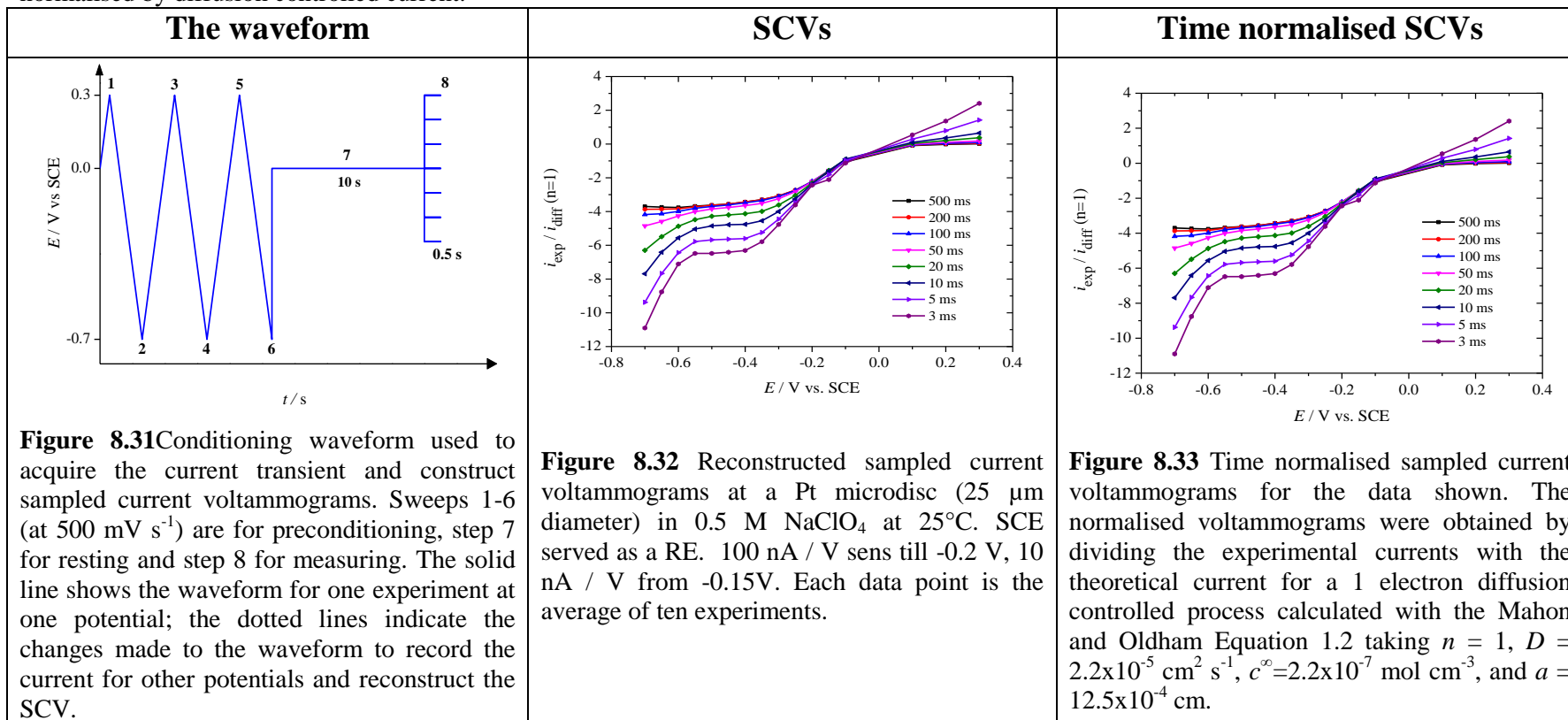| The waveform	SCVs	Time normalised SCVs
Figure 8.28 Conditioning waveform used to acquire the current transient and construct sampled current voltammograms. Sweeps 1-6 (at 500 mV s^{-1}) are for preconditioning, step 7 for resting and step 8 for measuring. The solid line shows the waveform for one experiment at one potential; the dotted lines indicate the changes made to the waveform to record the current for other potentials and reconstruct the SCV.	**Figure** 8.29 Sampled current voltammograms at a Pt microdisc (25 μm diameter radius) in 0.5 M NaOH at 25 °C. SCE served as a RE and Pt mesh as a CE. Sensitivity 100 nA/ V till -0.65 V, 10 nA/ V from -0.6V). Each data point is the average of three experiments.	**Figure 8.30** Time normalised sampled current voltammograms for the data shown. The normalised voltammograms were obtained by dividing the experimental currents with the theoretical current for a 1 electron diffusion controlled process calculated with the Mahon and Oldham Equation 1.2 taking $n = 1$, $D=2.45 \times 10^{05}$ cm^2 s^{-1}, $c^{\infty}=9 \times 10^{-8}$ mol cm^{-3} and $a = 12.5 \times 10^{-4}$ cm.

ORR in 0.5 M NaClO$_4$: Below figures describe the conditioning waveforms to acquire the current transients and constructing SCVs which are normalised by diffusion controlled current.

| The waveform	SCVs	Time normalised SCVs
Figure 8.31 Conditioning waveform used to acquire the current transient and construct sampled current voltammograms. Sweeps 1-6 (at 500 mV s^{-1}) are for preconditioning, step 7 for resting and step 8 for measuring. The solid line shows the waveform for one experiment at one potential; the dotted lines indicate the changes made to the waveform to record the current for other potentials and reconstruct the SCV.	**Figure 8.32** Reconstructed sampled current voltammograms at a Pt microdisc (25 µm diameter) in 0.5 M NaClO$_4$ at 25°C. SCE served as a RE. 100 nA / V sens till -0.2 V, 10 nA / V from -0.15V. Each data point is the average of ten experiments.	**Figure 8.33** Time normalised sampled current voltammograms for the data shown. The normalised voltammograms were obtained by dividing the experimental currents with the theoretical current for a 1 electron diffusion controlled process calculated with the Mahon and Oldham Equation 1.2 taking $n = 1$, $D = 2.2 \times 10^{-5}$ cm^2 s^{-1}, $c^{\infty} = 2.2 \times 10^{-7}$ mol cm^{-3}, and $a = 12.5 \times 10^{-4}$ cm.

183

Dopamine Oxidation

There is an increasing demand for the determination of biological compounds using suitable analytical methods. One of the important topics in neuroscience research and development of pharmaceutical products is dopamine measurement. Dopamine is well known as a neurotransmitter in the mammalian central nervous system. It plays a major role in the regulation and control of movement and motivation. The lack of brain dopamine or its deficiency can lead to psychiatric disorders including Parkinson's disease. It can be detected electrochemically due to its electroactivity. It was reported it undergoes a 2 electron irreversible oxidation process with transfer of two protons at carbon based electrodes [157]. The mechanism of the oxidation involves some intermediates as shown in the following reactions and the reaction is reported to be slow [158].

First, the oxidation of dopamine [158] occurs to form the open-chain o-quinone (Reaction1).
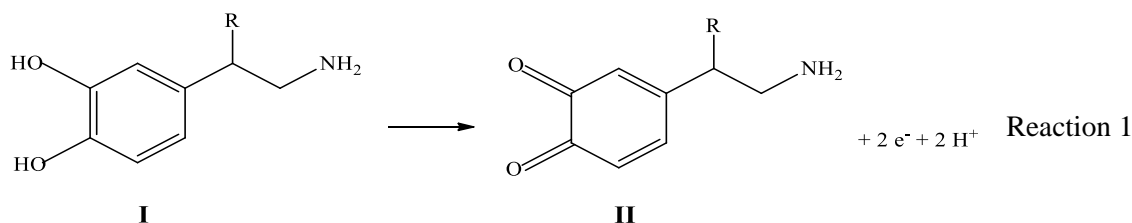
Second, intracyclization of the o-quinone proceeds within seconds, producing the 5,6-dihydroxyindoline (Reaction 2).
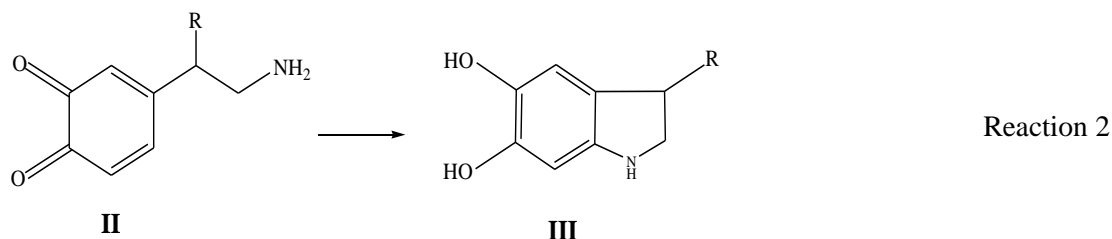
Lastly, the cyclic intermediate, **III**, is more easily oxidizable than the parent catecholamine, **I**, and accordingly, is rapidly oxidized by the o-quinone, **II**, to produce an aminochrome, **IV**, Reaction 3.
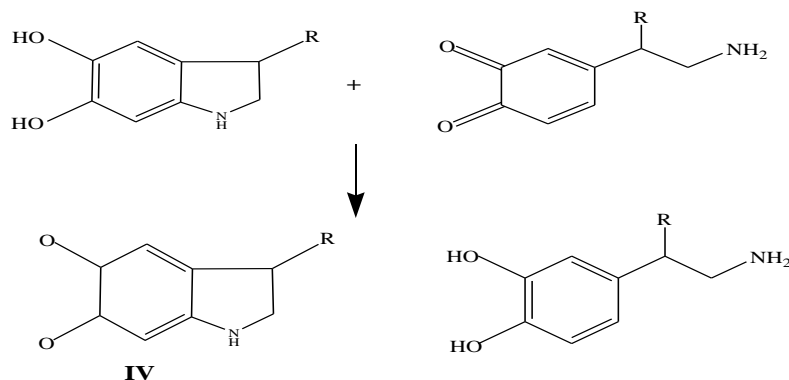
Reaction 3 Mechanism of dopamine oxidation

There are some problems encountered in dopamine measurement. Generally, minimal tissue damage can be achieved in *in vivo* analysis using electrodes of suitably small diameter in both electroactive area and in total structural diameter. However, electrode fouling remains a serious limitation in the measurements thus far obtained using the carbon probes. Using Pulse Amperometric Detection (PAD) with Pt and Au microelectrode for Dopamine (DA) sensing was reported to minimise electrode fouling [159]. The application of waveform coupled with FSV at CF microelectrodes for the detection of dopamine has been recently reported [160]. This treatment was beneficial in the creation of adsorption sites for dopamine to oxidise. Some other challenges were reported with this kind of measurements which related to very low concentration (µL) of neurotransmitter. In addition measurements suffer interferences from other species such as ascorbic acid over the potential range of interest. Its electrochemical oxidation occurs in the same potential range as that of dopamine. Moreover, it is presents in high concentration 10^2 to 10^3 higher than those for dopamine [161-164].

The electrode modification should enhance the electron transfer kinetics for dopamine oxidation. There are considerable interests in the chemical modification of the electrodes for some applications such as electrocatalysis, electrosynthesis and

photosensitization [5]. One of these methods is polymeric films. Hence the demand for designed sensors is to achieve improved sensitivity and selectivity with modified electrodes in addition to sufficient versatility to detect a wide variety of analytes. Also, modification of carbon fibre microelectrodes with carbon nanotube and Nafion was reported recently [163, 165]. It has proved superior in the discrimination of the oxidation peaks for both dopamine and ascorbic acid. Recently, some work was also carried out for detecting dopamine at CF microelectrode at sub-second FSV in human brain [166]. The recent development in DA sensing is in exploiting nanoparticles [167] as they offer a prolonged storage stability due to the unique activity of the Au nanoparticle network. Self-Assembled Monolayer (SAM) [168-169] or Polyethylene glycol (PEG) was coated at Au electrode in order to prevent protein adsorption during DA detection [161].

Dopamine Investigation at bare electrode

Detection of dopamine was carried out first at bare Pt microelectrodes in this study. In order to prevent oxidative degradation of dopamine over the course of the experiment, both phosphate buffered saline (PBS) and dopamine (DA) in PBS electrolyte solutions were argon degassed.

PBS (0.1 M NaH_2PO_2 + 0.1 M Na_2HPO_4 + 0.15 M NaCl) was set to have pH=7.4. The total current is for 100 μL of 10 mM dopamine hydrochloride + 0.15 M NaCl + phosphate buffer (pH=7.4), whereas the background is for 0.15 M NaCl + phosphate buffer (pH=7.4). Stock solution of dopamine was prepared in 10 ml (10 mM). When dopamine was injected, the solution was again degassed with argon for few minutes to avoid the oxidation by air. All experiments were conducted at 37 ℃. A slow scan rate was applied and limiting current was obtained. Figure 8.34 shows a sigmoidal shape for the dopamine oxidation response. However, it does not look like a perfect sigmoidal curve compared to that for ruthenium hexaammine. There is a fair amount of hysteresis. Also, there is decay in current with the increase in the number of scans and that is probably due to the adsorption of dopamine. Using Equation 9, D_{DA} was found to be in a good agreement with the reported value [158]. The limiting current was measured at

0.2 V and $n = 2$. The diffusion coefficient of dopamine was determined to be $D_{DA} = 4.9 \times 10^{-6}$ cm^2 s^{-1}.
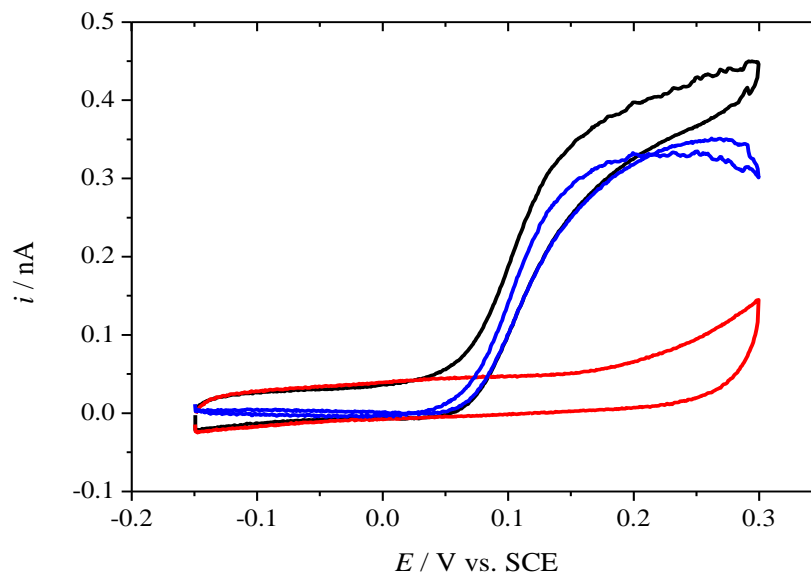

Figure 8.34. Steady state voltammogram (3rd scan) for dopamine oxidation, in PBS electrolyte at 37° C at Pt microdisc electrode (25 μm diameter) at 10 mV s^{-1}. 100 μL of 10 mM dopamine + 0.15 M NaCl (pH=7.4). Pt mesh serves as a counter electrode. Red line for the background CV, black for CV in dopamine and NaCl whereas blue colour for the background subtracted CV.

When the applied scan rate was increased, the magnitude of the oxidation current (at 0.13 V *vs* SCE) increased and the voltammetric response changed to peaked shape, as expected for a voltammogram showing a mix of planar and hemispherical diffusion. Figure 5.2 illustrates the responses at different scan rates. A poisoning of the platinum electrode was observed due to adsorption of dopamine in physiological pH condition [158]. The electropolymerisation of dopamine can be attributed to the decrease in current as the number of sweeps increases. This was evidenced from the fact that platinum is well known to be prone to biofouling and chlorine contamination [170]. The use of exclusion layer coatings could help to reduce this effect.

First, the products of catecholamine electrooxidation undergo subsequent chemical reactions to form solid deposits on the electrode (See mechanism of dopamine oxidation- Reactions 1, 2 and 3. This results in a continual decline in the measured

current with continuous cycling and prevents quantitative interpretation of the results. Chemisorption of numerous species on conventional platinum electrodes caused marked and variable inhibition of the electron transfer process, which interfered with the analysis [158].
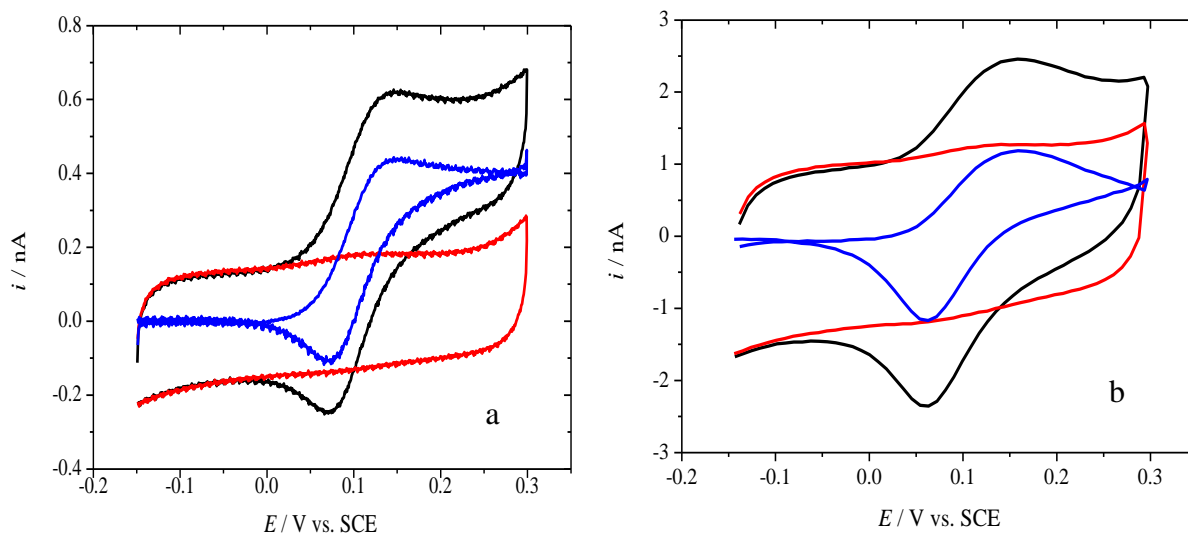

Figure 8.35 Eighth scan cyclic voltammograms at a) 100 and b) 1000 mV s^{-1}, in PBS electrolyte, 100 µL of 10 mM Dopamine + 0.15 M NaCl (pH=7.4), and background subtracted at 25 µm Ø Pt microdisc electrode as working electrode recorded at 37 ºC under deaerated conditions. Red line for the background CV, black for CV in dopamine and NaCl whereas blue colour for the background subtracted CV.

In Figure 8.35, the Pt electrode exhibits some irreversibility in the dopamine oxidation reaction: the oxidation peak of dopamine to quinone and reduction peak back to dopamine shift with scan rate. Pt electrodes develop an oxide monolayer when cycled in electrolytic solution [31][158]. Oxide layers have promoted the adsorption of species such as dopamine [21].

A 50 µm Ø Pt microdisc electrode was also used to investigate both dopamine oxidation and ORR. It is clearly observed that the recorded current on the background voltammogram at 50 µm Ø Pt microdisc is twice that at 25 µm Ø Pt microdisc (see Figure 8.36). The response for dopamine oxidation is not as good as those recorded at 25 µm Ø Pt microdisc (see Figure 5.3). The electrode was transferred to an acid solution to check its cleanliness after the dopamine oxidation experiments, and a

distorted voltammogram (not shown) was observed. Clearly, in order to eliminate the expected electrode poisoning caused by electropolymerisation of dopamine at the electrode surface, the modification of the electrode could be an alternative to bare electrode.
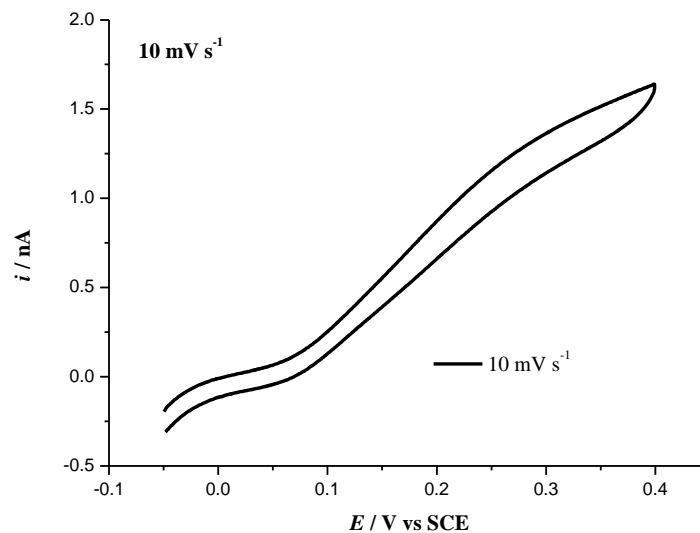

Figure 8.36 Steady state voltammogram for dopamine oxidation (100 μL of 10 Mm dopamine + 0.15 M PBS, pH=7.4) at a 50 μm diameter Pt microdisc electrode at 10 mV s⁻¹. Pt mesh serves as a counter electrode at 37° C.

In Figures 8.37, the ORR response at a Pt microelectrode showed well-behaved waves for the ORR and dopamine oxidation at low sweep rates but large hysteresis was observed as the scan rate increased to 1 and 10 V s⁻¹, not shown. The background signal was significant especially at high scan rates.
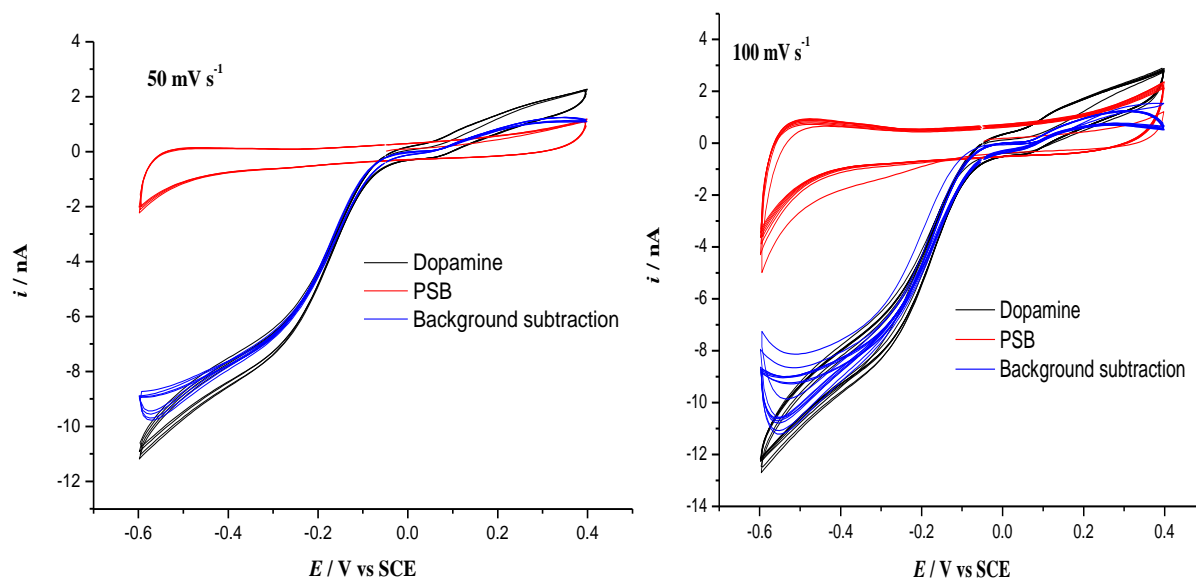
Figure 8.37 Eight cyclic voltammograms, in aerated PBS electrolyte, 100 μL of 10 Mm dopamine + 0.15 M PBS, pH=7.4 and background subtracted at a 50 μm Ø Pt microdisc electrode recorded at 37º C.

The detection of dopamine at CF surface using background subtracted fast scan voltammetry was accomplished [170]. Since the electrochemical properties of CF differ from those of Pt, an investigation was carried out. Under the same conditions, the dopamine oxidation and oxygen reduction experiment was tried at carbon fibre electrodes to compare the electrochemical responses. First, the diameter of the CF electrode was determined as it can be seen from Figure 8.38, using ruthenium hexaammine reduction or ferrocene oxidation by measuring the limiting current and calculating the radius of the electrode using Equation 9, the diameter was found to be circa 7 μm.
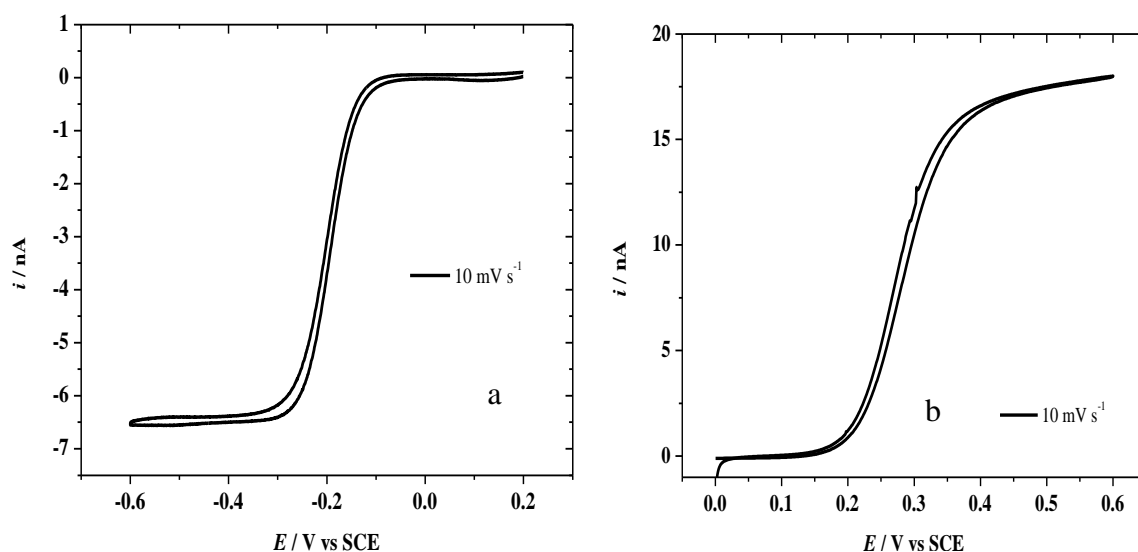
Figure 8.38 Cyclic voltammograms for a) reduction of 5 mM $Ru(NH_3)_6^{3+}$ to $Ru(NH_3)_6^{2+}$ in 0.5 M KCl , b) oxidation of 5 mM ferrocene in 0.1 M TBTFA in acetonitrile at bare CF microdisc working electrodes. First cycle recorded at 25 ℃.

A carbon fibre microelectrode has outstanding mechanical and electrical properties [171]. A CF with longer tip length has a greater active surface, therefore it is preferable for this kind of biological applications and it has been used for a while for the determination of neurotransmitters. Additionally, due to its low cost and renewable surface it has been used in biological applications such as ascorbic detection [172]. The carbon fibre surface seems to promote faster electron transfer with biomolecules than metal electrodes [170].

The simultaneous measurements of both dopamine oxidation and oxygen reduction were carried out. Particularly high scan rates were also tested since FSV was demonstrated to help prevent surface fouling by the products of the oxidation of dopamine [112]. From Figure 8.39, it can be seen that at slow scan rate, a sigmoidal shape for dopamine oxidation is consistent with observation in the literature. At large scan rates, not shown, the appearance of some voltammetric waves in the background CV has been attributed to electroactive quinones and phenolic groups on the CF electrode [112].
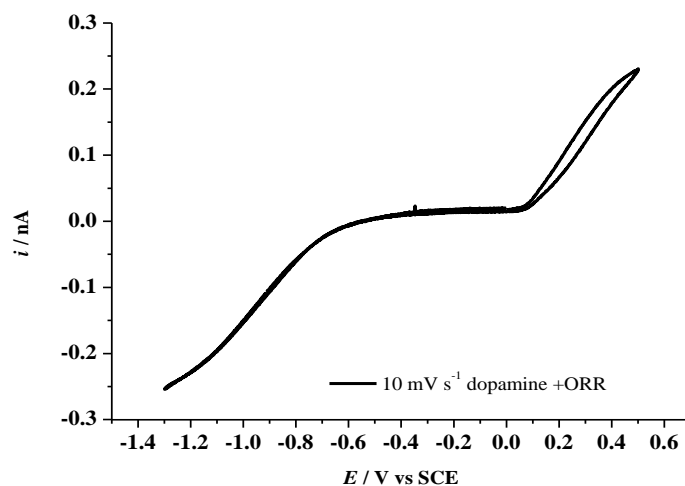
Figure 8.39 Eight cyclic voltammograms, in aerated PBS electrolyte, 100 μL of 10 mM dopamine + 0.15 M PBS, pH=7.4 and background subtracted at 7 μm Ø CF microdisc working electrode; recorded at 37 °C with different scan rates.

The potential window in PBS is wider at CF electrode compared to Pt electrode. The irregular background current properties at carbon fibre electrode are attributable to surface-bound redox couples. The contribution of this current can interfere with the measured signal. Any change in the properties of CF surface can affect the electron transfer.

The choice of carbon fibre was based on the advantages provided in terms of the wide potential window compared with metal electrodes [173]. This ensures the detection of more redox couples such as biomolecules. In addition, it is of interest due to its easiest way of modification or manipulation. Also, it was reported that the fouling of the carbon based electrode upon dopamine oxidation was not a problem at fast scan [112] as a results of sweeping away any products that could adsorb on the surface. The adsorption of dopamine stems from the interaction with the surface functional groups at carbon. There was an increase in peak current at various applied scan rates. However, carbon is not known to be a good catalyst for detecting reduced oxygen species, yet the oxygen reduction wave seen in figure 8.39 at low scan rate is stable with no hysteresis.

Dopamine and ORR investigations

The coated electrode was subjected to further experiment in biological media. This coating was tested in PBS solution containing dopamine and oxygen species. The voltammograms were recorded at different scan rates.

Figure 8.40 illustrates the simultaneous detection of dopamine oxidation and reduction of oxygen. The polypyrrole coated electrode catalysed the oxidation of dopamine and showed a nice wave for ORR, although it hindered the ORR signal. This is probably due to the presence of carbonyl and carboxylic groups that attract dopamine cation. Due to high electron density of these groups, this coating does not promote a strong adsorption with dopamine at the surface.

It was found that the sensitivity of the oxidation of dopamine is enhanced by the presence of polyprrrole at CF electrode. This is consistent with our results for Pt coated with poly pyrrole. OPPy was electropolymerised previously at CF disc microelectrodes. The previously published work showed that the sensitivity resulting from the modification of the electrode surface is more pronounced at Pt rather than CF. Here, CF has not been tried for coating. A paper discussed the effect of OPPy covered CF cylindrical and elliptical electrode in efficiency detection in identification of dopamine [138]. However the slow response time was one of the problems encountered with this coating. The steric congestion effect when detecting dopamine at overoxidized PPy coated electrode was proposed.
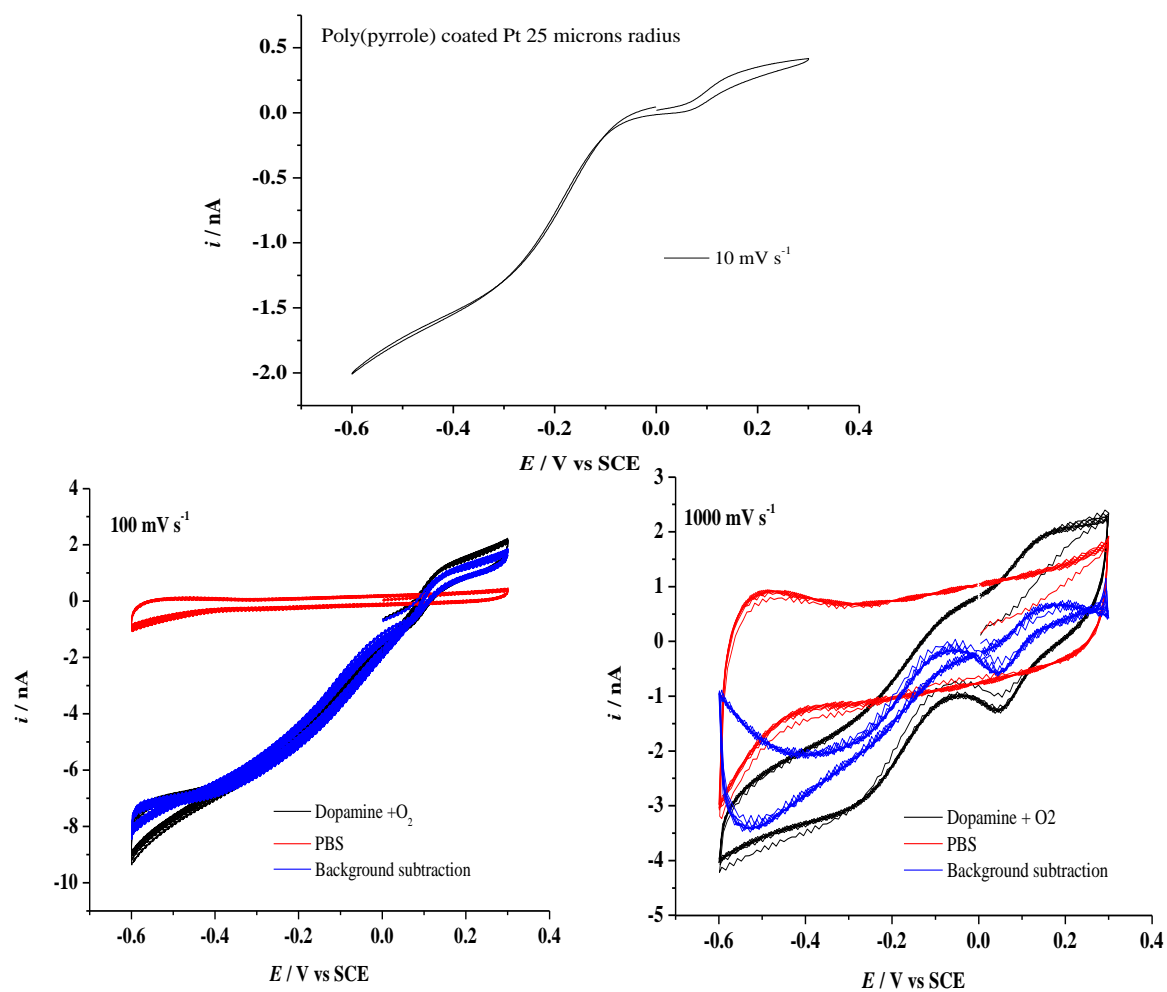
Figure 8.40 Eight cyclic voltammograms, in PBS electrolyte, Dopamine + PBS, and background subtracted at polypyrrole coated 25 μm Ø Pt microdisc electrode; recorded at 37ºC.